PN AAS-327

IAN: 39239

ASSESSMENT OF TSUNAMI HAZARD PRESENTED BY POSSIBLE SEISMIC EVENTS: NEAR-SOURCE EFFECTS

SAI-82-651-WA

SCIENCE APPLICATIONS, INC.

Post Office Box 1303, 1710 Goodridge Drive, McLean, Virginia 22102, (703) 821-4300

ASSESSMENT OF TSUNAMI HAZARD PRESENTED BY POSSIBLE SEISMIC EVENTS: NEAR-SOURCE EFFECTS

SAI-82-651-WA

TR-424-81-216-11

November 1981

Contract Number:
AID/SOD/PDC-C-0404

Prepared by:
Gerald T. Hebenstreit
and Robert E. Whitaker

Prepared for:
Agency for International Development
U.S. Department of State

SCIENCE APPLICATIONS, INC.
1710 Goodridge Drive
P.O. Box 1303
McLean, Virginia 22102
(703) 821-4300

ACKNOWLEDGMENTS

This report combines the efforts of many individuals. Thanks must go to Gene Molinelli and Fred Newman, who acted as reviewers and editors. This report is significantly stronger thanks to their efforts.

Special thanks go to Paul Krumpe of the Office of Foreign Disaster Assistance, USAID, who provided the funding and many of the ideas for this study.

The Spanish translation of this report was done by Linguamundi International, Inc., McLean, Virginia.

ABSTRACT

The purpose of this study is to model the propagation of tsunamis along the continental shelf up and down coast of earthquake source regions near the Peru-Chile Trench. The simulations were carried out by numerically solving the linear, inviscid equations for long waves. Potential generating areas were chosen by identifying seismic gaps in the Peru-Chile Trench area. Ocean bottom displacements in each source area were specified on the basis of representative earthquake parameters (depth, dip angle, fault length and width, slip displacement) chosen from an examination of historical seismicity patterns in the area.

Areas of maximum offshore wave height were identified along the coastline in response to each earthquake/tsunami event. Several coastal areas were subjected to high concentrations of wave energy no matter where the source was located. These areas warrant more detailed study. Recommendations are made concerning the use of the present study in tsunami hazard education and planning efforts, as well as for further work based on these results.

Table of Contents

Page

Acknowledgments

Abstract

Section 1 INTRODUCTION 1-1

1.1 Tsunamis. 1-1
1.2 The South American Threat 1-5
1.3 Purpose of the Study. 1-5
1.4 Structure of the Report 1-7

Section 2 THE NUMERICAL MODEL. 2-1

2.1 Introduction. 2-1
2.2 Model Equations 2-2
2.3 Solution Scheme 2-4
2.4 Boundary Conditions 2-6
2.5 Bottom Topography 2-8
2.6 Source Motions. 2-12

Section 3 CHOICE OF EARTHQUAKE SITES AND SOURCE MOTIONS. 3-1

3.2 Focal Mechanisms. 3-5
3.2.1 Peru 3-5
3.2.2 Chile. 3-8
3.2.3 Fault Motions. 3-8
3.2.4 Representative Mechanisms. . . . 3-9
3.3 Earthquake Energy 3-11
3.4 Source Motions. 3-21
3.5 Bottom Displacement Patterns. 3-24
3.6 Effect of Source Duration 3-26

Section 4 SOURCE ZONE A. 4-1

4.1 Introduction. 4-1
4.2 Uniform Uplift Case 4-1
4.2.1 Immediate (First Hour) Effects. 4-3
4.2.2 Longer Duration Effects. 4-3
4.2.3 Maximum Elevations 4-4
4.3 Variable Uplift Case. 4-22
4.3.1 Immediate Effects. 4-22
4.3.2 Longer Duration Effects. 4-22
4.3.3 Maximum Elevations 4-23
4.4 General Hazard Assessment 4-37
4.5 Hazard Assessment - Zone A. 4-38

Table of Contents (continued)

Page

Section 5 SOURCE ZONE B. 5-1

5.1 Introduction. 5-1
5.2 Northern Zone - Uniform Uplift Case. 5-1
5.2.1 Immediate Effects. 5-1
5.2.2 Longer Duration Effects. 5-3
5.2.3 Maximum Elevations 5-4
5.3 Northern Zone - Variable Uplift Case 5-18
5.3.1 Immediate Effects. 5-18
5.3.2 Longer Duration Effects. 5-18
5.3.3 Maximum Elevations 5-19
5.4 Southern Zone - Uniform Uplift Case 5-33
5.4.1 Immediate Effects. 5-33
5.4.2 Longer Duration Effects. 5-33
5.4.3 Maximum Elevations 5-34
5.5 Southern Zone - Variable Uplift Case 5-48
5.5.1 Immediate Effects. 5-48
5.5.2 Longer Duration Effects. 5-48
5.5.3 Maximum Elevations 5-49
5.6 Hazard Assessment - Zone B. 5-63
5.6.1 Northern Subzone 5-63
5.6.2 Southern Subzone 5-63
5.6.3 Summary. 5-64

Section 6 SOURCE ZONE C. 6-1

6.1 Introduction. 6-1
6.2 Uniform Uplift Case 6-1
6.2.1 Immediate Effects. 6-1
6.2.2 Longer Duration Effects. 6-1
6.2.3 Maximum Wave Heights 6-3
6.3 Variable Uplift Case. 6-17
6.3.1 Immediate Effects. 6-17
6.3.2 Longer Duration Effects. 6-17
6.3.3 Maximum Elevations 6-17
6.4 Hazard Assessment - Source C. 6-31

Section 7 SOURCE ZONE D 7-1

7.1 Introduction. 7-1
7.2 Uniform Uplift Case 7-1
7.2.1 Immediate Effects. 7-1
7.2.2 Longer Duration Effects. 7-1
7.2.3 Maximum Elevations 7-3
7.3 Variable Uplift Case. 7-17

Table of Contents (continued)

Page

7.3.1 Immediate Effects. 7-17
7.3.2 Longer Duration Effects. 7-17
7.3.3 Maximum Elevations 7-17
7.4 Hazard Assessment - Source Zone D . . . 7-32

Section 8 SOURCE ZONE E. 8-1

8.1 Introduction. 8-1
8.2 Uniform Uplift Case 8-1
8.2.1 Immediate Effects. 8-1
8.2.2 Longer Duration Effects. 8-3
8.2.3 Maximum Elevations 8-4
8.3 Variable Uplift Case. 8-18
8.3.1 Immediate Effects. 8-18
8.3.2 Longer Duration Effects. 8-18
8.3.3 Maximum Elevations 8-19
8.4 Hazard Assessment - Source Zone E . . . 8-33

Section 9 CONCLUSIONS AND RECOMMENDATIONS. 9-1

9.1 Introduction. 9-1
9.2 Conclusions 9-2
9.2.1 Threat from Specific Earthquakes 9-2
9.2.2 Threats to Specific Areas. . . . 9-3
9.2.3 Summary. 9-5
9.3 Historical Perspective. 9-5
9.4 Recommendations 9-6

References. R-1

Appendix A SOUTH AMERICAN TSUNAMIS A-1

Appendix B NUMERICAL TECHNIQUE B-1

Section 1
INTRODUCTION

1.1 TSUNAMIS

Tsunamis are very long ocean surface gravity waves generated by sudden displacements of large volumes of water. While tsunamis have been generated by landslides (both submarine and coastal) and volcanoes, the predominant source of tsunamis is the rapid displacement of the sea floor due to shallow focus submarine earthquakes. The displacement of a volume of sea water (usually a vertical displacement) moves the sea surface in the vicinity of the displacement away from the quasi-equilibrium state known as mean sea level (MSL). The action of gravity and buoyancy in trying to return the surface to its equilibrium state produces wave energy in the form of tsunamis, which propagate away from the disturbance into the surrounding ocean. Tsunami waves propagate very rapidly and can cross a basin the size of the Pacific Ocean in less than a day.

Most tsunamis seem to be generated by shallow, thrust type earthquakes, such as are associated with the subduction of one tectonic plate under another. Since many subduction zones are located on the margins of the Pacific basin, most of the tsunamis recorded to date have occurred in the Pacific Ocean. Figure 1.1 depicts the locations of epicenters of tsunamigenic earthquakes in the Pacific. We can see that epicenters tend to cluster in several geographic regions: South and Central America, Alaska and Aleutian Islands, Kamchatka and the Kurile Islands, Japan, and the Southwest Pacific. The Southwest Pacific source area rarely

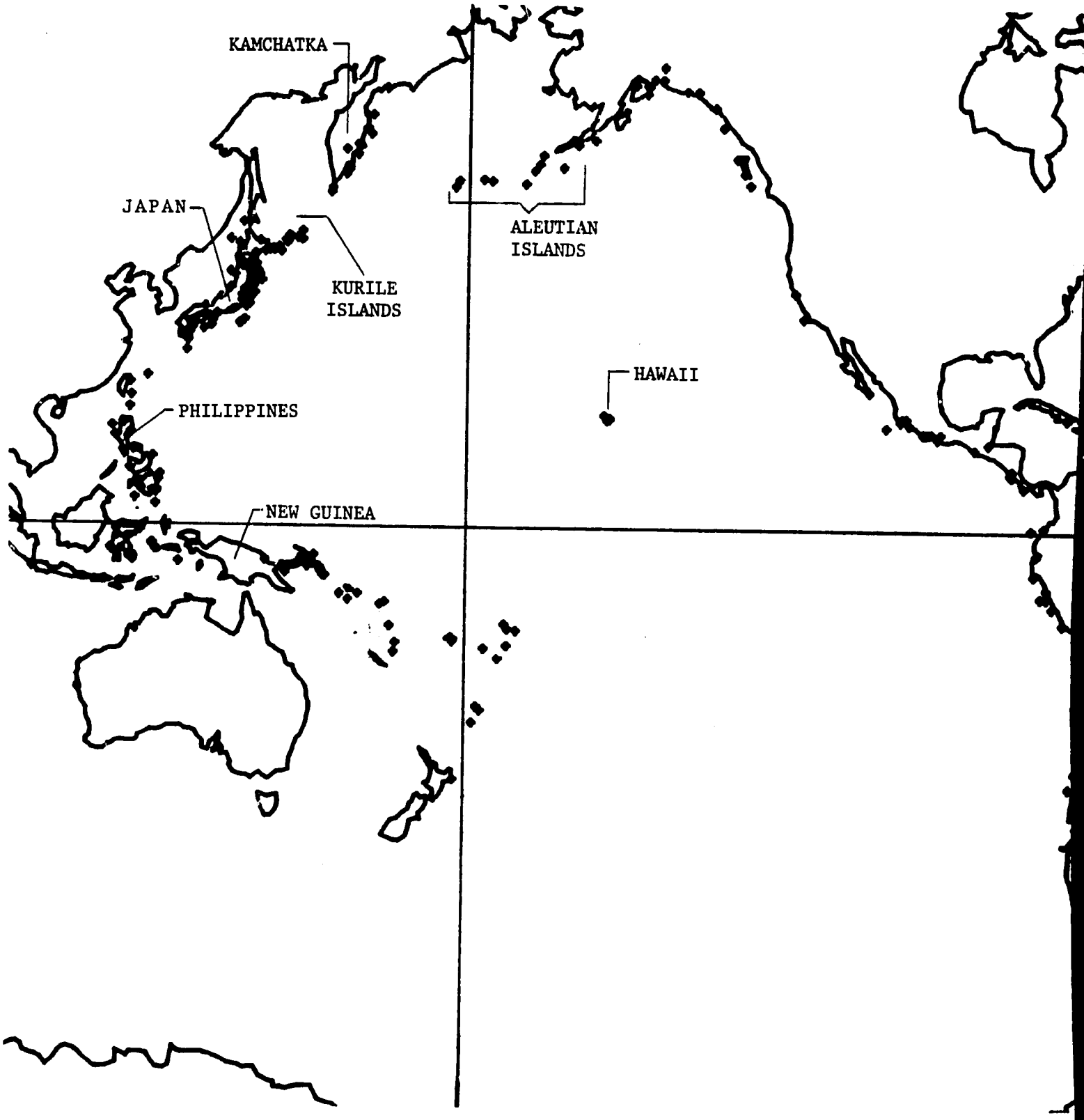

Figure 1.1. Epicenters of tsunamigenic earthquakes in the Pacific Ocean during the period 1900-1969. (courtesy EDIS/NGSDC/NOAA, Boulder, Colorado.)

produces tsunamis which cause serious effects throughout the entire Pacific region. But tsunamis generated in the other areas do potentially pose a Pacific-wide threat.

Tsunamis pose a twofold threat to the Pacific community. The most generally known is the far-field threat. If the energy pumped into the ocean is sufficiently great, the resulting waves can cross the open ocean as very long, low amplitude waves and reappear as large amplitude, highly destructive waves on coasts tens of thousands of kilometers from their source area. For example, the earthquake of 22 May 1960, which occurred off the coast of southern Chile, produced waves which caused 61 deaths and $22M in damage in the Hawaiian Islands and 199 deaths and the destruction of nearly 5,000 structures in Japan. Tsunamis which cause such far-reaching destruction are, fortunately, rare. Since 1946 only five tsunamis in the Pacific Ocean have been that destructive. Table 1.1 lists the cost in lives and dollars to the United States alone because of these events.

The second threat can be termed the near-source threat. The waves generated by a tsunamigenic earthquake in a shallow coastal area not only spread out into the Pacific, but also up and down the coast in the vicinity of the source. Tsunamis always produce a near-source threat, but not always a far-field threat. For example, Berninghausen (1962) lists 49 tsunamis which produced, at the very least, measurable waves on the coasts of South America between 1562 and 1960. Only 4 of these were generated anywhere else but the coastal waters of South America. Let us examine the threat posed by South American tsunamis more closely.

TABLE 1.1

Major Tsunamis since 1946
which caused loss of life and property in the U.S.*

Date	Places of Major Impact	Source Location	Tsunami Fatalities	Tsunami Damage** 1980 $ ($ Millions)
1946	Hawaiian Islands	E. Aleutian Islands	173	119.2
1952	Hawaiian	Kamchatka	0	2.1
1957	Hawaiian Islands	Aleutian Islands	0	10.5
1960	Hawaiian Islands	S. Chile	61	66.9
1964	Alaska N. California Hawaiian Islands	Prince William Sound, Alaska	119	282.3
1975	Hawaiian Islands	Hawaiian Islands	2	4.2
		TOTAL	335	485.2

* Supplied by
E. N. Bernard
PMEL - NOAA
Seattle, Washington

** Adjustment of damage to 1980 dollars aided by:
Significant Earthquake File
R. A. Ganse and J. B. Nelson
NGSDC-NOAA
Boulder, Colorado 1980

1.2 THE SOUTH AMERICAN THREAT

The west coast of South America is the site of the subduction of the oceanic Nazca Plate under the continental South American Plate. The result is a band of strong seismicity running the length of the continent and roughly parelleling the axis of the Peru-Chile Trench. As Figure 1.1 shows, tsunamigenic earthquakes have occurred all along this zone. Since 1687, between 10,000 and 30,000 people living on the South American coast, have lost their lives due to tsunamis originating in this region. (The wide spread in the number of deaths is due to the occasional difficulty in separating deaths due to tsunamis from deaths due to earthquakes in areas near the source.) Fortunately, destructive tsunamis do not occur frequently. The average tsunami recurrence rate for South America, based on Berninghausen's listing, is over 8 years. But this includes events that produced only low, non-destructive waves. The recurrence time for destructive tsunamis is presumably greater. Appendix A contains a listing of 21 locally destructive tsunamis which have occurred in the last 400 years in South America. Many of these events also produced destructive waves in other areas of the Pacific basin.

1.3 PURPOSE OF THE STUDY

If we accept the two basic assumptions of this study - (1) that tsunamis pose a threat to life and property throughout the Pacific, and (2) that the South American coast is a likely source of tsunamis - then the purpose of this study is quite easily stated: we examine the western coasts of Chile and Peru to determine what areas are most likely to

be the sites of large* tsunami-producing earthquakes in the near future (say within 50 years), what types of tsunamis these earthquakes could produce, and to what extent these tsunamis would pose a threat to South American coastal areas. The scientific tools to carry out this plan are available. Somewhat similar studies have been performed in recent years (see Section 2), but this is the first time that the historical seismicity patterns of potential source areas have been taken into account.

Having stated in general terms what this study attempts to accomplish, we now lay out explicitly what it does and does not do. This report describes numerical simulations of tsunami waves (in terms of energy, elevation, direction) as they propagate away from the immediate vicinity of an hypothetical earthquake with specific characteristics (seismic moment, rupture length, rupture width, displacement pattern, etc.) and travel up and down the continental shelf near the generating area.

This study does not attempt to predict actual earthquakes and resulting tsunamis. The uncertainties involved in describing actual bottom motions are so great that detailed agreement between historic or future earthquakes and the possible events outlined in this study could only be classed as coincidence. To the extent that the

---

*Throughout this document the terms large, major, and great will be used to describe earthquakes. A large or major earthquake has a Richter magnitude (see Section 3) greater than 7.0. A great earthquake has a magnitude greater than 7.8, and also a rupture length of at least several hundred km. This usage is described by Kelleher et al. (1974).

source motion scenarios developed for this study are, in fact, representative of those which could occur in a given area, it is believed that the tsunamis simulated in the study are also representative.

Nor do we attempt to examine the far-field threat due to tsunamis generated off South America. This facet of the problem is the subject of another SAI study (Hebenstreit, 1981).

1.4 STRUCTURE OF THE REPORT

The first part of this report (Section 2) describes common approaches to modeling tsunami generation and propagation and provides a detailed look at the wave model used here. The second part (Section 3) describes the seismological characteristics of the South American coast used to develop hypothetical but realistic source motions to provide the impulse for the simulated tsunamis. The next five sections are devoted to an examination of each individual case, following each tsunami from its generation to its interactions with adjacent shorezones. Each section concludes with a discussion of the threat posed by tsunamis leaving the specific source area.* Section 8 examines the general threat due to South American tsunamis. Section 9 summarizes the results of the study and translates them into recommendations for use by disaster mitigation authorities.

---

*We have included an extensive set of figures to illustrate the results of each simulation. To avoid forcing the reader to waste time searching for text among the pictures we have structured Sections 4 through 8 so that all the figures pertaining to each separate case are grouped immediately following the complete text describing the case.

Section 2
THE NUMERICAL MODEL

2.1 INTRODUCTION

The generation of a tsunami by a sudden bottom displacement and the propagation of the resulting waves along the shore near the source is a complex process. Very little research has been done on this subject. Most of the available studies have concentrated on the behavior of tsunamis in the immediate vicinity of the source (for example, Momoi, 1964; Tuck and Hwang, 1972; Yamashita and Sato, 1974; Lee, 1980). These studies are usually quite sophisticated and make few assumptions about the physical processes involved. These models have been applied largely to simplified situations (where, for example, bottom depth is a known analytic function and uplift patterns are quite simple) which can be solved analytically. Simulations of real ocean conditions (such as rapidly varying bottom topography and irregular coastlines) have rarely been attempted. The work of Chen et al., (1975) is an exception. They used two sophisticated models of tsunami propagation--one based on nonlinear wave equations and one based on high-order linear equations--to carry out numerical simulations of tsunamis generated in the immediate vicinity of a nuclear power plant site.

It is generally agreed that the behavior of tsunamis in the brief period following generation is nonlinear (Kajiura, 1963; Hammack, 1973; Chen et al., 1975), although Chen et al. showed that the difference between nonlinear and high-order linear solutions is not great close to the source.

The problem we are considering here, however, is how tsunamis behave at some distance from the source but still in relatively shallow water. This is a problem which has rarely been examined. Two studies which begin to address it are those by Aida (1978) and Sklarz et al. (1980). In the former a linear model was used to follow tsunamis from generating areas on the continental slope off Japan, over the shelf, and to the land/sea boundary. The latter used a linear model to simulate the generation of a tsunami on the shelf of the island of Hawaii and its propagation around the island shelf. The fact that both of these studies produced reasonably good results leads us to choose to apply a model based on linear equations of motion to examine the behavior of tsunamis along the South American coast due to local seismic activity.

2.2 MODEL EQUATIONS

The numerical model used in this study is based on the inviscid, vertically integrated, linear equations of motion for the propagation of long waves (i.e., waves whose length, λ, is much larger than the depth, h, of the water in which they propagate). These equations, in spherical coordinates, are

$$\partial_t U - fV + ghR^{-1}\partial_\theta \eta = 0, \tag{2.1}$$

$$\partial_t V + fU + gh\,(R \sin\theta)^{-1}\partial_\phi \eta = 0, \tag{2.2}$$

$$\partial_t (h+\eta) + (R \sin\theta)^{-1}\,[\partial_\phi V + \partial_\theta (U \sin\theta)] = 0. \tag{2.3}$$

The variables in these equations are defined as:

η - displacement of the free surface from mean sea level (MSL),

ϕ - longitude measured eastward from 0° at Greenwich, England,

V - horizontal transport in the eastward (ϕ) direction per unit width,

θ - co-latitude (i.e., measured from 0° at the North Pole,

U - horizontal transport in the southward (θ) direction per unit width,

t - time,

g - acceleration due to gravity,

h - depth of water below MSL,

R - radius of the earth, and

f - Coriolis parameter ($f = 2\Omega \cos\theta$, where Ω = angular velocity of the earth.

The notation ∂_x denotes partial differentiation with respect to the subscripted variable. The transport terms are obtained by vertically integrating the horizontal water particle velocity components (u,v) from the bottom to the surface:

$$U = \int_h^\eta u \, dz, \tag{2.4}$$

and

$$V = \int_h^\eta v \, dz, \tag{2.5}$$

Note the lack of a vertical velocity component, w, implying neglect of vertical accelerations. Note also the presence in (2.3) of a $\partial_t h$ term. This is the term through which time-varying bottom displacements generate sea surface deformations.

2.3 SOLUTION SCHEME

Numerical solutions to equations (2.1)-(2.3) are obtained by using a finite-difference analog to these continuum equations. The code used is a modified version of SSURGE, which is a model originally developed to simulate the propagation of storm surges in coastal waters. The fact that it has been proven useful in shallow water simulations makes its application in this project quite attractive. The details of the finite-difference algorithm are described in Appendix B.

The general approach used in the model is to integrate eqs. (2.1) through (2.3) over time using the multioperational, alternating direction implicit (ADI) algorithm described by Leendertse (1967). A staggered computational mesh, shown in Figure 2.1 is used in the numerical model formulation. At each cell, η_{ij} at time $n\Delta t$ is the average anomaly over the cell area centered at $i\Delta\phi$, $j\Delta\theta$ where Δt is

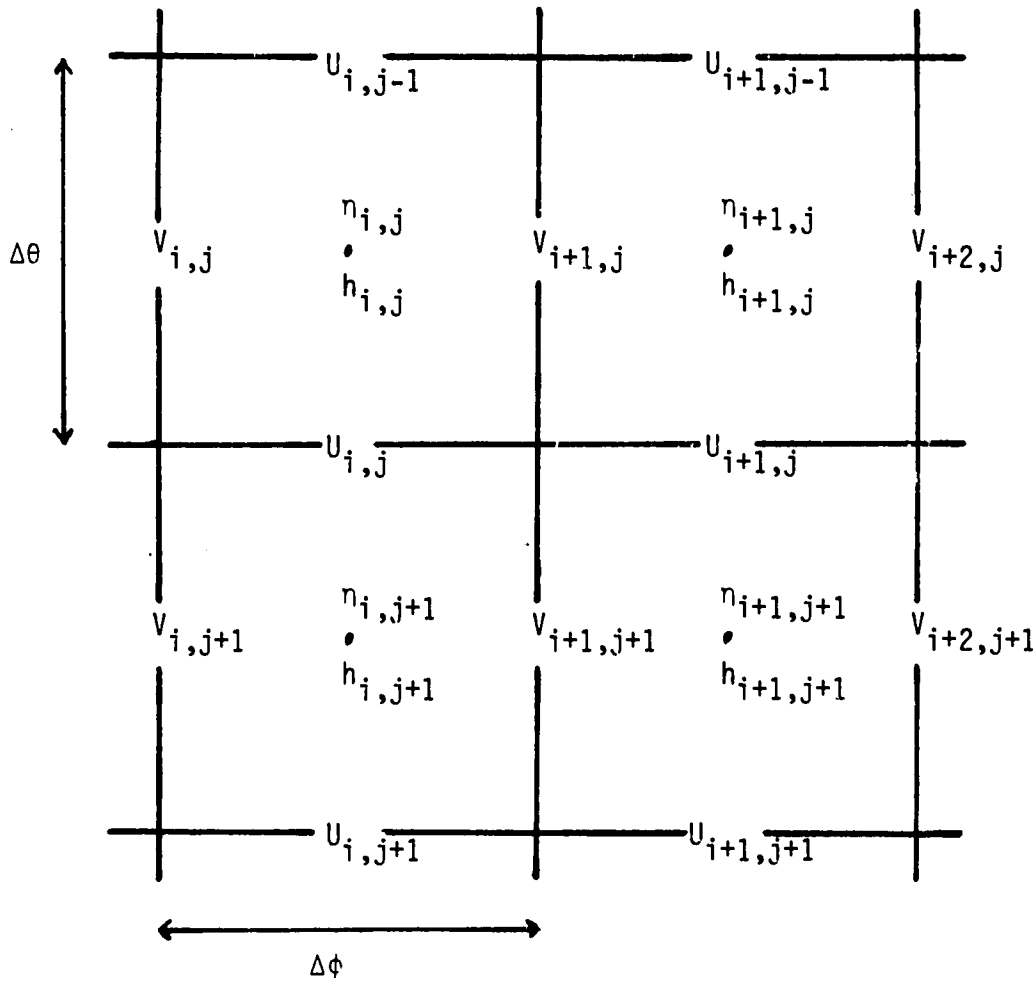

Figure 2.1 The staggered spatial grid used in the Finite-difference solutions of model equations.

the time increment and $\Delta\phi, \Delta\theta$ are increments in longitude and latitude, respectively. The transport V_{ij} is taken at the center of the left-hand face and U_{ij} is taken at the center of lower face. The depths are defined at the same locations as the η's.

2.4 BOUNDARY CONDITIONS

Two types of boundaries occur along the edges of the model grid: shoreline boundaries and open-ocean boundaries. Different boundary conditions are applied in each case.

Since in this study we are not concerned with predicting coastal runup and inundation zones, we can require that waves striking the coasts be fully reflected. This can be expressed, in terms of the velocity component perpendicular to the shore, as

$$u_n = 0 \qquad \text{at land boundaries.} \tag{2.6}$$

Setting the normal component of velocity to zero at the coastal boundary implies that no wave energy crosses the shore onto dry land.

At open-ocean boundaries (that is, when the region defined by the model grid ends not on dry land but in water) we require that wave energy approaching the boundary from within the model area pass through the boundary without reflection. This is referred to as a radiation-type condition. One way that it can be expressed is:

$$\partial_t \eta = -c\ [R^{-1}(\cos\delta)\ \partial_\theta \eta + (R \sin \theta)^{-1}(\sin\delta)\partial_\phi \eta]. \qquad (2.7)$$

Here c is the wave phase speed, approximated by $c = [g(h+\eta)]^{1/2}$, and δ is the angle of incidence between the direction of wave propagation and the open boundary.

The boundary condition expressed in (2.7) is satisfactory as long as the angle of incidence of the outgoing waves is known. If the outgoing waves are plane (i.e., the wave front has no curvature), then it is possible to determine δ quite readily. In the situation being modeled, however, the waves are not plane. Instead, they spread radially outward from the source zone and still have a definite curvature when they cross the open boundary. Reflected waves from the land/sea boundaries also add to the confusion. Techniques for calculating the angle of incidence at every point along the boundary at every time step would wind up taking more computation time than the finite-difference calculations themselves (Bennett, 1976).

A technique for taking into account the radially spreading nature of the waves leaving the source area was developed by Mungall and Reid (1978). The assumption is that the waves can be considered to be radiating outward from a point source and that each open ocean boundary point is located a distance r_b from that point. Then the radiation condition can be expressed as

$$U_b^r = c\eta_b + \frac{c^2}{2r_b} \int_o^t \eta_b \, dt, \tag{2.8}$$

where U_b^r is the outward transport in a radial direction. The time integral on the right hand side takes into account the spreading of the wave front. Mungall and Reid showed that this condition could be used effectively even if the origin of the waves is not a point but a well-defined region. Hebenstreit et al. (1980) used this boundary condition in their study of tsunami interactions in the Hawaiian Islands.

2.5 BOTTOM TOPOGRAPHY

Sea floor topography plays a major role in determining how the tsunami-borne energy spreads out from the source. Thus the model must employ realistic values of $h(\phi,\theta)$ to obtain reasonable simulations. Because of computational considerations SSURGE requires that the bottom depth data be provided on a regularly spaced grid; that is, the spacing in degrees latitude and longitude between adjacent points must be uniform (which does not imply uniform physical distances between points). In addition, the spacing should be as small as possible in order to ensure that the model can adequately resolve waves throughout the tsunami wavelength and period range (that is, lengths of hundreds of kilometers and periods of tens of minutes.)

We choose a resolution of 10' in both latitude and longitude for the model grid in the generation phase. Spacing this fine allows resolution of wavelengths as short as roughly 30 km. Since bottom data with 10' resolution for the southeast Pacific Ocean was not readily available in digital

form at the time of this study, we used fine resolution bathymetry charts from the Naval Oceanographic Office* and hand-digitized the data at the needed intervals. An example of the NAVOCEANO charts is presented in Fig. 2.2. Originally the depth field was digitized to 20' resolution for use in the far-field portion of this study (Hebenstreit, 1981). In order to avoid re-digitizing to higher resolution, the 20' depths were first interpolated to a 10' grid. Then depth values from 1° seaward of the Peru-Chile Trench to the shore were edited with depths from coastal nautical charts. In this way, we were able to build up a detailed rendition of the entire modeling region.

The overall region modeled ranges in latitude from 5°N to 40°S and in longitude from 70°W to 90°W. Note that these are reckoned in the normal fashion as north/south of the equator and east/west of Greenwich, rather than in the fashion used to obtain ϕ and θ for SSURGE. This model area is shown in Figure 2.3. The closely spaced contours near the coast are a rough indicator of the location of the Peru-Chile Trench, although they do not always represent the absolute axis of the trench. This would only happen at those places where the deepest portion of the trench fell at a grid point. The actual axis is usually within $\pm$15 km of the line. The line of deepest model depth could fall on the landward or seaward slope of the trench, or, in regions where the trench is very narrow (<15 km wide), may not actually be in the trench. We feel that this lack of resolution in the depth field around the trench does not greatly affect the results of the study and thus have not altered the grid or the topography to include all the deepest portions of the trench.

*Charts SP-3A and SP-6A/SA-3A were obtained from the World Bathymetry Unit, NAVOCEANO, NSTL Station, Bay St. Louis, MS 39522.

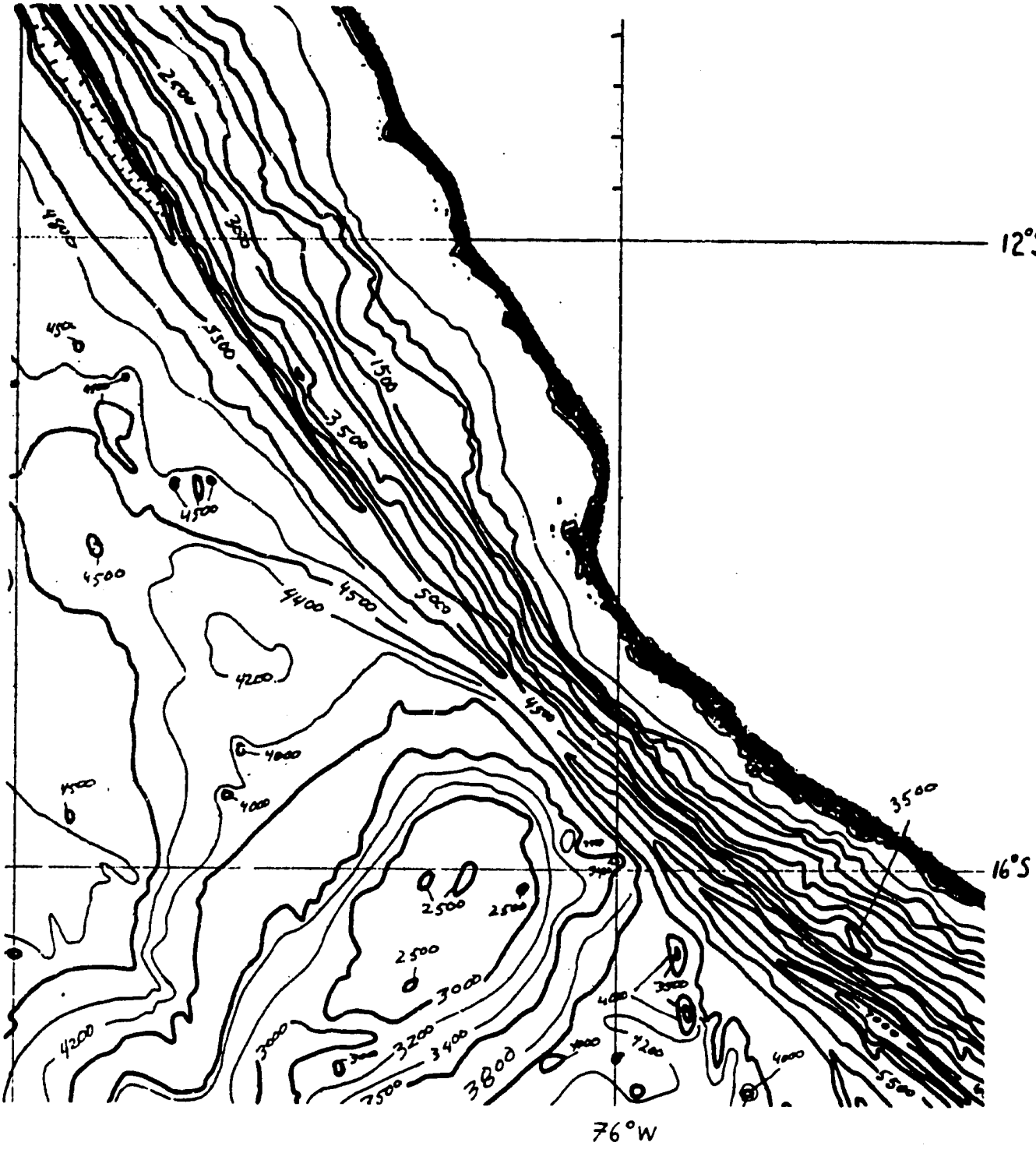

Figure 2.2. Example of bottm topography chart used to obtain depth field in this study. The primary contour interval is 500 m.

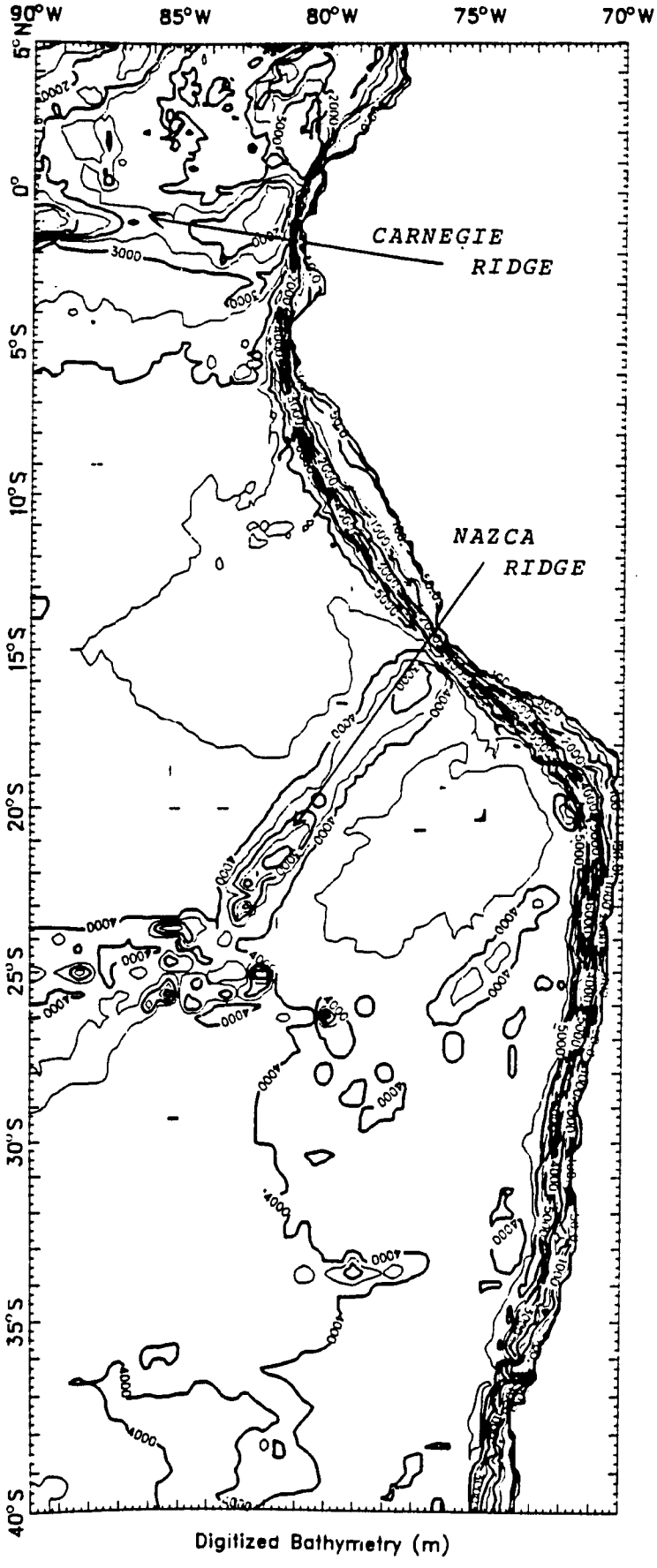

Figure 2.3:

Contours of bottom topography based on the digitized depth field described in the text. The primary contour interval is 500 m, with heavy contours every 1000 m.

Comparison of Figures 2.2 and 2.3 also shows that some of the fine detail of the NAVOCEANO chart is lost in digitizing. Since the horizontal scale of such features is usually less than 10', and thus much less than a typical tsunami wavelength, their presence or absence in the model topography is not significant.

2.6 SOURCE MOTIONS

The heart of the application of SSURGE to the generation phase is the specification of the submarine bottom motion which displaces a volume of water and sets the surface waves in motion. The ground motion in the source area can be specified in a number of ways, depending on the user's assumption about the tsunami generation process. If we assume that the water column reacts nearly instantaneously to bottom motion, then the displacements (either as an analytical function of (ϕ,θ) or as arbitrary values specified at each grid point in the source area) are simply added to the bottom depth so that the resulting depth is

$$d(\phi,\theta) = h(\phi,\theta) - e(\phi,\theta), \tag{2.9}$$

where $e(\phi,\theta)$ is the ground motion taken so that uplift implies $d<h$. Then the initial sea surface (usually taken to be at rest at MSL) is adjusted so that

$$\eta(\phi,\theta) = e(\phi,\theta).^{*} \tag{2.10}$$

*We seem to be saying that depth below MSL is positive, while elevation above MSL is also positive. This apparent confusion of coordinates does not affect the model equations, which can be looked on as predicting the time variation of the height of the sea surface above the bottom, i.e., the change in $h+\eta$ with time.

A second approach depicts the sea floor motion as occuring over a finite time period (longer than a single time step of the model) and allows the sea surface, initially undisturbed, to adjust to the movement.

If the "instantaneous response" approach to generation is taken, then the model requires specification of the final displacement due to fault motion in the source area. The information requirements for this approach include the spatial orientation of the fault in the model grid and the uplift pattern.

If the "time evolution" approach to generation is taken, then the information requirements increase. In addition to the orientation of the faulting and the pattern of displacement, the model must also be supplied with information concerning the location of the epicenter, the velocity of fault propagation away from the epicenter, and the time over which uplift occurs. The program, as initially configured, does not contain a time varying bottom displacement algorithm.

Most previous large-scale tsunami simulation studies have employed the instantaneous response approach with remarkable success (Brandsma et al., 1975; Garcia, 1976; for example). The time evolution approach has largely been restricted to studies of near-field (i.e., within the immediate vicinity of the source) behavior, without any attempt to simulate specific historical events or specific geographical locations. However, some seismological evidence does seem to indicate that long period ($\leq$100 sec) motions can impart large amounts of energy to the water column (Kanamori, 1977). This is longer than the time step used in this study. We employ

the instantanous response technique in all but one case examined in this report. For the one exception, in which a fault length of nearly 2000 km is considered, a very simple time variation scheme for the displacement has been adopted.

Section 3 contains a description of the process by which we arrived at the specific bottom displacement patterns for the various source zones.

Section 3
CHOICE OF EARTHQUAKE SITES AND SOURCE MOTIONS

In order to specify the bottom displacement needed to drive SEAWAVE we must supply the location of the source area, type of focal mechanism, and energy level in the earthquake. Section 3.1 describes the choice of sites in terms of seismic gap information. Section 3.2 shows how historical data on the seismicity of the region is used to specify focal mechanisms. Section 3.3 describes the use of historical data and seismic theory to estimate the energy released by various size earthquakes. Section 3.4 shows how this information is consolidated to provide the various source scenarios which will be used in this study.

3.1 SITE SELECTION

The Pacific coast of South America has a long history of strong shallow seismic activity caused in large part by the subduction of the oceanic Nazca Plate beneath the continental South America Plate (Stauder, 1973, 1975). A number of these earthquakes have generated tsunamis. Silgado (1978) described data from 21 tsunamigenic earthquakes which have occurred in the region between 1749 and 1968. One of these events, the earthquake of 22 May 1960, is among the largest seismic events ever recorded.

The Peru-Chile Trench, which is the result of the subduction process, forms the seaward limit for a band of intense activity all along the coast. Analysis of historical seismicity patterns of the region indicate

several areas with strong potential as sites of large earthquakes. Since this zone coincides with the zone of tsunami-producing earthquakes, we examine these locations to determine the sites of the hypothetical sources used to drive the SEAWAVE model.

McCann et al. (1978) examined the tectonic plate boundaries of the world for evidence of the existence of seismic gaps, which they defined as "any region along an active plate boundary that has not experienced a large thrust or strike slip earthquake for more than 30 years." As two plates collide, strain tends to increase along the interface zone. If strain release does not occur over an extended period of time, by either seismic or aseismic mechanisms, tension may accumulate to the point that a large earthquake occurs to release the stress. The lack of large seismic events may thus be evidence of long-term stress buildup. Kelleher (1972) pointed out that a history of major shallow earthquakes increases a region's potential as a gap. The basic assumption is that an area which has experienced large earthquakes as a means of relieving stress is likely to do so again.

In their survey of the South America-Nazca plate boundary McCann et al. indicated several areas between 0° and 45°S as likely gaps (see Figure 3.1). The first gap, spanning the coast from 0°-9°S, has been quiet for so long (roughly 400 years) that large earthquakes are highly unlikely unless their recurrence period is quite long.

The region spanning roughly 16°-24°S is postulated to be an extremely likely candidate for a large earthquake. The last large earthquakes in this zone

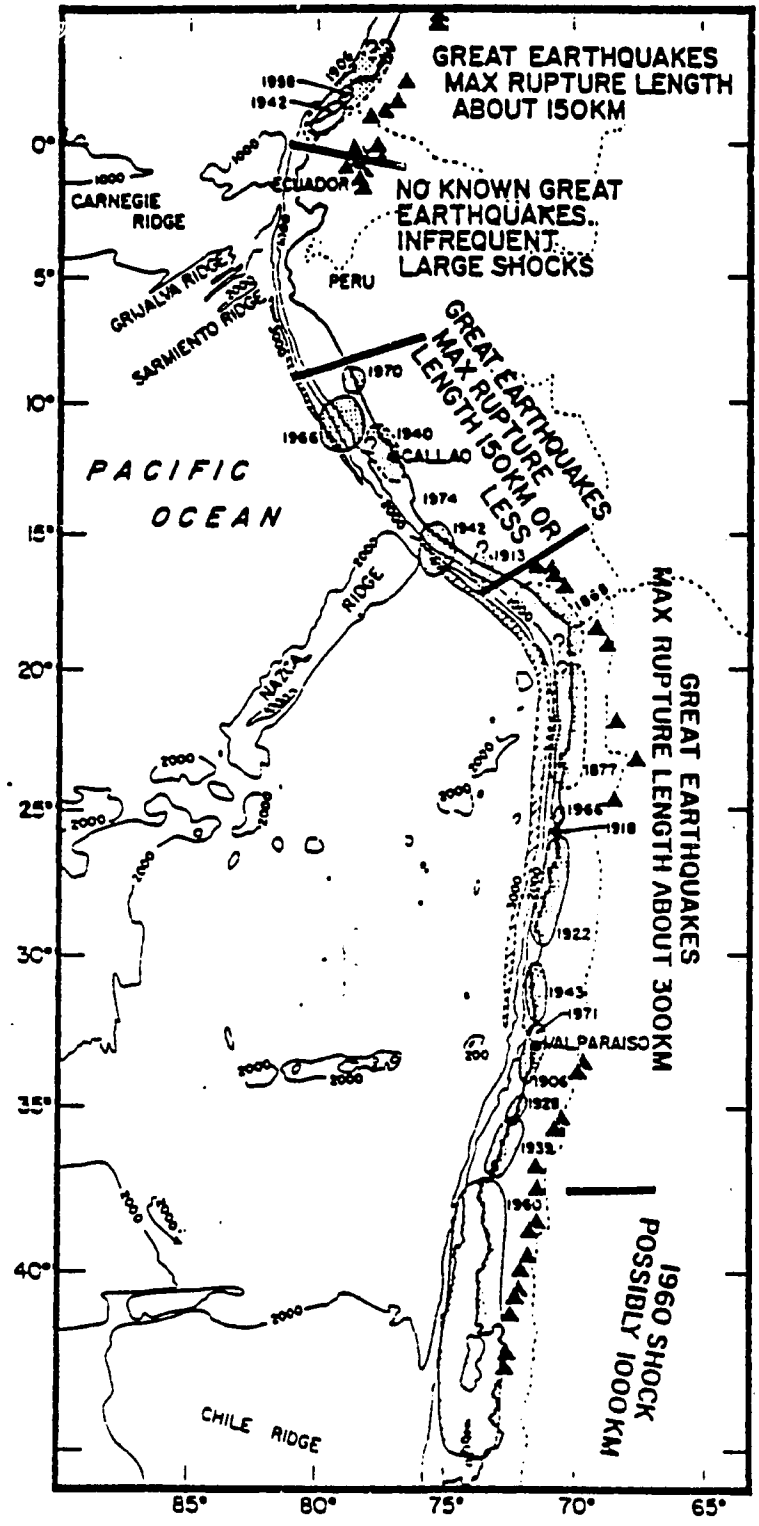

Figure 3.1. Potential seismic gaps along the western coast of South America (from McCann et al., 1978).

occurred in 1868 (northern end) and 1877 (southern end). Both events produced destructive tsunamis (Pararas-Carayannis and Calebaugh, 1977). McCann et al. assigned this zone "highest seismic potential.

Two smaller gaps exist farther south. Both are assigned moderate seismic potential levels because of recent activity. The first, with a recurrence period of roughly 40 years, is the zone from 25°-26°S; the second, with a somewhat longer period of 85 years, is the zone south of Valparaiso, Chile along 33°-35°S.

McCann et al. stated that a long-existing gap south of Callao, Peru (12.5°S to 14°S as described by Kelleher, 1972) was filled by a great earthquake (magnitude of 8.1) in 1974. B. Brady (Bureau of Mines) and W. Spence (U.S. Geological Survey) have amassed a body of evidence which indicates that this event was not, in fact, gap-filling. Brady has developed a theory of earthquake mechanisms which leads him to ascribe strong seismic potential to two adjacent zones. The larger zone follows the Peru-Chile Trench from 12°S to roughly 28°S. A gap-filling event in this area would have an extremely high energy level (Kanamori magnitude,* $M_W \geq 9.4$). The smaller zone runs northward from 12°S-8°S. A gap-filling event in this region would be a lesser magnitude ($M_W = 8.7$) great earthquake.

---

*See Section 3.3 for a discussion of the implications of this magnitude scale.

Since the difference of opinion over the existence of gaps originating in the region from 8°S-15°S is unresolved, we will assume that they do indeed exist. Thus we model possible tsunamigenic bottom motions in five source zones along the South American coast. These are listed in Table 3-1.

Figure 3.2 depicts the various source regions used in this study.

3.2 FOCAL MECHANISMS

In general, earthquakes occurring in a specific region tend to follow common patterns; that is, the focal mechanisms of the earthquakes tend to be similar. Stauder (1973, 1975) performed a detailed survey of seismicity patterns in Peru and Chile. We use his data and conclusions to piece together representative focal mechanisms such as dip-slip, strike-slip, normal fault, and reverse fault, (see Billings (1954) for examples of these mechanisms), applicable to the source zones under study. These are then used to model possible ocean bottom displacements resulting from these events.

3.2.1 Peru

Stauder (1975) examined 40 earthquakes which occurred in the period 1963-1972 in the zone along western South America from the equator to 18°S. Of these, 14 were

TABLE 3-1

Potential Tsunami Generation Sites

Location	Code	Latitude Range	Seismic Potential	Source
Central Peru	A	8° - 12°	High	Brady
Southern Peru-Northern Chile	B	16°S-24°S	High	McCann, et al. (1978)
Capiapo, Chile	C	25°-26°S	Moderate	"
Valparaiso, Chile	D	33°-35°S	Moderate	"
Lima, Peru	E	12°-28°S	High	Brady

Figure 3.2 Approximate zones of possible major earthquakes used as tsunami sources. Zones A,B,C, and D are represented by cross-hatched areas. The open area beginning at 12°S and continuing through zones B and C to end at 28°S is zone E.

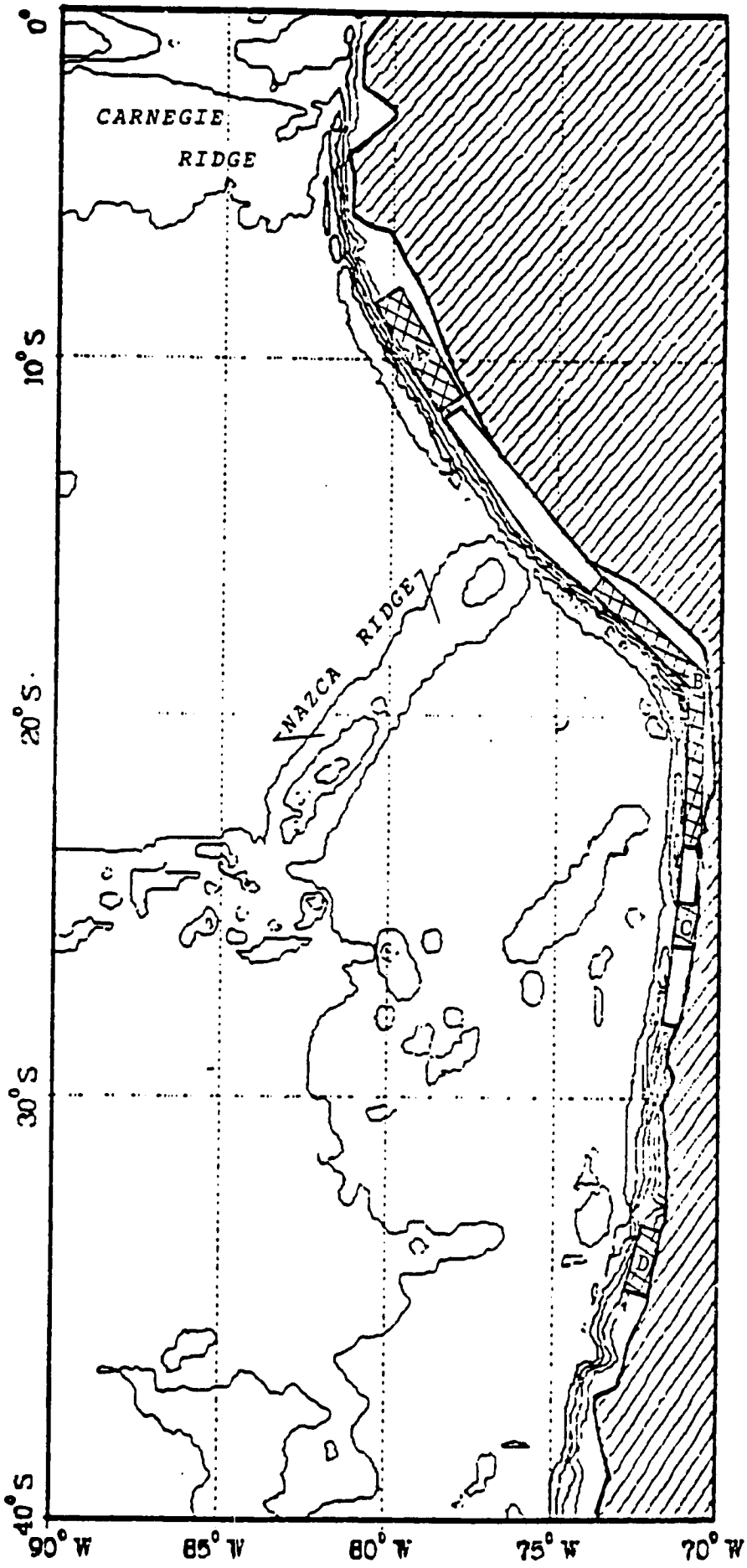

shallow focal depth events which were located between the coast line and the axis of the Peru-Chile Trench. They had a mean focal depth of 46 km. Focal plane solutions indicated that dip-slip faulting* predominated, with the fault planes lying along the interface between the underthrusting oceanic plate and the continental plate. The dip of the fault planes was 10° to 15° from the horizontal and the direction of dip was roughly normal to the coast.

3.2.2 Chile

In a similar study, Stauder (1973) examined 61 earthquakes occurring in the period 1962-1970 in the zone extending from 20°S to 45°S. For 19 shallow focus events in northern Chile (20°S to 34°S) the mean focal depth was approximately 44 km and the dip of the focal plane was approximately 20° normal to the coast. In central Chile (35°S to 47°S), an examination of 9 shallow focus coastal events showed a mean focal depth of 40 km and an average dip of 15° roughly normal to the coast.

3.2.3 Fault Motions

Tsunamigenic earthquakes tend to be predominantly dip-slip events, in which one side of the fault plane is displaced vertically relative to the other (Iida, 1970). Stauder's solutions showed most of the shallow focus events having dip-slip motions. In order to reduce the level of complexity of the modeling by one parameter, we assume that the representative events are solely dip-slip, with no strike-slip (horizontal) component.

---

*Dip-slip faulting implies that most of the fault motion takes place in the direction of the dip of the fault. Thus the motion of the fault bed has a vertical component. The final result is that the two sides of the fault wind up being vertically offset from each other.

We also assume, again for simplicity, that motion is thrust type. That is, the overhanging bed moves upward relative to the underhanging bed. Figure 3.3 shows the difference between thrust and normal or gravity faulting. If the thrust fault motion breaks the sea floor, the result would be an initial hump in the sea surface, whereas the normal fault would produce a depression. The primary difference in the resulting tsunamis would be the sense of the motion of the leading wave. While for a specific harbor or coastal area the difference between a tsunami producing an initial rise or an initial drawdown of water can be quite crucial in terms of type and magnitude of damage, the difference is not significant in terms of threat assessment along a broad coastal zone.* Thus the specification of exclusively thrust faulting should not significantly alter results.

3.2.4 Representative Mechanisms

We specify representative focal mechanisms for possible source motions on the basis of Stauder's study. We should point out that while this study was quite thorough, it did cover a relatively short time span and included only a small number of events for which reliable focal plane solutions could be developed. We cannot, therefore, allow the reader to assume that the representative mechanisms are the average mechanisms for the source zones. Instead, we must represent them as fairly typical of events in this area.

---

* Experiments with a simplified version of the SEAWAVE code showed that the difference in wave amplitude between a tsunami generated by an initial hump on the sea surface and one generated by an identically shaped depression was less than 5% of the initial disturbance amplitude after nearly three hours of propagation.

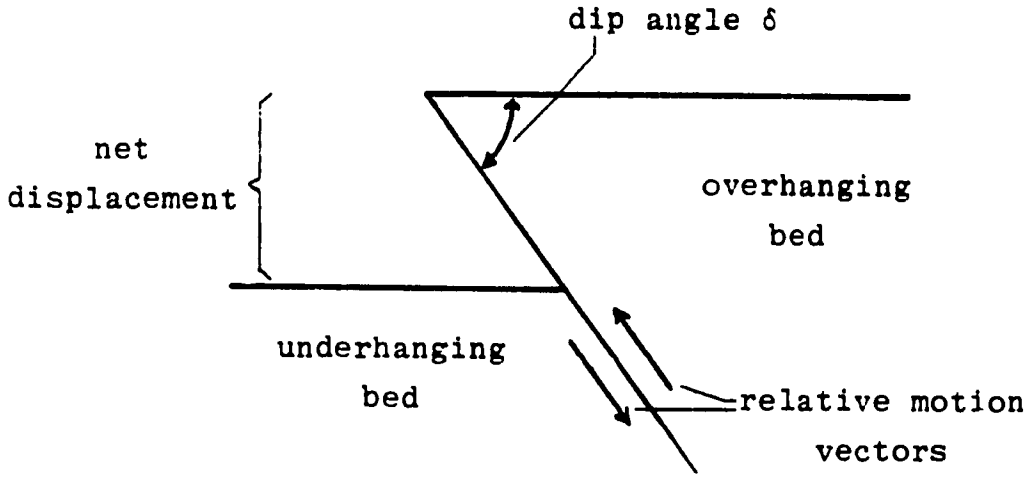

(a)

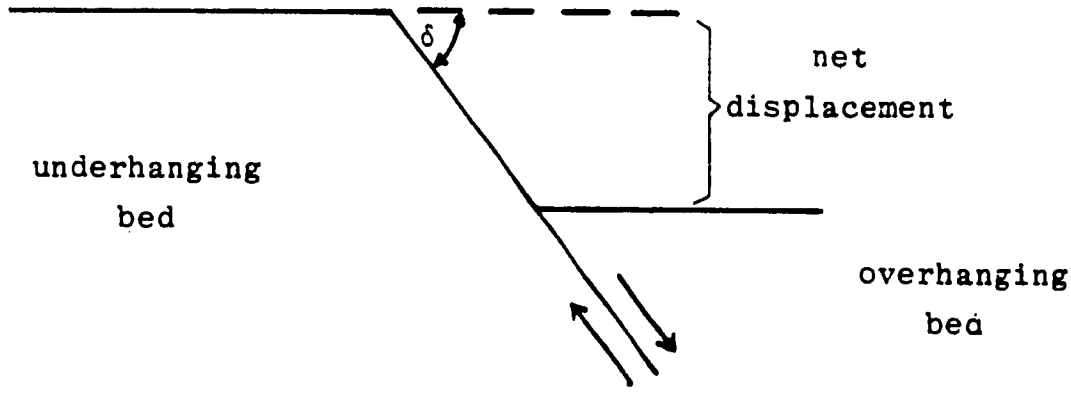

(b)

Figure 3.3: (a) Thrust faulting, in which the overhanging bed is displaced upward along the fault plane.
(b) Normal faulting, in which the overhanging bed is displaced downward along the fault plane.

We must also point out that of the 101 events Stauder examined, only 8 could be classed as large earthquakes. Thus, these mechanisms may not be truly typical of tsunamigenic events. They do, however, represent the best estimates we could make based on available information.

The specific values assigned to source motions in the various zones are detailed in Section 3.4.

3.3 EARTHQUAKE ENERGY

The key factor in determining how large a tsunami will be produced by a specific earthquake is the amount of seismic energy expended in displacing a volume of the earth's crust. One estimation of earthquake energy is the magnitude assigned to the event. The commonly quoted Richter magnitude, or M_S*, is based on the spectral amplitude of the 20 sec period seismic surface waves which radiate from the source. This magnitude is a sufficient description for small and intermediate earthquakes, which have $M_S<7.0$. However, the use of M_S for large earthquakes can be misleading, because in these events a good deal of the energy is released at periods longer than 20 sec. The result can be a saturation of the M_S scale, because the energy estimate based on 20/sec amplitudes is too low to be a good indicator of overall energy. Thus M_S seems to approach a limit even as the energy level rises.

---

* M_S is not truly the classical Richter or Gutenberg-Richter magnitude, because the empirical constants used in obtaining M_S have been refined from the original form of the expression.

Another parameter related to earthquake energy is the seismic moment, M_O. This can be estimated from the spectral amplitude of the seismic waves at very long periods (100 sec or larger). This quantity is not limited in the same way as the 20 sec amplitude. Figure 3.4 illustrates schematically how M_S and M_O are estimated for small and large earthquakes.

Kanamori (1977) argued that M_O is a much better indicator of seismic energy in major earthquakes than M_S because it is based on the amplitude of the spectrum at periods much longer than 20/sec. He proposed a new magnitude, M_W, defined as

$$M_W = (\log M_O - 16.1)/1.5. \qquad (3.1)$$

This scale is not susceptible to saturation and for small earthquakes $M_W \approx M_S$. Table 3.2 lists a number of tsunamigenic events for which M_S, M_O, and M_W have been calculated. Note that the largest M_W value is assigned to the Chilean earthquake of 22 May 1960. This event had a seismic moment of over 10^{30} dyne-cm. Chinnery and North (1975), in their correlation of M_O versus frequency of occurrence for great earthquakes, indicated that events of this size should have a return period of 15-20 years. Their empirical relationship implied that events with return period of 50-100 years would have moments in the range 2-8 x 10^{31} dyne-cm. This provides an upper limit to the M_O values of the hypothetical earthquakes.

Seismic moment can be calculated from parameters of the earthquake in one of two ways. If we know S, the area of the fault, and D, the mean slip dislocation on the

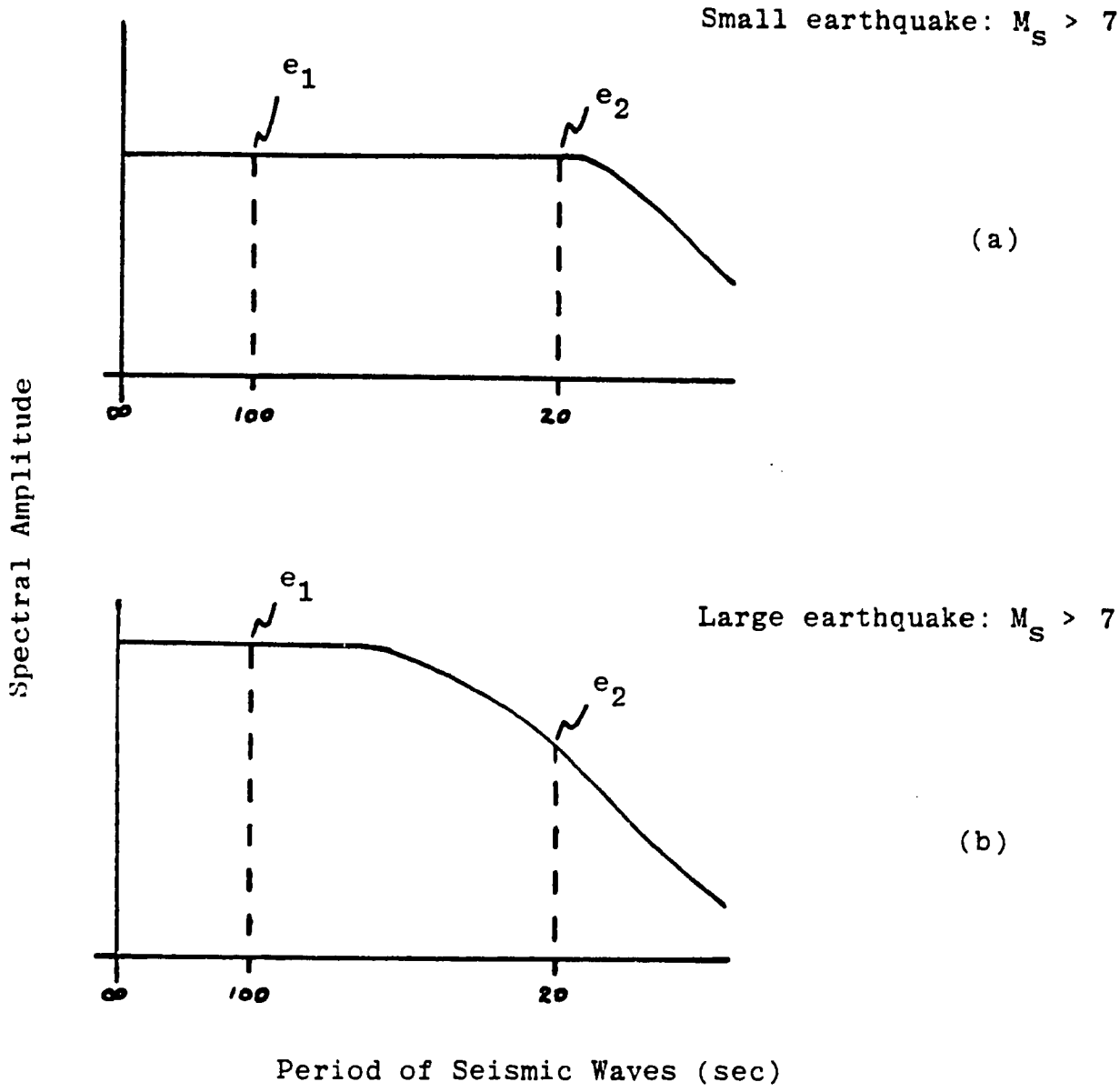

Figure 3.4 Schematic representation of seismic spectrum vs period for (a) small earthquakes and (b) large earthquakes. e_1 is the amplitude used to estimate M_o: e_2 is the parameter used to estimate M_s. Note that e_1 is a more consistent estimator of the highest energy level in the earthquake.

TABLE 3-2

Tsunami-Producing Great Earthquakes for which M_o is Reported (Kanamori, 1977)

Date	Latitude	Longitude	Location	M_s	M_o (10^{27} dyne-cm)	M_w
18 Apr 06	38N	123W	San Francisco	8.25	10	7.9
17 Aug 06	33S	72W	Chile	8.4	29	8.2
11 Nov 22	28.5S	70W	Chile	8.3	69	8.5
3 Feb 23	54N	161E	Kamchatka	8.3	37	8.3
1 Sep 23	35.3N	139.5E	Kanto	8.2	8.5	7.9
7 Mar 29	51N	170W	Fox Island	8.1	6.7	7.8
3 Jun 32	19.5N	104.3W	Mexico	8.1	15	8.1
2 Mar 33	39.3N	144.5E	Sanriku	8.5	43	8.4
10 Nov 38	55.5W	158W	Alaska	8.3	28	8.2
24 Aug 42	15S	76W	Peru	8.1	27	8.2
7 Dec 44	33.8N	136E	Tonankai	8.0	15	8.1
20 Dec 46	32.5N	134.5E	Nankaido	8.2	15	8.1
22 Aug 49	53.8N	133.3W	Alaska	8.1	15	8.1
4 Mar 52	42.5N	143E	Tokachi-Oki	8.3	17	8.1
4 Nov 52	52.8N	159.5E	Kamchatka	8.25	350	9.0
9 Mar 57			Aleutians	7.25	585	9.1
10 Jul 58	58.6N	137.1W	Alaska	8.9	29	8.2
6 Nov 58	44.5N	148.5E	Kurile Islands	8.7	40	8.3
4 May 59	52.5N	159.5E	Kamchatka	8.25	26	8.2
22 May 60			Chile	8.3	2000	9.5
13 Oct 63	44.8N	149.5E	Kurile Islands	8.1	67	8.5
28 Mar 64	61.1N	147.6W	Alaska	7.4	820	9.2
4 Feb 65			Aleutians	7.75	125	8.7
17 Oct 66	10.7S	78.6W	Peru	7.5	20	8.1
16 May 68			Tokachi-Oki	7.9	28	8.2
11 Aug 69	43.6N	147.8E	Kurile Islands	7.8	22	8.2
3 Oct 74	12.3S	77.8W	Peru	7.6	15	8.1

fault, then we can calculate M_o from the expression (Abe, 1973):

$$M_o = \mu SD. \tag{3.2}$$

The quantity μ is the rigidity of the earth's crust. This is usually taken to have a constant value of 5×10^{11} dyne cm^{-2}.

If, on the other hand, we only have an estimate of the fault area, then we can use geometric arguments about faulting to calculate the moment and the average slip dislocation from (Abe, 1975)

$$M_o = k_1 S^{3/2} \tag{3.3}$$

and

$$D = k_2 S^{1/2}, \tag{3.4}$$

where $k_1 = 1.23 \times 10^{22}$ dyne cm/km^3 and $k_2 = 2.46$ cm/km. In (3.2), S is in units of cm^2 and D in cm. In (3.3) and (3.4), S is in units of km^2 and D in cm.

Equations (3.3) and (3.4) are derived on the basis of the following assumptions:

(a) stress drop in large earthquakes is total (i.e., all the accumulated stress is relieved in a single event),

(b) stress drop is relatively constant in these earthquakes, and

(c) the ratio of fault length (L) to fault width (W) is roughly as 2:1 on a rectangular fault plane.

Kanamori (1977) pointed out that the evidence for or against complete stress drop in major earthquakes is inconclusive; Purcaru and Berckhemer (1978) argued strongly that stress drop varies significantly from event to event; and, as Figure 3.5 illustrates, the L vs. W relationship is by no means exact. Despite these difficulties, however, (3.2) is probably accurate enough to allow for reasonable modeling. The degree to which M_O and S are related can be seen in Figure 3.6. This figure also depicts the relationship between M_O and stress drop. Note that the Pacific events do cluster between 10 and 50 bars.

The difference between the two appproaches is that use of (3.2) allows some flexibility in the choice of both S and D. That is, a family of (S,D) pairs can produce a given M_W. This is shown in Figure 3.7, where the solid lines represent constant values of M_W. Use of (3.3) and (3.4), on the other hand, implies that any specified value of S leads directly to single values of D and M_W. This is illustrated by the line of x's in Fig. 3.7. The points at which this line crosses the lines of constant M_W are points at which the two methods are equivalent.

The relations between M_W, M_O, S, and D allow us to specify the magnitude of events based on estimates of fault area and slip displacement. Area is relatively easy to estimate from the seismological literature, while displacement is less easily estimated. We assume that

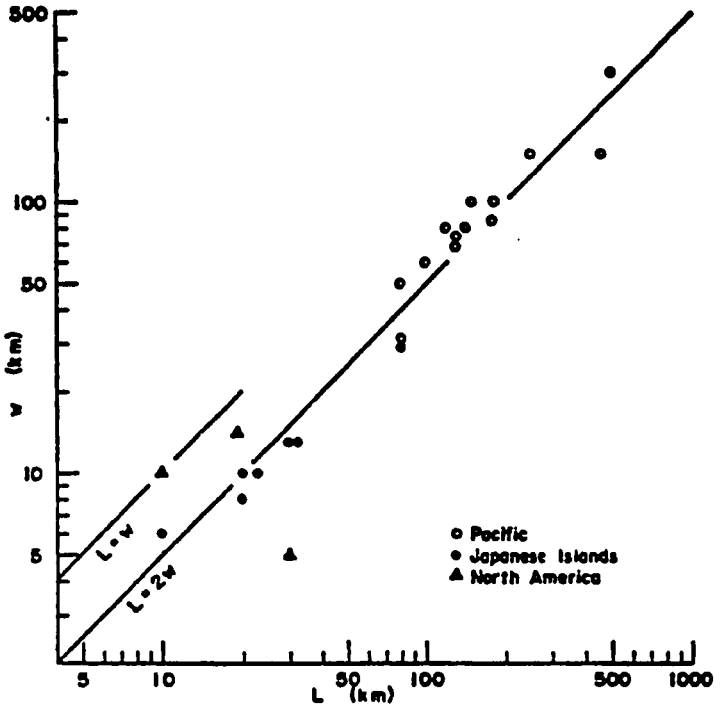

Figure 3.5 Fault length L vs. fault width W for large earthquakes (Abe, 1975).

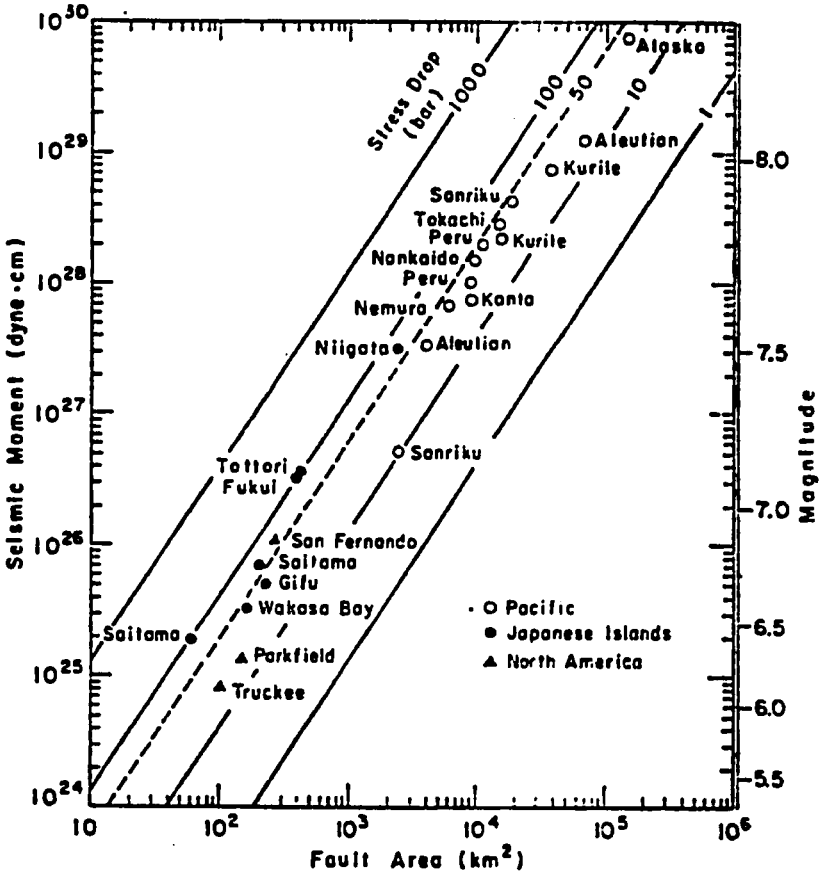

Figure 3.6 Relationship among fault area, seismic moment, and stress drop for large earthquakes. (Abe, 1975).

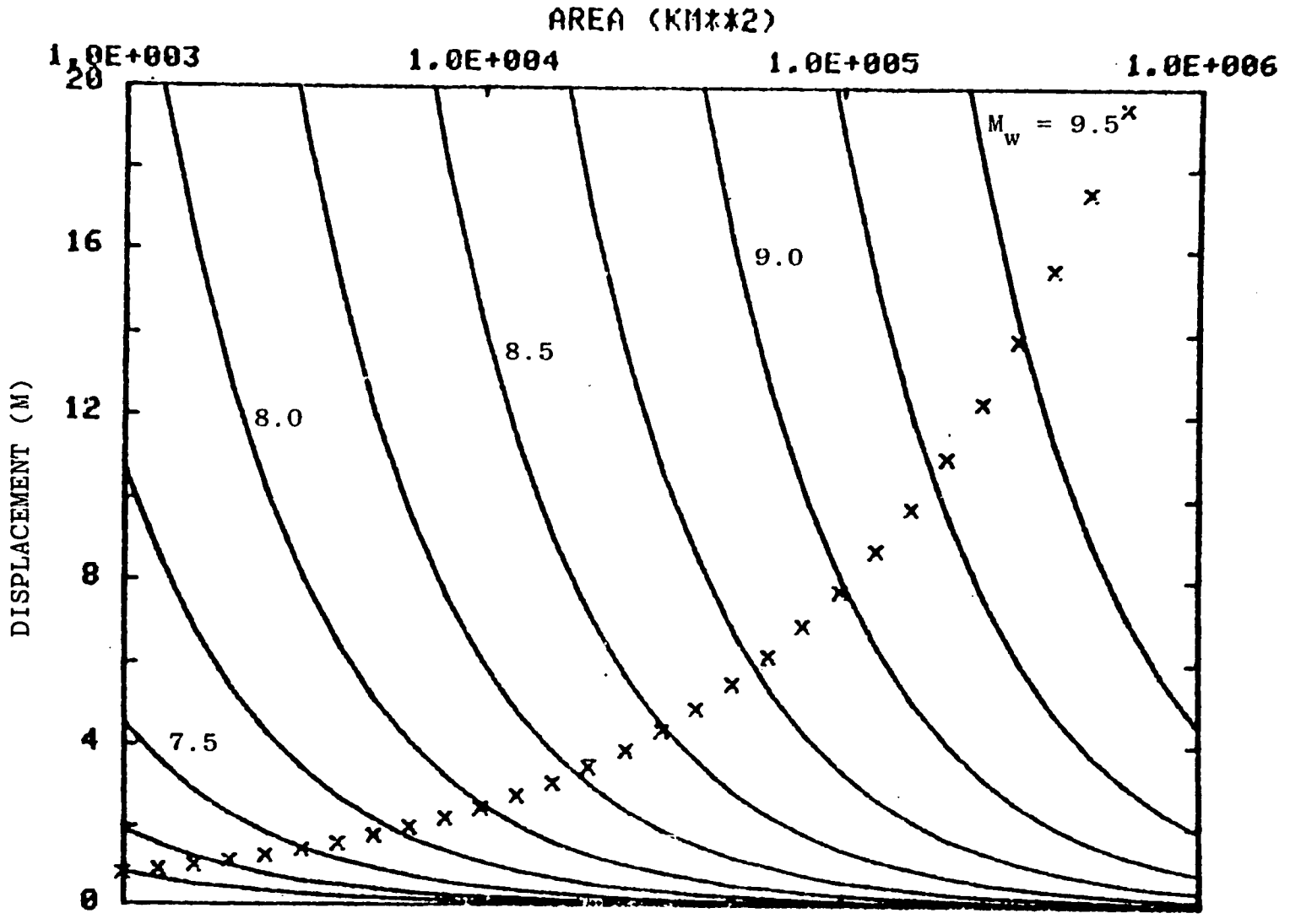

Figure 3.7 Fault area (km^2) vs. slip displacement (m). Solid lines are calculated from (3.2) with M_w (and, via (3.1), M_o) held fixed and S allowed to vary. X's are displacements calculated from (3.4). Intersections points are (S,D) pairs for which M_o from (3.3) equals M_o from (3.2).

each source zone is a rectangle of length L and width W. The upper limits to the length of the postulated faults can be estimated from historical evidence. McCann et al. (see Fig. 3.1) showed lengths of great earthquake ruptures to be increasing from north to south. Site A is in a zone with historical lengths of 150 km or less, although Brady (personal communication) expects that ruptures the length of the entire zone are possible (i.e. 550 km). Sites B, C, and D fall in a region with a 300 km upper limit. Site E begins in the 150 km limit zone and runs into the 300 km zone. Again, Brady contends a rupture encompassing the entire roughly 1800 km length of the zone is possible. These upper limit values were used to estimate lengths for events that fill or partially fill the source zones.

Widths of the source areas are less readily estimated. As illustrated in Fig. 3.5, a general relationship of L = 2W seems to hold, at least for large earthquakes with lengths up to 500 km. This relationship probably breaks down for ruptures of greater extent.

Kelleher et al. (1974) postulated an upper limit to L in great thrust earthquakes based on the geometry of the interface between underthrust (oceanic, in this case) and overthrust (continental) lithosphere slabs in subduction zones. Shallow dipping subduction zones will have a wider contact interface between slabs and, apparently, potential for longer rupture lengths. Figure 3.8 illustrates the interface zone geometry. The estimates of interface width for the Peru-Chile region are shown in Figure 3.9. While these estimates were not intended to provide absolute values of interface width, they could be

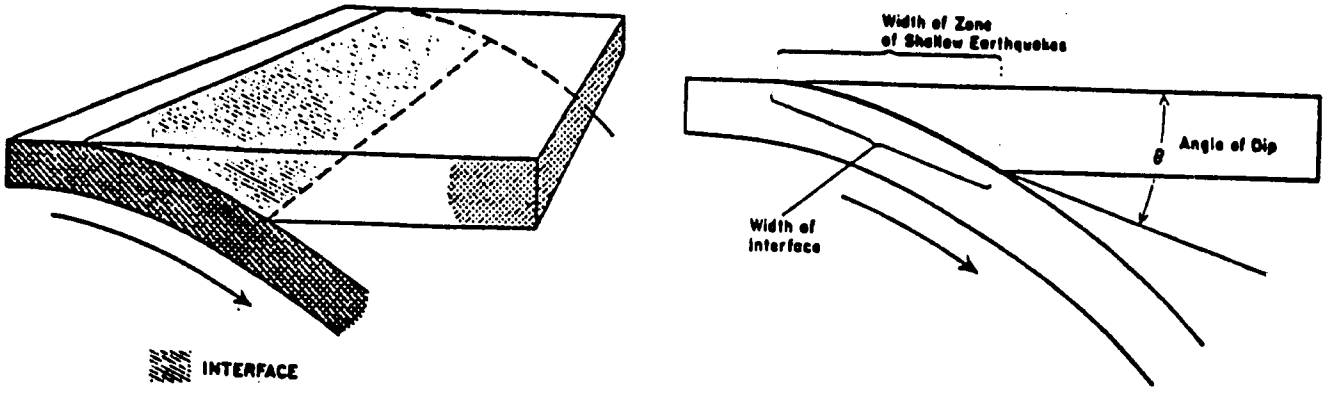

Figure 3.8 Interface area between overthrust and underthrust slabs of lithosphere at a subduction zone. (a) Perspective view. (b) Side view showing relationships among width of interface, zone of shallow earthquakes, and angle of dip. (Kelleher et al., 1974.)

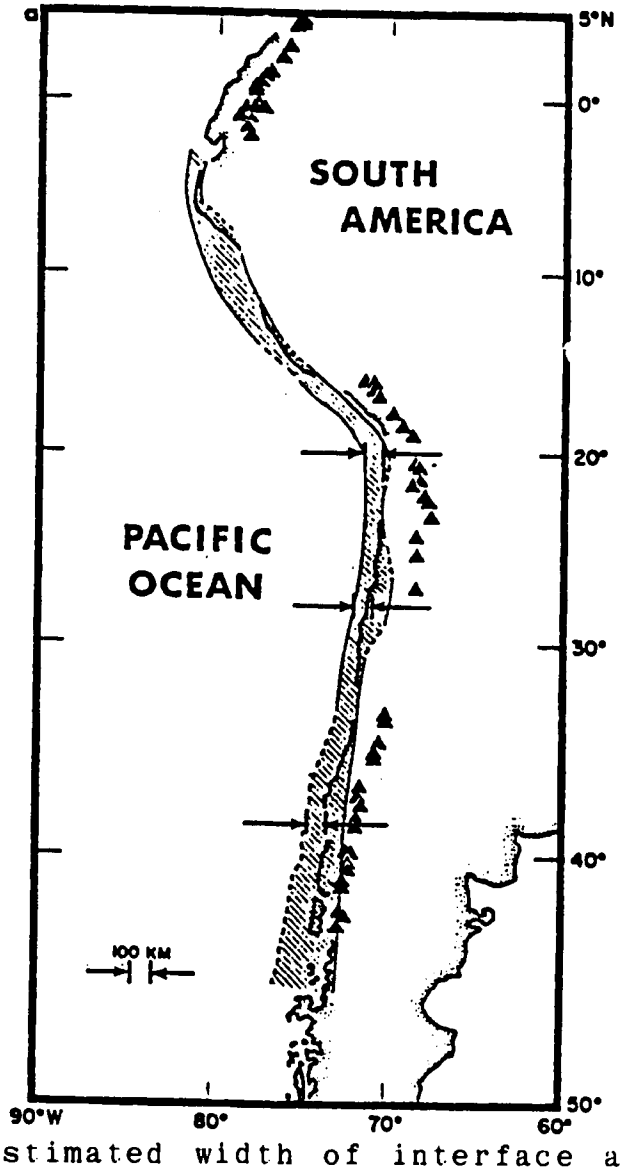

Figure 3.9: Estimated width of interface along western South America. (Kelleher et al., 1974.)

combined with Fig. 3.5 to provide limiting values for W in the different source areas. For example, for site A the L-W relation would lead to an estimate of W = 75 km, which is within the approximate limit of 100-150 km taken from Fig. 3.9. Sites B and C would seem to have an upper width limit of 100-120 km, while site D could be as wide as 150 km. The widths chosen for the postulated source motions will be listed in the next section.

Hypothetical values of slip dislocation can be developed from estimates of sea floor spreading rates and elapsed time since the last decoupling earthquake. LePichon (1968) indicated a convergence rate for the Nazca-South America plate boundary of approximately 6 cm/yr, while Spence (personal communication) estimates a rate closer to 10 cm/yr. If we assume that the subduction process slowly builds up stress between the two plates that is essentially unrelieved except by great, decoupling earthquakes, and that these events totally relieve stress, then some of the source areas could have potential slip values of up to 10-15 m. We will outline our choice of values in the next section.

3.4 SOURCE MOTIONS

The source motions used in this study were developed by combining various parameters discussed in previous sections. Table 3-3 lists the source parameters used in the simulations. These are similar to the parameters used in the earlier report on this study (Hebenstreit, 1981), but reflect modifications made in light of additional information about historical seismicity in the region.

TABLE 3-3
SOURCE PARAMETERS USED IN EARTHQUAKE SIMULATIONS

Case	Focal depth (km)	Dip Angle	L (km)	W (km)	D (m)	M_0 (10^{27} dyne cm)	M_W
A	45	15°	550	100	5.8	159	8.7
B (North)	45	20°	300	100	10.0	150	8.7
B (South)	45	20°	300	100	10.0	150	8.7
C	45	20°	125	125	3.0	23	8.2
D	40	15°	150	125	8.0	75	8.5
E	20	15°	1800	130	10.0	1667	9.4

The number of individual source zones was reduced from 11 to the present 6 because of the experience gained earlier. For example, in the earlier report source zone A was studied by four separate cases -- three subintervals covering adjacent portions of the zone and one zone-long interval. The results, in terms of tsunami directionality, proved nearly insensitive to source location. Thus only one (modified) zone-long case was considered for this report.

Similarly zone B, which was treated as four cases in the previous report, is treated as two separate subzones in this version -- a zone north of the bend in the coastline and a similar zone south of the bend. We did not examine a third zone which straddled the bend in the coastline for two reasons:

- this bend is already a part of source zone E and little additional information would be gained by studying it separately, and

- the likelihood of a continuous rupture propagating from north to south and successfully "turning the corner" is remote (M. Wyss, Univ. of Colorado, personal communication).

Possible focal depth and dip angle for zone E were provided by Brian Brady.

Values of M_0 and M_W in Table 3-3 were calculated from (3.3) and (3.4).

The locations of these sources and bottom displacement scenarios are discussed in the following section.

3.5 BOTTOM DISPLACEMENT PATTERNS

The ultimate result of all of this manipulation of seismological concepts and data must be the specification of the bottom displacement pattern which drives the sea surface and initiates the tsunami. In each source zone we have applied two approaches. The first such pattern used, and by far the simplest, specifies uniform uplift over the entire source area. The slip displacement can be calculated from (3.4) or from values of plate convergence and estimates of earthquake recurrence time. The assumption operating here is that the slip on the fault plane is translated into an identical displacement at the ocean bottom. No account is taken of the depth of the faulting, since we essentially specify a 90° dip angle; that is, all slip motion is in the vertical plane.

The alternative approach takes into account the information deduced from local seismicity concerning focal depth, dip angle, etc. Mansinha and Smylie (1971) developed analytical expressions for the displacement fields of inclined faults based on their focal parameters. Figure 3.10 shows an example of the vertical displacement on a flat surface (that is, the ocean bottom or the land surface, without taking into account the curvature of the earth,) due to an earthquake with the parameters of case A. Note that the effects of the motion extend well beyond the area of the fault plane projected onto the surface.

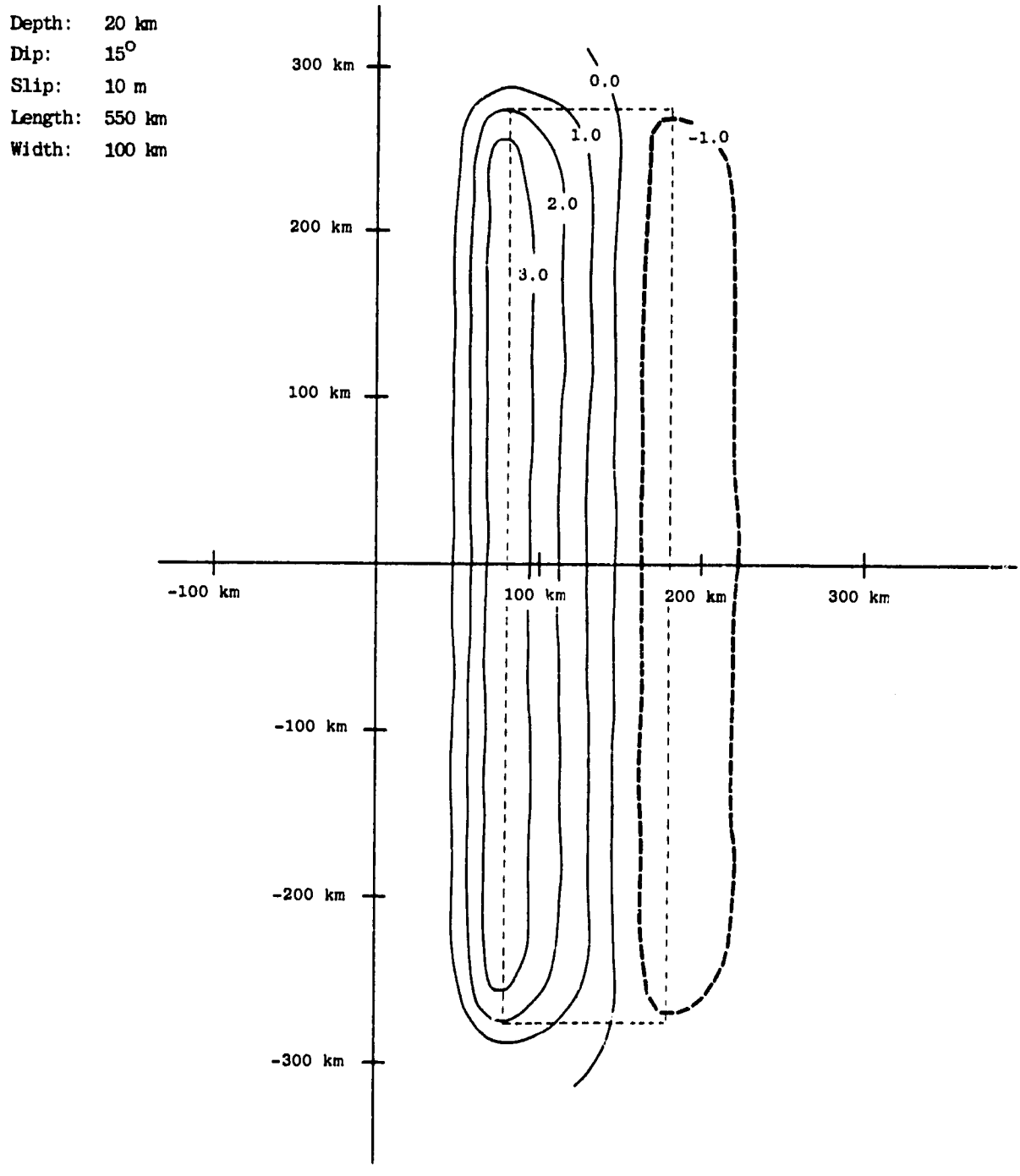

Figure 3.10: Contours of the bottom displacement pattern based on the parameters of Case A predicted by the Mansinha-Smylie Model. The dotted rectangle is the projection of the focal plane. Contour interval is 1 meter.

3.6 EFFECT OF SOURCE DURATION

Earlier studies (e.g., Kajiura, 1963; Hammack, 1973; Yamashita and Sato, 1974) have shown that the duration of the source motion is not a significant factor in the simulation of tsunami generation using a linear model as long as the motion only lasts on the order of 100 sec. For this reason we applied the instantaneous displacement assumption mentioned in Section 2 for source zones A-D, since these zones are comparatively short. Zone E, however, is so long that the instantaneous motion approach seems inappropriate. If we use an approximate rupture propagation speed of 3.5 km/sec, the rupture would take over 8 minutes to travel the 1800 km length of the zone. Thus we felt that some time dependence had to be added in this case. Since we are dealing with a discrete time increment model, we could not supply a continuous displacement. Instead, we broke zone E into 9 subzones, each 210 km long*. The bottom displacements in each subzone were instantaneous and occurred in sequence beginning at the north end of the zone and moving southward. The subzones are numbered in order of occurrence. Thus at time t=0 subzone 1 displaced *en masse*, at time t=60 sec subzone 2 displaced, and so on. In this way we developed a somewhat crude approximation to the time dependent evolution of the fault motion.

---

* This is the distance a rupture traveling at 3.5 km/sec would travel in 60 sec, which is the model time step required to maintain computational stability. See Brandsma *et al.*, (1975) for the method and rationale for computing the time step value.

Section 4
SOURCE ZONE A

4.1 INTRODUCTION

Source zone A is an area approximately 500 km long by 100 km wide centered near 11°S, 80°W (Figure 4.1). This places it northwest of Lima and between the trench axis and the slope. The long axis is roughly parallel to the coast and thus one would intuitively expect much of the wave energy from this region to radiate toward the southwest. Examination of the local topography (Figure 2.3) shows that the Carnegie Ridge lies to the north of the zone and the Nazca Ridge to the south.

We discuss each case (i.e., results using a uniform uplift and results using a variable uplift) in turn. Each discussion is accompanied by a number of figures depicting specific points. In order to reduce the confusion sometimes brought on by having to page back-and-forth from figure to figure, we have chosen to group all of the figures pertaining to each case in one spot immediately following the text for that case. We hope this will make this report more readable.

4.2 UNIFORM UPLIFT CASE

The source motion for this case is a uniform 5.8 m uplift of the entire area depicted in Figure 4.1. Because of the difficulties involved in projecting a rectangular area onto the model grid at any orientation not parallel to the (ϕ,θ) axis, the uplift pattern used in the simulation is actually a jagged, rectangle-like shape.

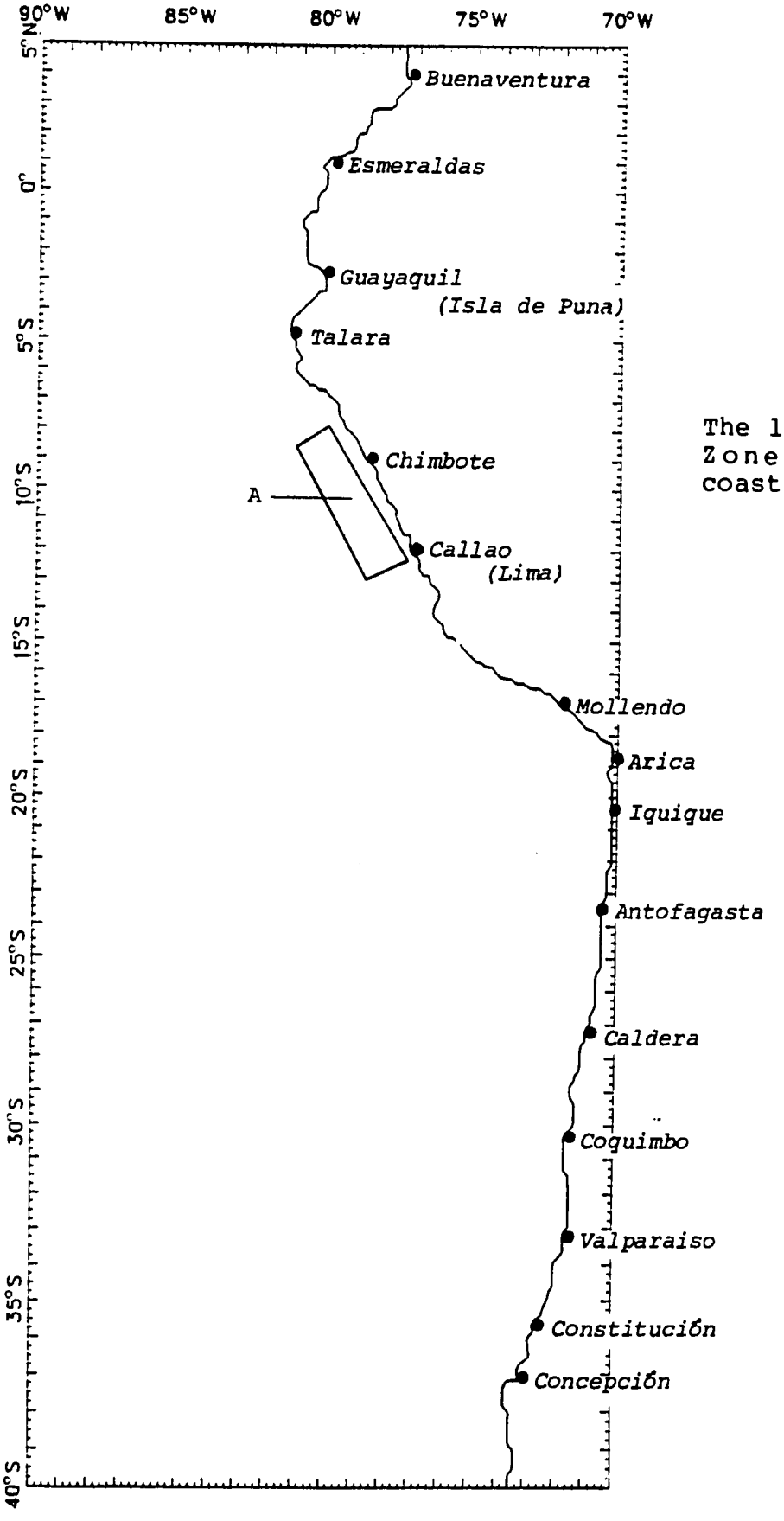

Figure 4.1

The location of source Zone A along the coastline.

4.2.1 Immediate (First Hour) Effects

The bulk of the potential energy imparted to the ocean by this uplift propagates out into the open ocean. This is apparent in Figure 4.2, which shows contours of wave height (i.e., lines connecting locations of equal wave elevation above MSL), in meters, one hour after the uplift. The initial waves are spreading radially outward from the source, with the highest leading waves (located in the ellipse labelled 2.00 at roughly 14°S, 85°W) heading toward the southwest. Note that only positive wave elevations are contoured to avoid confusion. The wave field will be made up of crests and troughs, since the sea surface in the source area will oscillate about MSL as it slowly returns to equilibrium after the initial vertical displacement.

Note also the very confused and, in many locations, quite intense wave concentration along the coastline. This is not surprising, in view of the proximity of the source area to the shoreline. The initial waves reaching the coast from the source should be nearly as high as the uplift-induced surface displacement. The fact that the intense concentrations remain after an hour (and, indeed, for quite a time later) shows that all of the wave energy is not leaving the source area immediately. The relatively narrow continental shelf in this area appears to be trapping some of the energy and keeping it from escaping seaward.*

4.2.2 Longer Duration Effects

Figure 4.3 shows the time dependent variation in wave height near Lima, Peru as a result of the uplift.

*An explanation of the shelf-trapping mechanism is provided by Miles (1972).

The initial crest is roughly 4 m high and occurs about 15 min after generation. But the largest crest occurs 2 hrs and 15 min later. Waves of significant amplitude near Lima continue for the entire 8 hrs of the simulation.

Wave energies drop off rapidly at coastal locations north and south of the source area. Wave time series near* five cities (Arica, Antofagasta, and Valparaiso, Chile to the south and Isla de Puna, Columbia and Buenaventura, Ecuador to the north) appear in Figures 4.4 to 4.8. Waves at Arica and Isla de Puna, which are closest to the source, are significant (crests roughly 1.5 m above MSL), but of much longer period than those at Lima. By the time waves reach Antofagosta and Buenaventura they are quite low and long. The time series at Valparaiso, which is the location farthest away from the source, shows a surprising level of activity. We can postulate two reasons for this. One is that the waves propagating southward along the shelf are amplified by bottom topography near Valparaiso. The second is that the initial waves reaching Valparaiso do not come along the shelf but instead cross the open Pacific seaward of the trench and actually approach from offshore. If this is the case, then refraction due to offshore topography would turn the wave fronts so that the angle of approach to the shore is more nearly perpendicular and amplification on the shelf would be accentuated.

4.2.3 Maximum Elevations

The wave records discussed in Section 4.2.2 contain valuable information about the temporal variation of wave

*We emphasize the word near since we are only talking about offshore waves and because the discrete model grid only allows us to locate a position to within 15-20 km.

height at a few specific sites up and down the coast. But limitations of computer resources prevent us from examining wave behavior in this fashion at more than just a few locations. The length of the South American coast (the section we have chosen to model is over 5000 km long) makes it desirable to be able to obtain information about the waves at a much greater number of locations. We have chosen to reduce the large amount of data required by recording only the maximum (positive) wave elevation calculated at 300 coastal points, as well as the time (in hours and minutes after the uplift) at which it is recorded. This will allow us to assess the maximum tsunami wave threat at each location (assuming that the highest wave poses the greatest hazard) and give some indication of when it arrives.

Figure 4.9a-f contains the maximum wave elevation information. Figure 4.9a (which will appear with each set of maximum elevation plots) depicts the coastline used in the simulation runs and the approximate locations of the 300 recording points. Because so many points are used, only the locations of the first point and every even-numbered point thereafter are shown. The odd-numbered points are usually equi-distant between adjacent even-numbered points. The approximate locations of a number of coastal cities are noted on this figure. We only intend to calculate wave heights in water on the continental shelf at least 20 m deep; therefore, the reader should not assume an exact correspondence between recording point locations and cities. The cities are noted only for orientation purposes.

Figures 4.9b-f show the variation in maximum elevation along the coast from point 1 to point 300. The elevations are not plotted as a continuous curve, but rather as a discontinuous histogram-like function. This method of

presentation is used to emphasize to the reader the discrete nature of these computations. Because of the resolution of the model grid we can only calculate wave heights at locations which are separated in space by approximately 20 km. We have no valid basis for making any statements about locations in between these points. We have specifically avoided the use of continuous, smooth maximum elevation plots to keep the reader from assuming that we can provide information about points closer together than the model allows.

The lower axis of the figure indicates the coastline index number (corresponding to points on Figure 4.9a). The maximum wave elevation in meters at each point is indicated by a horizontal line, directly over the appropriate tic-mark, at a height corresponding to the wave elevation. If the maximum is greater than the vertical extent of the plot, we have indicated this fact with a vertical arrow just below the upper axis of the figure. Since we are concerned here with the patterns of wave height, rather than absolute numbers, we have not attempted to indicate the calculated heights at those points which exceed the vertical extent of the plot.

Just above the upper axis of the plot we have listed the time after generation at which the maximum occurs. The time is indicated in hours and minutes. A value of 0437, for example, means that the maximum occurred 4 hours and 37 minutes after the uplift began. These times are also centered on the appropriate tic marks.

We have also indicated, by means of a thin horizontal line on each plot, the arithmetic mean (average) of all 300 maximum elevation values. We have found that this provides an extremely useful reference point for assessing the variations in wave height (and hazard) along the coast.

An examination of the maximum elevation plots for this case shows that the major portion of the severe threat is quite localized in the section of coastline extending from south of Lima (about point 167) to Talara (about point 234). In this region the maximum waves are extremely high, with the majority of elevations over 4 m. This is not too surprising, since this area is quite close to the source location. The wave threat drops off rapidly to the north, with only scattered values near or above average.

Wave elevations to the south die down to a steady elevation of between 1 and 2 m. The area of the continental bend near Arica does receive slightly higher waves than its neighbors, but only at one point is the maximum above average.

The occurrence of three localized above-average concentrations south of Valparaiso is a bit surprising. The fact that these occur near local small indentations or embayments in the coast would seem to indicate a resonance mechanism at work to produce these local peaks.

The pattern of observed arrival times is quite confusing. An examination of predicted travel times for first arrivals* would lead us to expect a steady increase in arrival time with increasing distance from the source. Indeed the times of arrival of the first crests observed on the time series (Figures 4.3 to 4.8) do agree well with the charts, but we have no real basis for comparison of calculated arrivals of the maximum waves. We have therefore chosen not to include these data in our threat analysis.

*Such as the Tsunami Travel Time Charts produced by the U.S. Department of Commerce (NOAA, 1971).

It is evident from these plots that in some cases a large maximum value will occur at one point, while the maximum at an adjacent point will be much smaller. Intuition would lead us to expect a fairly smooth variation along the coast. These variations could be due to several mechanisms: local offshore bottom topography variations, the local shape of the coastline, or numerical noise, among others. We decided to leave them in the results without any attempts at smoothing because we feel that the important information to be gained is not the actual numbers or the individual point-to-point variations but the wave height patterns over a number of adjacent locations. These patterns tell us whether or not a section of coastline several tens of kilometers long is threatened by tsunami waves.

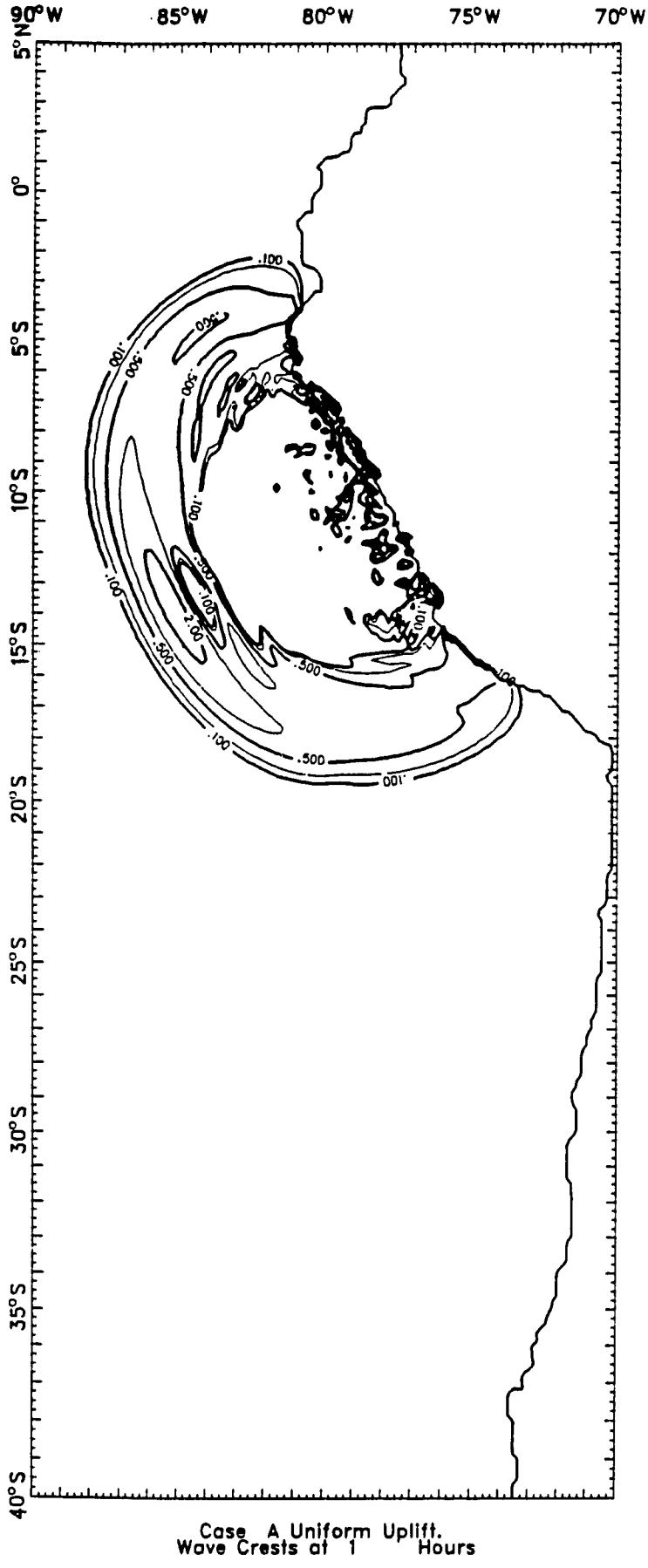

Figure: 4.2

Surface elevation (positive only) one hour after a uniform uplift in source Zone A. Contours correspond to 0.1, 0.2, 0.5, 1.0, and 2.0 m.

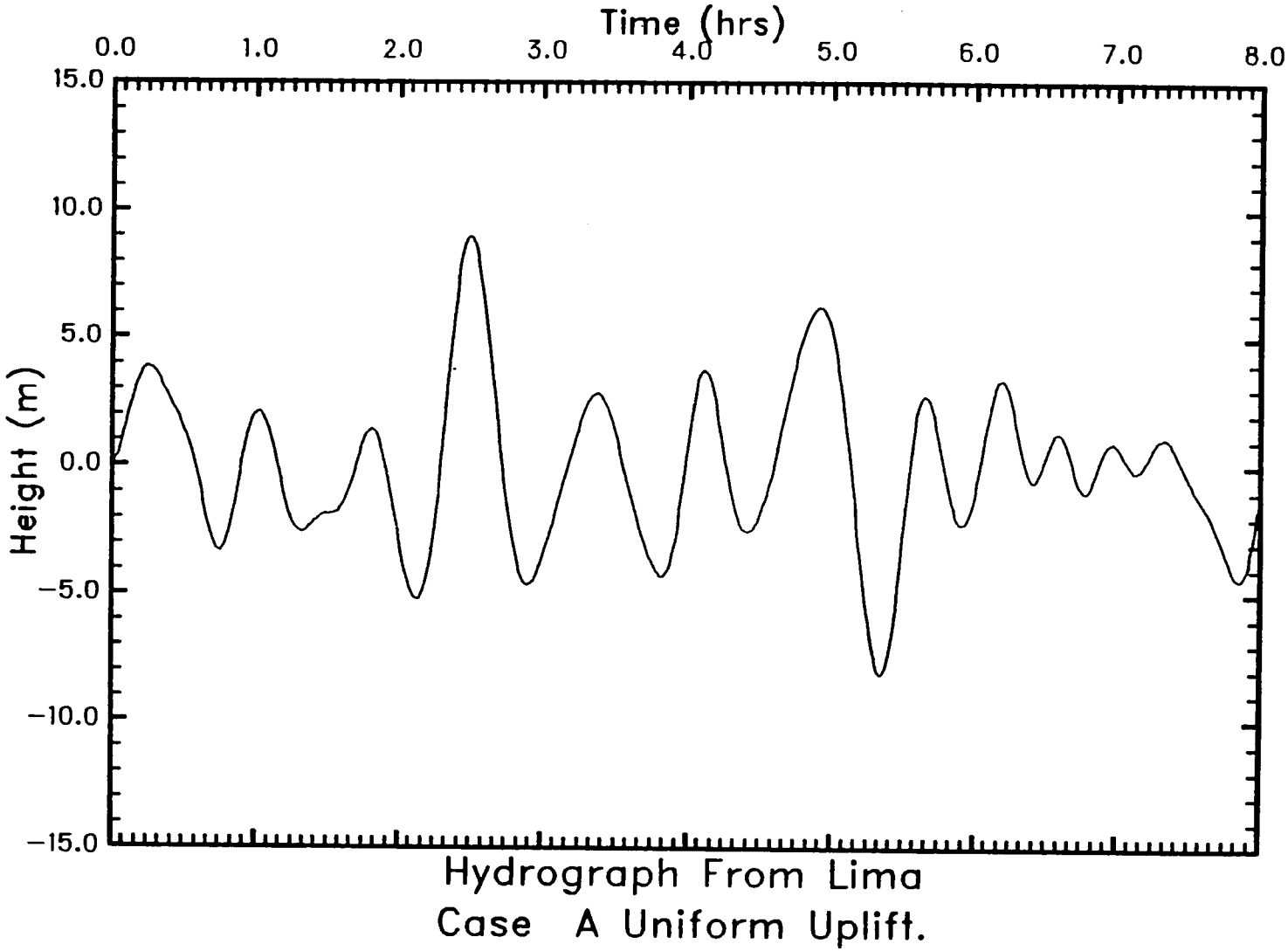

Figure 4.3: Wave elevation as a function of time at the recording point near Lima, Peru. These waves were generated by the uniform uplift of Zone A.

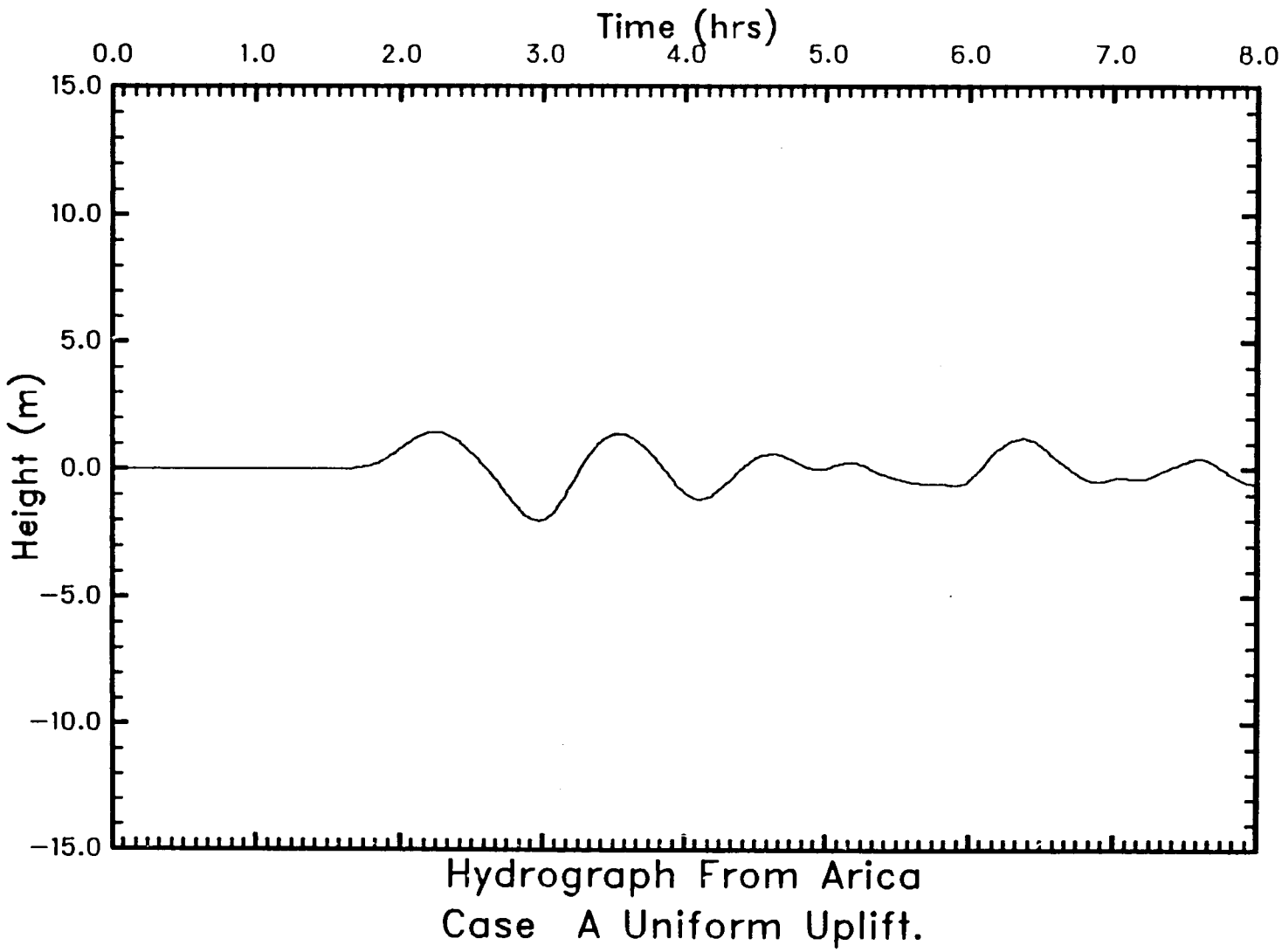

Figure 4.4: Wave elevation as a function of time at the recording point near Arica, Chile. These waves were generated by the uniform uplift of Zone A.

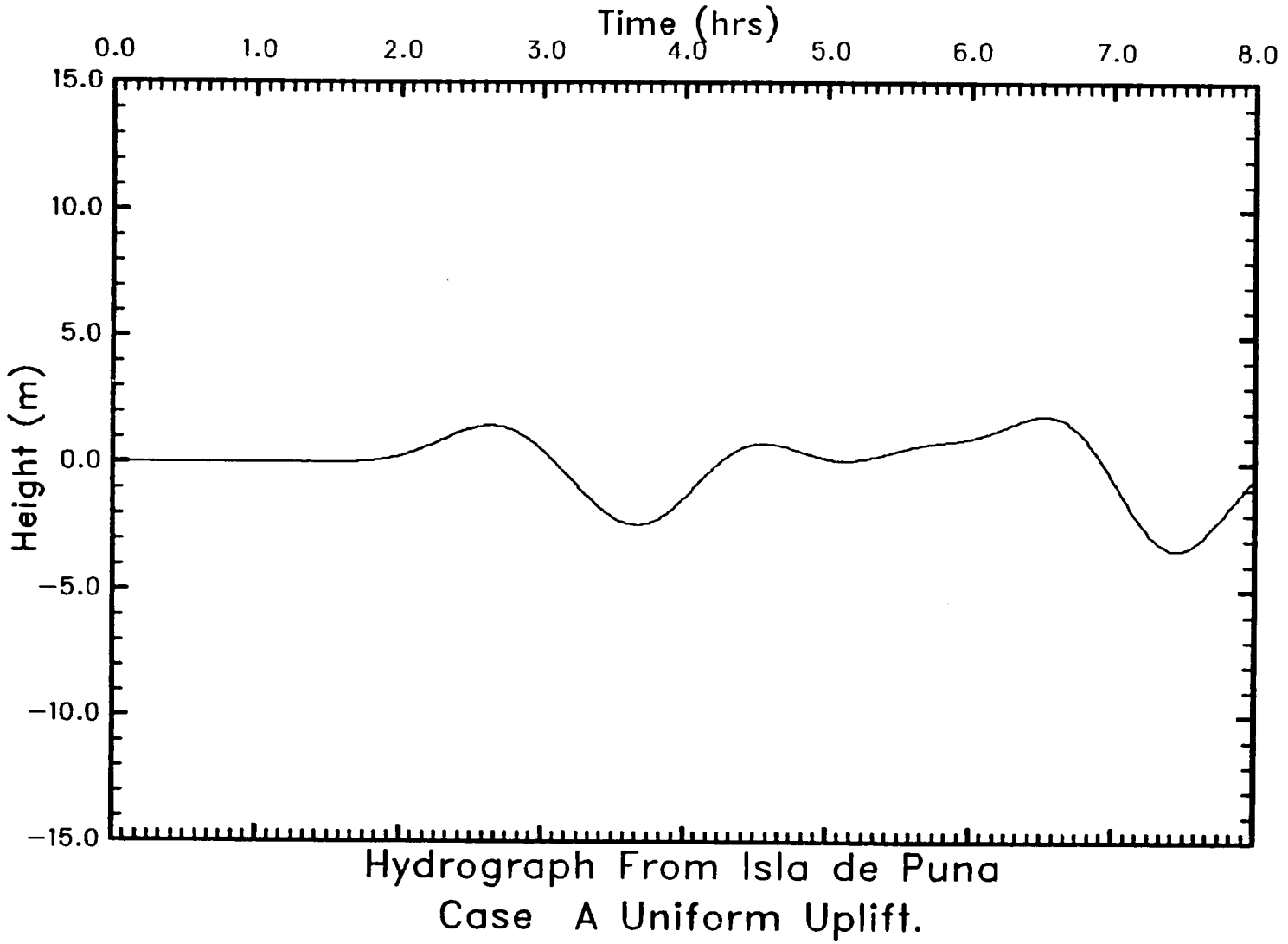

Figure 4.5: Wave elevation as a function of time at the recording point near Isla de Puna, Colombia. These waves were generated by the uniform uplift of Zone A.

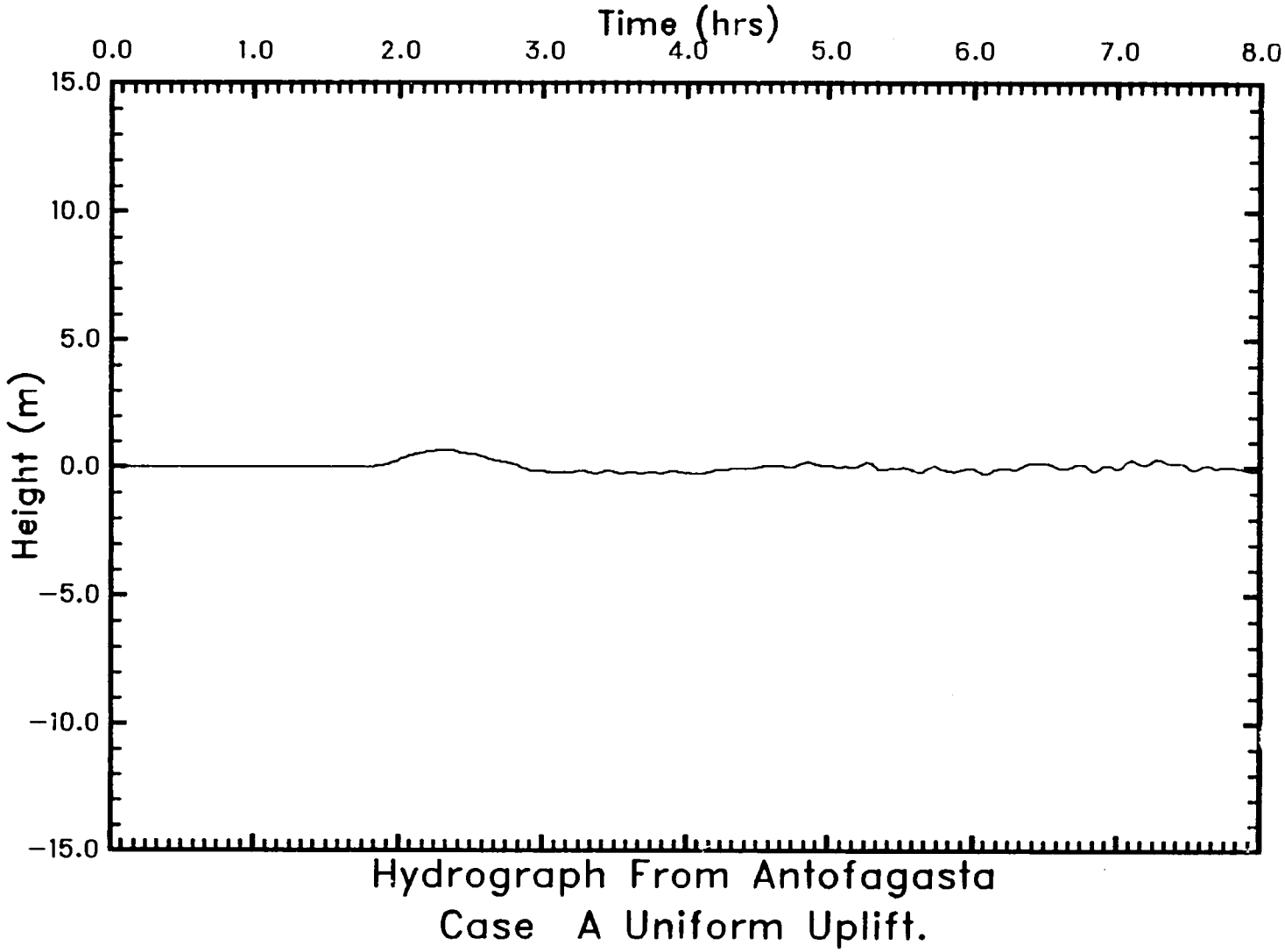

Figure 4.6: Wave elevation as a function of time at the recording point near Antofagasta, Chile. These waves were generated by the uniform uplift of Zone A.

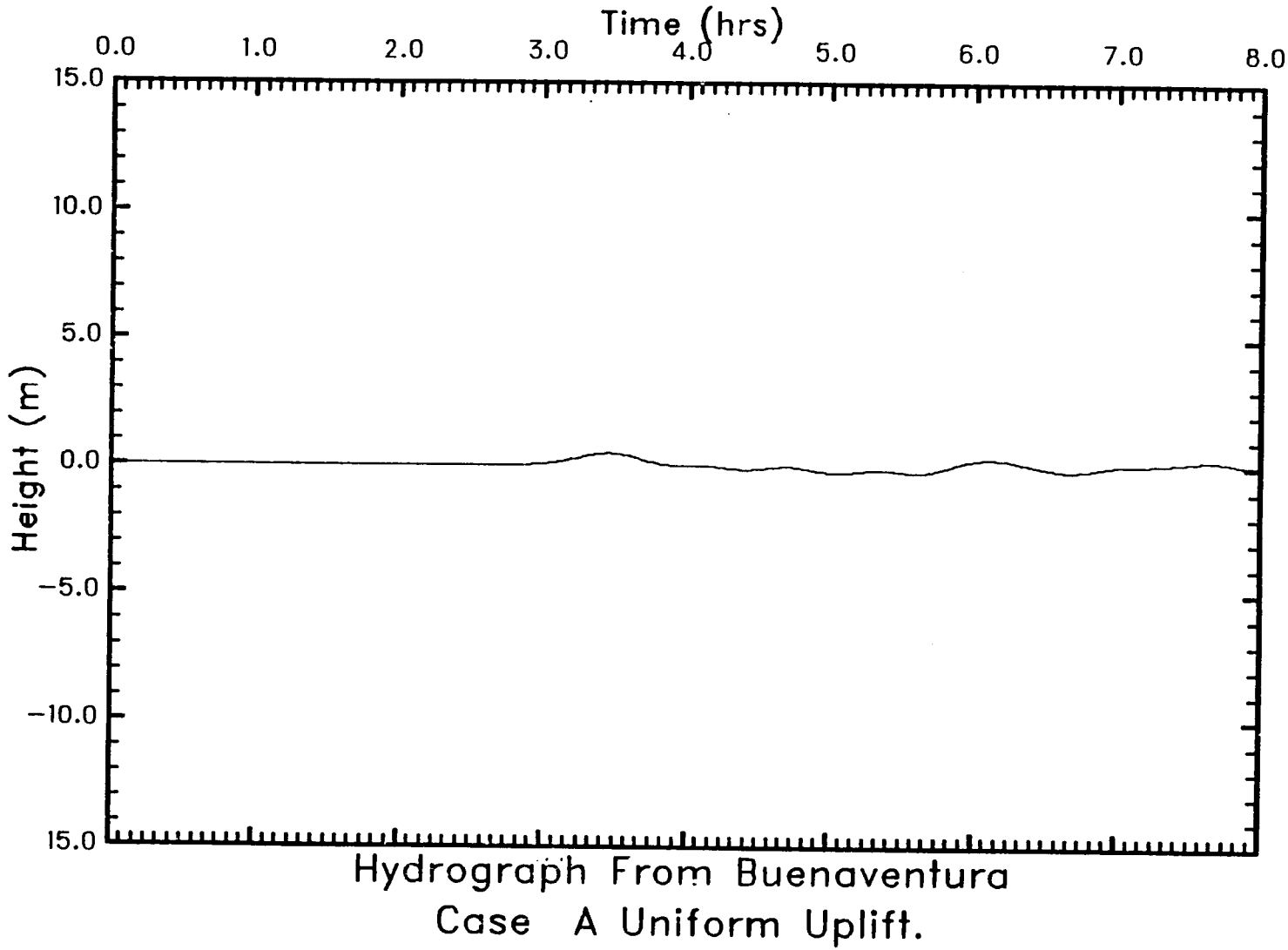

Figure 4.7: Wave elevation as a function of time at the recording point near Buenaventura, Ecuador. These waves were generated by the uniform uplift of Zone A.

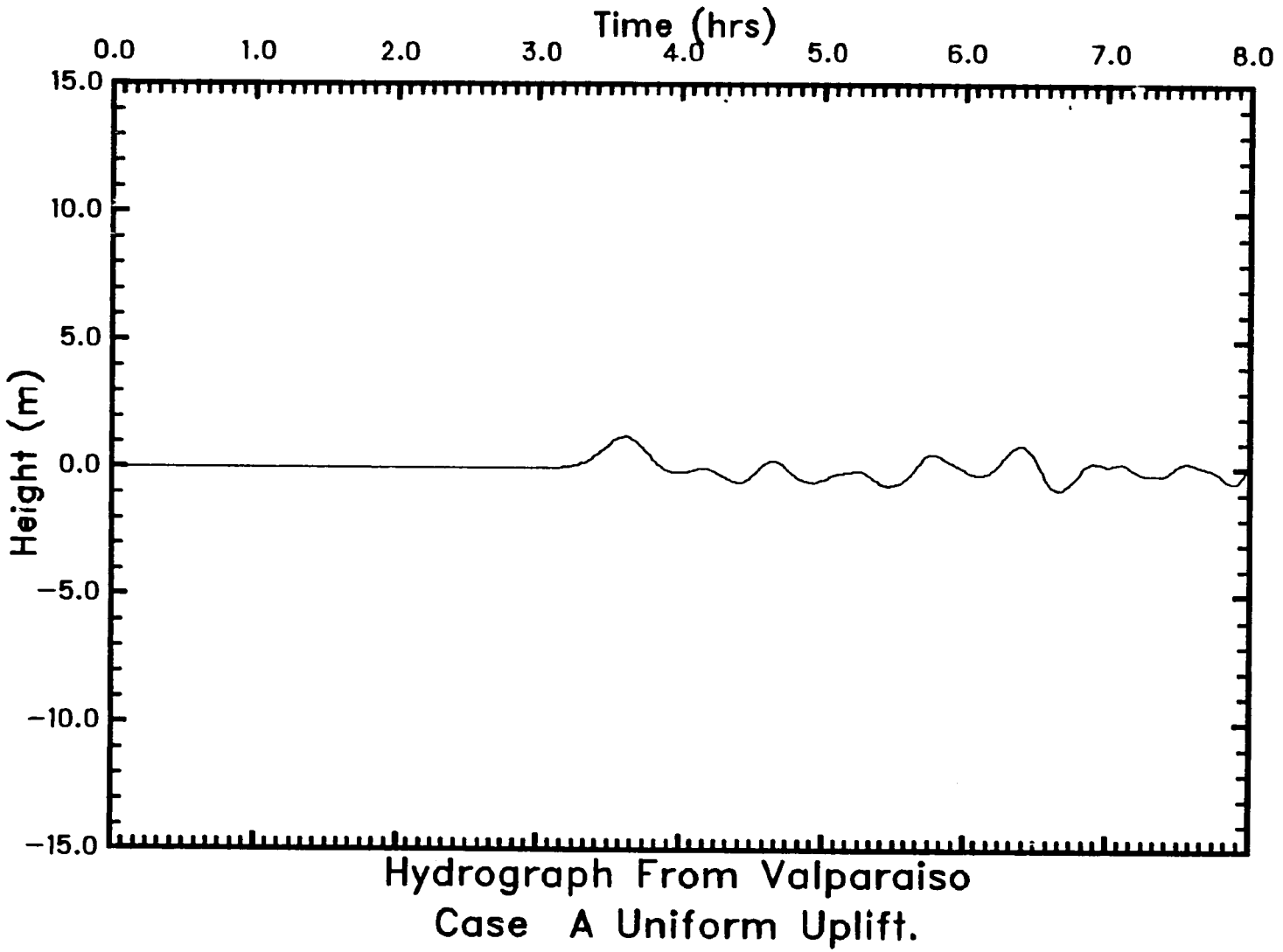

Figure 4.8: Wave elevation as a function of time at the recording point near Valparaiso, Chile. These waves were generated by the uniform uplift of Zone A.

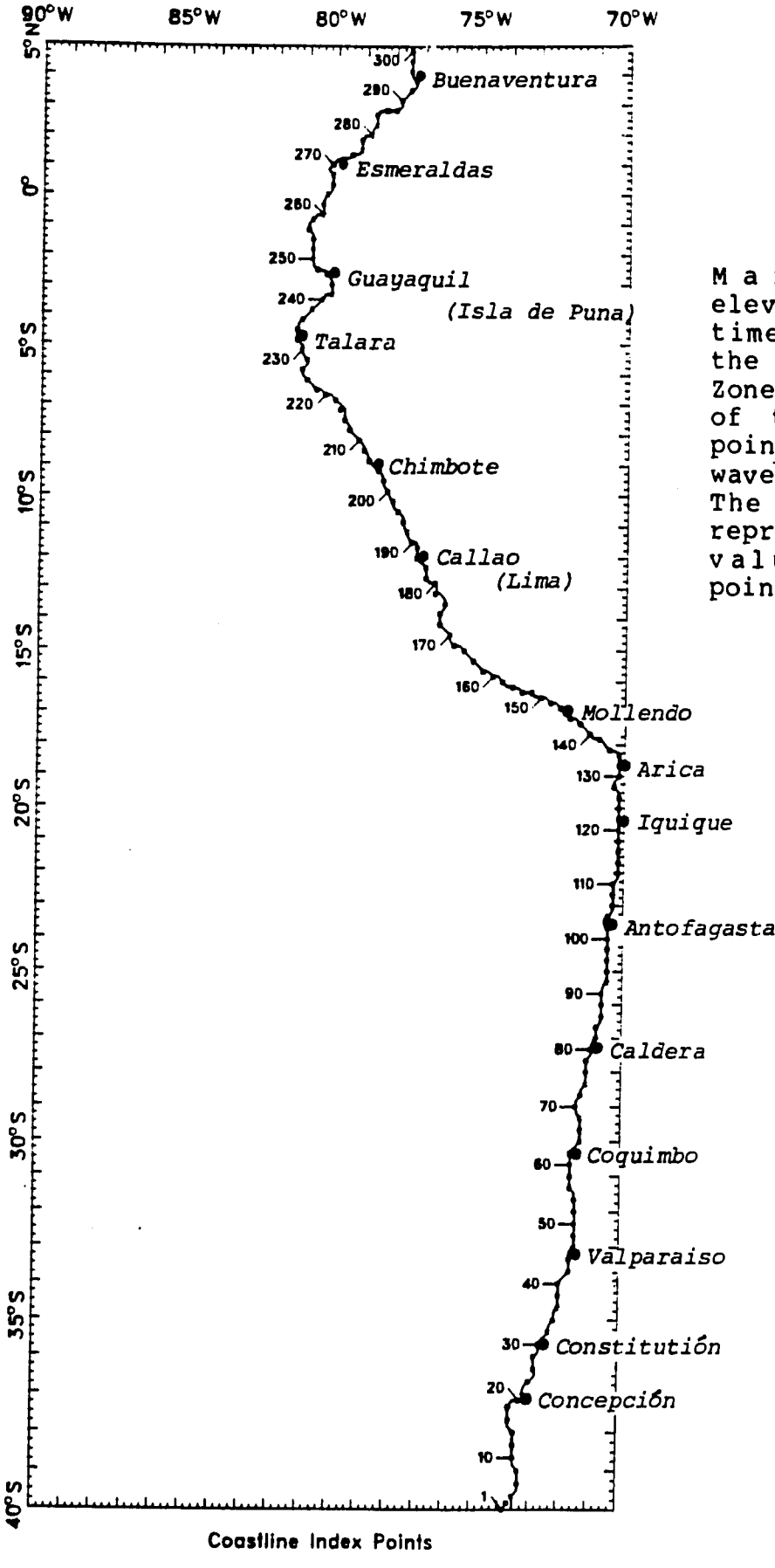

Figure: 4.9

Maximum wave elevations and arrival times of waves from the uniform uplift in Zone A. (a) Locations of the 300 recording points. (b-f) Maximum waves at each point. The horizontal line represents the average value of all 300 points.

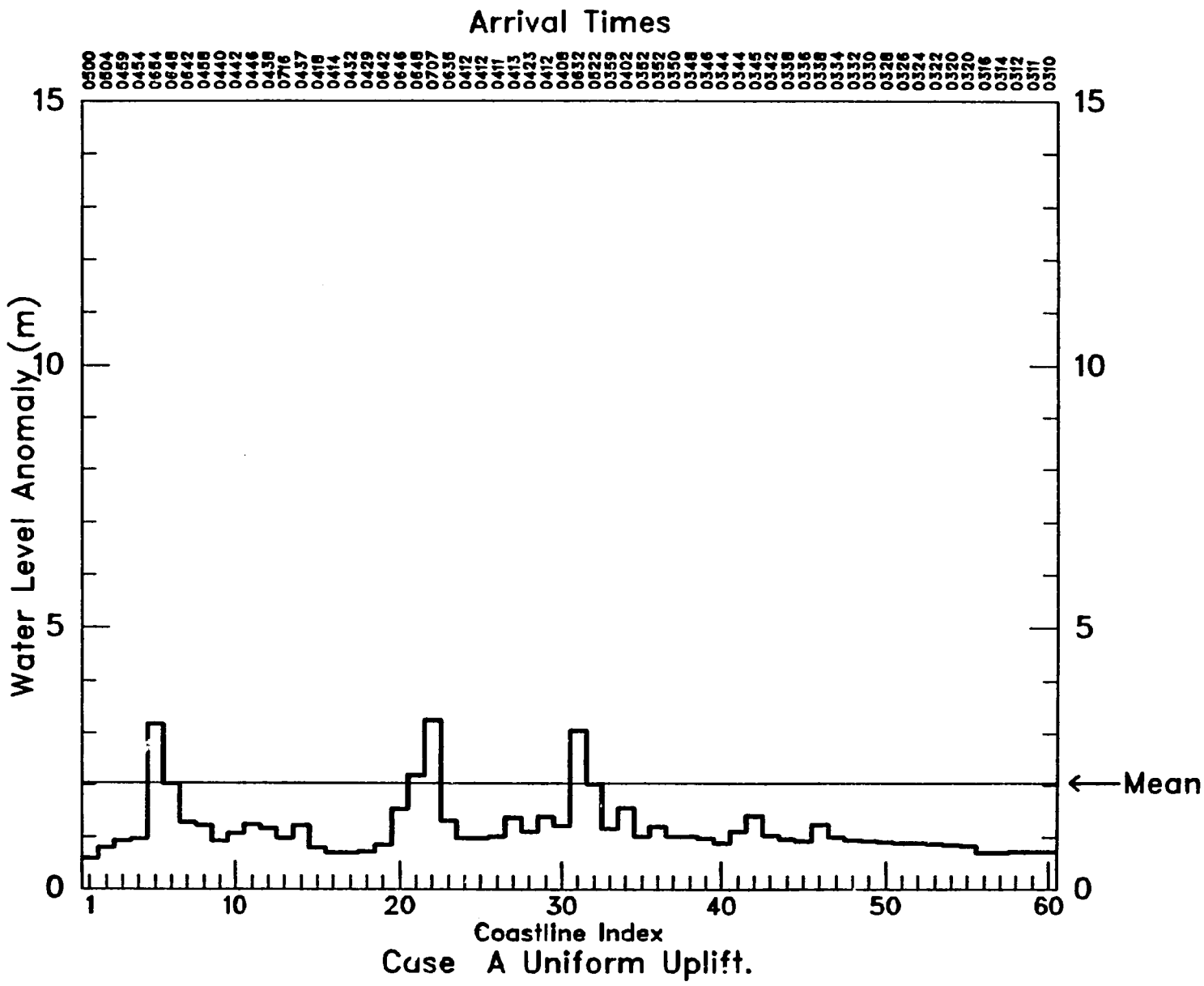
Arrival Times
0500 0504 0459 0454 0684 0648 0642 0458 0440 0442 0446 0438 0716 0437 0418 0414 0432 0429 0642 0646 0648 0707 0638 0412 0412 0411 0413 0423 0412 0408 0632 0622 0359 0402 0352 0352 0350 0348 0346 0344 0344 0345 0342 0338 0336 0338 0334 0332 0330 0328 0326 0324 0322 0320 0320 0316 0314 0312 0311 0310
Water Level Anomaly (m)
15
10
5
0
1
10
20
30
40
50
60
Coastline Index
Mean
Case A Uniform Uplift.

Figure: 4.9 (b)

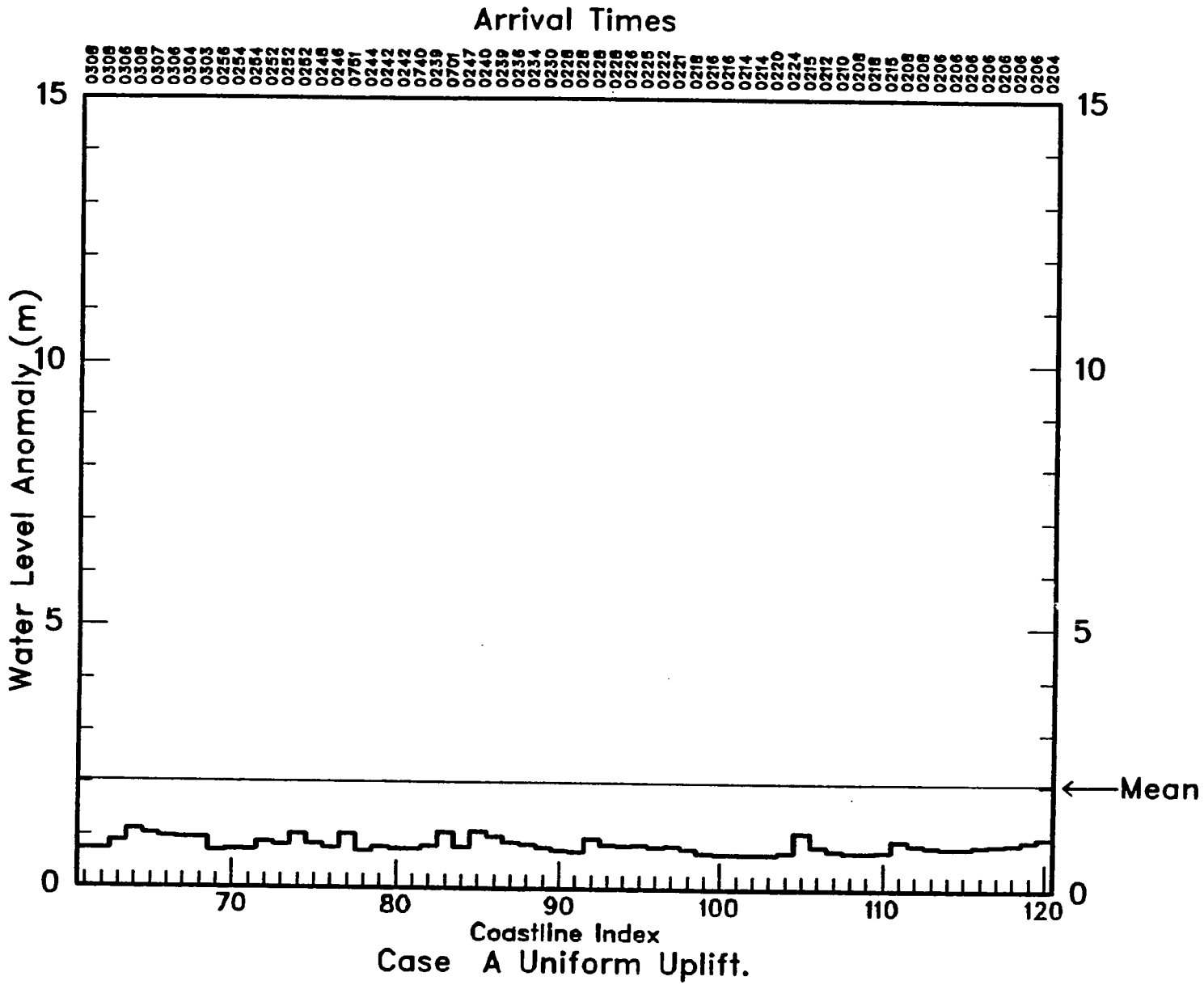
Arrival Times
0308 0308 0306 0308 0307 0306 0304 0303 0256 0254 0254 0252 0252 0252 0248 0246 0751 0244 0242 0242 0740 0239 0701 0247 0240 0239 0236 0234 0230 0228 0228 0228 0228 0226 0225 0222 0221 0218 0216 0216 0214 0214 0220 0224 0215 0212 0210 0208 0218 0215 0208 0208 0206 0206 0206 0206 0206 0206 0206 0206 0204
Water Level Anomaly (m)
15
10
5
0
70
80
90
100
110
120
Coastline Index
Mean
Case A Uniform Uplift.

Figure: 4.9 (c)

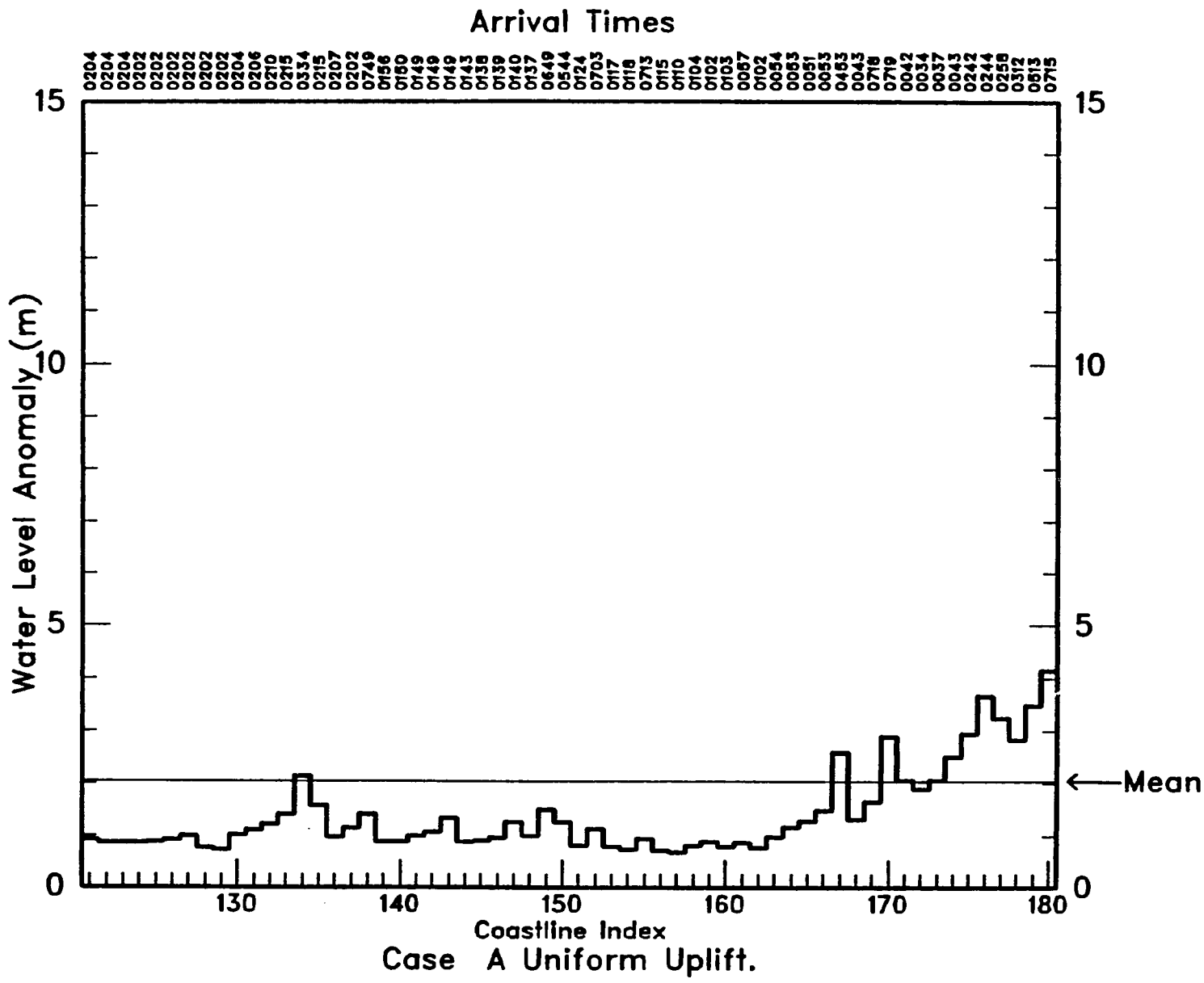
Arrival Times
0204 0204 0204 0202 0202 0202 0202 0202 0202 0204 0206 0210 0215 0334 0215 0207 0202 0749 0156 0150 0149 0149 0149 0143 0138 0139 0140 0137 0649 0544 0124 0703 0117 0118 0713 0115 0110 0104 0102 0103 0087 0102 0054 0053 0051 0053 0453 0043 0718 0719 0042 0034 0037 0043 0242 0244 0258 0312 0513 0715
Water Level Anomaly (m)
15
10
5
0
130
140
150
160
170
180
Coastline Index
Mean
Case A Uniform Uplift.

Figure: 4.9 (d)

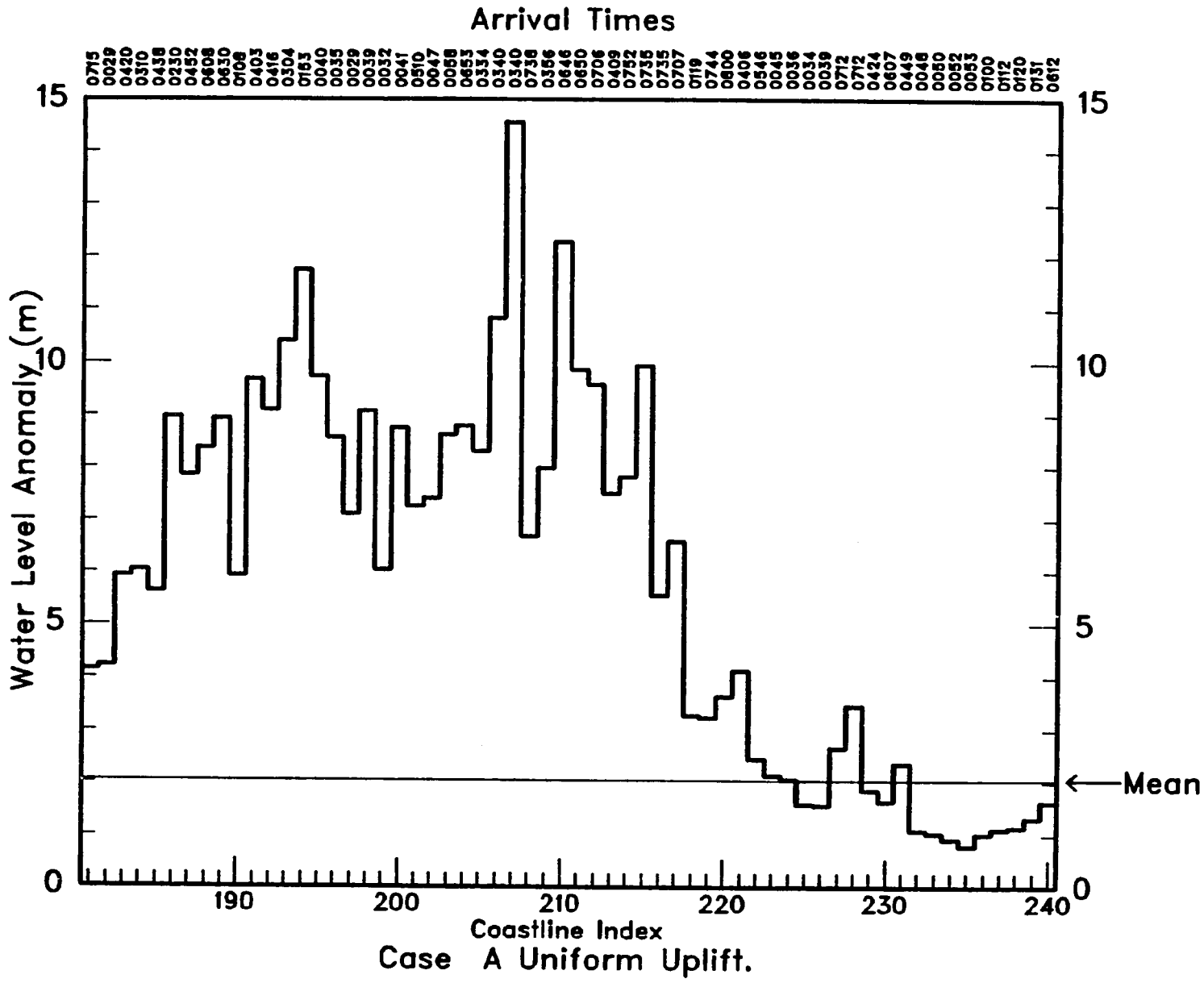
Arrival Times
0715 0029 0420 0310 0438 0230 0452 0408 0630 0108 0403 0416 0304 0153 0040 0035 0029 0039 0032 0041 0510 0047 0058 0653 0334 0340 0340 0738 0356 0646 0650 0706 0409 0752 0735 0735 0707 0119 0744 0800 0406 0546 0045 0036 0034 0039 0712 0712 0424 0607 0449 0048 0050 0052 0053 0100 0112 0120 0131 0612
Water Level Anomaly (m)
15
10
5
0
190
200
210
220
230
240
Coastline Index
Mean
Case A Uniform Uplift.

Figure: 4.9 (e)

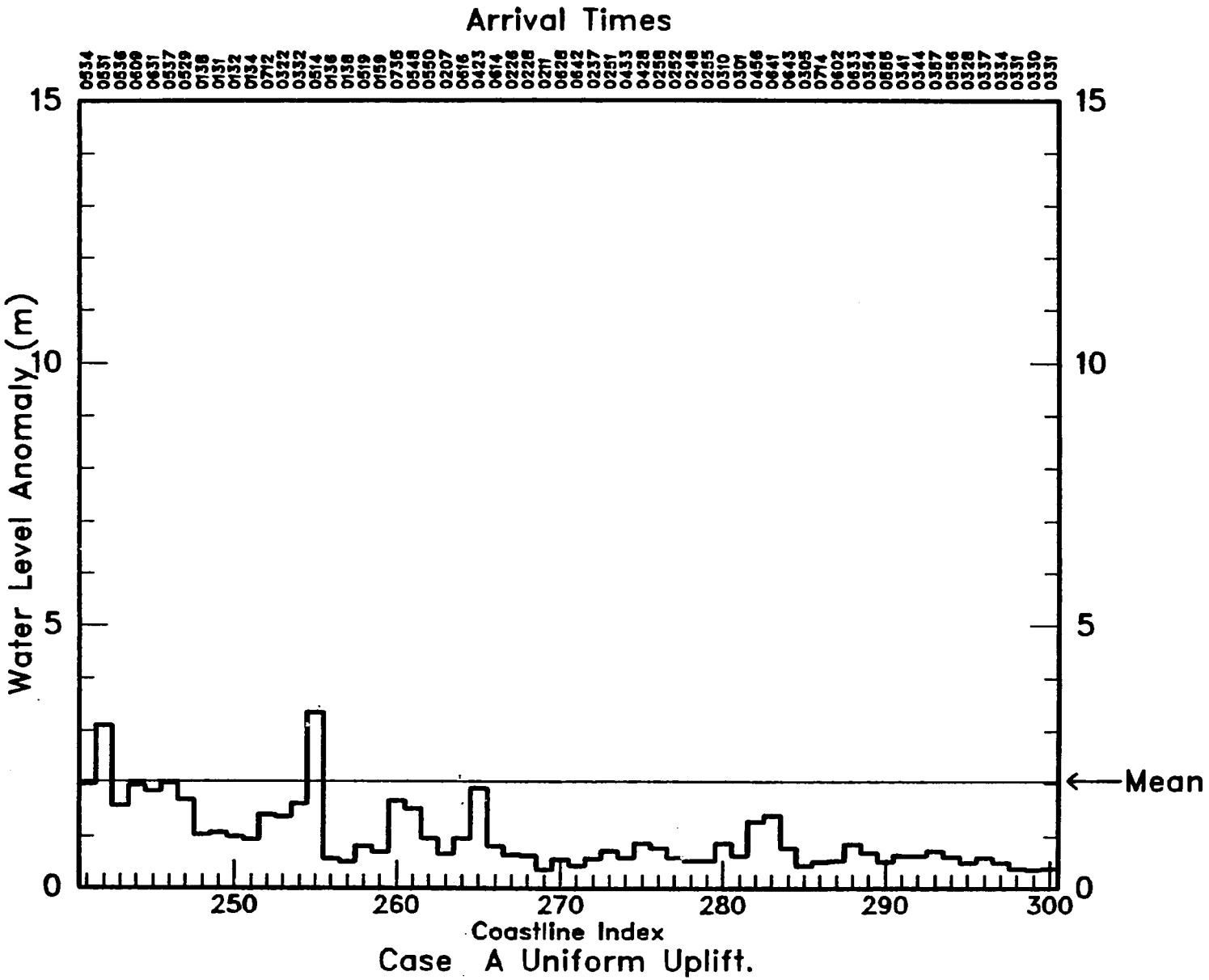
Arrival Times
0534 0531 0536 0609 0631 0537 0529 0138 0131 0132 0734 0712 0322 0332 0514 0138 0138 0519 0159 0735 0548 0550 0207 0616 0423 0614 0228 0228 0211 0628 0642 0237 0251 0433 0428 0258 0252 0248 0255 0310 0301 0456 0641 0643 0305 0714 0602 0633 0354 0555 0341 0344 0367 0356 0328 0337 0334 0331 0330 0331
Water Level Anomaly (m)
15
10
5
0
250
260
270
280
290
300
Mean
Coastline Index
Case A Uniform Uplift.

Figure: 4.9 (f)

4.3 VARIABLE UPLIFT CASE

The variable uplift pattern used in this case covers the entire area depicted in Figure 4.1. The mean slip displacement parameter, D, was adjusted to produce a peak displacement of 5.8 m. Displacements less than 0.05 m were set to zero in order to limit the area of the uplift field.

4.3.1 Immediate Effects

The surface elevation contours one hour after uplift are shown in Figure 4.10. The highest portion of the crest, as in Figure 4.2 for the uniform uplift case, is directed toward the southwest. Several low secondary waves are apparent trailing behind the leading wave. The wave field near the coast is quite confused. A good deal of energy remains behind the seaward propagating waves.

4.3.2 Longer Duration Effects

The wave time series produced at coastal points by this uplift are quite similar to those for the uniform uplift, but much lower in amplitude. Lima, which is close to the source, receives an initial crest, followed by a succession of long period waves with elevations of about 1 m (see Figure 4.11). This succession is occasionally broken by an extreme wave with a crest several meters high.

Waves farther south at Arica (Figure 4.12) are long and quite low. Similar waves reach Isla de Puna a short while later (Figure 4.13). The waves at Antofagasta are only barely noticeable (Figure 4.14), as are waves at Buenaventura (Figure 4.15).

Once again, the waves reaching Valparaiso (Figure 4.16) are higher than those at stations closer to the source, although in this case these waves are quite low.

4.3.3 Maximum Elevations

The plots of maximum elevation along the coast (Figure 4.17a-f) reflect the general low levels of wave energy which propagate along the coast from this source. The elevations along the coast from point 166 to point 231 are all at or above the mean level. And the majority of them are above 2 m. This, of course, is the immediate vicinity of the source.

Wave elevations up and down the coast from this region are generally low. Only a few places record waves much above the overall mean level. North of Esmerelda the coast is quiet. Only at a few locations far to the south (the same locations for which this was observed in the uniform uplift case) do elevations get above 1 m.

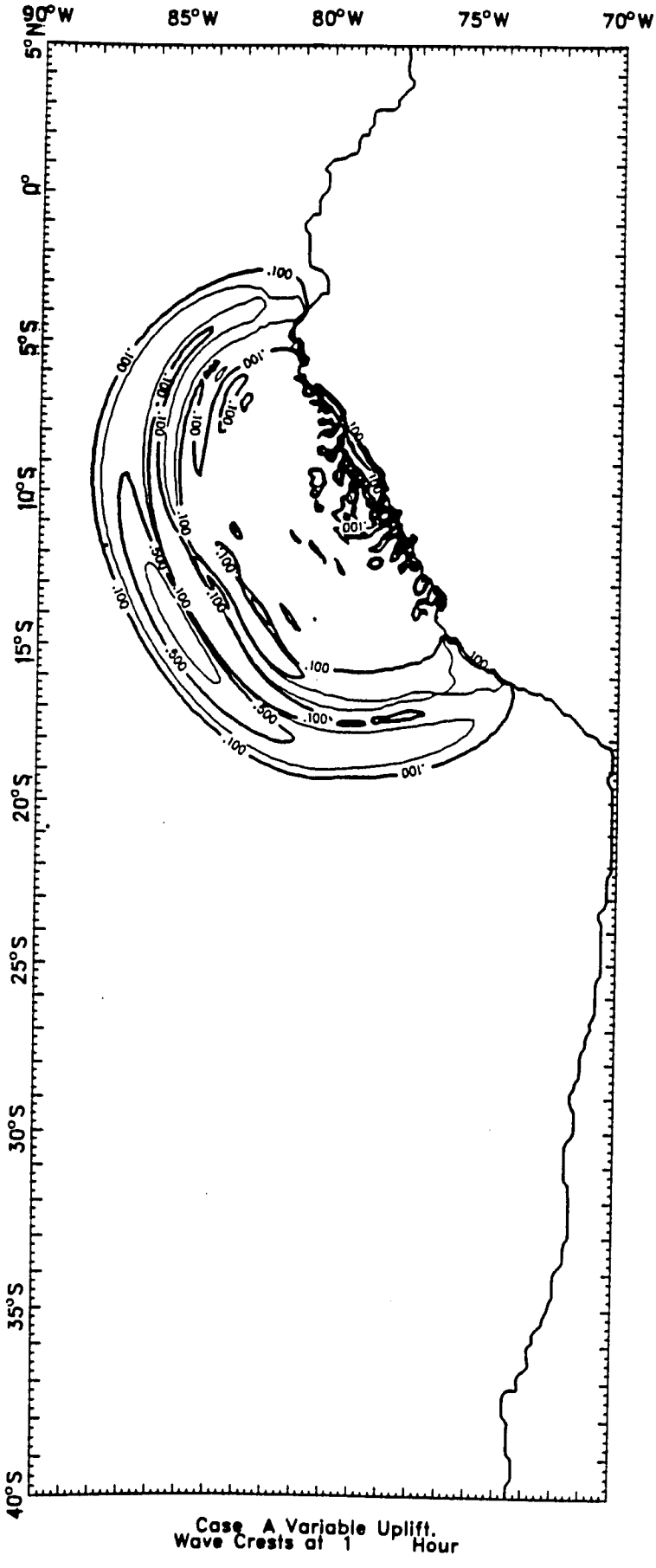

Figure: 4.10

Surface elevation (positive only) one hour after a variable uplift in source Zone A. Contours correspond to 0.1, 0.2, 0.5, 1.0, and 2.0 m.

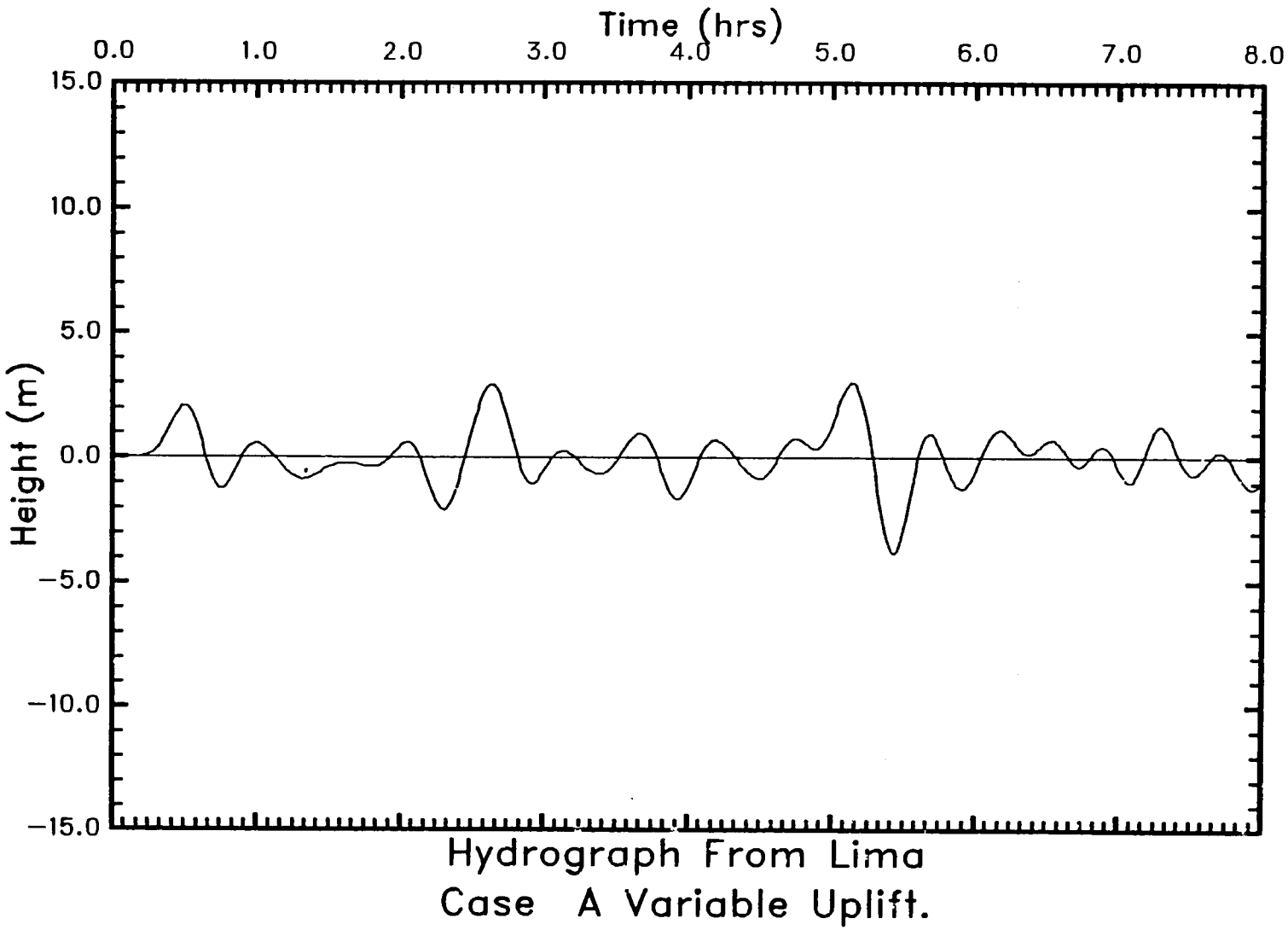

Figure 4.11: Wave elevation as a function of time at the recording point near Lima, Peru. These waves were generated by the variable uplift of Zone A.

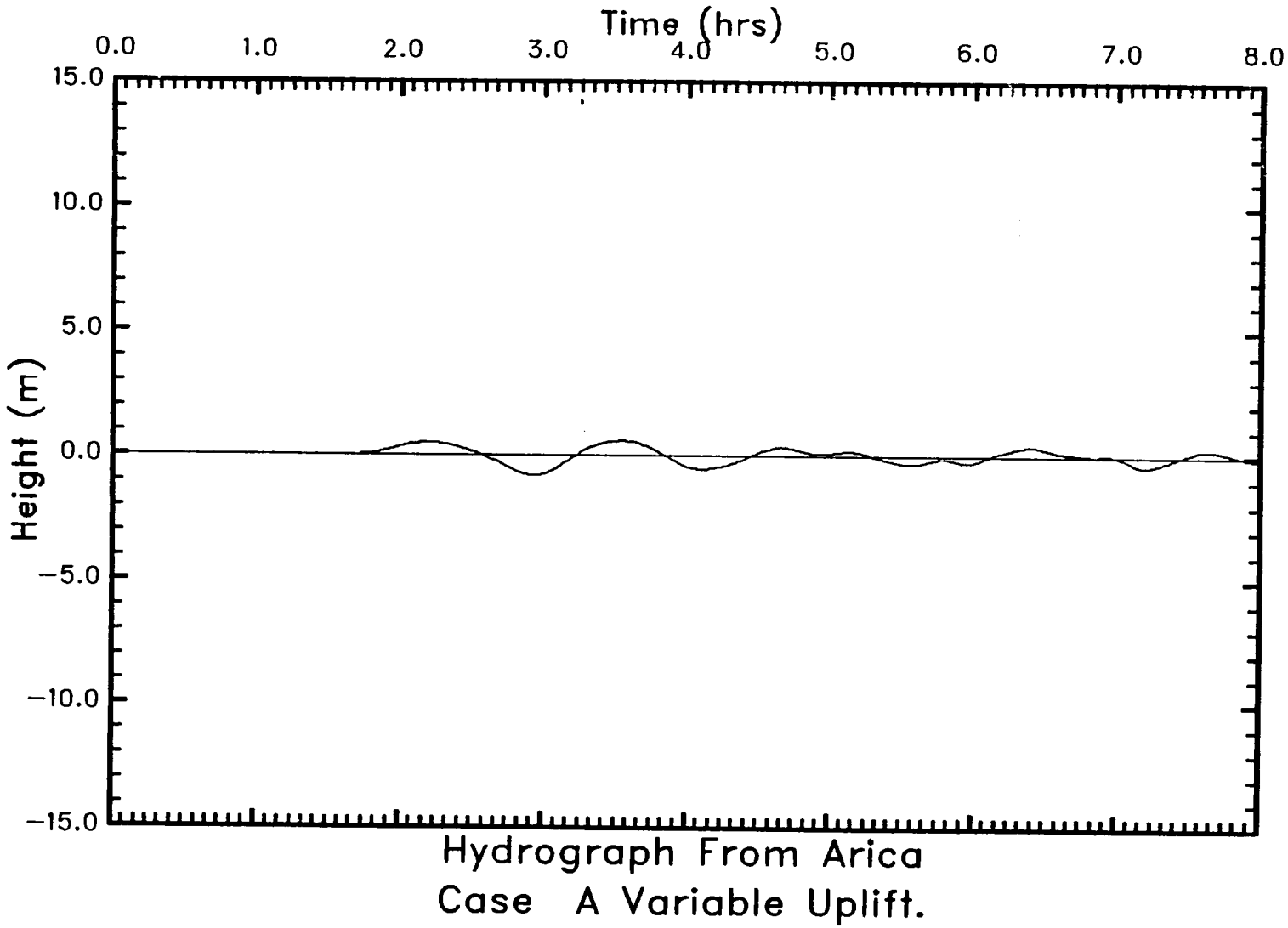

Figure 4.12: Wave elevation as a function of time at the recording point near Arica, Chile. These waves were generated by the variable uplift of Zone A.

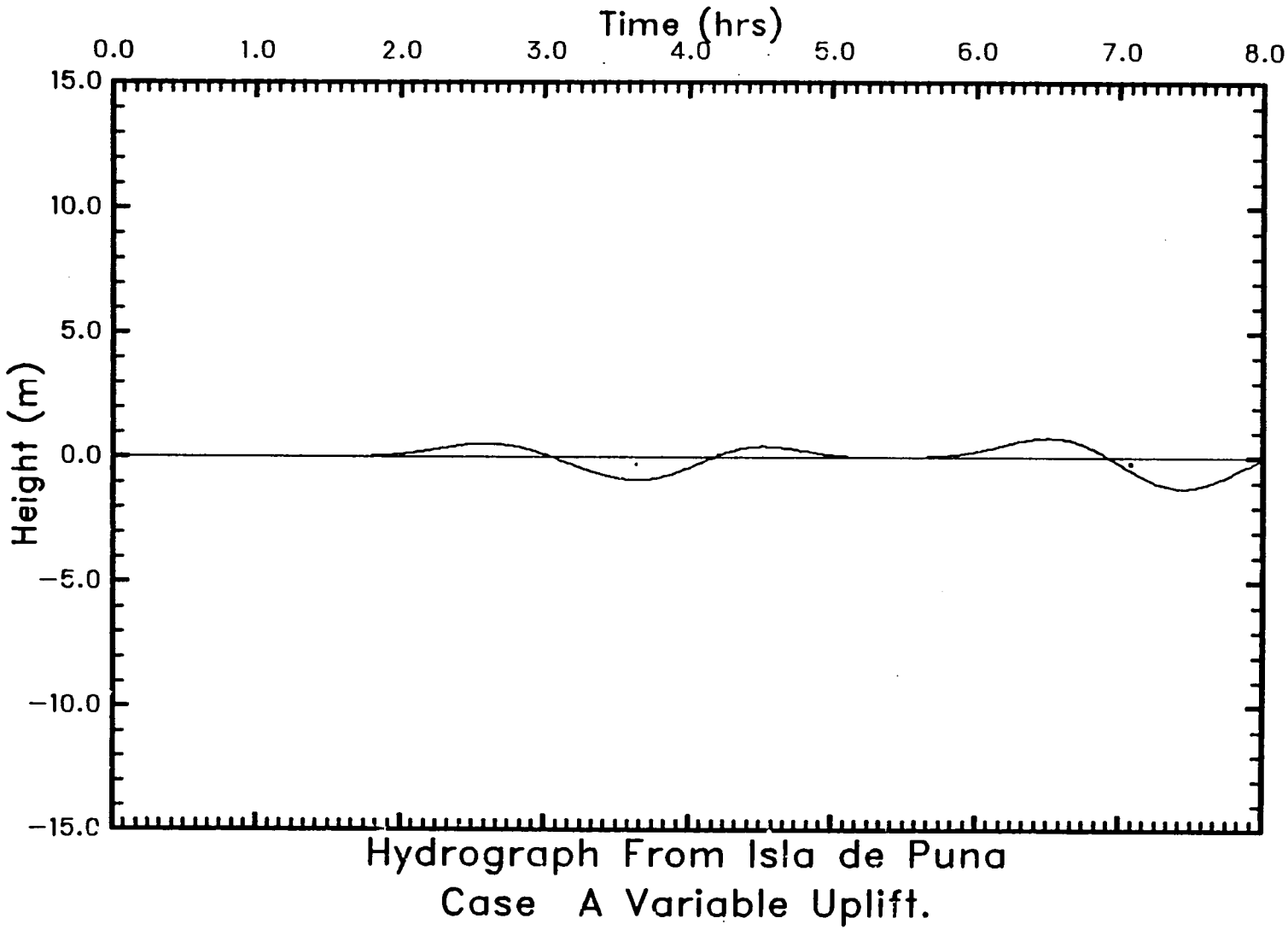

Figure 4.13: Wave elevation as a function of time at the recording point near Isla de Puna, Colombia. These waves were generated by the variable uplift of Zone A.

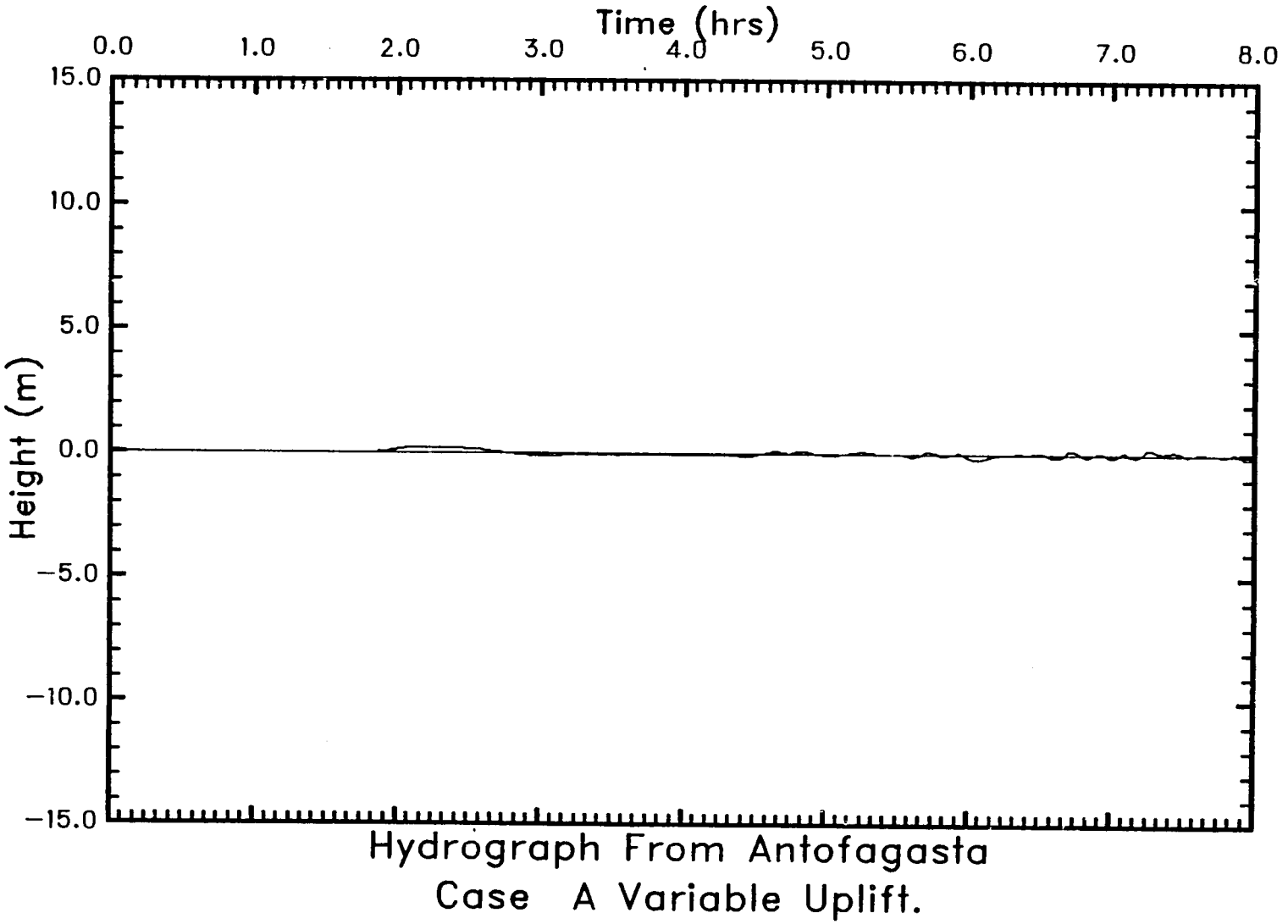

Figure 4.14: Wave elevation as a function of time at the recording point near Antofagasta, Chile. These waves were generated by the variable uplift of Zone A.

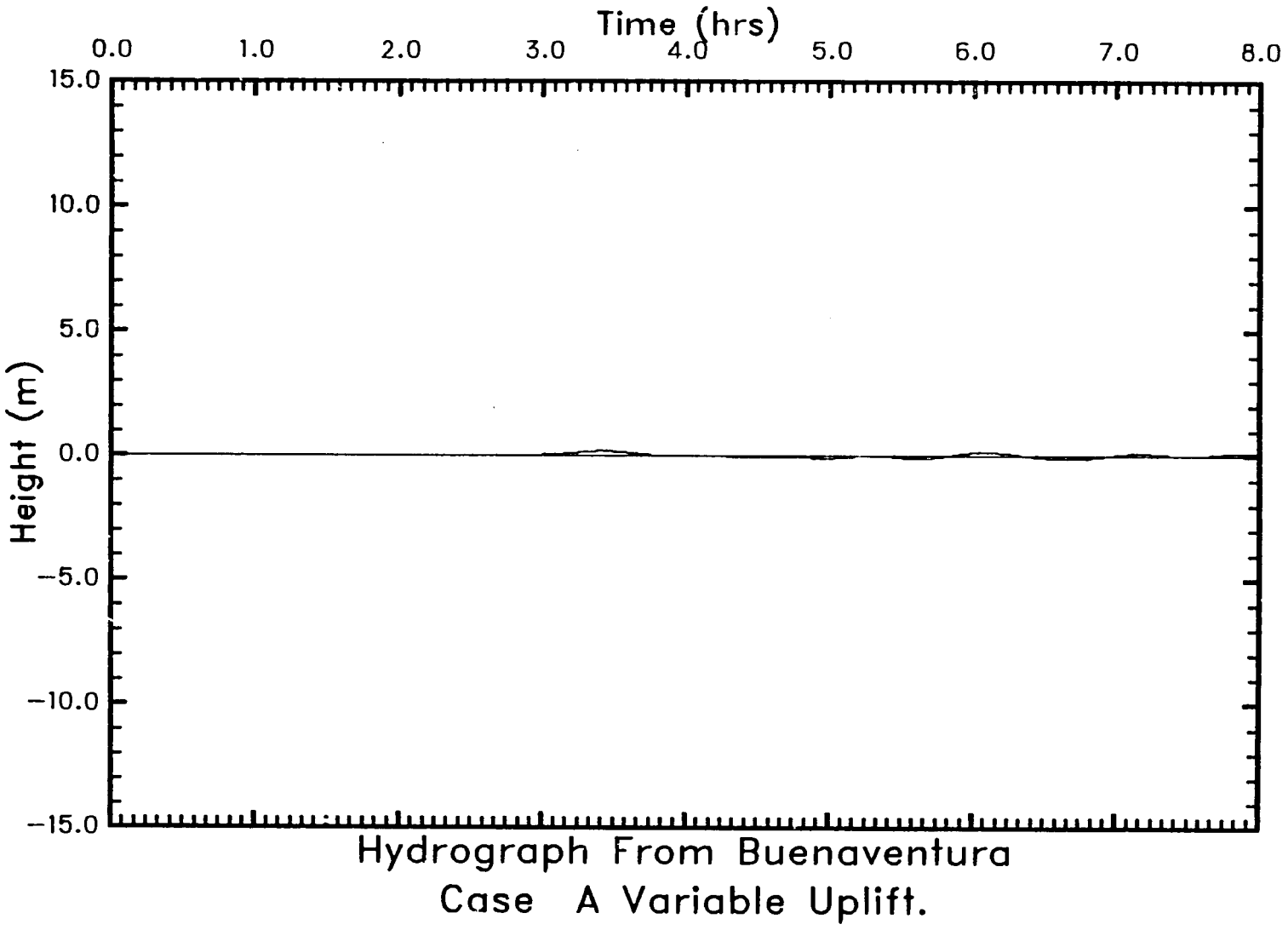

Figure 4.15: Wave elevation as a function of time at the recording point near Buenaventura, Ecuador. These waves were generated by the variable uplift of Zone A.

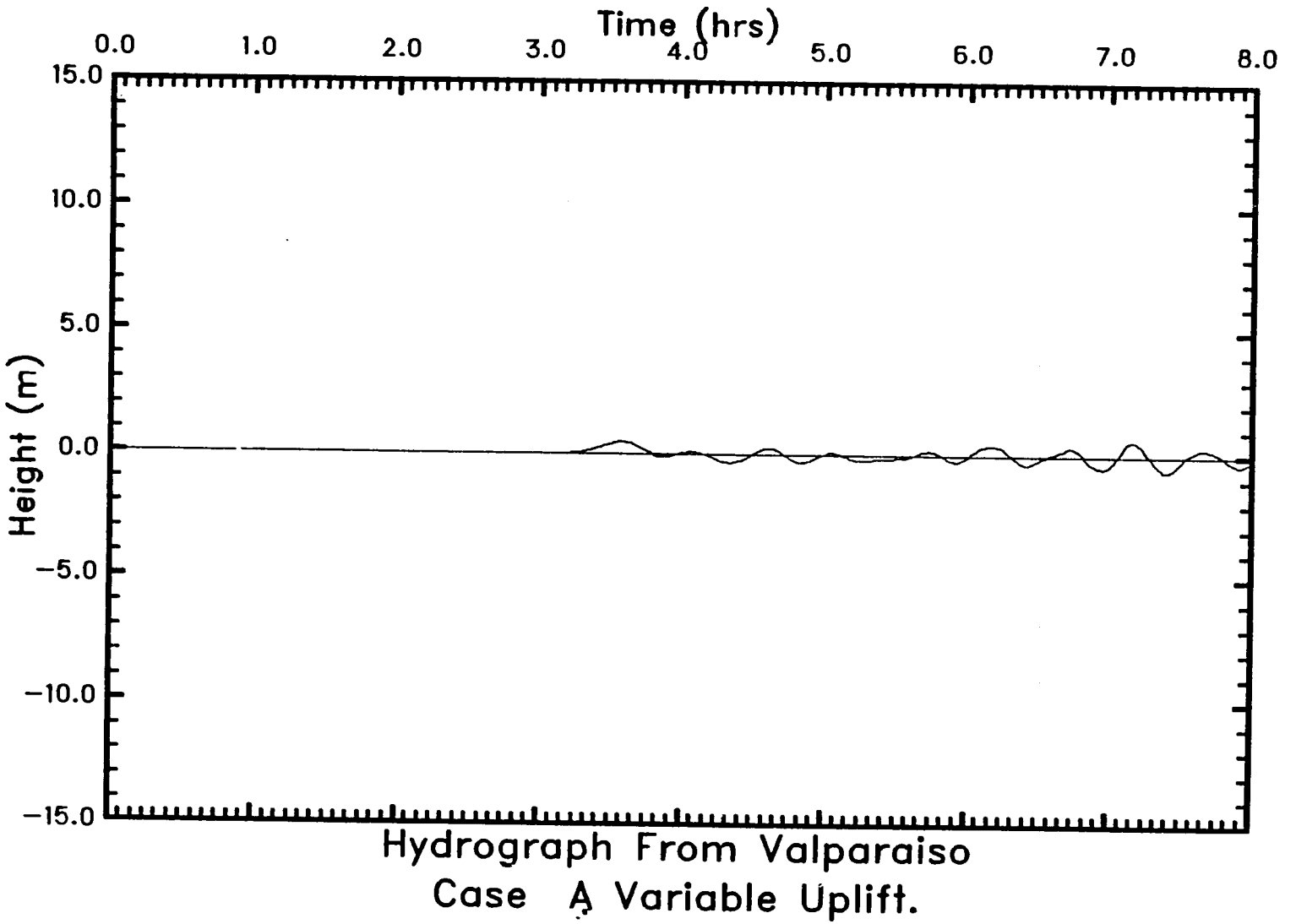

Figure 4.16: Wave elevation as a function of time at the recording point near Valparaiso, Chile. These waves were generated by the variable uplift of Zone A.

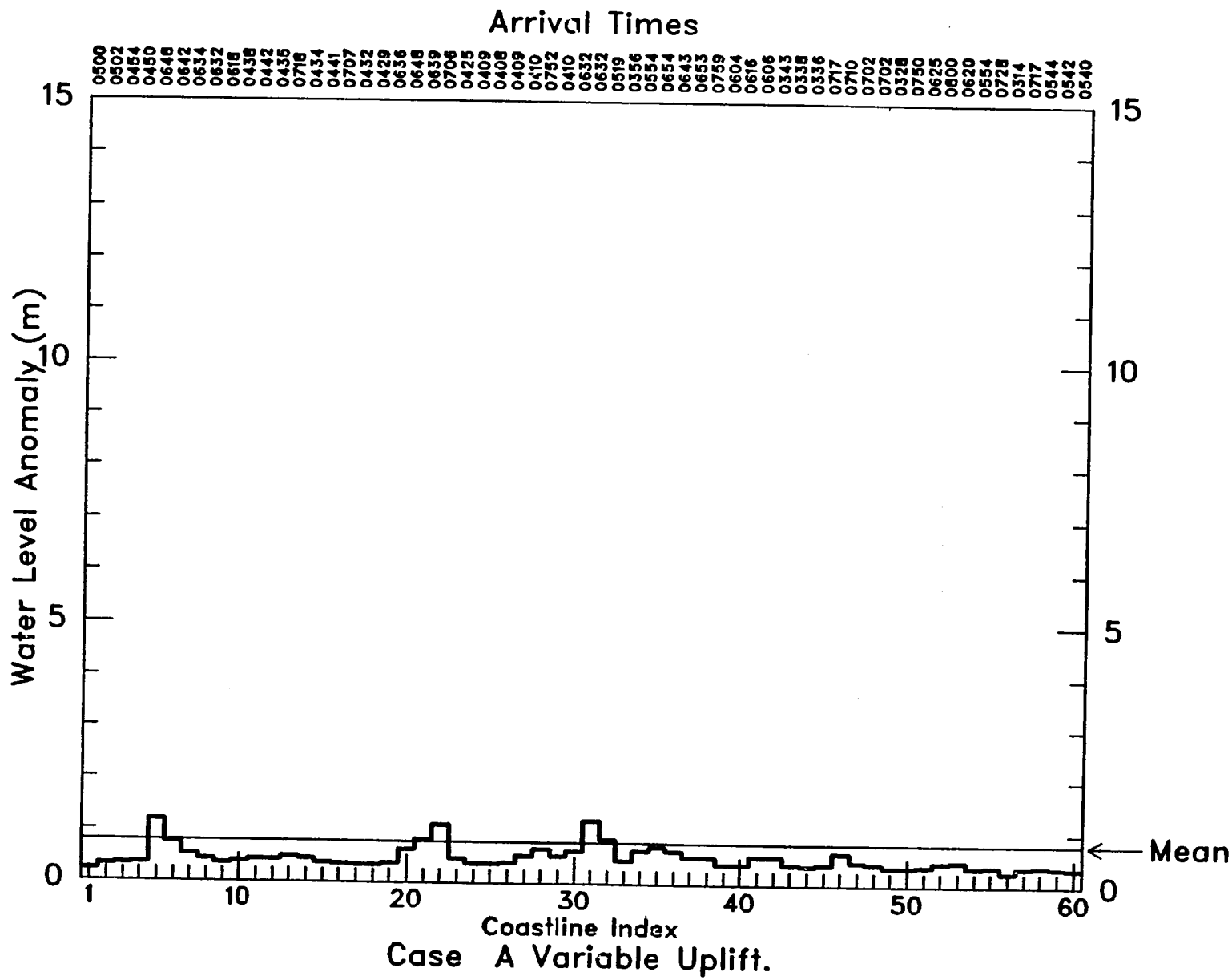

Figure: 4.17 (b)

Previous Page Blank

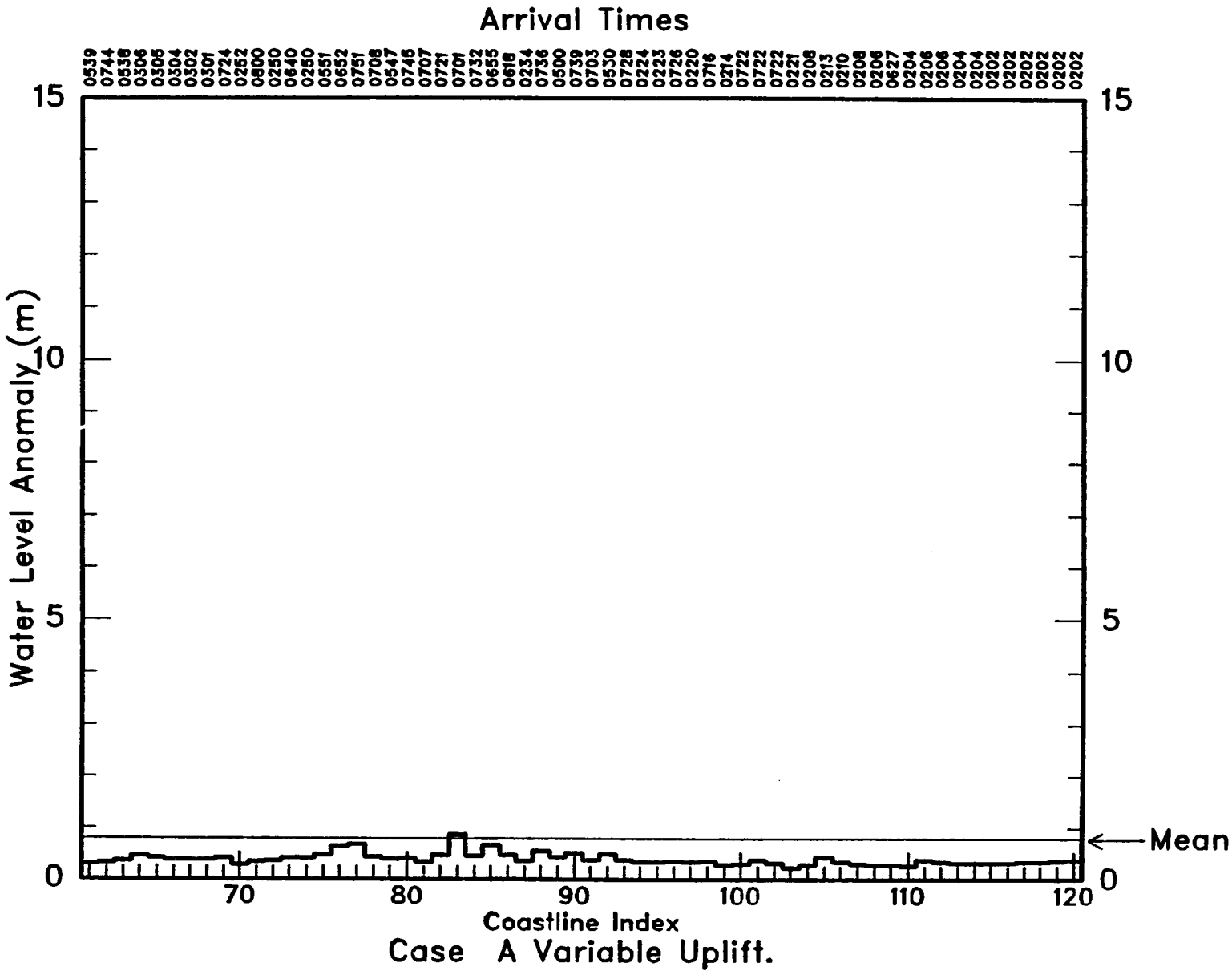
Arrival Times
0539 0744 0538 0306 0305 0304 0302 0301 0724 0252 0800 0250 0640 0250 0551 0652 0751 0708 0547 0746 0707 0721 0701 0732 0655 0618 0234 0736 0500 0739 0703 0530 0728 0224 0223 0726 0220 0716 0214 0722 0722 0721 0221 0208 0213 0210 0208 0206 0627 0204 0206 0206 0204 0204 0202 0202 0202 0202 0202 0202 0202
15
10
5
0
Water Level Anomaly (m)
70
80
90
100
110
120
Coastline Index
Mean
Case A Variable Uplift.

Figure: 4.17 (c)

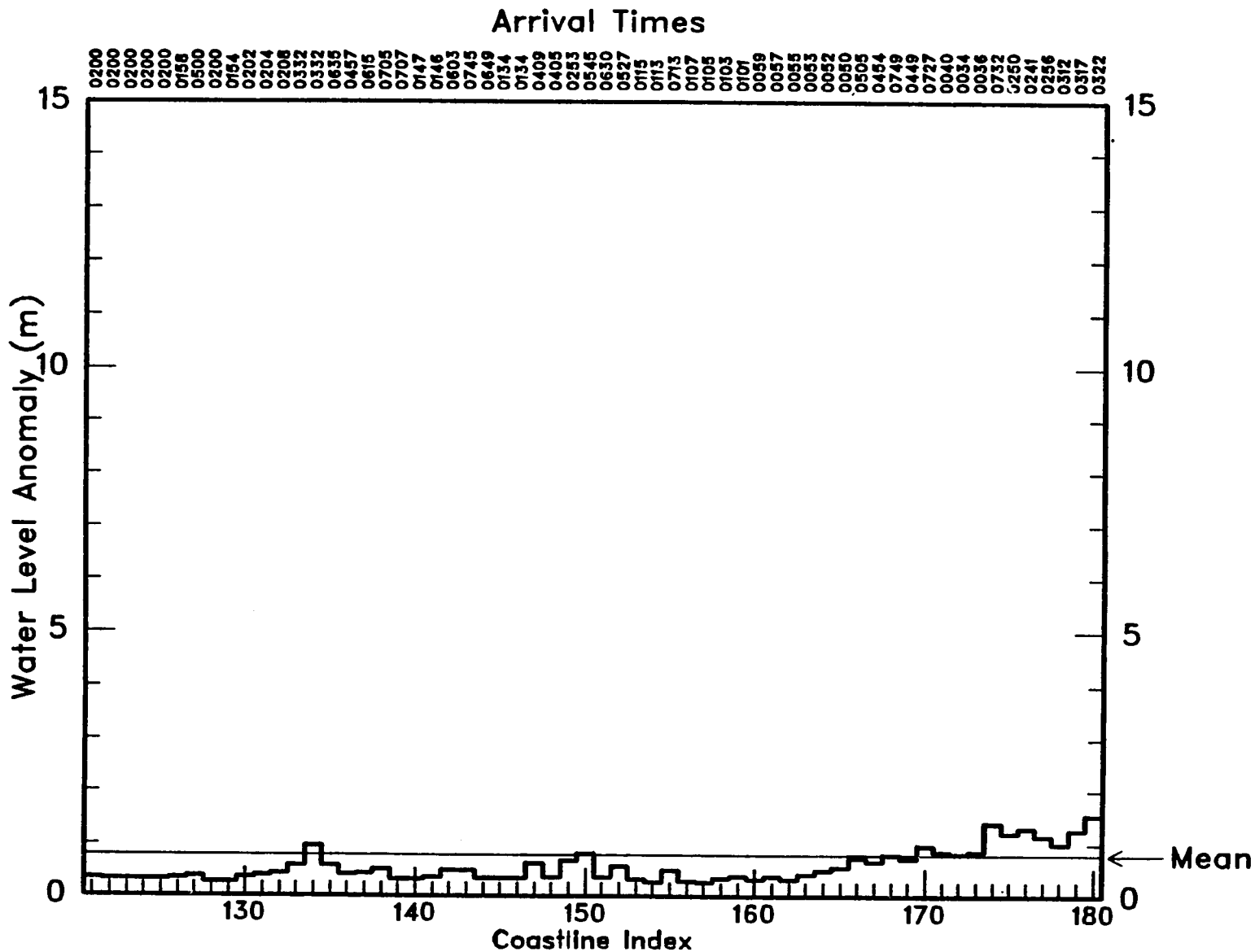

Case A Variable Uplift.

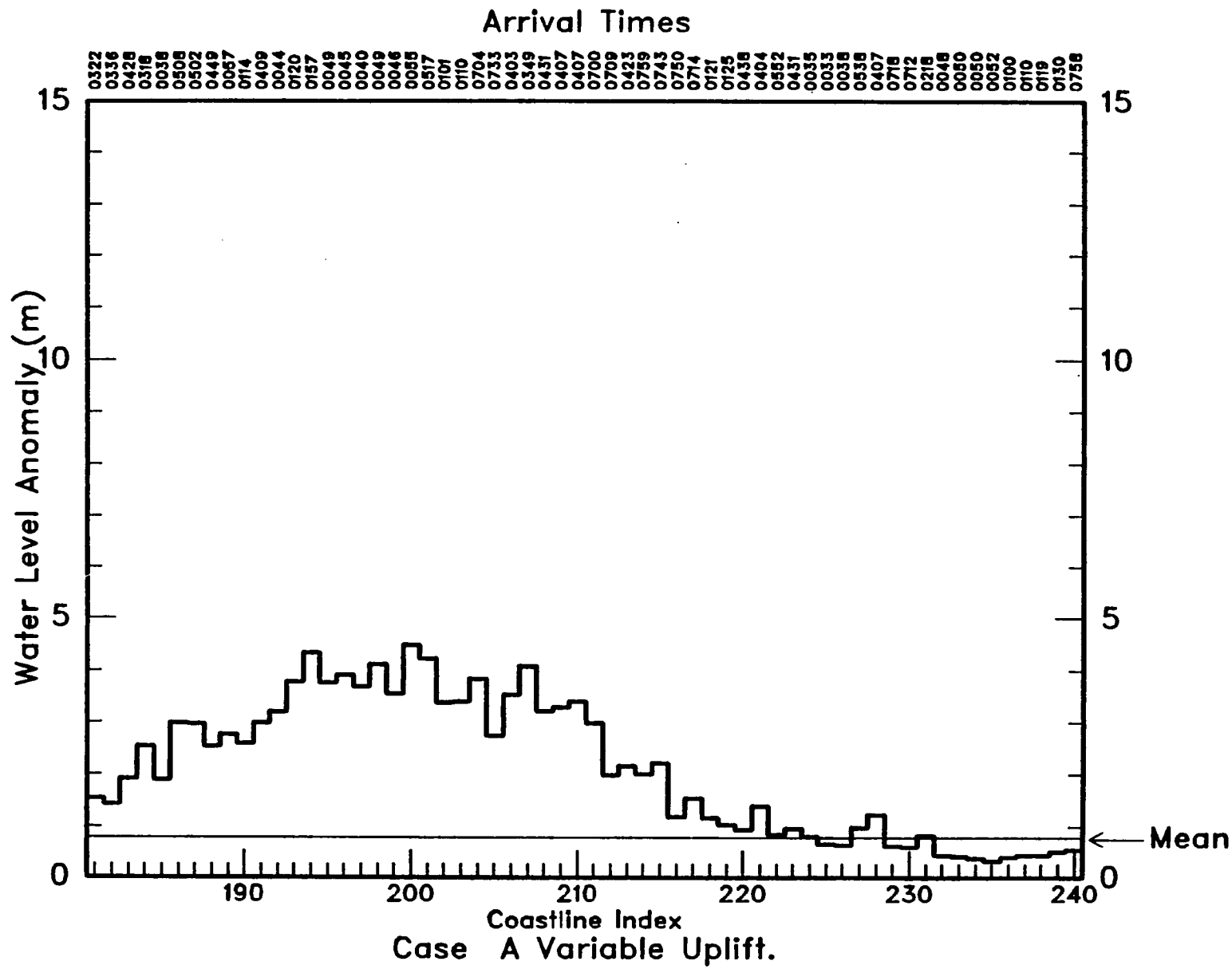
Arrival Times
0322 0336 0428 0318 0038 0508 0502 0449 0057 0114 0409 0044 0120 0157 0049 0045 0040 0049 0046 0055 0517 0101 0110 0704 0733 0403 0349 0431 0407 0407 0700 0709 0423 0759 0743 0750 0714 0121 0125 0438 0404 0552 0431 0035 0033 0038 0538 0407 0718 0712 0218 0048 0050 0050 0052 0100 0110 0119 0130 0758
Water Level Anomaly (m)
15
10
5
0
190
200
210
220
230
240
Mean
Coastline Index
Case A Variable Uplift.

Figure: 4.17 (e)

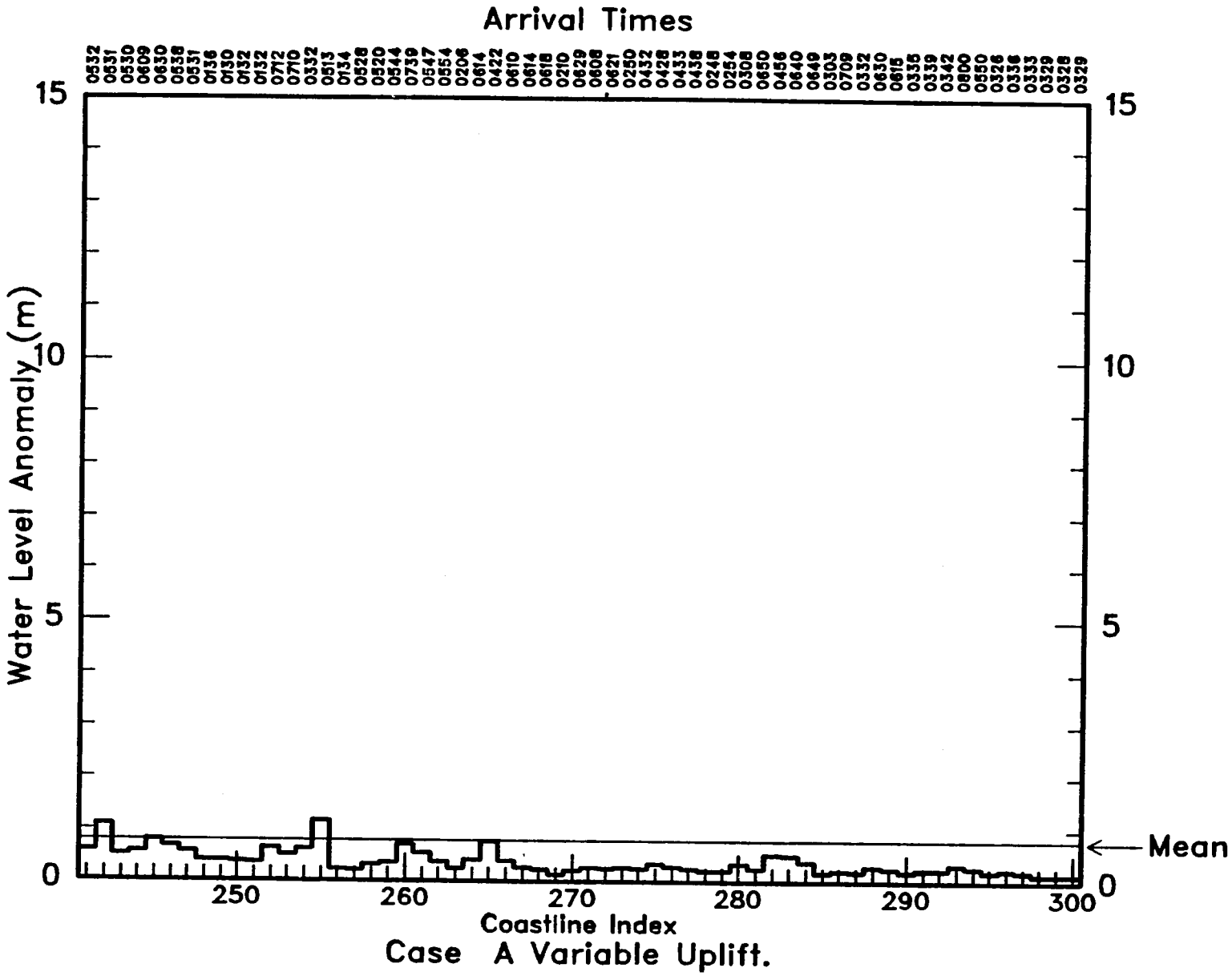
Arrival Times
0532 0531 0530 0609 0630 0538 0531 0136 0130 0132 0132 0712 0710 0332 0513 0134 0528 0520 0544 0739 0547 0554 0206 0614 0422 0610 0614 0618 0210 0629 0608 0621 0250 0432 0428 0433 0438 0248 0254 0308 0650 0456 0640 0649 0303 0709 0332 0630 0615 0335 0339 0342 0800 0550 0326 0336 0333 0329 0328 0329
Water Level Anomaly (m)
15
10
5
0
250
260
270
280
290
300
Coastline Index
Mean
Case A Variable Uplift.

Figure: 4.17 (f)

4.4 GENERAL HAZARD ASSESSMENT

In the previous subsections we have examined the results of each individual uplift simulation separately. While some intercomparison between the two cases is desirable, for the most part each case is evaluated on its own merits. The main purpose of these subsections is to help the reader interpret model results and develop an understanding of the evolution of a tsunami under a specific set of conditions. The primary orientation is toward the way in which wave height (and energy) is distributed along the coast.

The purpose of the following Hazard Assessment subsection (and similar subsections in the next four major sections) is to examine the similarities and differences between the simulations for two different types of uplift. Some repetition of information from the discussions of individual cases naturally occurs, but the emphasis is on treating the two cases as different facets of one phenomenon--tsunamis originating in a specific source zone. The result is an assessment of the threat to South American coastal zones from tsunamigenic earthquakes in each source area.

4.5 HAZARD ASSESSMENT - ZONE A

The major difference between the two simulations, of course, is the height of the waves calculated. The mean maximum water elevation along the coast is only 0.8 m for the variable uplift case, but just over 2.0 m for the uniform uplift case. The tsunami generated by the uniform uplift is the more energetic of the two, and as such poses a greater potential threat.

Once we look past the wave elevations we find that the two sets of results are quite similar. For example, comparing hydrographs at the same location between cases shows that the time variations in waves at each point are nearly identical. For example, not only do first arrival times agree to within a few minutes, but later arrivals agree well, also.

The patterns of wave height distribution are also quite similar, although the arrival times for the various maxima vary by as much as several hours. In both cases the most severe wave threat falls between points 165 and 235. Occasional, less extreme peaks appear to the north and south.

We cannot answer the question of how threatening is a 1 m or 5 m wave height offshore of a specific coastal area without further careful study. Thus any reference we make to "threatening" vs. "non-threatening" is purely subjective. We tend to decide that waves a meter or less in height do not pose a serious threat, and that anything higher than 3 m is very threatening. Using this rough rule of thumb leads us to conclude that many more coastal locations are under a potential threat from the uniform uplift than from the variable uplift, but that roughly the same coastal areas in the

immediate vicinity of the source are under a severe threat in either case.

Before leaving this case, we need to discuss the differences between the uniform and variable uplift sources. The uniform uplift obviously produces higher waves because more potential energy (taken as the square of the surface wave displacement integrated over the source area) is pumped into the ocean. But another key difference concerns the energy composition of the waves. The uniform uplift produces what is essentially a broad band (almost white) pulse, with nearly constant energy over a wide range of frequencies. The variable uplift produces a spectrum which is rich in energy over a narrower band and rolls off on either side of this band.

Each body of water, whether it be an ocean basin, a submarine canyon, or a continental shelf, responds to certain wave frequencies more than others. If an incoming wave has significant energy at one of these frequencies, the resulting resonance will act to increase wave amplitudes; conversely, if the wave is poor in energy at the resonant frequencies, little amplification will occur. The waves from the uniform uplift are more likely to contain energy at resonant frequencies because they contain high energy over a wider range of frequencies to begin with. This explains, at least in part, the occasionally dramatic differences between coastal results for the two types of uplift.

Section 5
SOURCE ZONE B

5.1 INTRODUCTION

Source zone B extends from 16°S to 24°S. The entire area is about 900 km long and straddles the bend in the continent near 18°S. Because of this bend we break the zone into two smaller zones, one north and one south of the bend. Both zones are taken to be 300 km long. The area of the bend itself is not used as a source zone for reasons stated previously. The northern zone lies just south of the Nazca Ridge. The locations of both source zones are shown in Figure 5.1.

5.2 NORTHERN ZONE - UNIFORM UPLIFT CASE

In this case the entire northern area depicted in Figure 5.1 displaces 10 m vertically. As we mentioned in Section 4, the actual uplift area used in the model is quasi-rectangular.

5.2.1 Immediate Effects

The contours of the surface waves an hour after generation by this uplift are shown in Figure 5.2. Again, it is obvious that, one hour after generation, the main direction of propagation is to the southwest, into the open Pacific. Notice, however, the large concentrations of wave energy along the Chilean coast between 18°S and 22°S. Presumably this is the result of topographic focussing by the great bend in the continent.

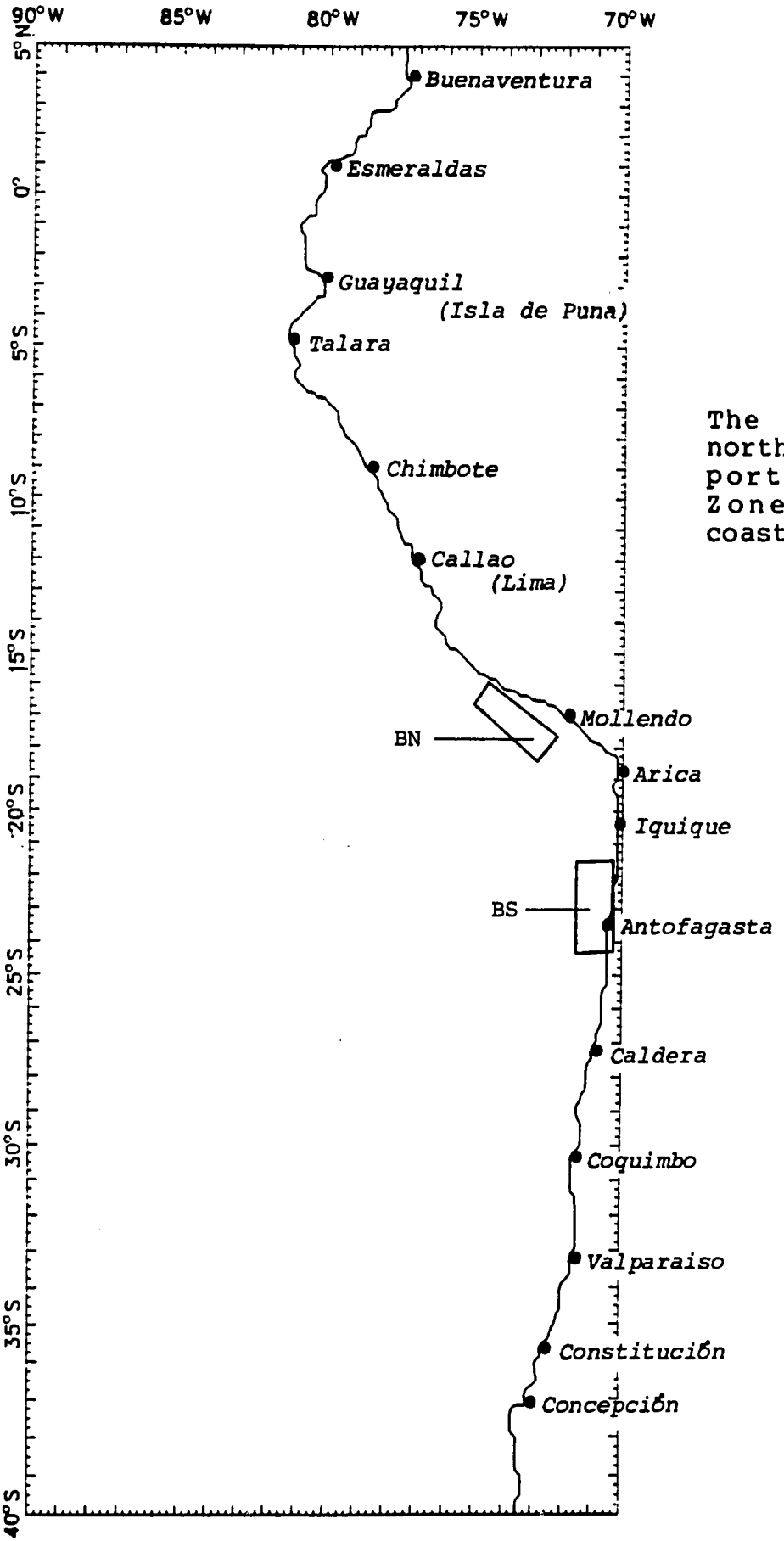

Figure 5.1:

The location of the northern and southern portions of source Zone B along the coastline.

5.2.2 Longer Duration Effects

The two coastal monitoring points which record the highest levels of wave activity are near Arica and Lima. Arica lies south of the zone, but near the continental bend. The time series at this point (Figure 5.3) shows an initial rise of nearly 5 m as the leading edge of the wave passes. Following this early surge is a long, fairly regular succession of extreme surges, which would indicate that a good deal of wave energy is trapped in the area.

The time series near Lima (Figure 5.4) also shows another, somewhat lower initial rise. During the next several hours wave activity is subdued to some extent, until a major surge arrives at about 5.5 hrs. These two occurrences indicate that most of the early wave energy travels along the shelf northward past Lima. The late surge could be due to a pumping-type action in the bend area, where wave energy does persist.

Waves south of Arica are lower and more regular. The record at Antofagasta (Figure 5.5) rises initially but quickly dies off. The waves near Valparaiso (Figure 5.6) are also regular, but are much higher. This may be due to the offshore wave approach described in Section 4.

To the north of the source wave activity drops off quite rapidly. The record near Isla de Puna (Figure 5.7) shows a series of long, low waves, while that near Buenaventura (Figure 5.8) shows only very slight disturbance.

5.2.3 Maximum Elevations

The plots of maximum elevation for this case show that the mean elevation is slightly above 3 m. Thus any concentrations of wave height near or above the mean level would have to be considered a serious threat. In this case the most intense wave activity occurs close to the source. The region extending from the vicinity of Arica to point 170, south of Lima is marked by extreme wave heights, with few maximum values less than 5 m. But wave elevations at or above the mean occur for a long distance north and south of the source. The last such point to the north is close to Talara, Peru, while they occur all the way south past Concepcion, Chile. Only on the coast north of Talara can we say that wave energies are uniformly low.

The peaks south of point 40 are surprisingly high. This is probably due both to local refraction effects and to wave propagation across deep water rather than along the coast.

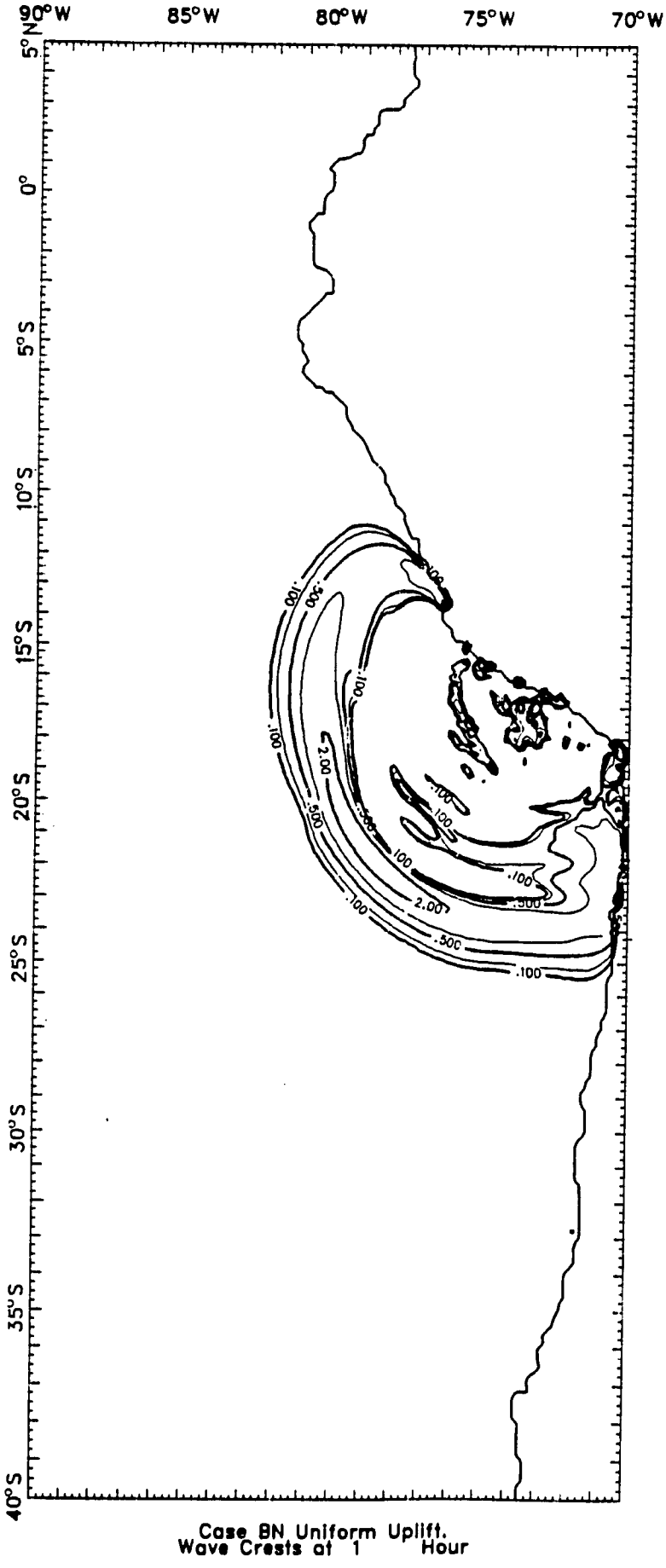

Figure: 5.2

Surface elevation (positive only) one hour after a uniform uplift in the northern portion of source Zone B. Contours correspond to 0.1, 0.2, 0.5, 1.0, and 2.0 m.

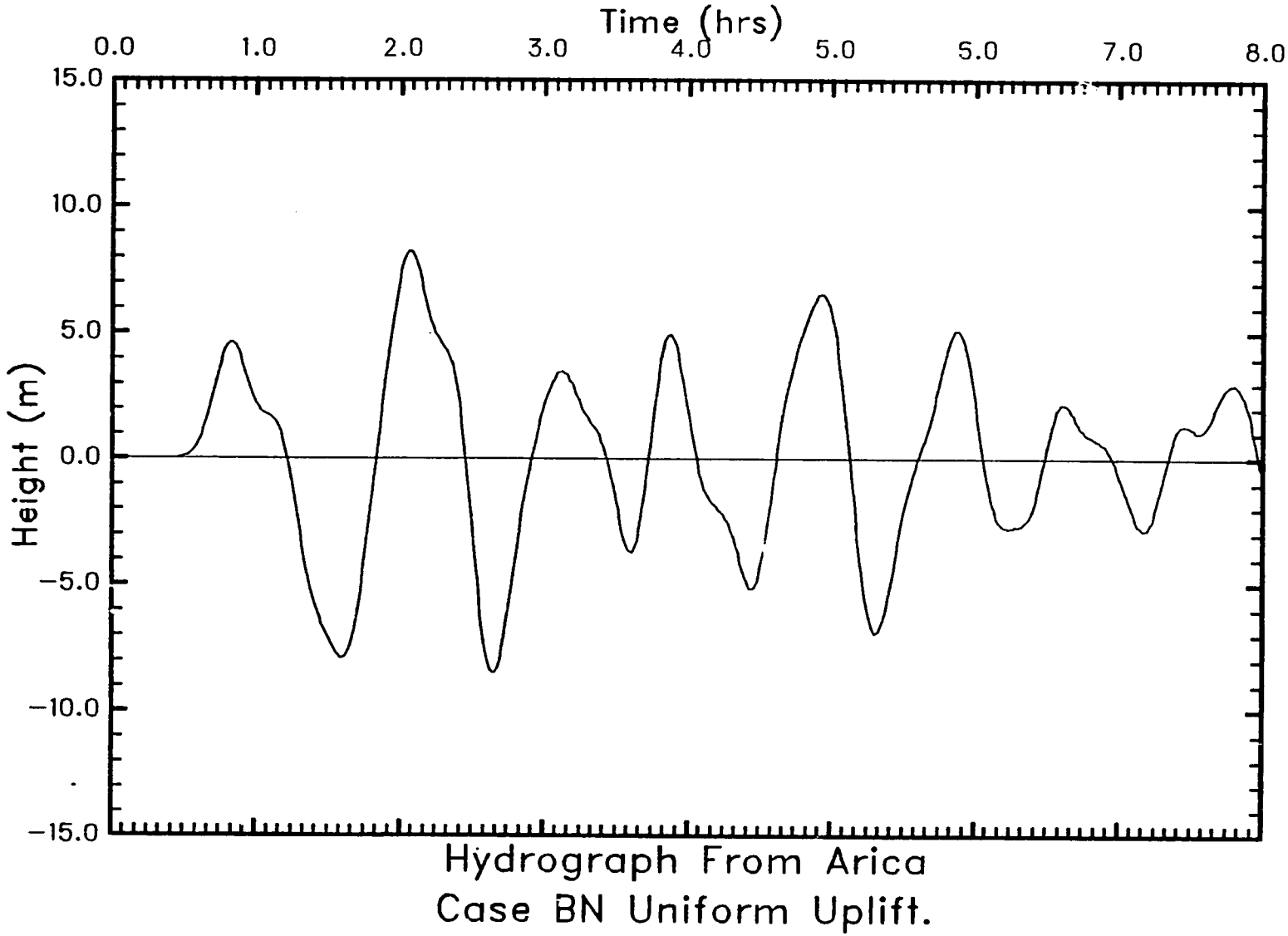

Figure 5.3: Wave elevation as a function of time at the recording point near Arica, Chile. These waves were generated by the uniform uplift of the northern portion of Zone B.

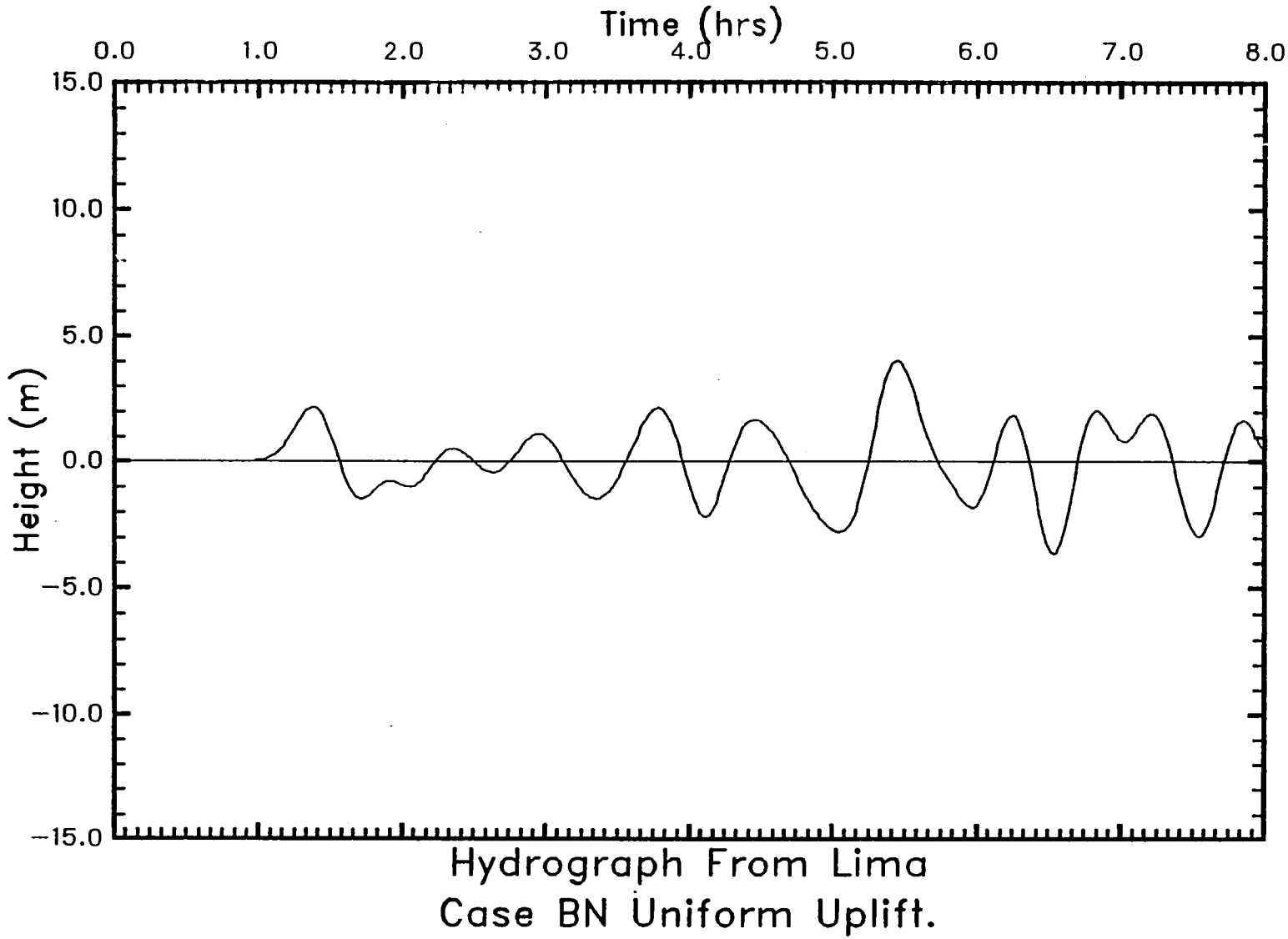

Figure 5.4: Wave elevation as a function of time at the recording point near Lima, Peru. These waves were generated by the uniform uplift of the northern portion of Zone B.

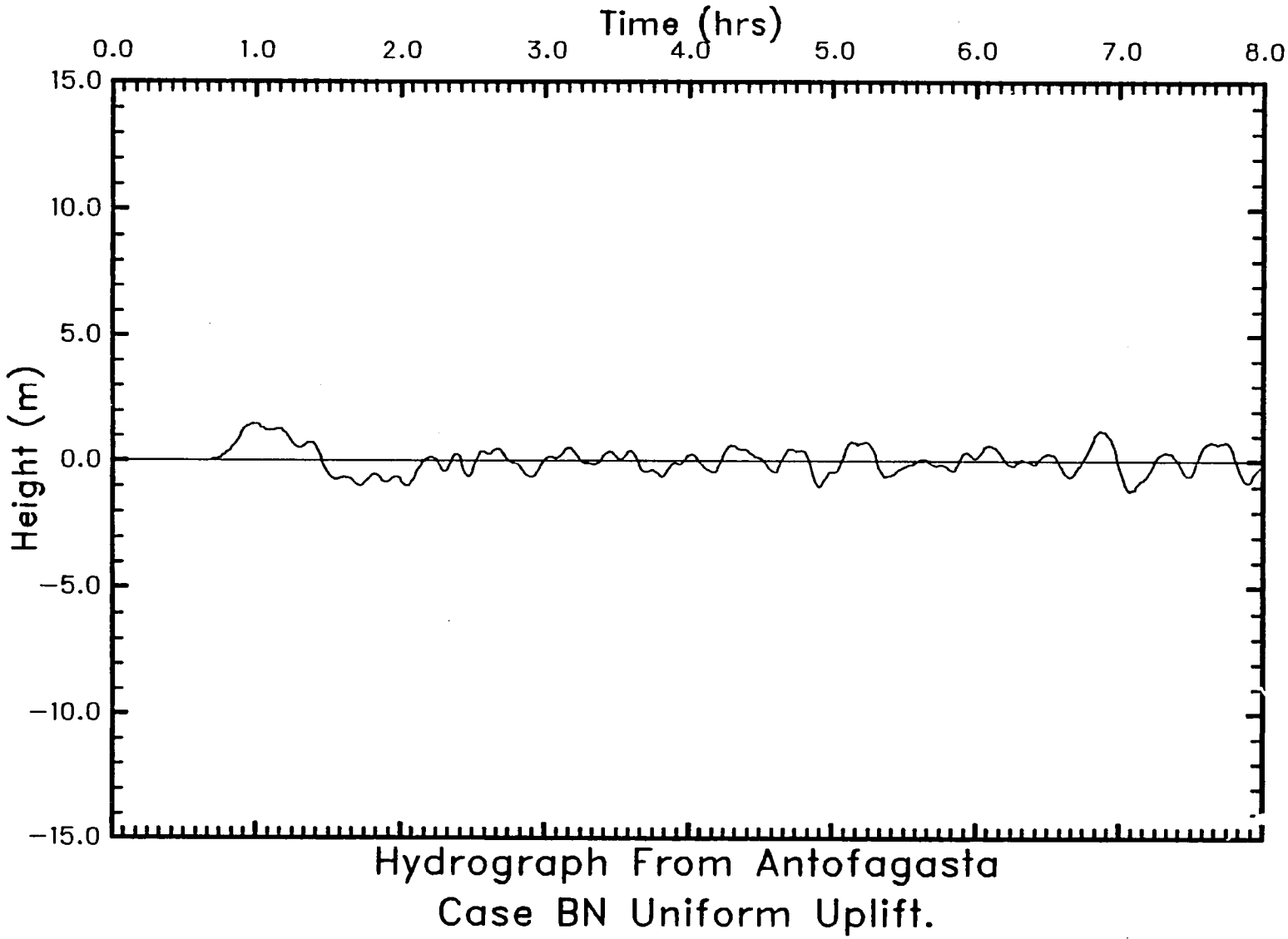

Figure 5.5: Wave elevation as a function of time at the recording point near Antofagasta, Chile. These waves were generated by the uniform uplift of the northern portion of Zone B.

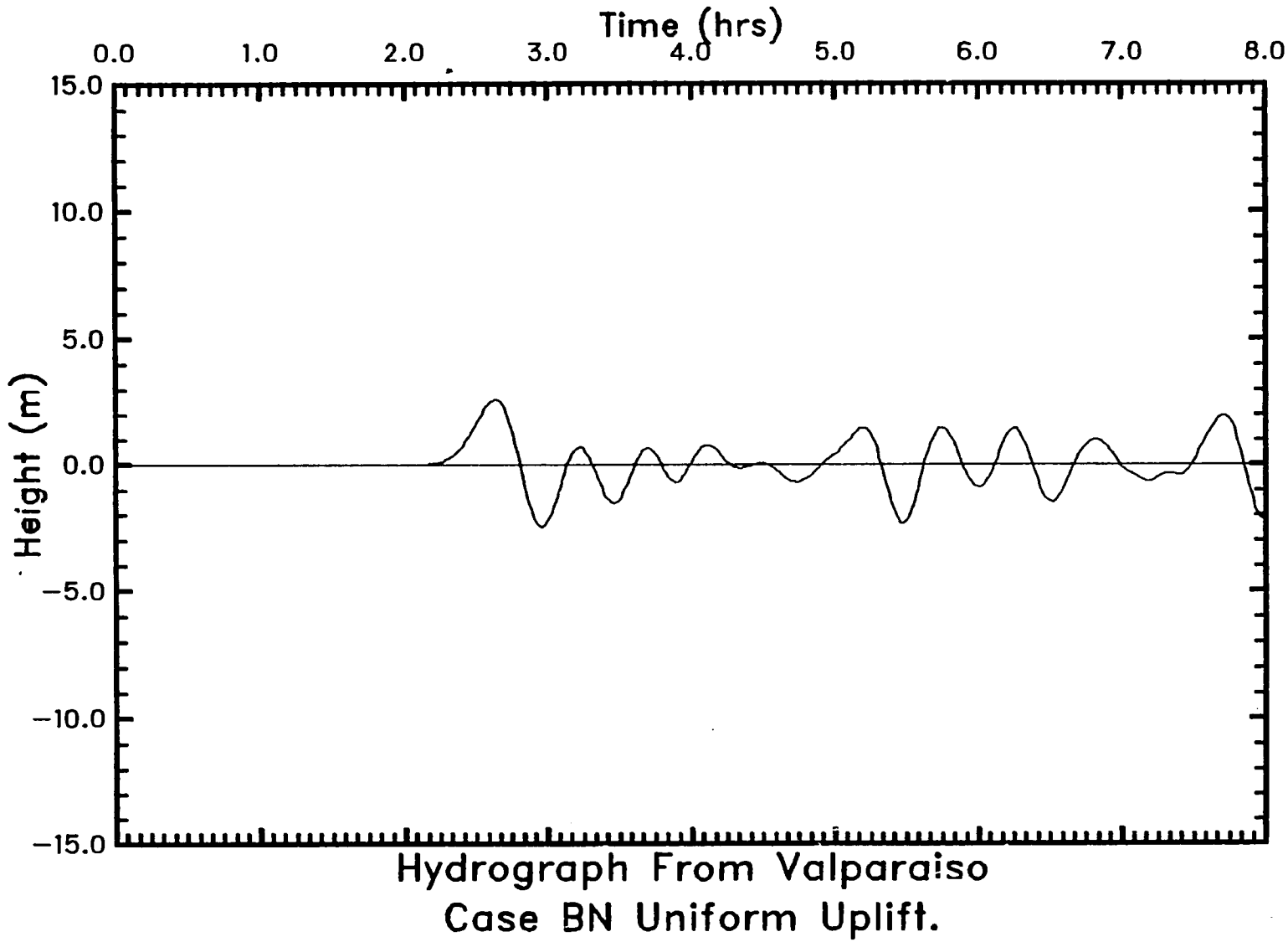

Figure 5.6: Wave elevation as a function of time at the recording point near Valparaiso, Chile. These waves were generated by the uniform uplift of the northern portion of Zone B.

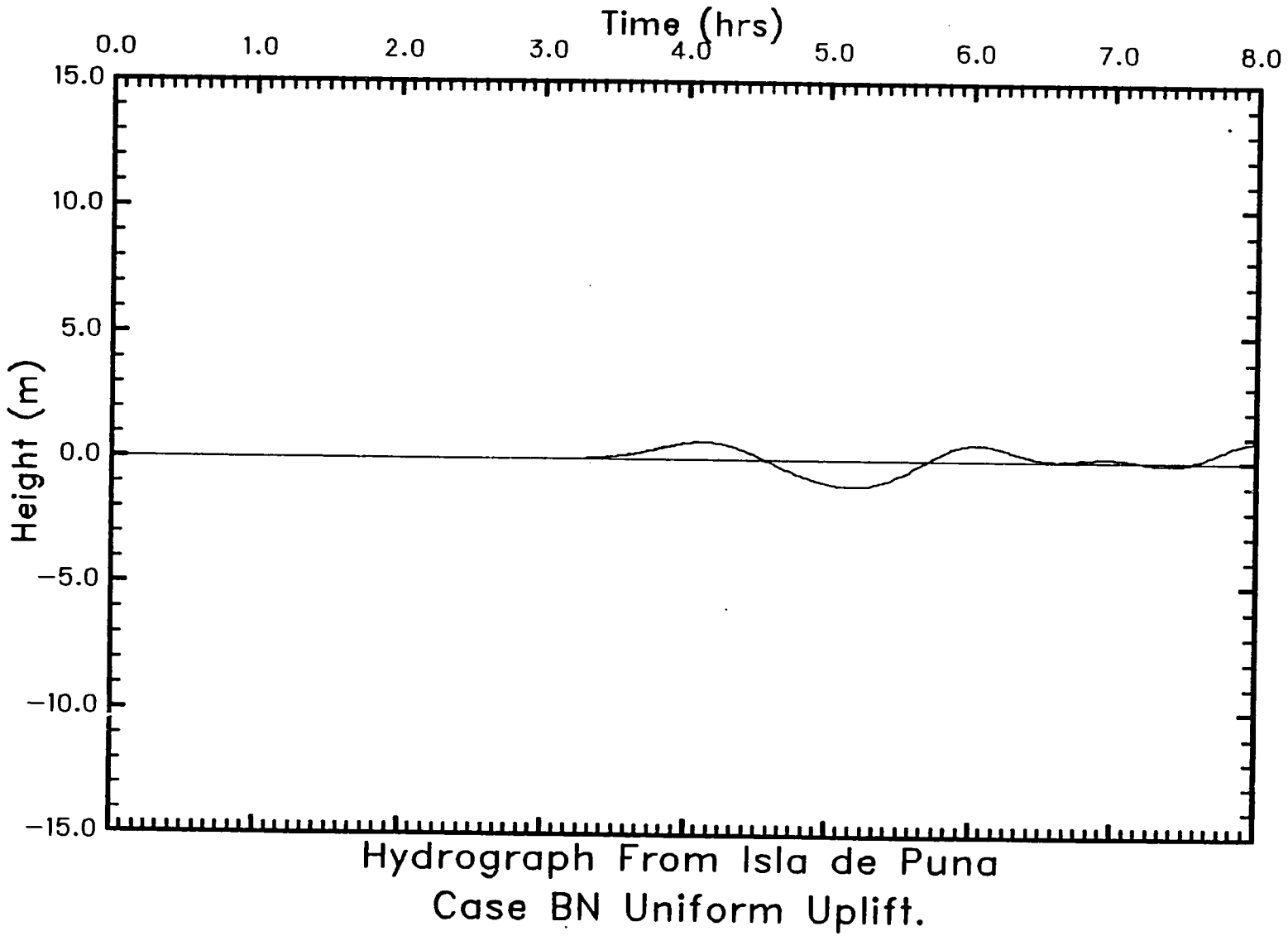

Figure 5.7: Wave elevation as a function of time at the recording point near Isla de Puna, Colombia. These waves were generated by the uniform uplift of the northern portion of Zone B.

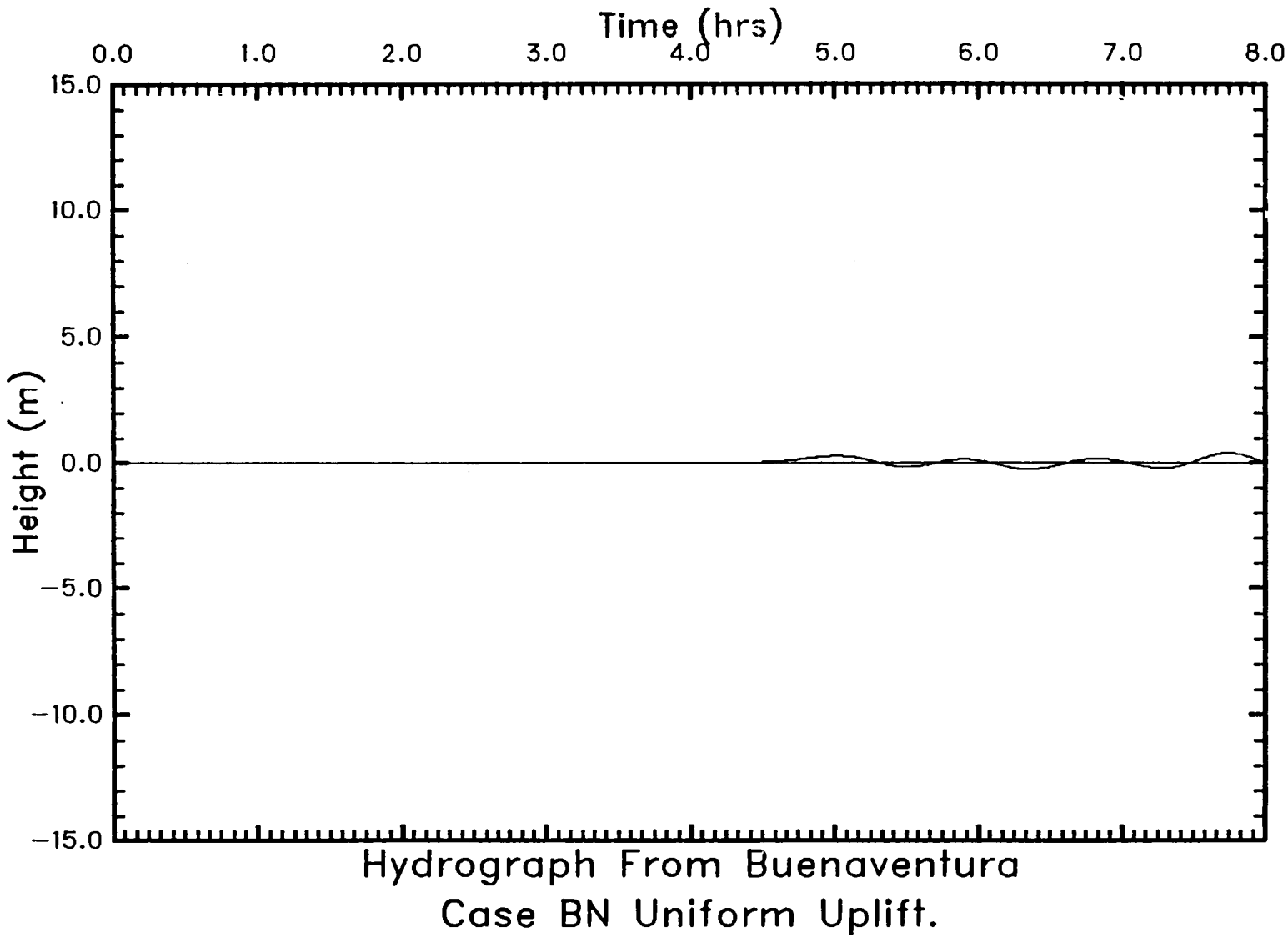

Figure 5.8: Wave elevation as a function of time at the recording point near Buenaventura, Ecuador. These waves were generated by the uniform uplift of the northern portion of Zone B.

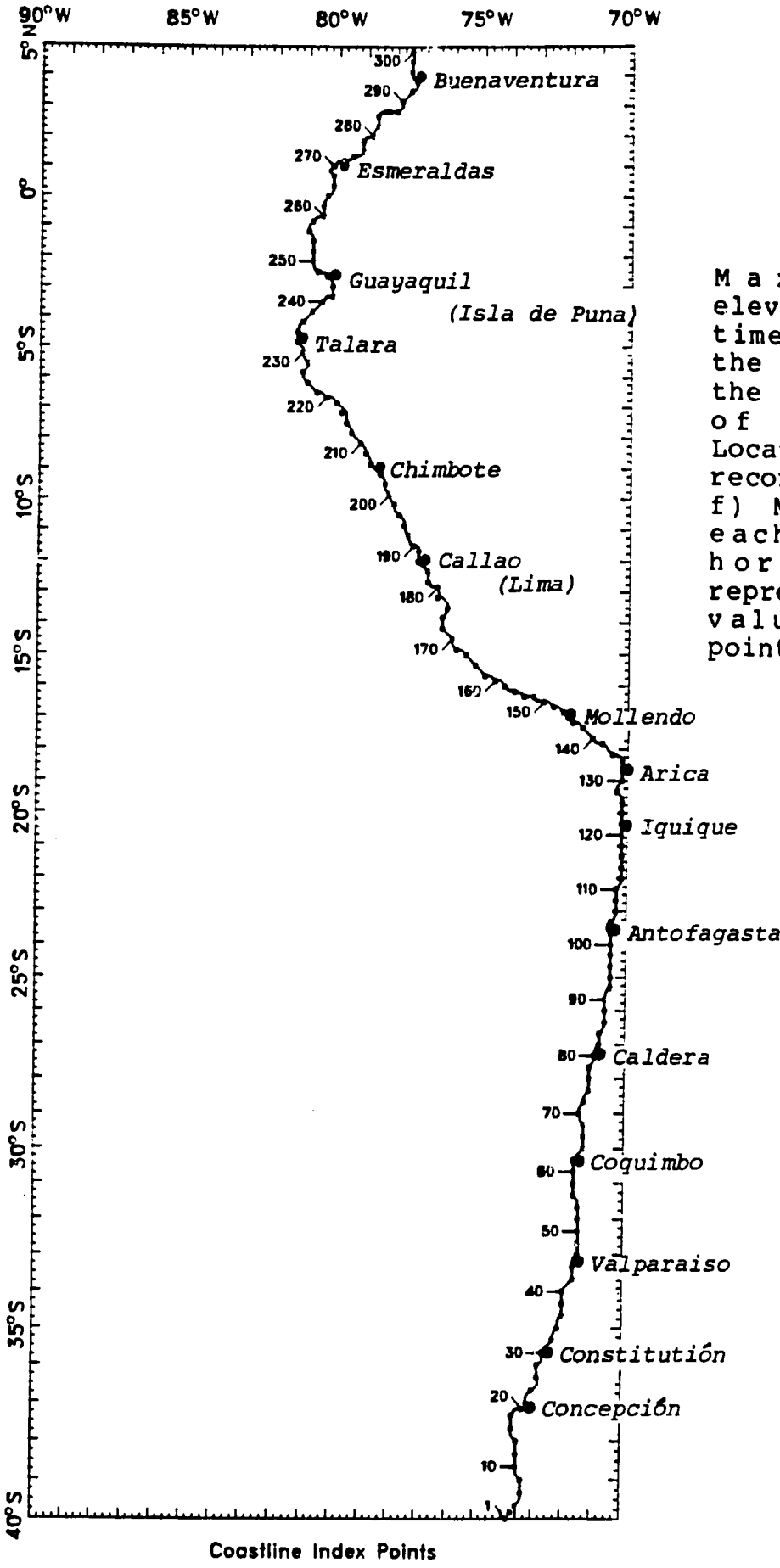

Figure: 5.9

Maximum wave elevations and arrival times of waves from the uniform uplift in the northern portion of Zone B. (a) Locations of the 300 recording points. (b-f) Maximum waves at each point. The horizontal line represents the average value of all 300 points.

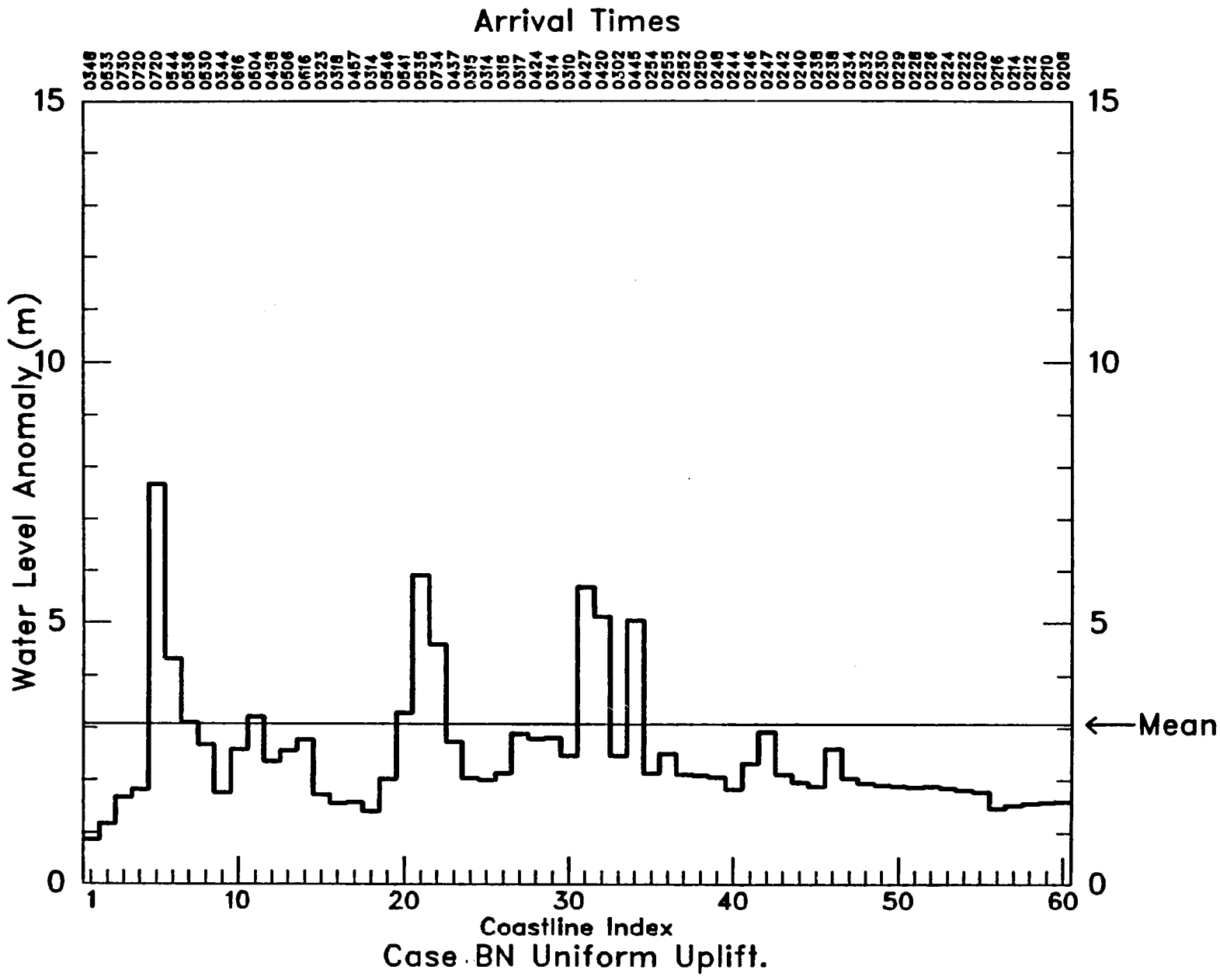
Arrival Times
0348 0533 0730 0720 0720 0544 0536 0530 0344 0616 0504 0438 0506 0616 0323 0318 0457 0314 0546 0541 0535 0734 0437 0315 0314 0315 0317 0424 0314 0310 0427 0420 0302 0445 0254 0255 0252 0250 0248 0244 0246 0247 0242 0240 0238 0238 0234 0232 0230 0229 0228 0226 0224 0222 0220 0216 0214 0212 0210 0208
Water Level Anomaly (m)
15
10
5
0
1
10
20
30
40
50
60
Coastline Index
Mean
Case BN Uniform Uplift.

Figure: 5.9 (b)

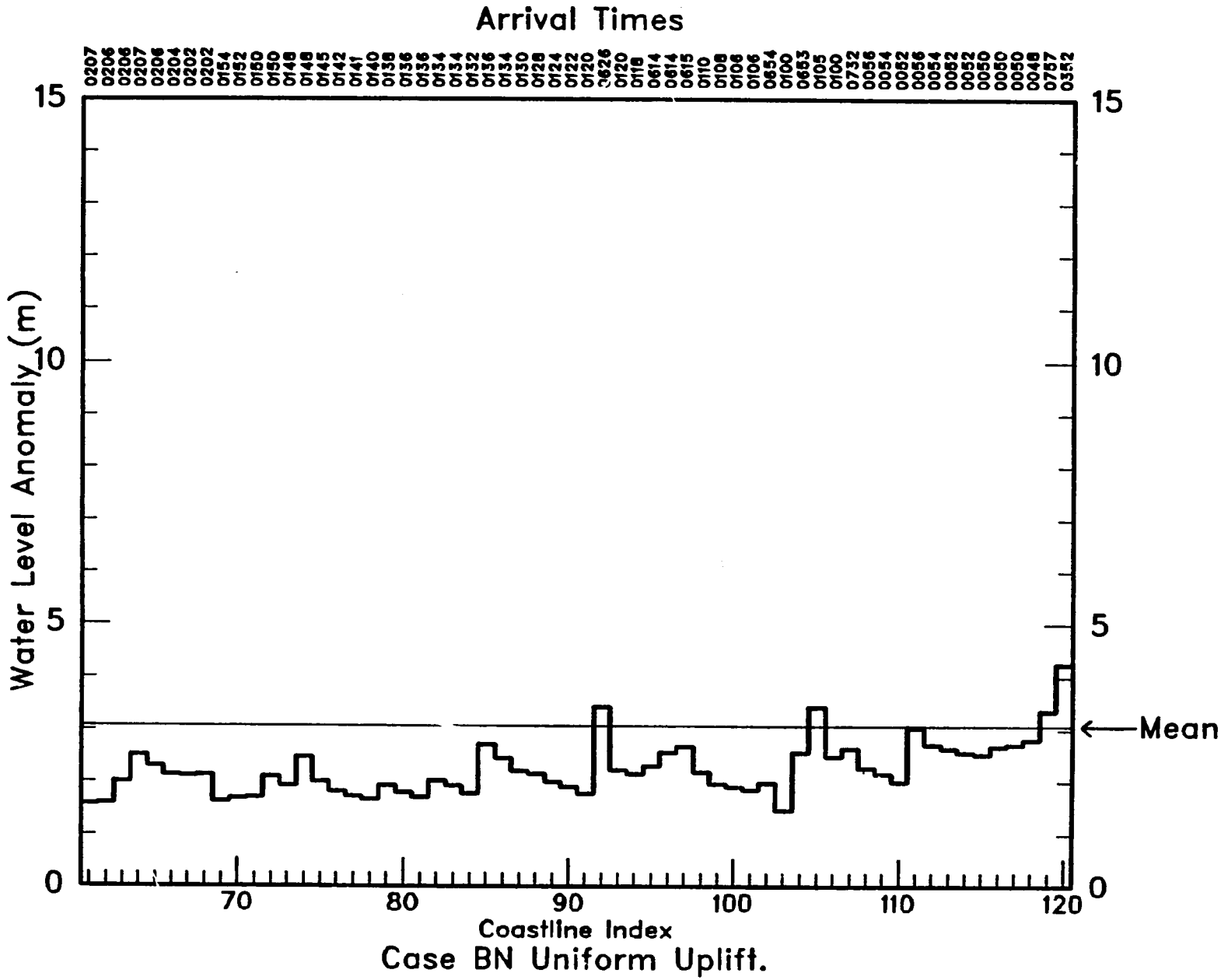
Arrival Times
0207 0206 0206 0207 0206 0204 0202 0202 0154 0152 0150 0150 0148 0148 0145 0142 0141 0140 0138 0136 0136 0134 0134 0132 0136 0134 0130 0128 0124 0122 0120 0626 0120 0118 0614 0614 0615 0110 0108 0106 0106 0654 0100 0653 0105 0100 0732 0056 0054 0052 0056 0054 0052 0052 0050 0050 0050 0048 0757 0352
Water Level Anomaly (m)
15
10
5
0
70
80
90
100
110
120
Mean
Coastline Index
Case BN Uniform Uplift.

Figure: 5.9 (c)

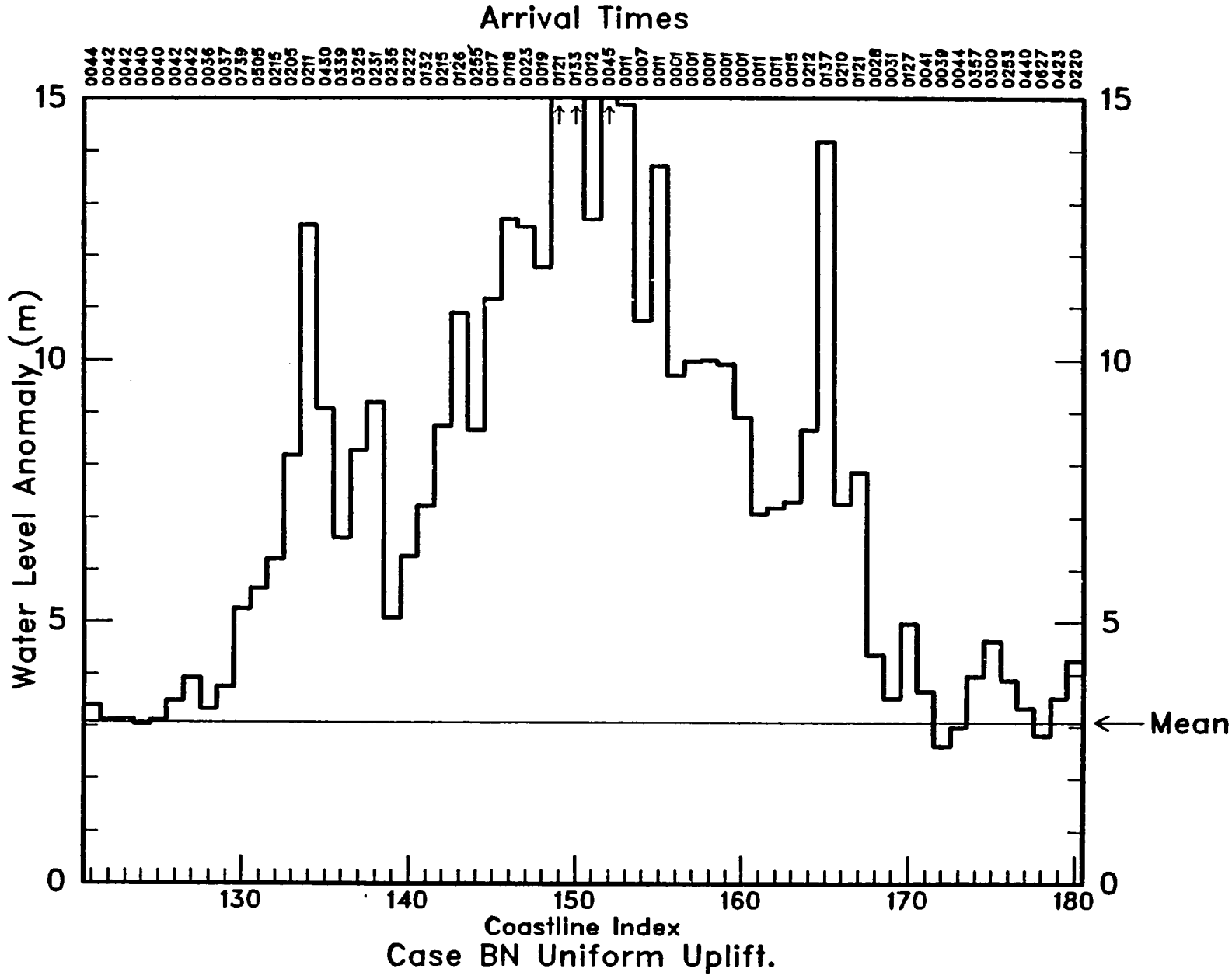
Arrival Times
0044 0042 0042 0040 0040 0042 0042 0036 0037 0739 0505 0215 0205 0211 0430 0339 0325 0231 0235 0222 0132 0215 0126 0255 0017 0018 0023 0019 0121 0133 0012 0045 0011 0007 0011 0001 0001 0001 0001 0001 0011 0011 0015 0212 0137 0210 0121 0028 0031 0127 0041 0039 0044 0357 0300 0253 0440 0627 0423 0220
15
10
5
0
Water Level Anomaly (m)
130
140
150
160
170
180
Coastline Index
Mean
Case BN Uniform Uplift.

Figure: 5.9 (d)

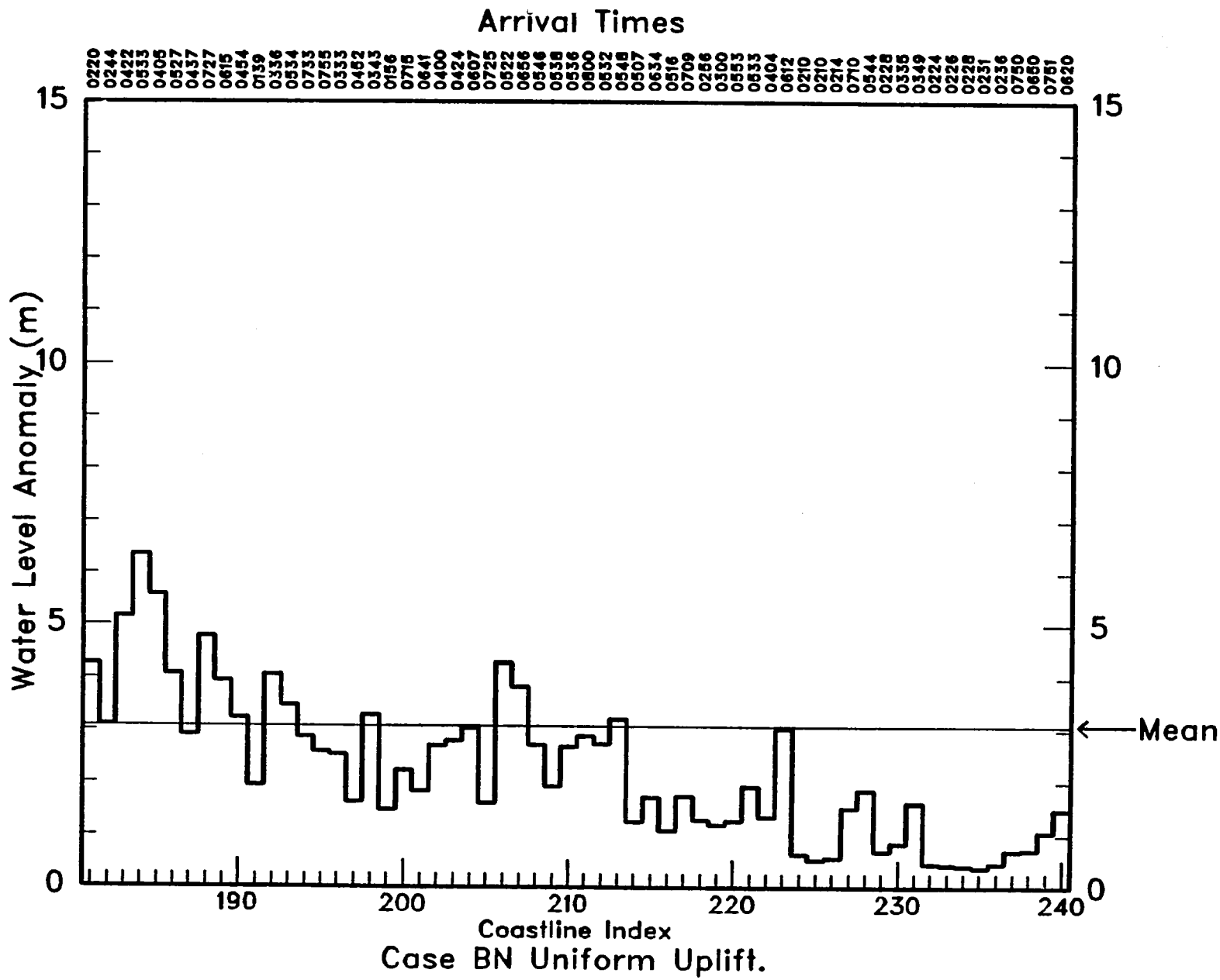
Arrival Times
0220 0244 0422 0533 0405 0527 0437 0727 0615 0454 0139 0336 0534 0733 0755 0333 0452 0343 0156 0715 0641 0400 0424 0607 0725 0522 0656 0546 0538 0536 0800 0532 0548 0507 0634 0516 0709 0256 0300 0553 0533 0404 0612 0210 0210 0214 0710 0544 0228 0335 0349 0224 0226 0228 0231 0236 0750 0650 0751 0620
Water Level Anomaly (m)
0
5
10
15
190
200
210
220
230
240
Mean
Coastline Index
Case BN Uniform Uplift.

Figure: 5.9 (e)

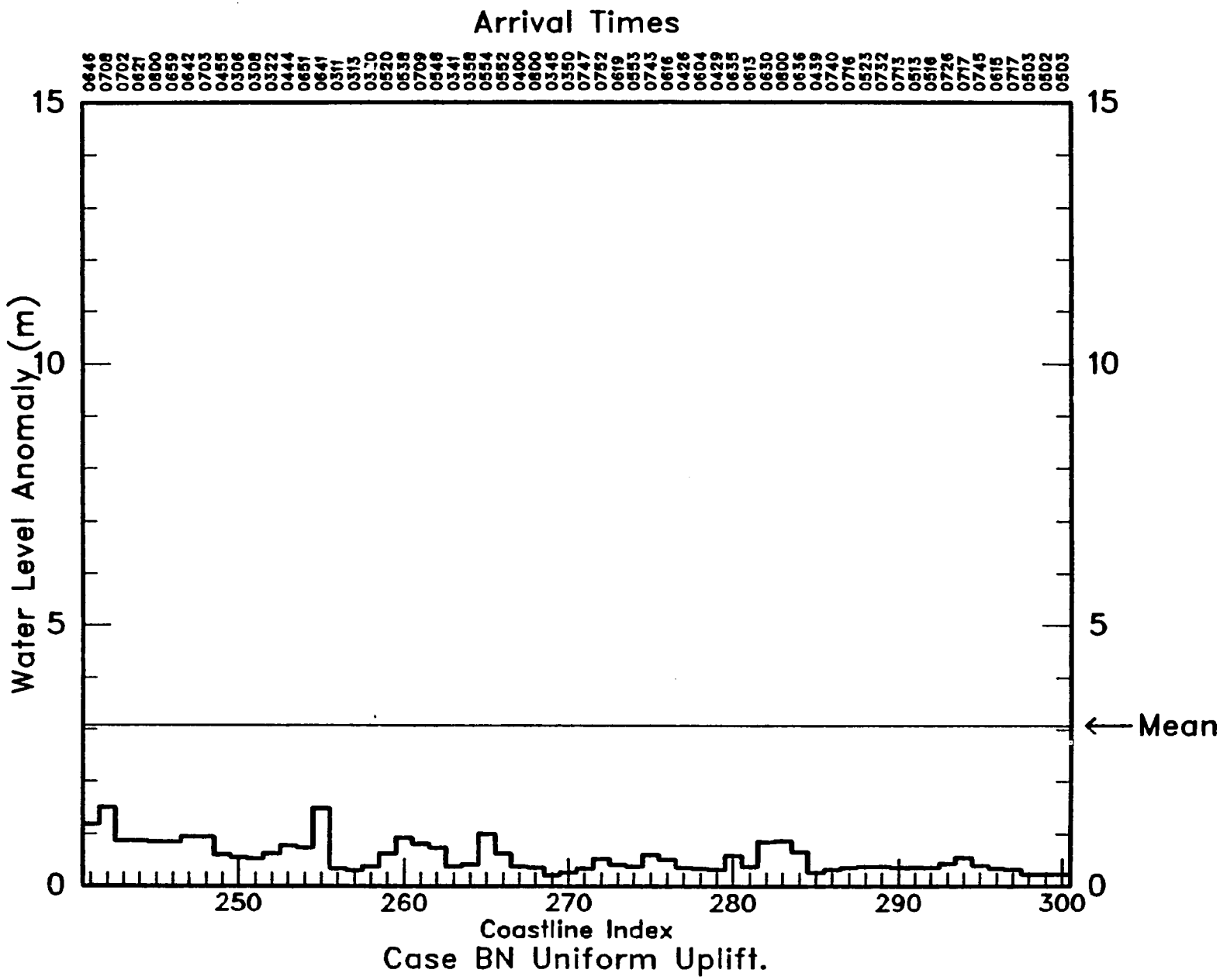
Arrival Times
0646 0708 0702 0621 0800 0659 0642 0703 0455 0306 0308 0322 0444 0651 0641 0311 0313 0320 0520 0538 0709 0548 0341 0358 0554 0552 0400 0800 0346 0350 0747 0752 0619 0553 0743 0616 0426 0604 0429 0635 0613 0630 0800 0636 0439 0740 0716 0523 0732 0713 0513 0516 0726 0717 0745 0615 0717 0503 0502 0503
15
10
5
0
Water Level Anomaly (m)
250
260
270
280
290
300
Coastline Index
Mean
Case BN Uniform Uplift.

Figure: 5.9 (f)

5.3 NORTHERN ZONE - VARIABLE UPLIFT CASE

The uplift pattern in this case fills the northern zone depicted in Figure 5.1. The maximum displacement is taken to be 10 m.

5.3.1 Immediate Effects

The wave elevation contours after one hour are shown in Figure 5.10. As in the uniform uplift case, the main body of waves is moving seaward toward the southwest. Several strong secondary crests are apparent, also. Some of this is due to reflections from the coastline as the initial mound breaks into two components--the seaward wave and the shoreward wave. This latter wave reaches the coast and is reflected back to sea sometime after the initial crest has left the source zone.

Some of this trailing wave activity is also the result of reflections from the coast in the vicinity of the coastal bend. Much of the wave pattern between 20°S and 22°S is no doubt due to this.

Note that wave elevations are concentrated at several locations along the coast, and not exclusively in the source zone.

5.3.2 Longer Duration Effects

The waves first reach Arica (Figure 5.11). Here they are quite high (crests close to 5 m) and persist for a long period of time. Once again this leads us to believe that wave energy is trapped in the vicinity of the coastline bend.

Waves reaching Lima (Figure 5.12) are somewhat longer and a good deal lower. But they also persist for the full simulation.

Antofagasta receives low, fairly high frequency waves which also persist (Figure 5.13); once again the waves farther south at Valparaiso have higher elevations and longer periods (Figure 5.14). Waves to the north of the source at Isla de Puna (Figure 5.15) and Buenaventura (Figure 5.16) are very long and low.

5.3.3 Maximum Elevations

This uplift pattern sends wave energies at fairly high levels all along the coast, except to the portion north of Talara (see Figure 5.17a-f). The extreme wave amplitudes are nearly all clustered near the source zone, between points 130 and 170. But a large number of locations outside that range receive wave elevations at or above (in some southern locations, far above) the overall mean level of 2.0 m. Waves at or near that level could pose a severe threat to low-lying coastal areas and would have to be considered a potential hazard.

This source motion produces a very energetic tsunami which has at least the potential to threaten areas over nearly the entire coastline, even though the greatest danger lies close to the source.

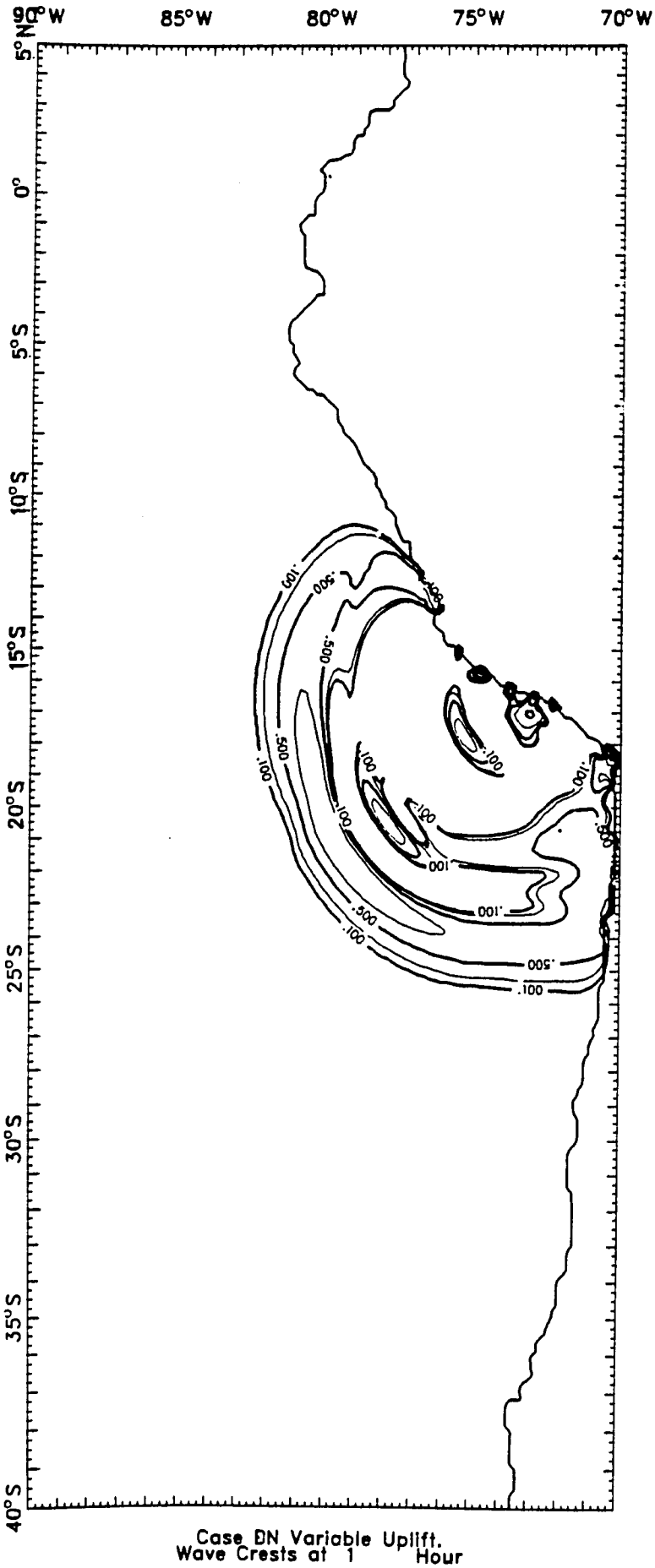

Figure: 5.10

Surface elevation (positive only) one hour after a variable uplift in the northern portion of source Zone B. Contours correspond to 0.1, 0.2, 0.5, 1.0, and 2.0 m.

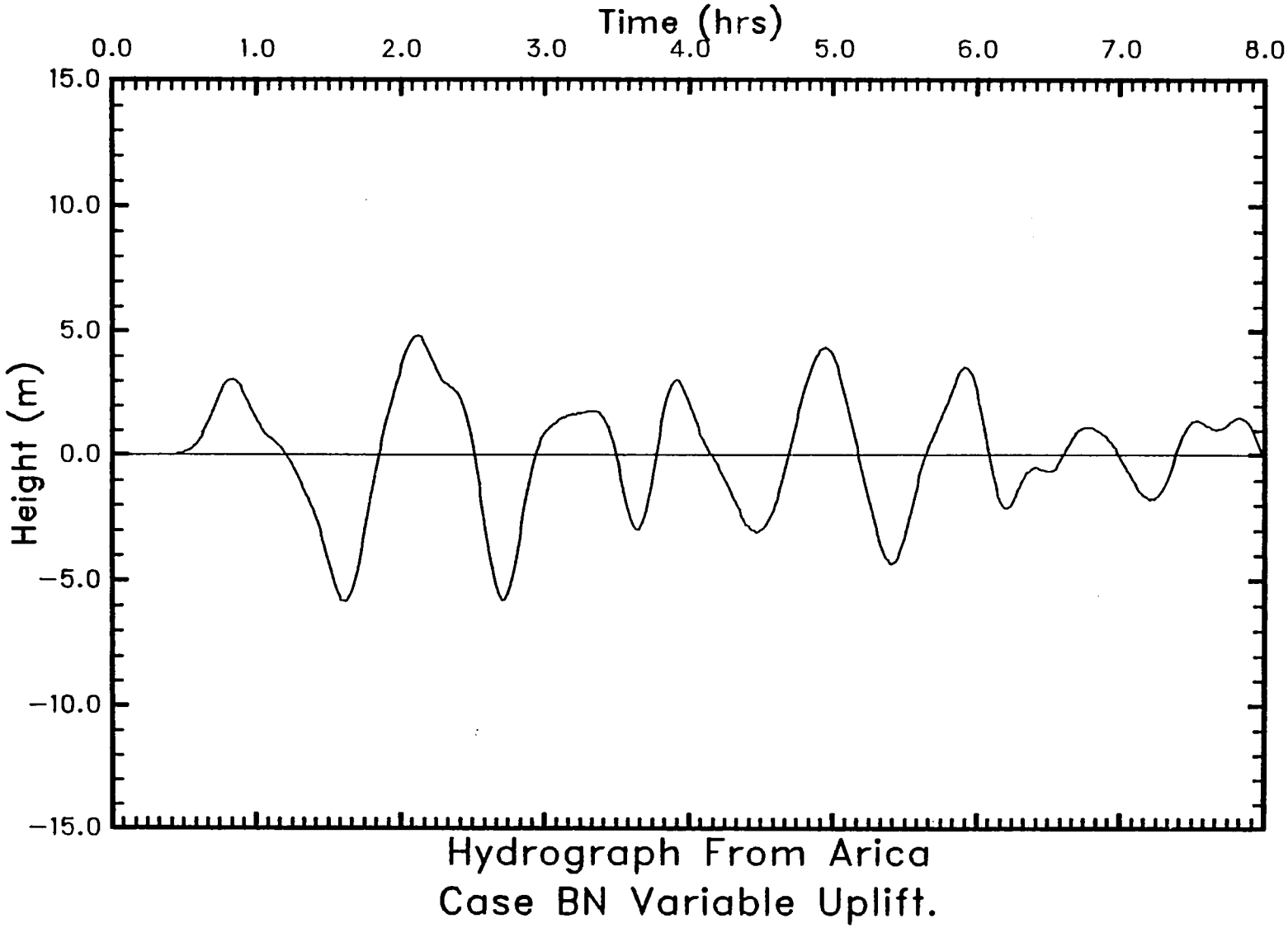

Figure 5.11: Wave elevation as a function of time at the recording point near Arica, Chile. These waves were generated by the variable uplift of the northern portion of Zone B.

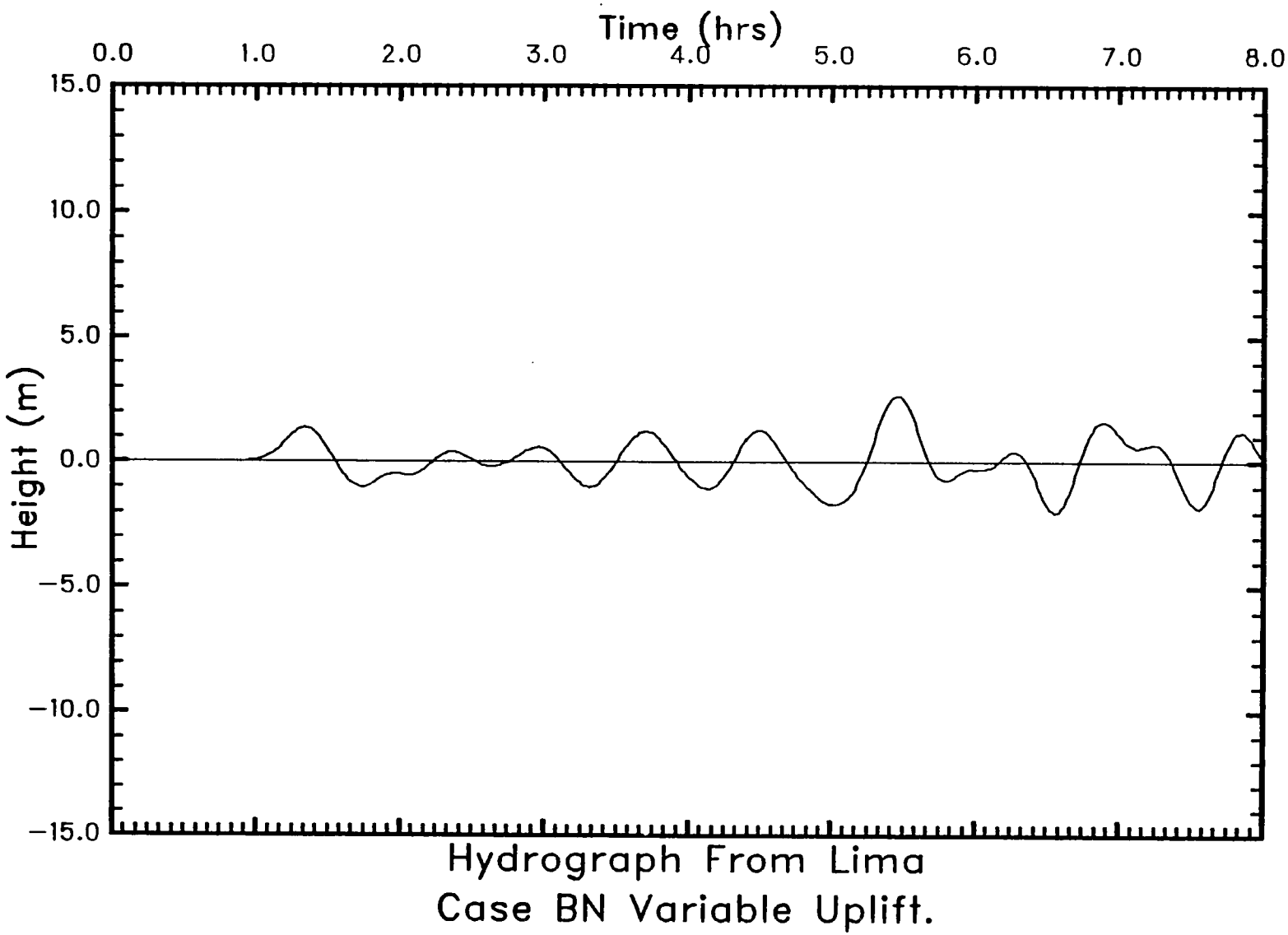

Figure 5.12: Wave elevation as a function of time at the recording point near Lima, Peru. These waves were generated by the variable uplift of the northern portion of Zone B.

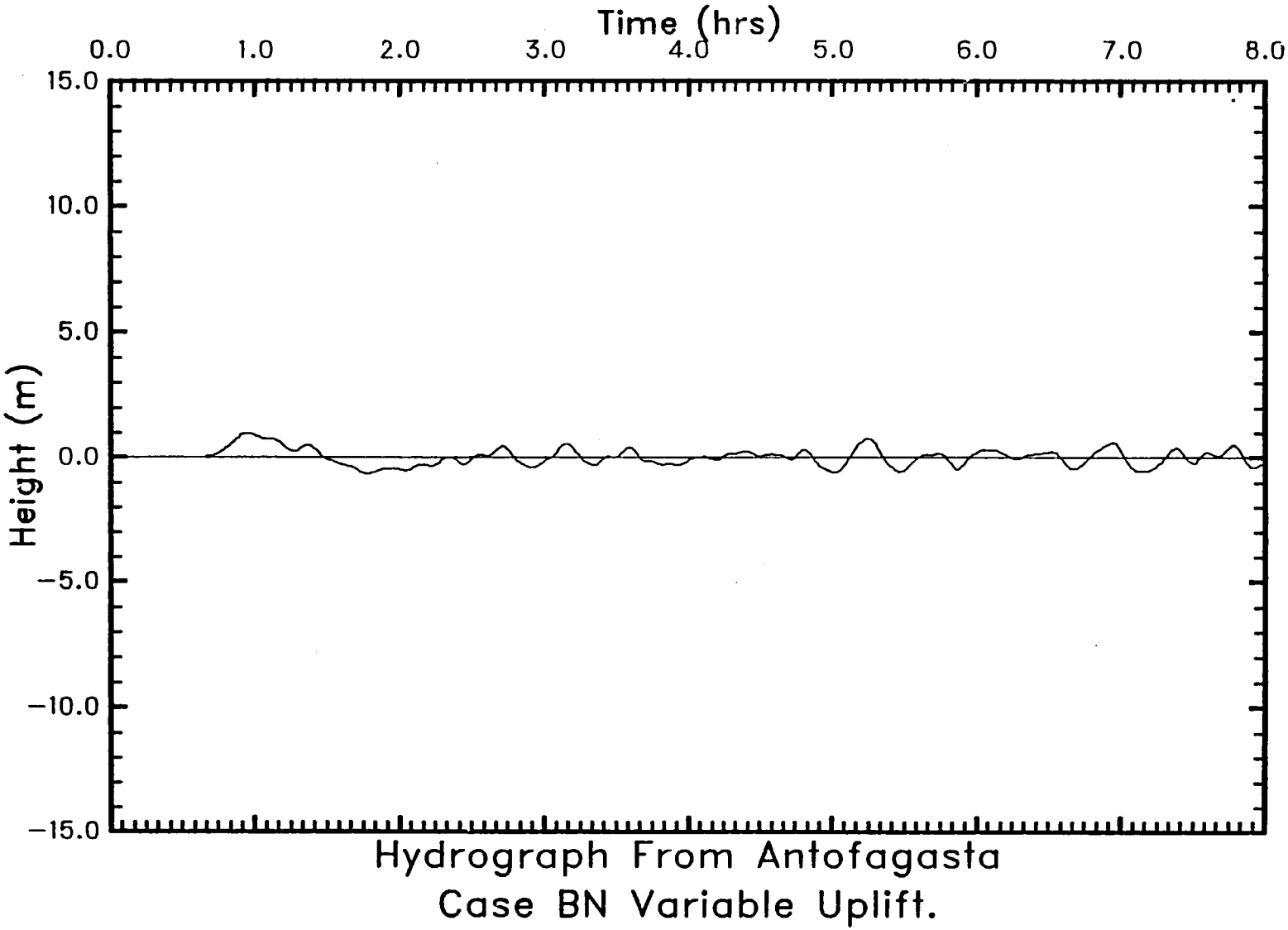

Figure 5.13: Wave elevation as a function of time at the recording point near Antofagasta, Chile. These waves were generated by the variable uplift of the northern portion of Zone B.

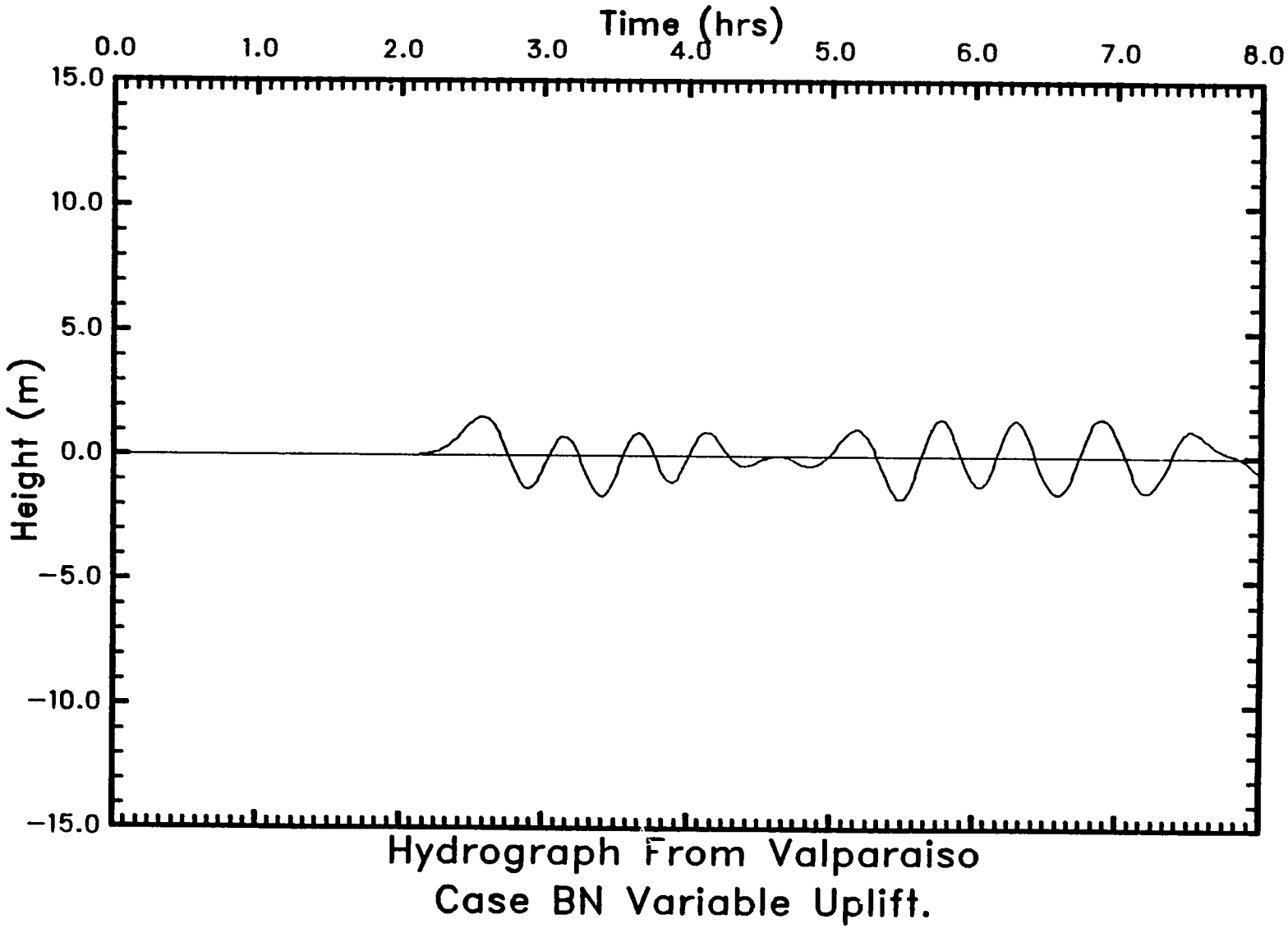

Figure 5.14: Wave elevation as a function of time at the recording point near Valparaiso, Chile. These waves were generated by the variable uplift of the northern portion of Zone B.

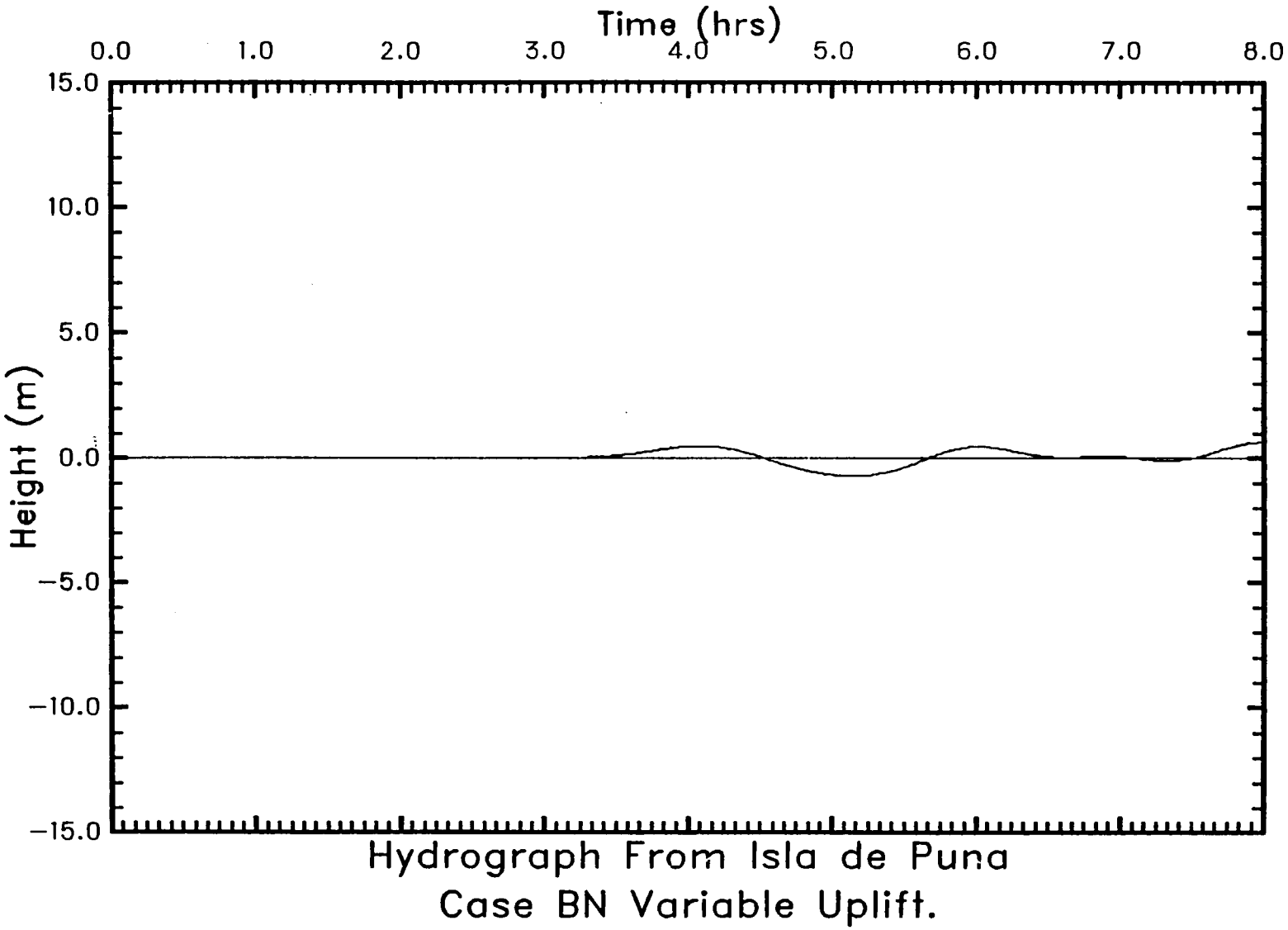

Figure 5.15: Wave elevation as a function of time at the recording point near Isla de Puna, Colombia. These waves were generated by the variable uplift of the northern portion of Zone B.

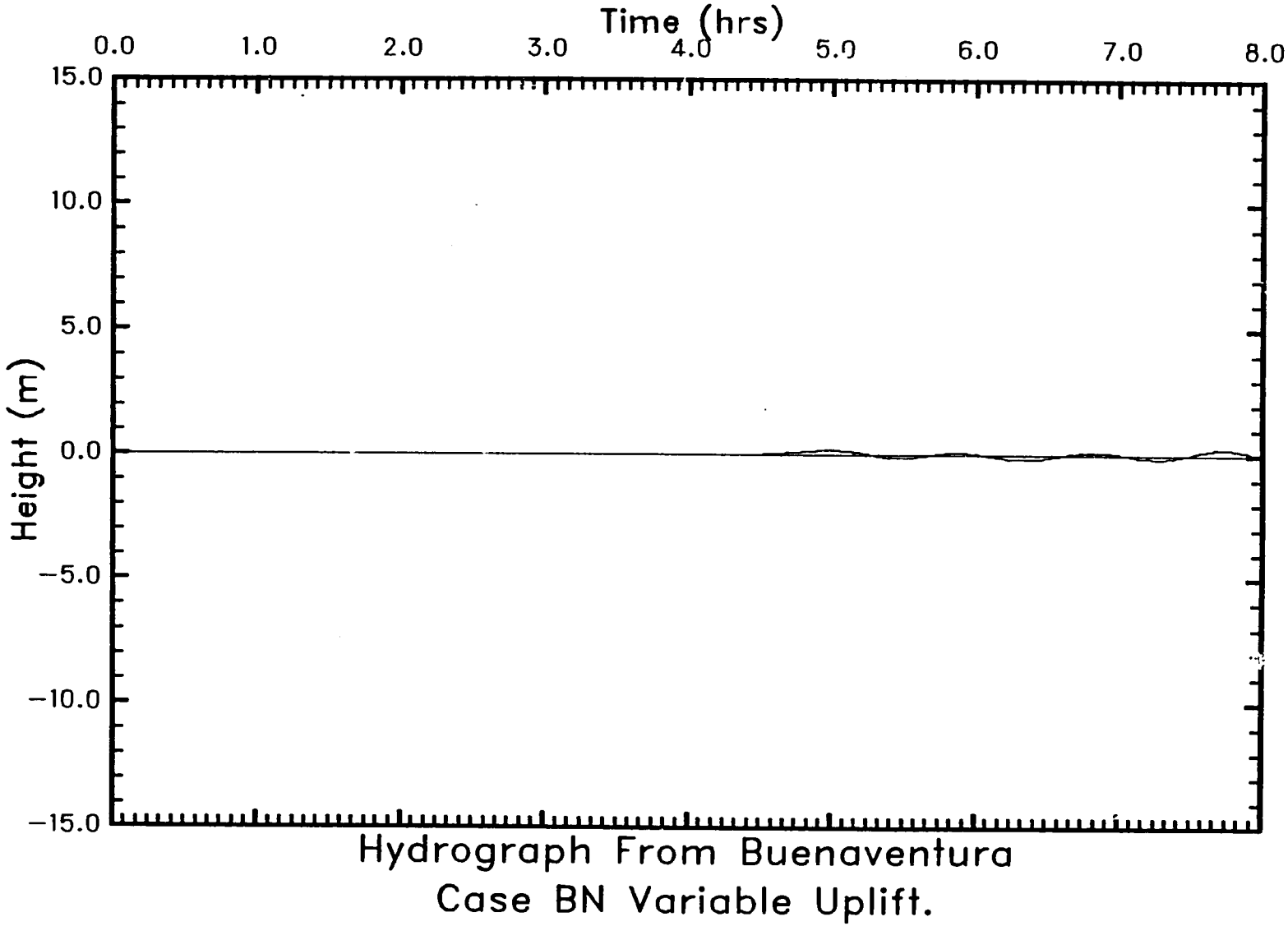

Figure 5.16: Wave elevation as a function of time at the recording point near Buenaventura, Ecuador. These waves were generated by the variable uplift of the northern portion of Zone B.

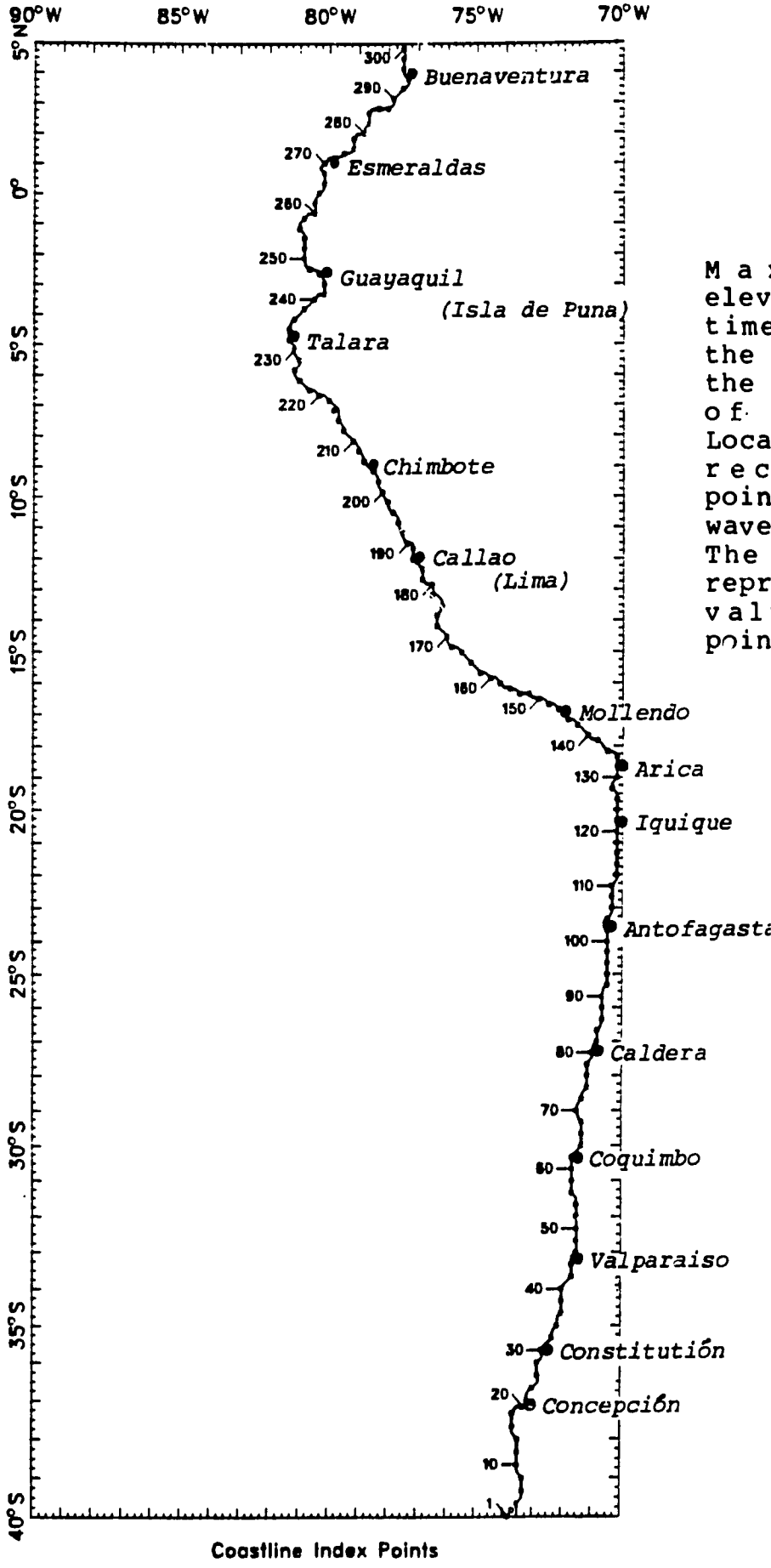

Figure: 5.17

Maximum wave elevations and arrival times of waves from the variable uplift in the northern portion of Zone B. (a) Locations of the 300 recording point points. (b-f) Maximum waves at each point. The horizontal line represents the average value of all 300 points.

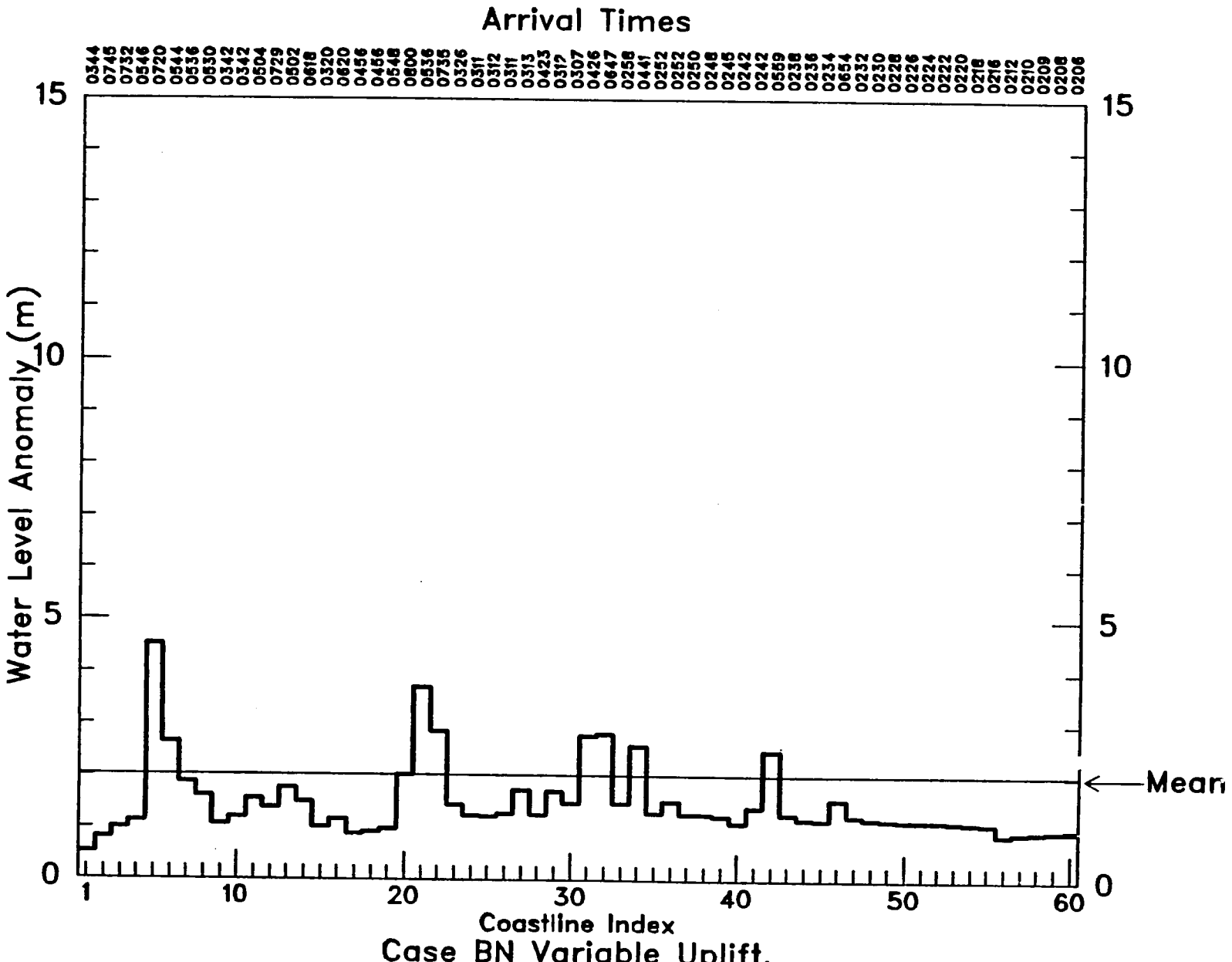
Arrival Times
0344 0745 0732 0546 0720 0544 0536 0530 0342 0342 0504 0729 0502 0618 0320 0620 0456 0456 0548 0800 0536 0735 0326 0311 0312 0311 0313 0423 0317 0307 0426 0647 0258 0441 0252 0252 0250 0248 0245 0242 0242 0559 0238 0236 0234 0654 0232 0230 0228 0226 0224 0222 0220 0218 0216 0212 0210 0209 0208 0206
Water Level Anomaly (m)
0
5
10
15
1
10
20
30
40
50
60
Coastline Index
Mean
Case BN Variable Uplift.

Figure: 5.17 (b)

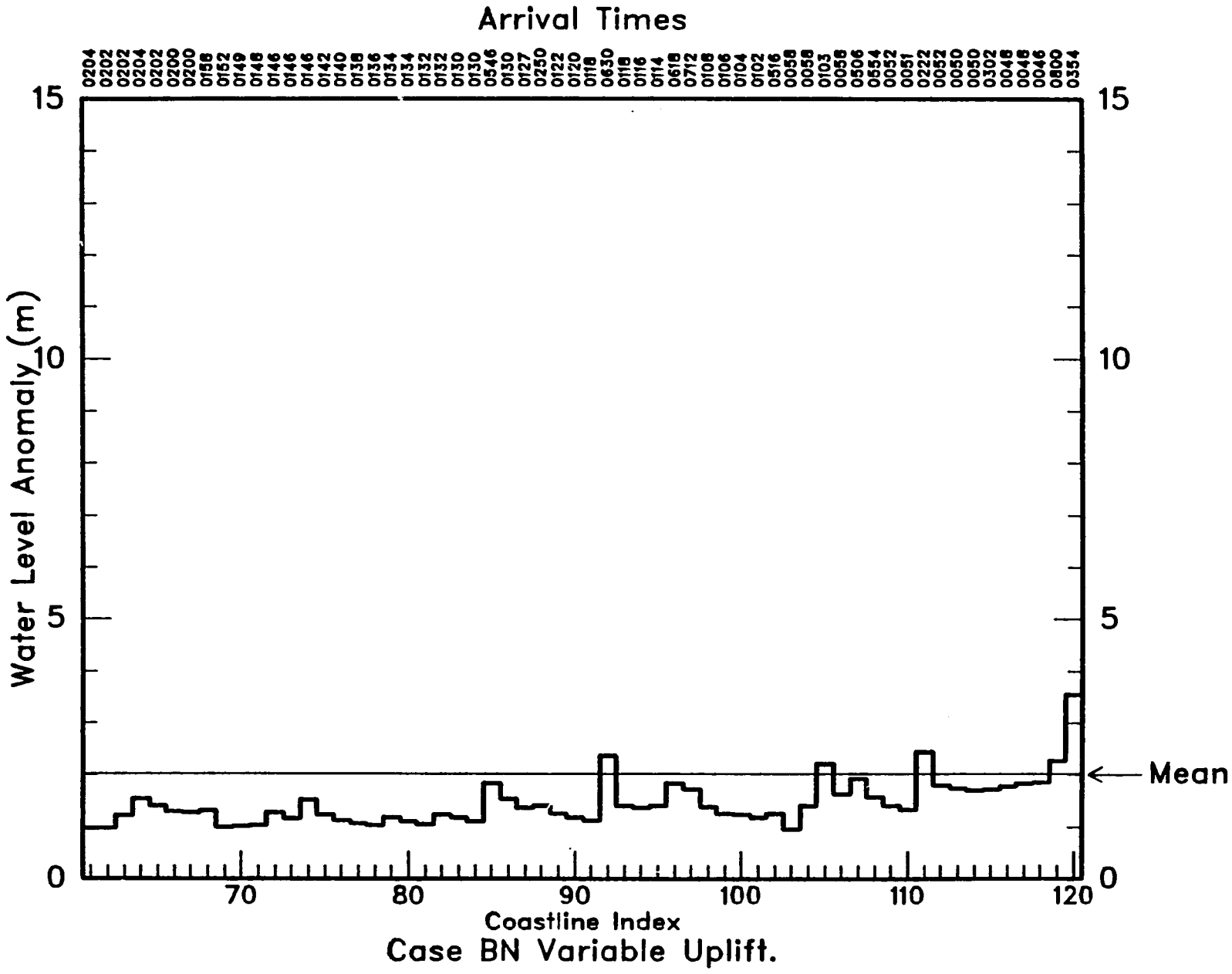
Arrival Times
0204 0202 0202 0204 0202 0200 0200 0158 0152 0149 0148 0146 0146 0146 0142 0140 0138 0136 0134 0134 0132 0132 0130 0130 0546 0130 0127 0250 0122 0120 0118 0630 0118 0116 0114 0618 0712 0108 0106 0104 0102 0516 0058 0058 0103 0058 0506 0554 0052 0051 0222 0052 0050 0050 0302 0048 0048 0046 0800 0354
15
10
5
0
Water Level Anomaly (m)
70
80
90
100
110
120
Coastline Index
Mean
Case BN Variable Uplift.

Figure: 5.17 (c)

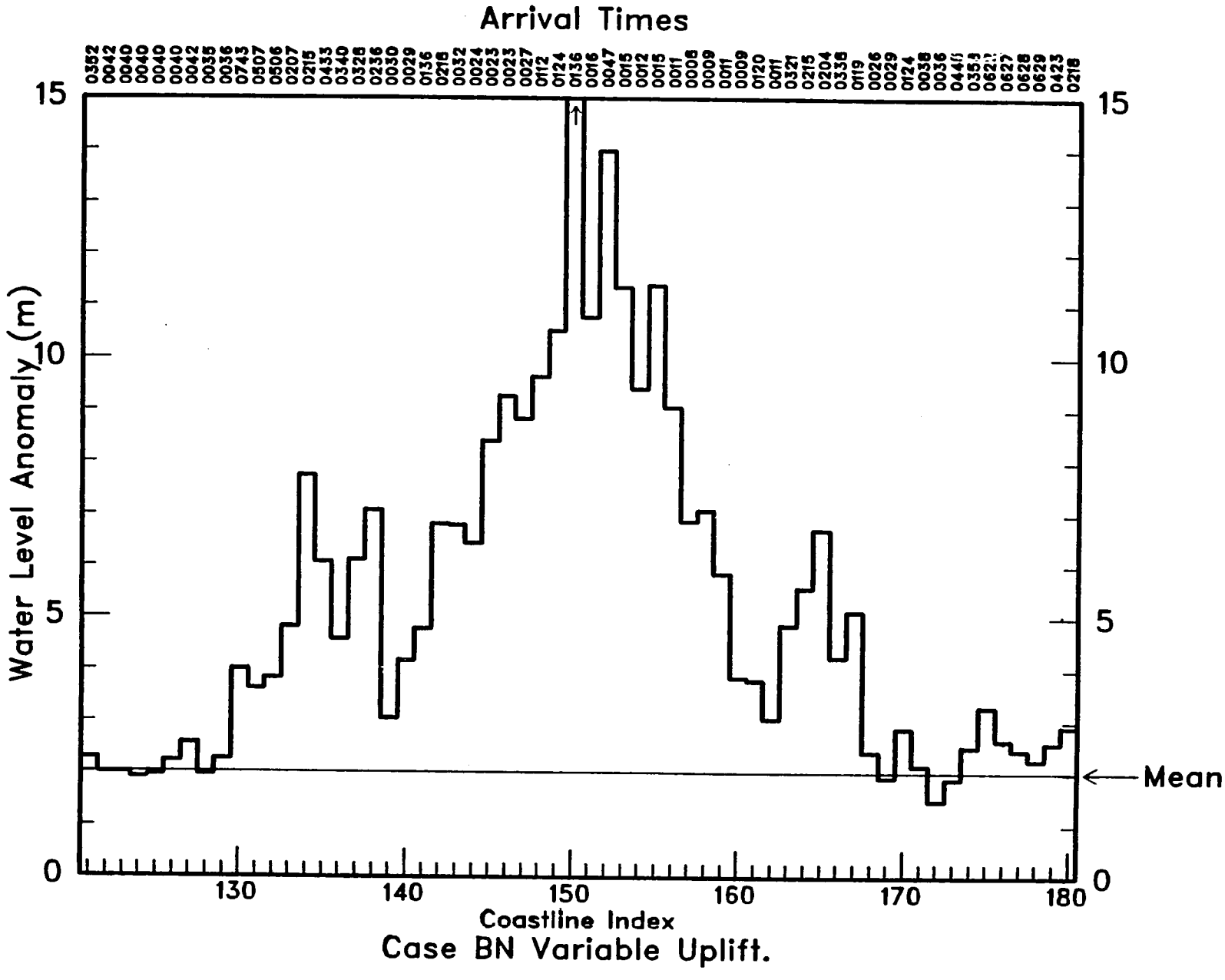
Arrival Times
Water Level Anomaly (m)
15
10
5
0
130
140
150
160
170
180
Coastline Index
Mean
Case BN Variable Uplift.

Figure: 5.17 (d)

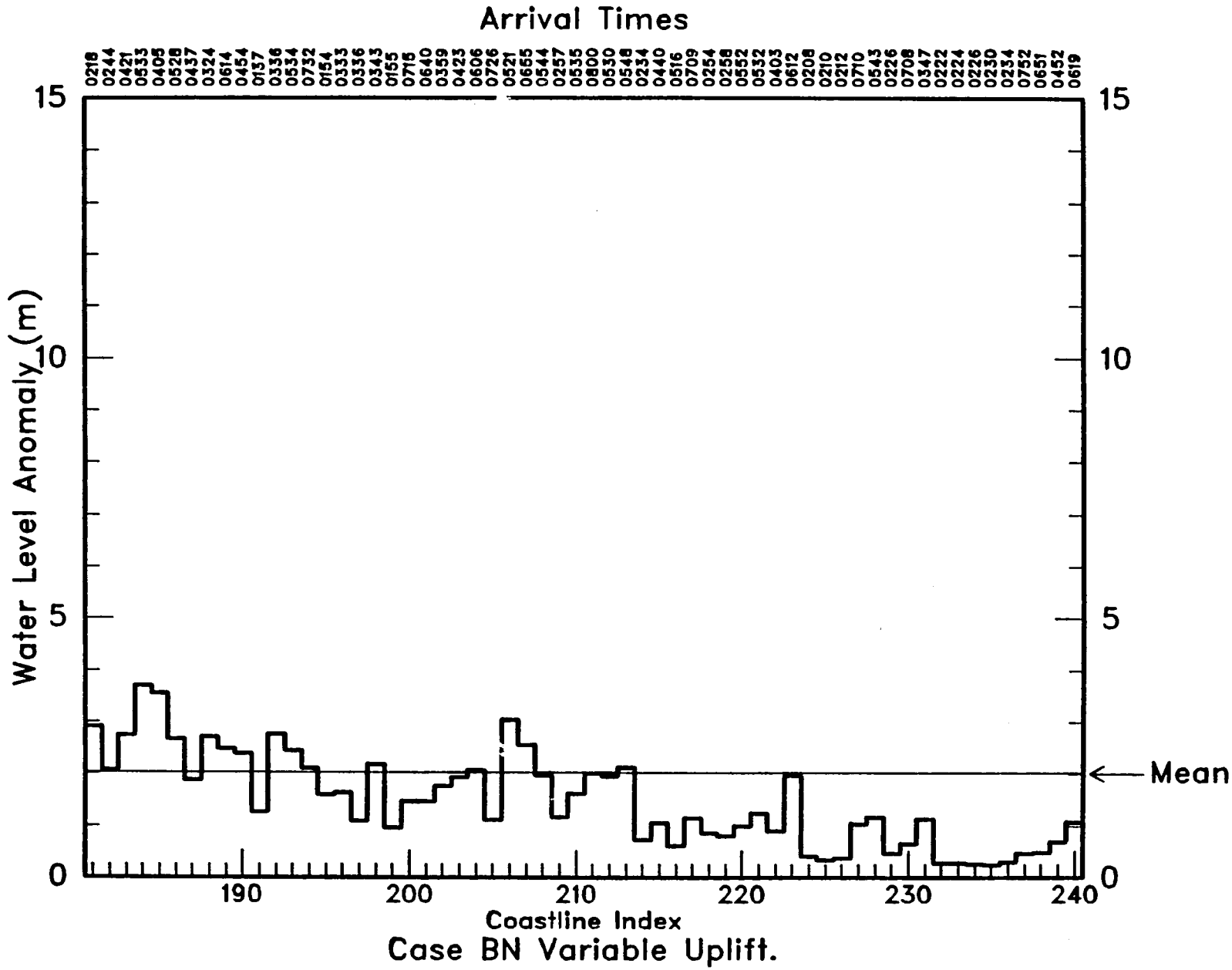
Arrival Times
0218 0244 0421 0533 0405 0528 0437 0324 0614 0454 0157 0336 0534 0732 0154 0333 0336 0343 0155 0716 0640 0359 0423 0606 0726 0521 0655 0544 0257 0535 0800 0530 0548 0234 0440 0516 0709 0254 0258 0552 0532 0403 0612 0208 0210 0212 0710 0543 0226 0708 0347 0222 0224 0226 0230 0234 0752 0651 0452 0619
15
10
5
0
Water Level Anomaly (m)
190
200
210
220
230
240
Coastline Index
Mean
Case BN Variable Uplift.

Figure: 5.17 (e)

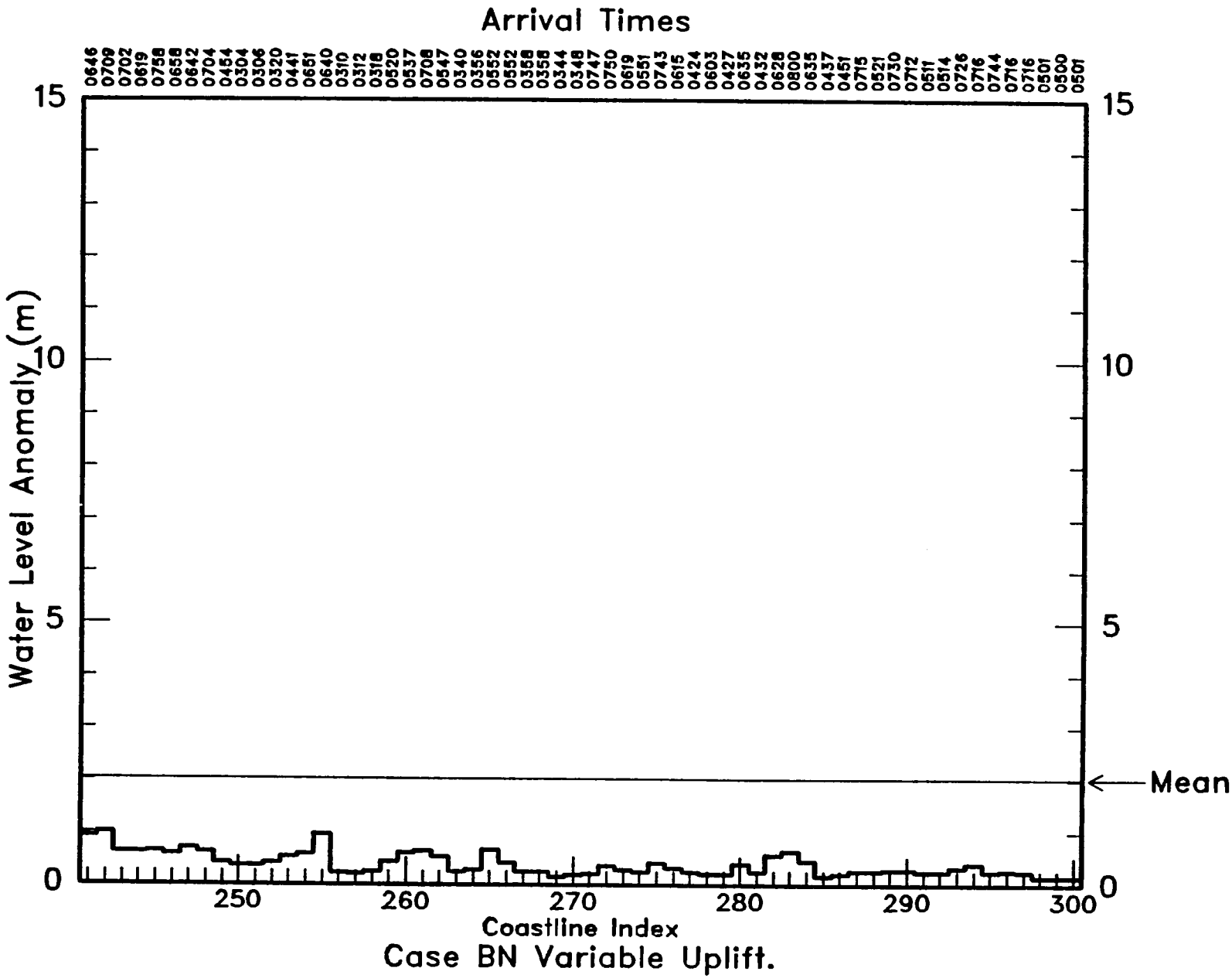
Arrival Times
0646 0709 0702 0619 0758 0658 0642 0704 0454 0304 0306 0320 0441 0651 0640 0310 0312 0318 0520 0537 0708 0547 0340 0356 0552 0552 0358 0358 0344 0348 0747 0750 0619 0551 0743 0615 0424 0603 0427 0635 0432 0628 0800 0635 0437 0451 0715 0521 0730 0712 0511 0514 0726 0716 0744 0716 0716 0501 0500 0501
Water Level Anomaly (m)
15
10
5
0
250
260
270
280
290
300
Mean
Coastline Index
Case BN Variable Uplift.

Figure: 5.17 (f)

5.4 SOUTHERN ZONE - UNIFORM UPLIFT CASE

The area for this source extends from 21°S to 24°S over some of the deepest portions of the trench. The area of the source is depicted in Figure 5.1. The uniform uplift scenario specifies a 10 m uplift over this whole zone. Portions of the zone on land do not effect the model, which does not allow water onto land areas.

5.4.1 Immediate Effects

After one hour, much of the wave energy has spread seaward in all directions, but especially to the west (Figure 5.18). High concentrations of wave energy are apparent both in the source region and to the north of Arica.

5.4.2 Longer Duration Effects

The wave record at Antofagasta (Figure 5.19), which is in the source zone, immediately rises to 10 m and then drops off. By the end of the first hour the waves have dropped to amplitudes of 1-2 m and persist at high frequency for the rest of the simulation. To the north and south of the source, at Arica (Figure 5.20) and Valparaiso (Figure 5.21), the waves are more intense, but of much longer period. The waves at Arica, especially, remain quite high, probably because of energy trapped between the source (which oscillates for some time after the initial uplift) and the bend in the continent.

By the time the waves reach Lima (Figure 5.22) they are even longer and much lower than those at Arica. The oscillations do, however, persist for quite a time.

The waves reaching Isla de Puna (Figure 5.23) and Buenaventura (Figure 5.24) are very long and low.

5.4.3 Maximum Elevations

The effects of this tsunami are severe for a long distance along the coast (see Figure 5.25a-f) since the mean maximum wave is nearly 4 m high. The most immediate effects are felt in the source area, where 10 m amplitudes occur within minutes of uplift. Extreme maximum values occur at intervals along the coast between points 85 and 150, although the general trend is a slow decrease from the initial maximum uplift. This decrease continues to the north, broken only by occasional local peaks. Elevations north of Guayaquil are generally low enough to pose little or no threat.

The decrease to the south is broken by a number of sharp peaks south of Valparaiso. Most of these peaks occur in locations which we have already seen to be susceptible to wave amplification. But the open ocean propagation mechanism which we proposed to explain such peaks previously is probably not valid here, since the source is located to the south of the bend in the continent. The alternative explanation of local amplification of longshore waves is more likely to be the case in this instance.

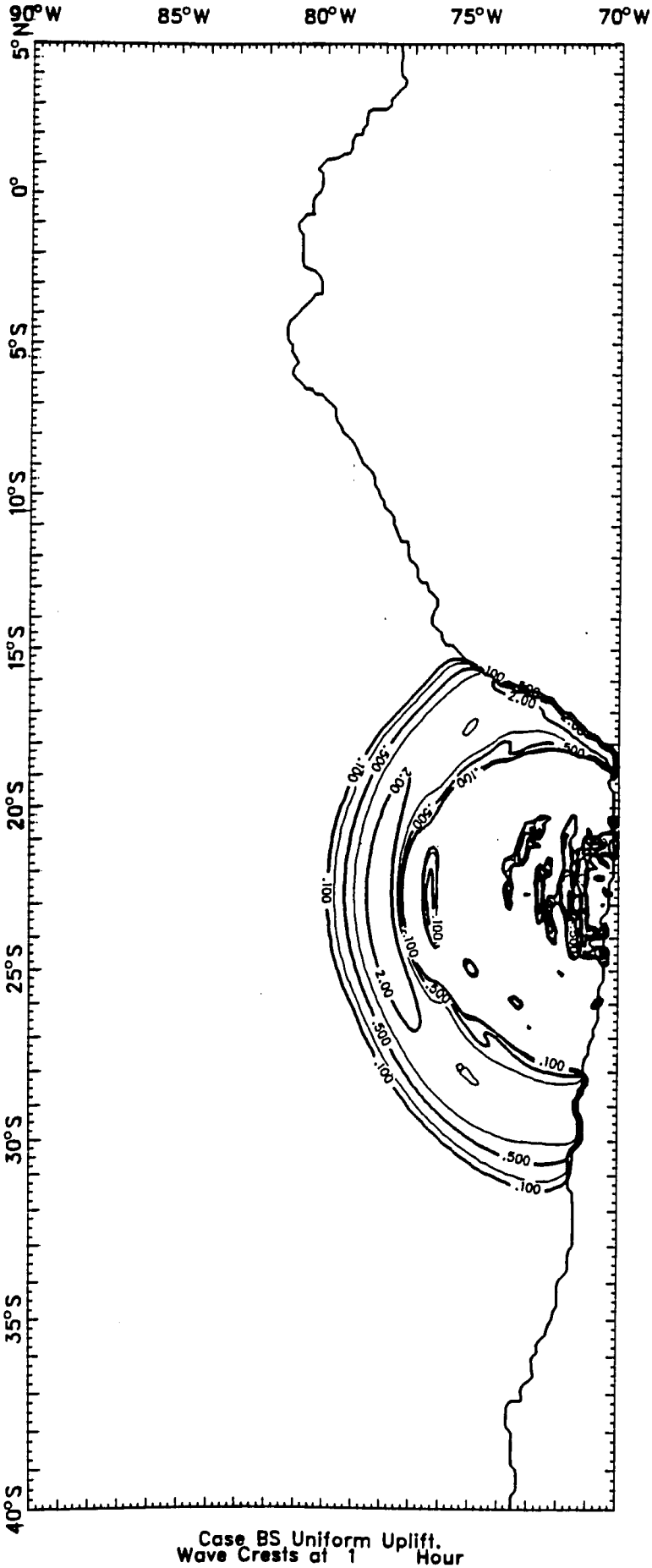

Figure: 5.18

Surface elevation (positive only) one hour after a uniform uplift in the southern portion of source Zone B. Contours correspond to 0.1, 0.2, 0.5, 1.0, and 2.0 m.

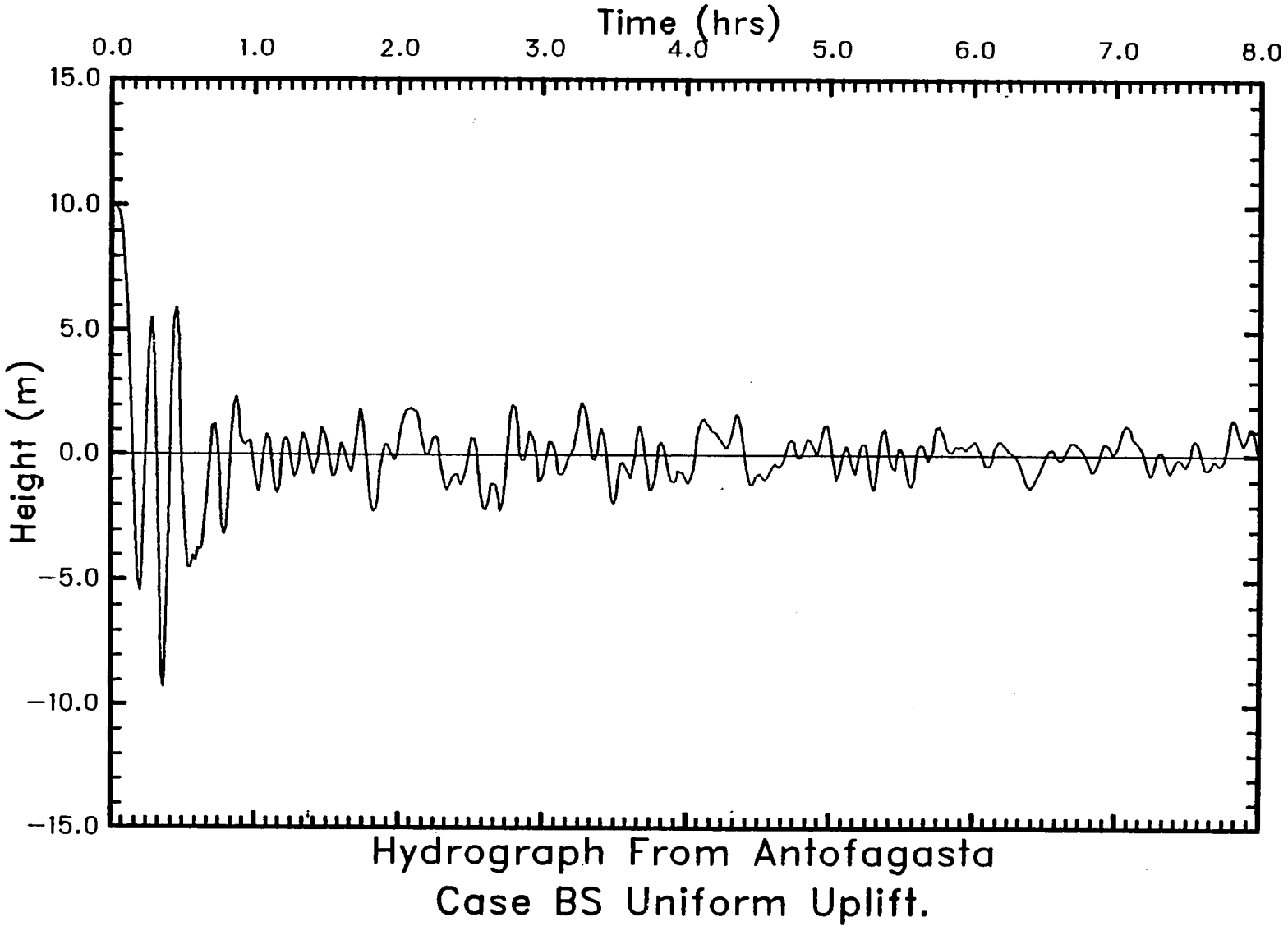

Figure 5.19: Wave elevation as a function of time at the recording point near Antofagasta, Chile. These waves were generated by the uniform uplift of the southern portion of Zone B.

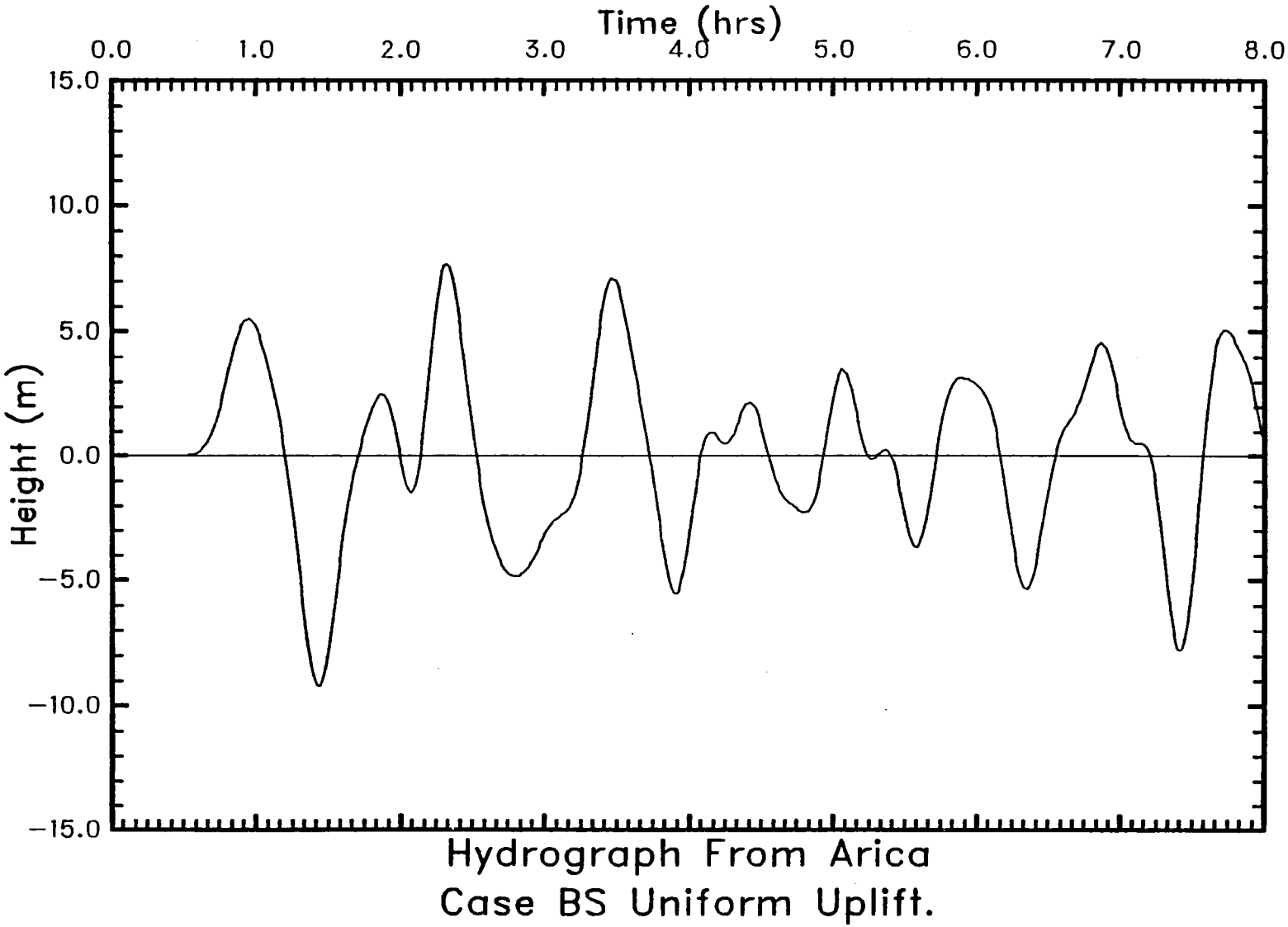

Figure 5.20: Wave elevation as a function of time at the recording point near Arica, Chile. These waves were generated by the uniform uplift of the southern portion of Zone B.

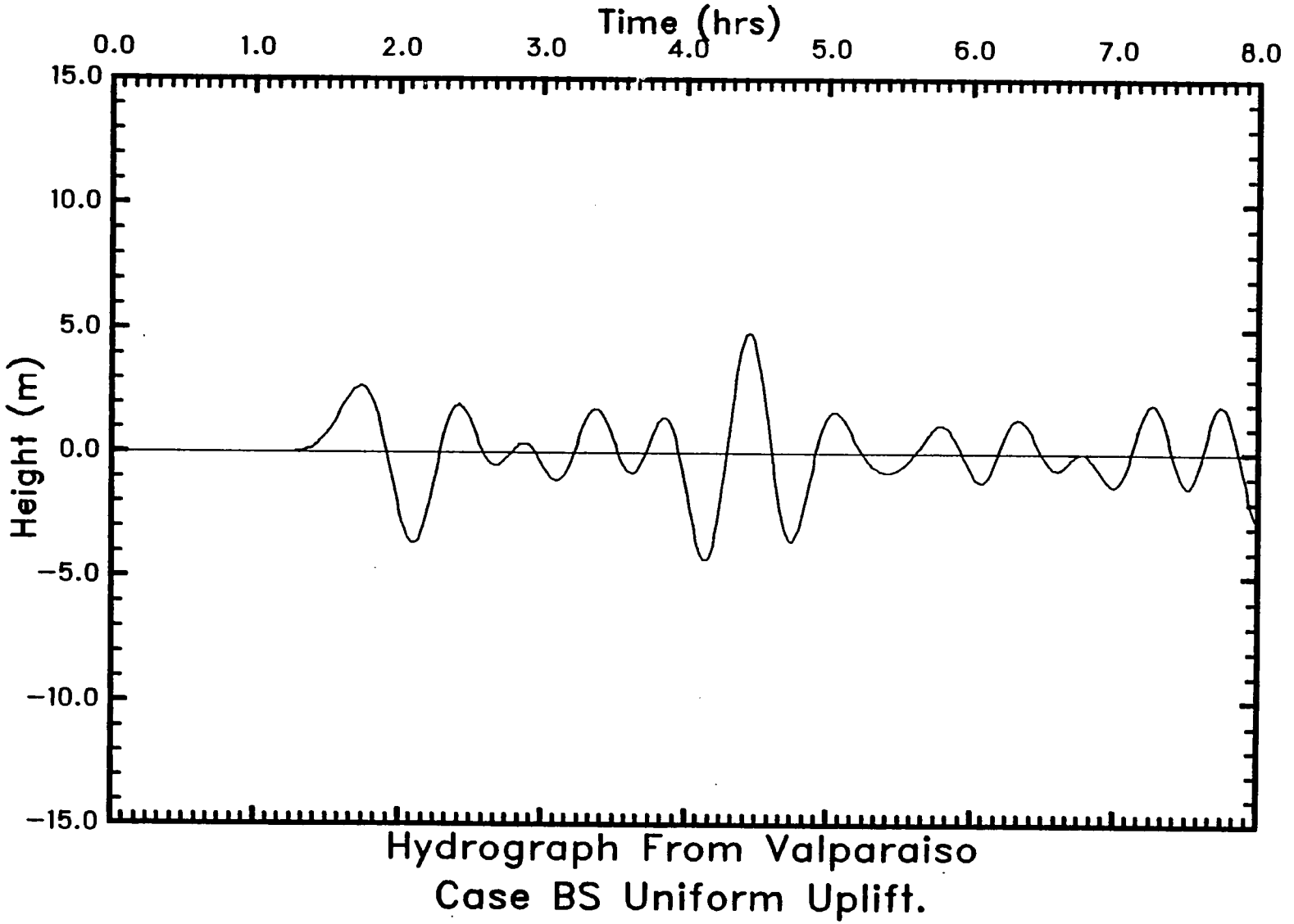

Figure 5.21: Wave elevation as a function of time at the recording point near Valparaiso, Chile. These waves were generated by the uniform uplift of the southern portion of Zone B.

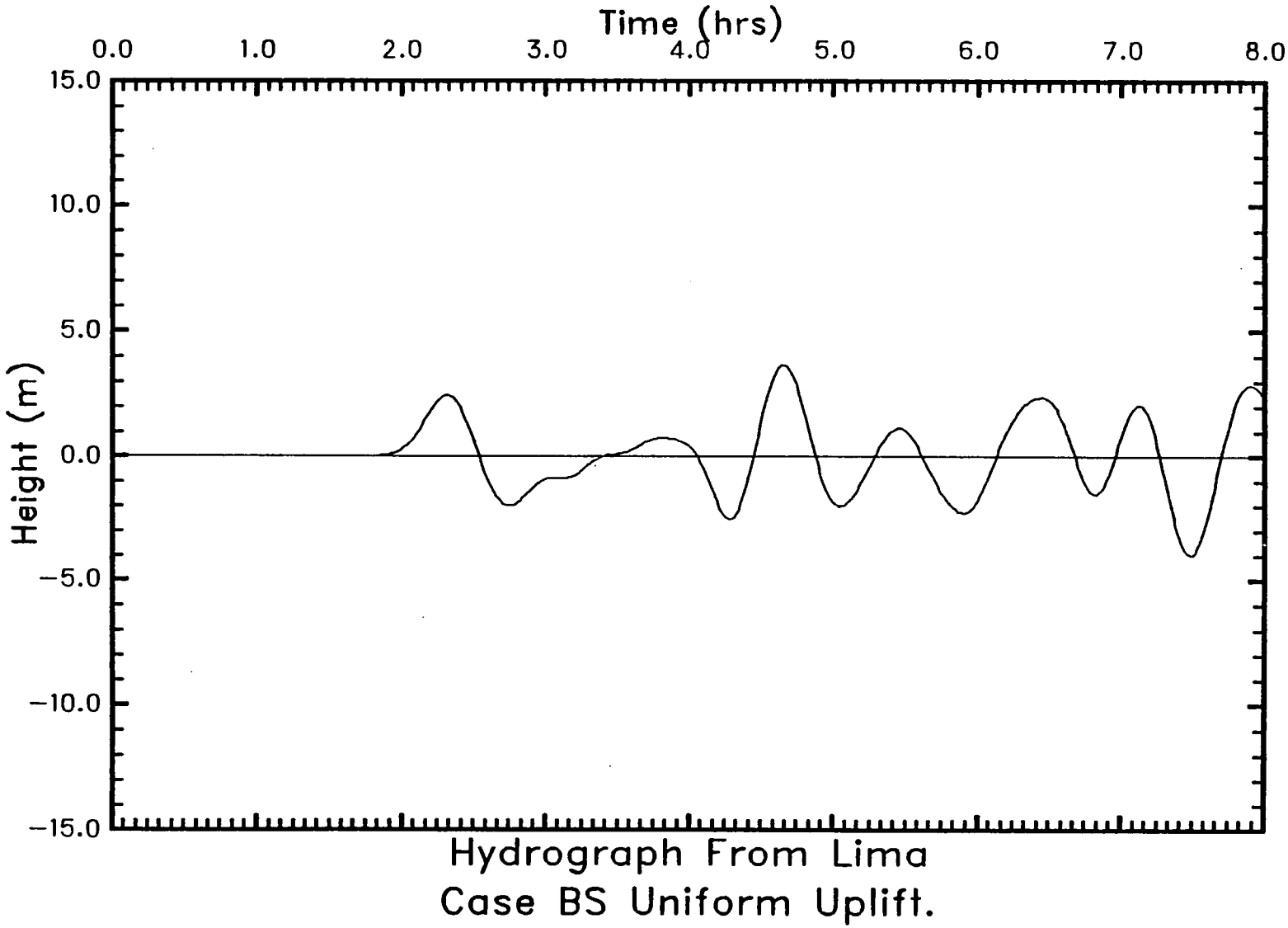

Figure 5.22: Wave elevation as a function of time at the recording point near Lima, Peru. These waves were generated by the uniform uplift of the southern portion of Zone B.

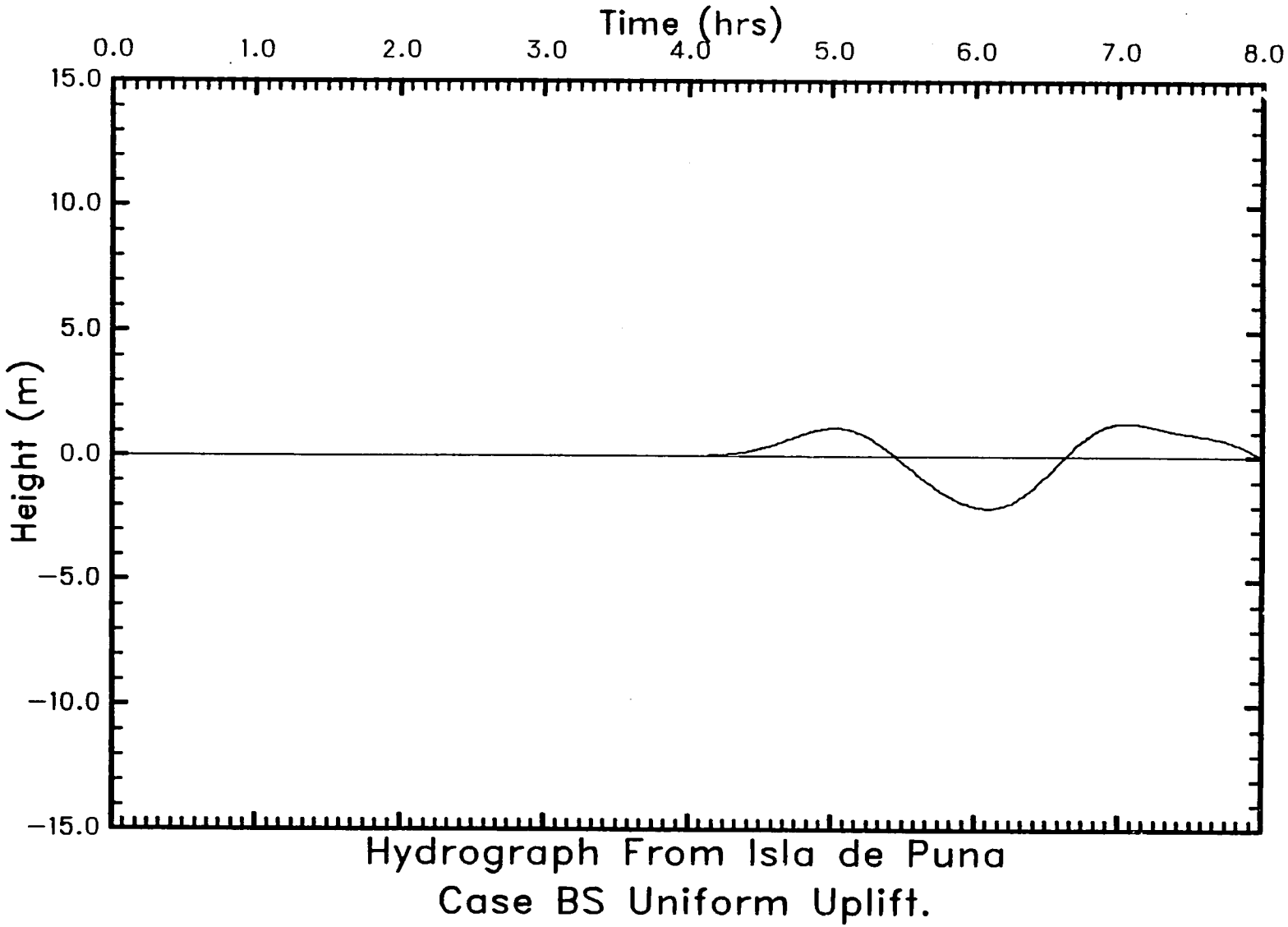

Figure 5.23: Wave elevation as a function of time at the recording point near Isla de Puna, Colombia. These waves were generated by the uniform uplift of the southern portion of Zone B.

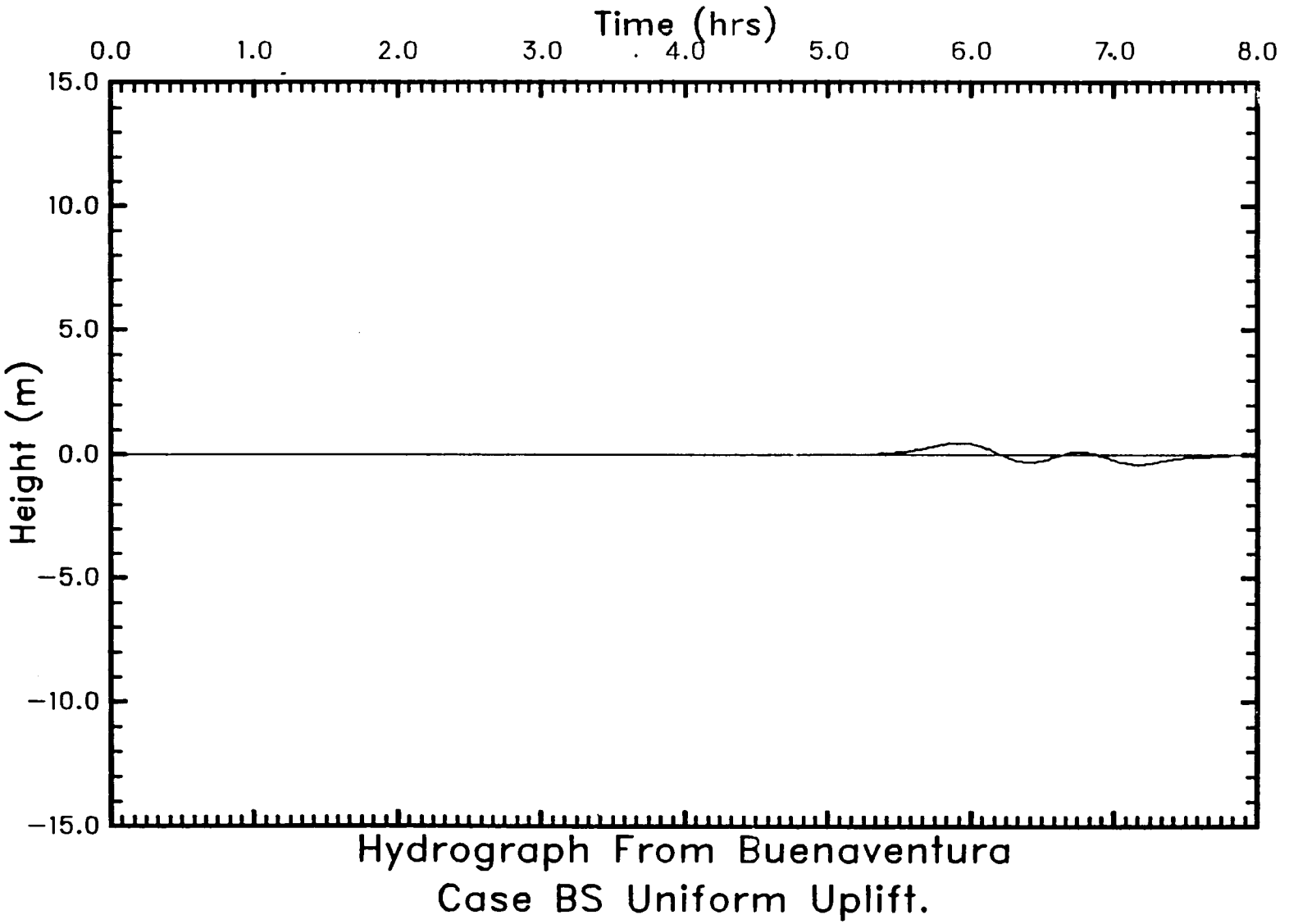

Figure 5.24: Wave elevation as a function of time at the recording point near Buenaventura, Ecuador. These waves were generated by the uniform uplift of the southern portion of Zone B.

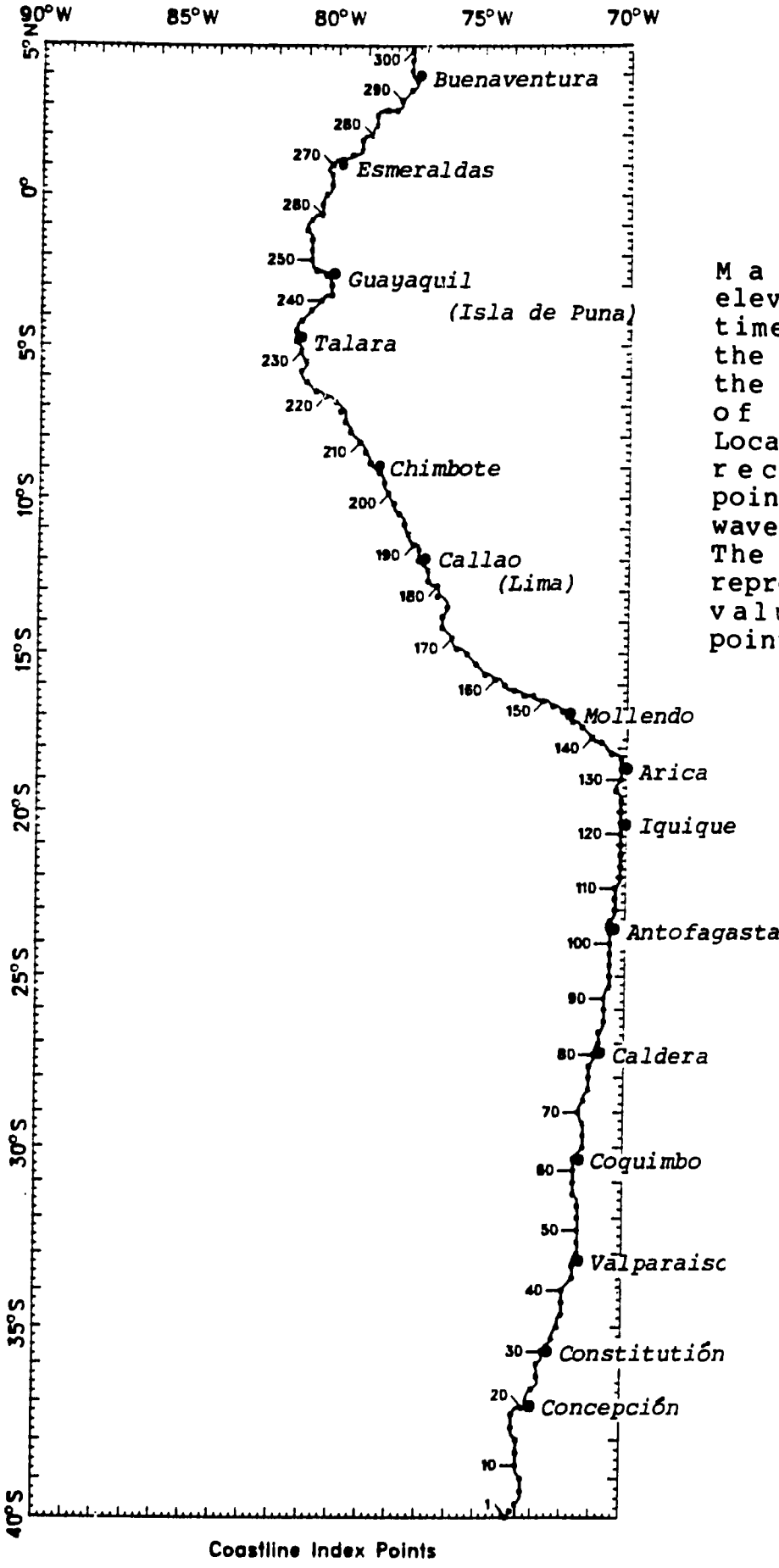

Figure: 5.25

Maximum wave elevations and arrival times of waves from the uniform uplift in the southern portion of Zone B. (a) Locations of the 300 recording point points. (b-f) Maximum waves at each point. The horizontal line represents the average value of all 300 points.

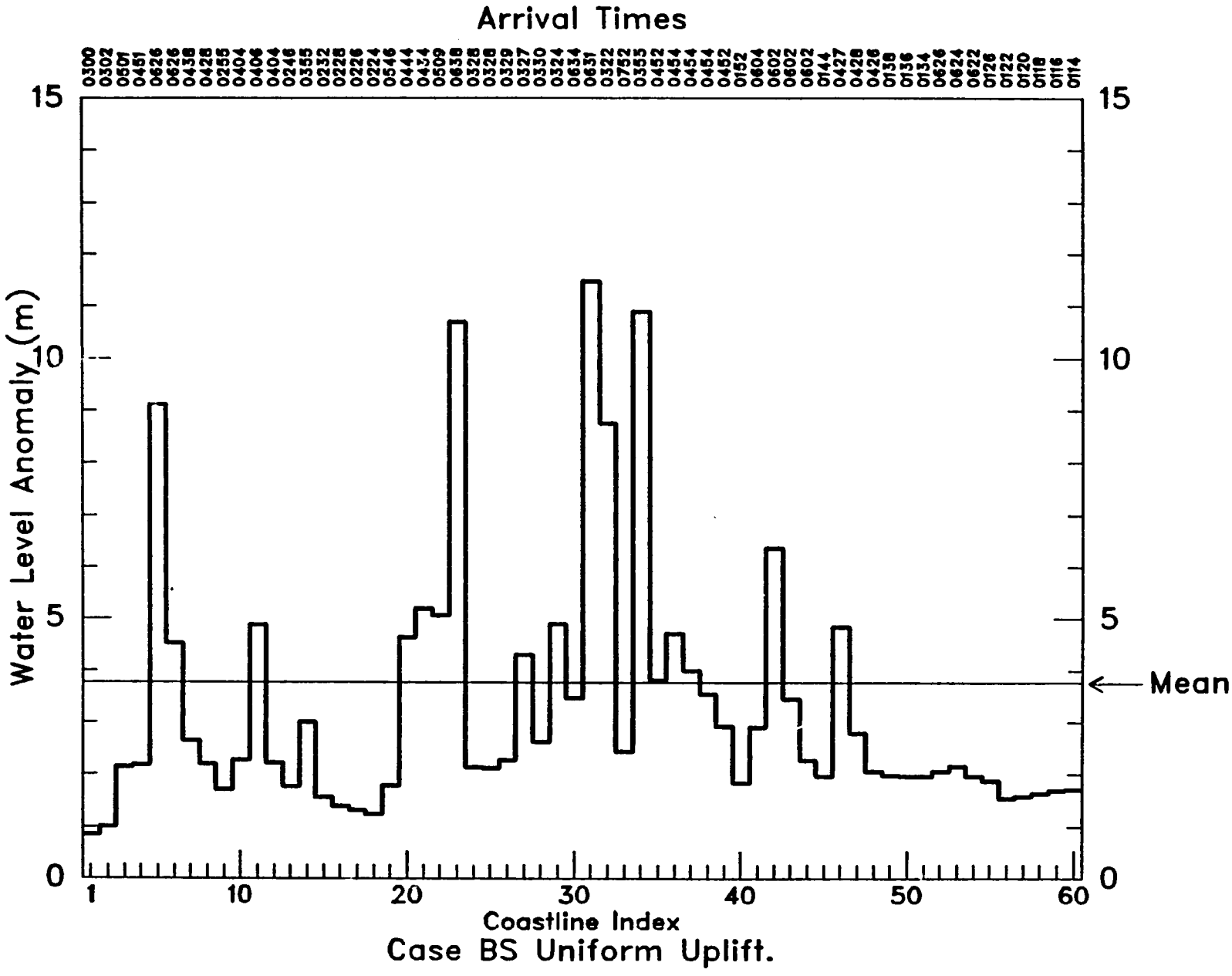
Arrival Times
0300 0302 0501 0451 0626 0626 0438 0428 0255 0404 0406 0404 0246 0355 0232 0228 0226 0224 0546 0444 0434 0509 0638 0328 0328 0329 0327 0330 0324 0634 0631 0322 0752 0355 0452 0454 0454 0452 0152 0604 0602 0602 0602 0144 0427 0428 0428 0138 0136 0134 0626 0624 0622 0126 0122 0120 0118 0116 0114
15
10
5
0
Water Level Anomaly (m)
1
10
20
30
40
50
60
Coastline Index
Mean
Case BS Uniform Uplift.

Figure: 5.25 (b)

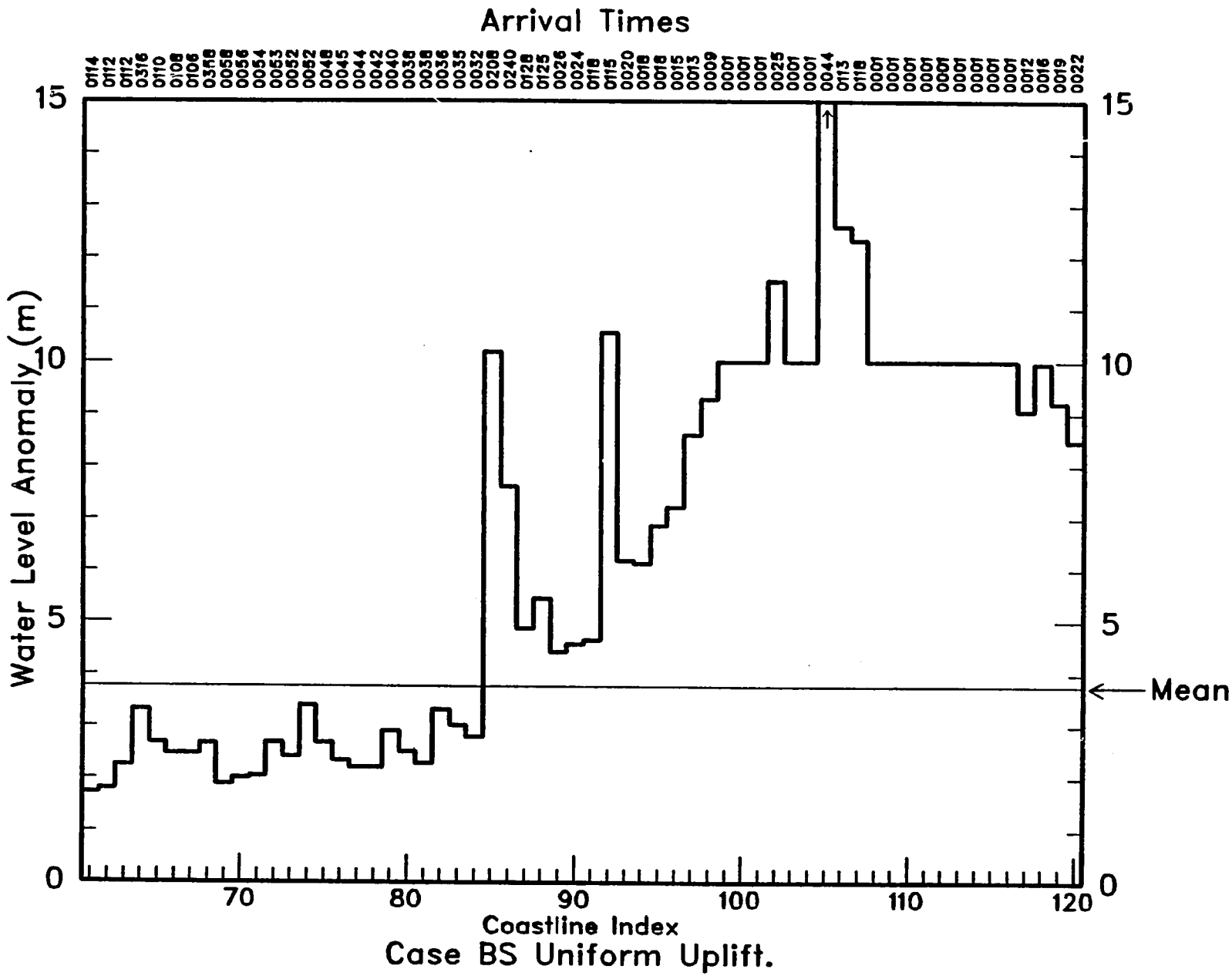
Arrival Times
Water Level Anomaly (m)
15
10
5
0
70
80
90
100
110
120
Mean
Coastline Index
Case BS Uniform Uplift.

Figure: 5.25 (c)

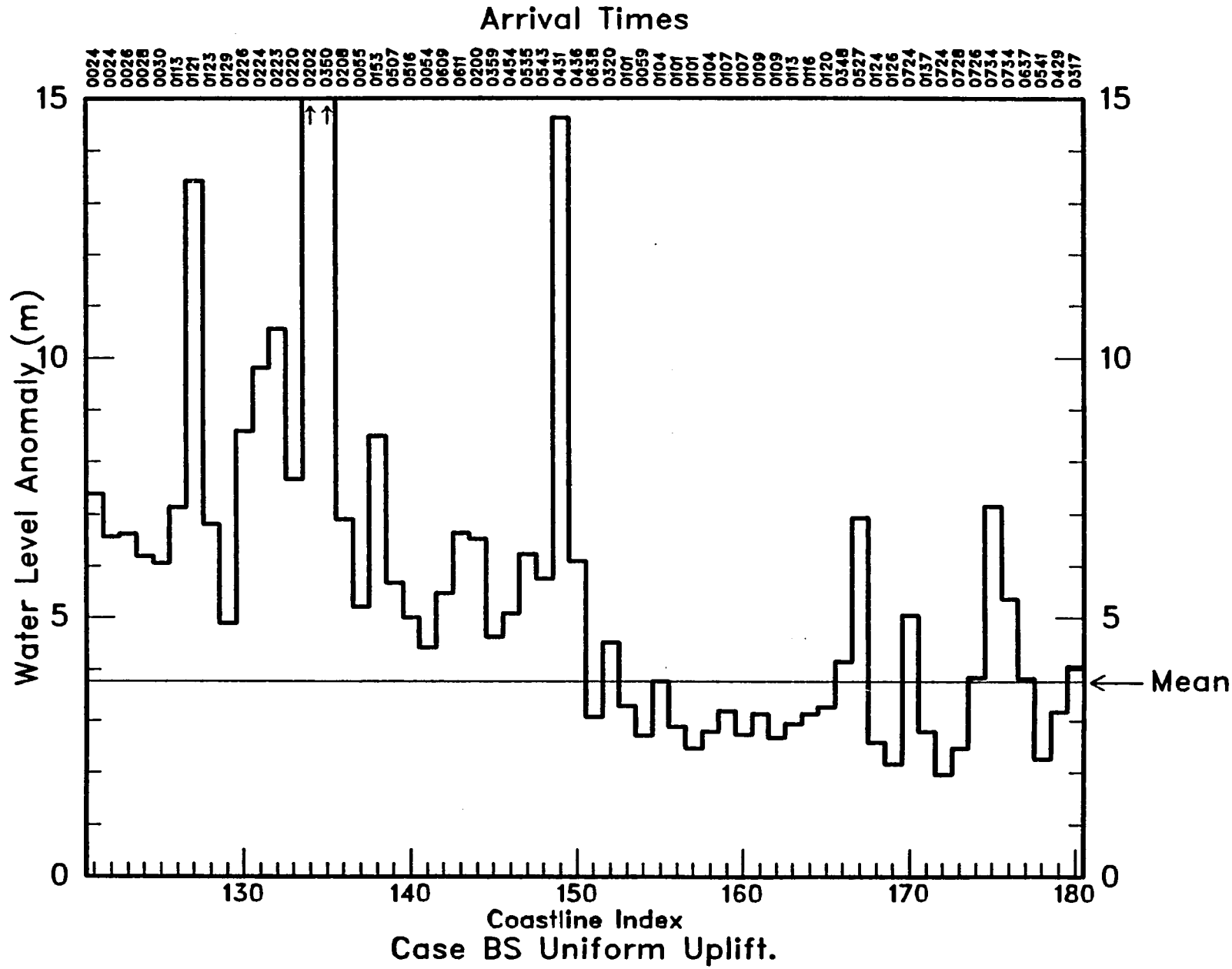
Arrival Times
0024 0024 0026 0028 0030 0113 0121 0123 0129 0226 0224 0223 0220 0202 0350 0208 0055 0153 0507 0516 0054 0609 0611 0200 0359 0454 0535 0543 0431 0436 0638 0320 0101 0059 0104 0101 0101 0104 0107 0107 0109 0109 0113 0116 0120 0348 0527 0124 0126 0724 0137 0724 0728 0726 0734 0734 0637 0541 0429 0317
Water Level Anomaly (m)
0
5
10
15
130
140
150
160
170
180
Mean
Coastline Index
Case BS Uniform Uplift.

Figure: 5.25 (d)

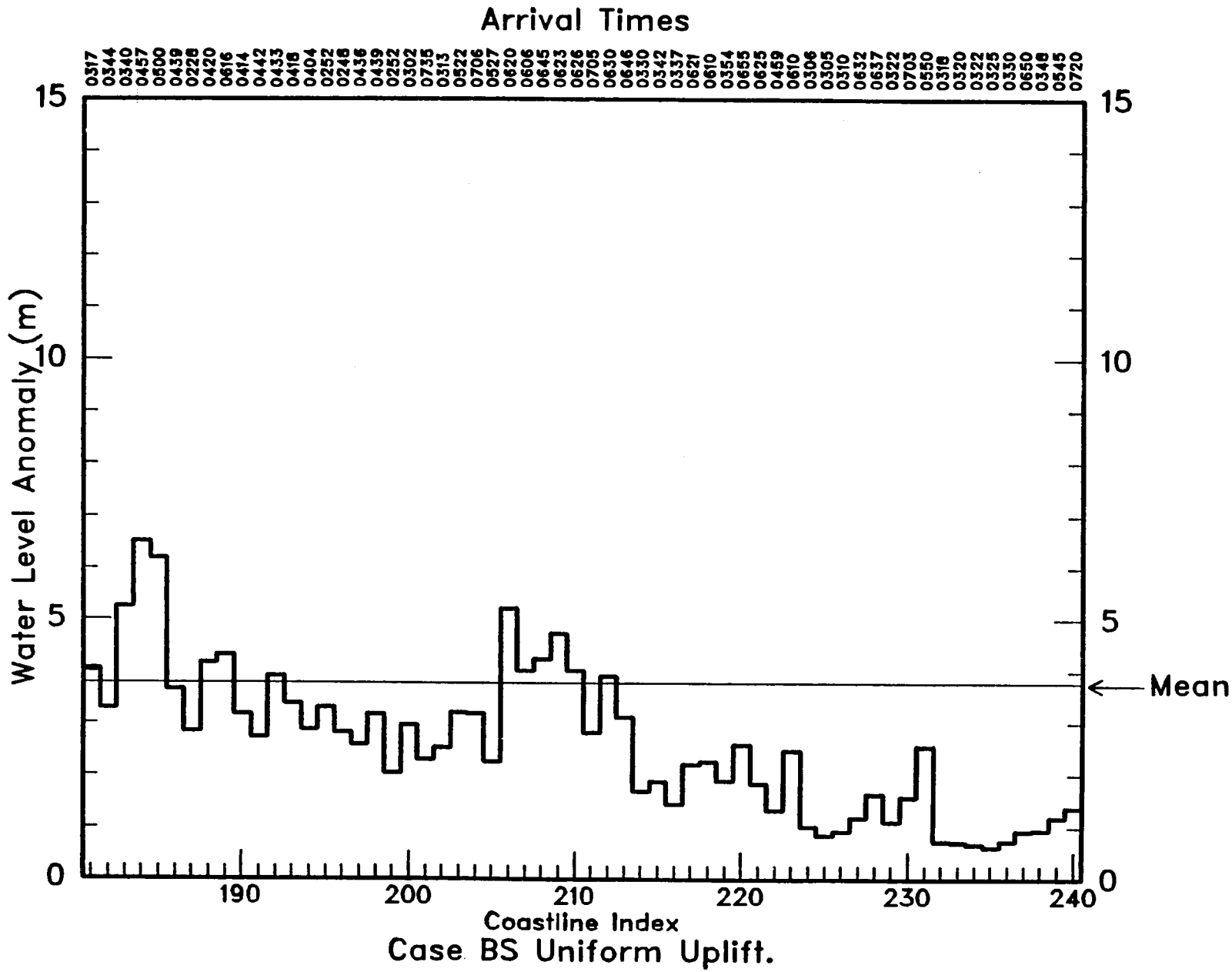
Arrival Times
0317 0344 0340 0457 0500 0439 0228 0420 0616 0414 0442 0433 0418 0404 0252 0248 0436 0439 0252 0302 0735 0313 0522 0706 0527 0620 0606 0645 0623 0626 0705 0630 0646 0330 0342 0337 0621 0610 0354 0655 0625 0459 0610 0306 0305 0310 0632 0637 0322 0703 0550 0318 0320 0322 0325 0330 0650 0348 0545 0720
Water Level Anomaly (m)
0
5
10
15
190
200
210
220
230
240
Coastline Index
Mean
Case BS Uniform Uplift.

Figure: 5.25 (e)

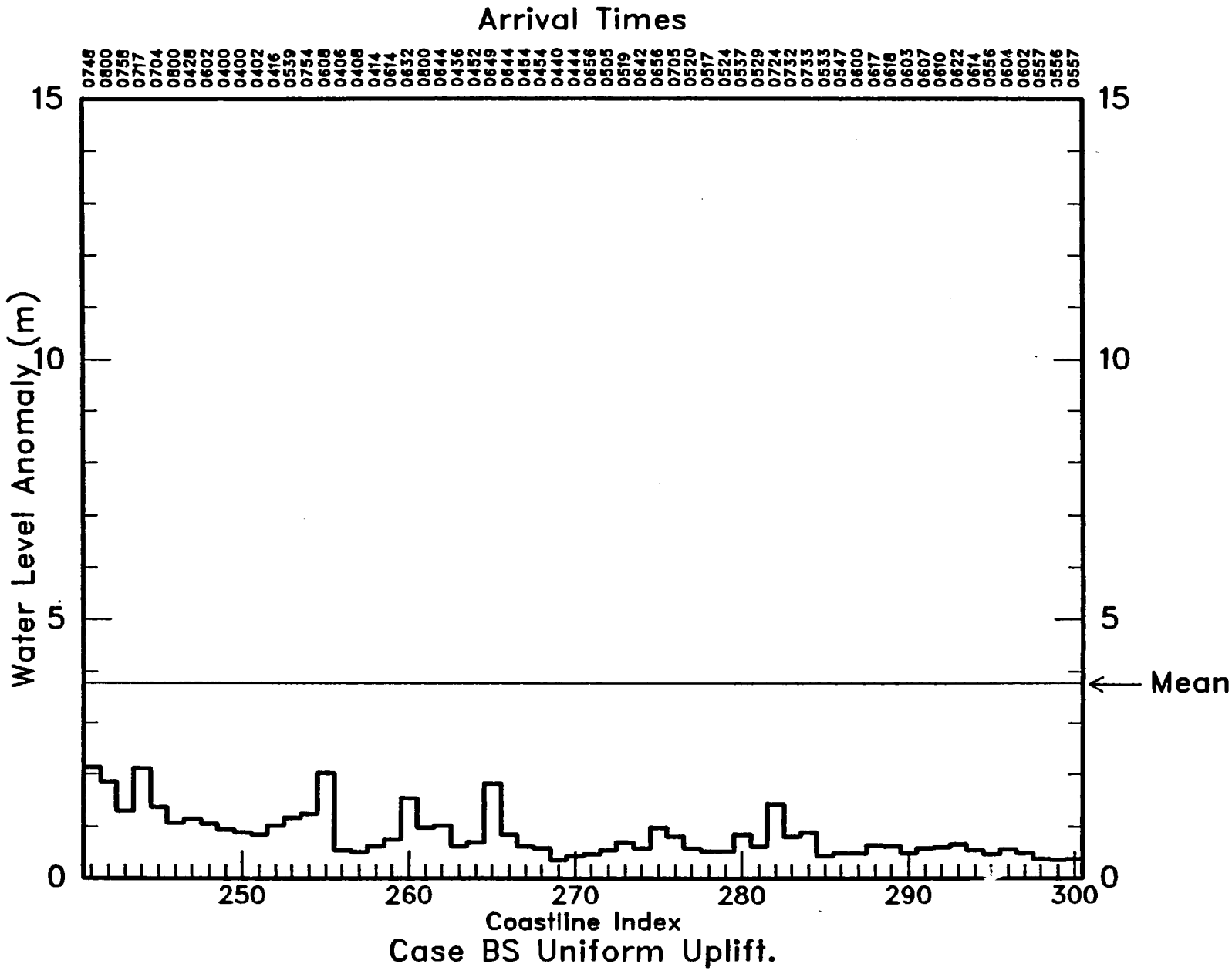
Arrival Times
0748 0800 0758 0717 0704 0800 0428 0602 0400 0400 0402 0416 0539 0754 0608 0406 0408 0414 0614 0632 0800 0644 0436 0452 0649 0644 0454 0454 0440 0444 0656 0505 0519 0642 0656 0705 0520 0517 0524 0537 0529 0724 0732 0733 0533 0547 0600 0617 0618 0603 0607 0610 0622 0614 0556 0604 0602 0557 0556 0557
Water Level Anomaly (m)
15
10
5
0
250
260
270
280
290
300
Coastline Index
Mean
Case BS Uniform Uplift.

Figure: 5.25 (f)

5.5 SOUTHERN ZONE - VARIABLE UPLIFT CASE

This uplift pattern fills the entire southern area indicated in Figure 5.1. The maximum vertical displacement is 10 m.

5.5.1 Immediate Effects

The surface wave contours after one hour (Figure 5.26) are in some ways quite similar to those for the northern zone (Figure 5.10). A large portion of the energy is propagating seaward, secondary crests follow the initial wave, and reflections due to the coastal bend are apparent. A large concentration of wave energy remains in the source area, also.

5.5.2 Longer Duration Effects

The hydrograph at Antofagasta (Figure 5.27) shows an initial steep rise at the start of the simulation. This quickly (in less than an hour) damps down to a long, slowly diminishing series of oscillations with elevations of no more than a meter.

Arica, to the north of the source, receives a long train of high waves which persists for the full 8 hours (Figure 5.28). It is striking that in most cases the troughs on this record are quite deep, while the crests are relatively low. Valparaiso (Figure 5.29) also receives a persistent wave train, but the elevations are markedly lower than those at Arica.

As the waves move north past Lima (Figure 5.30), Isla de Puna (Figure 5.31), and Buenaventura (Figure 5.32),

they become longer and lower, until the waves at Buenaventura barely register.

5.5.3 Maximum Elevations

The maximum elevation plots (Figure 5.33a-f) for this case show that the effects of this tsunami are greatest near the source zone, but that high waves occur at intervals all along the coast from the southern end of the model area to the vicinity of Chimbote, Peru. The greatest concentration of extreme wave heights occurs in the short length of coast between Antofagasta and Iquique, but local extremes appear fairly often. Only in the region north of Talara are wave elevations low enough to be considered only a weak threat.

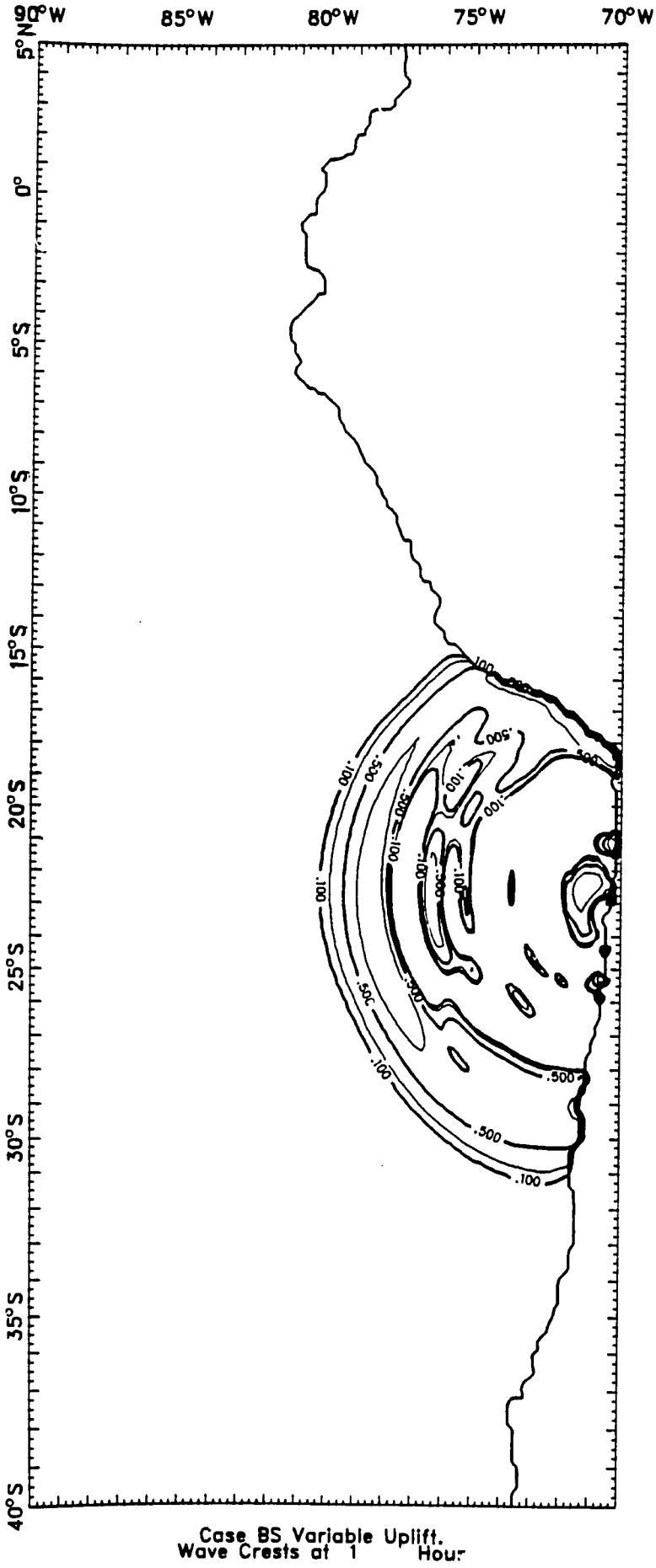

Figure: 5.26

Surface elevation (positive only) one hour after a variable uplift in the southern portion of source Zone B. Contours correspond to 0.1, 0.2, 0.5, 1.0, and 2.0 m.

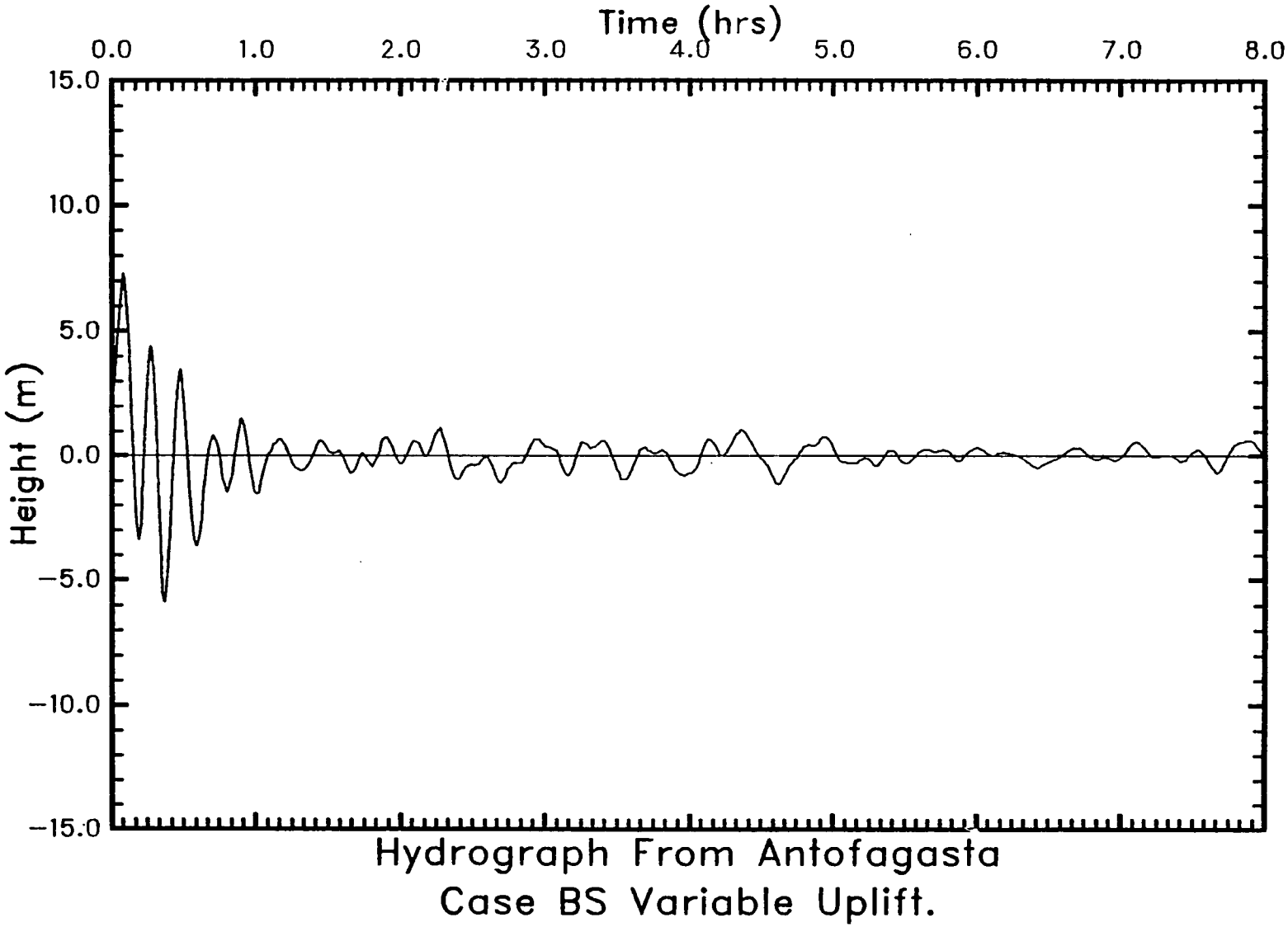

Figure 5.27: Wave elevation as a function of time at the recording point near Antofagasta, Chile. These waves were generated by the variable uplift of the southern portion of Zone B.

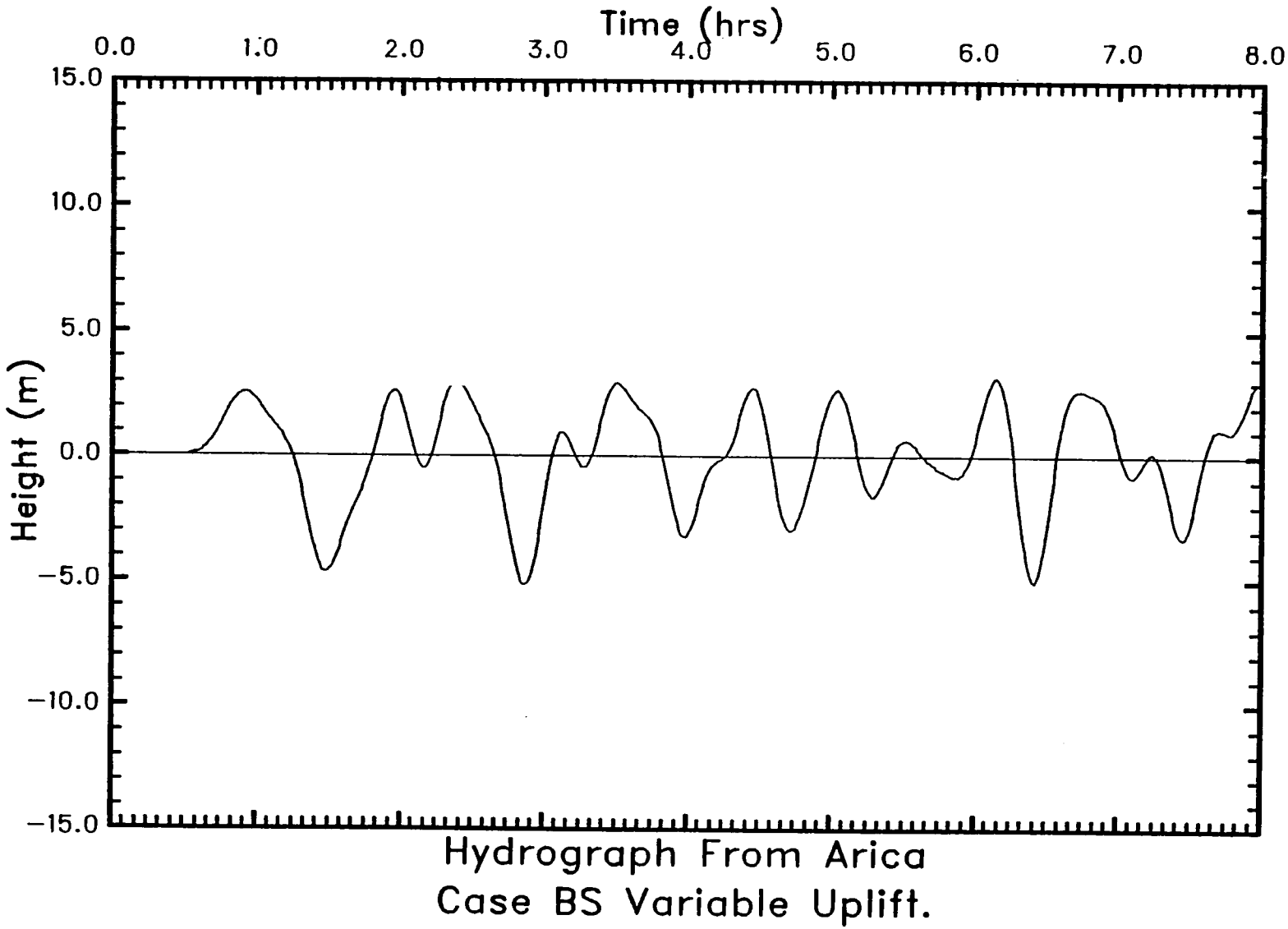

Figure 5.28: Wave elevation as a function of time at the recording point near Arica, Chile. These waves were generated by the variable uplift of the southern portion of Zone B.

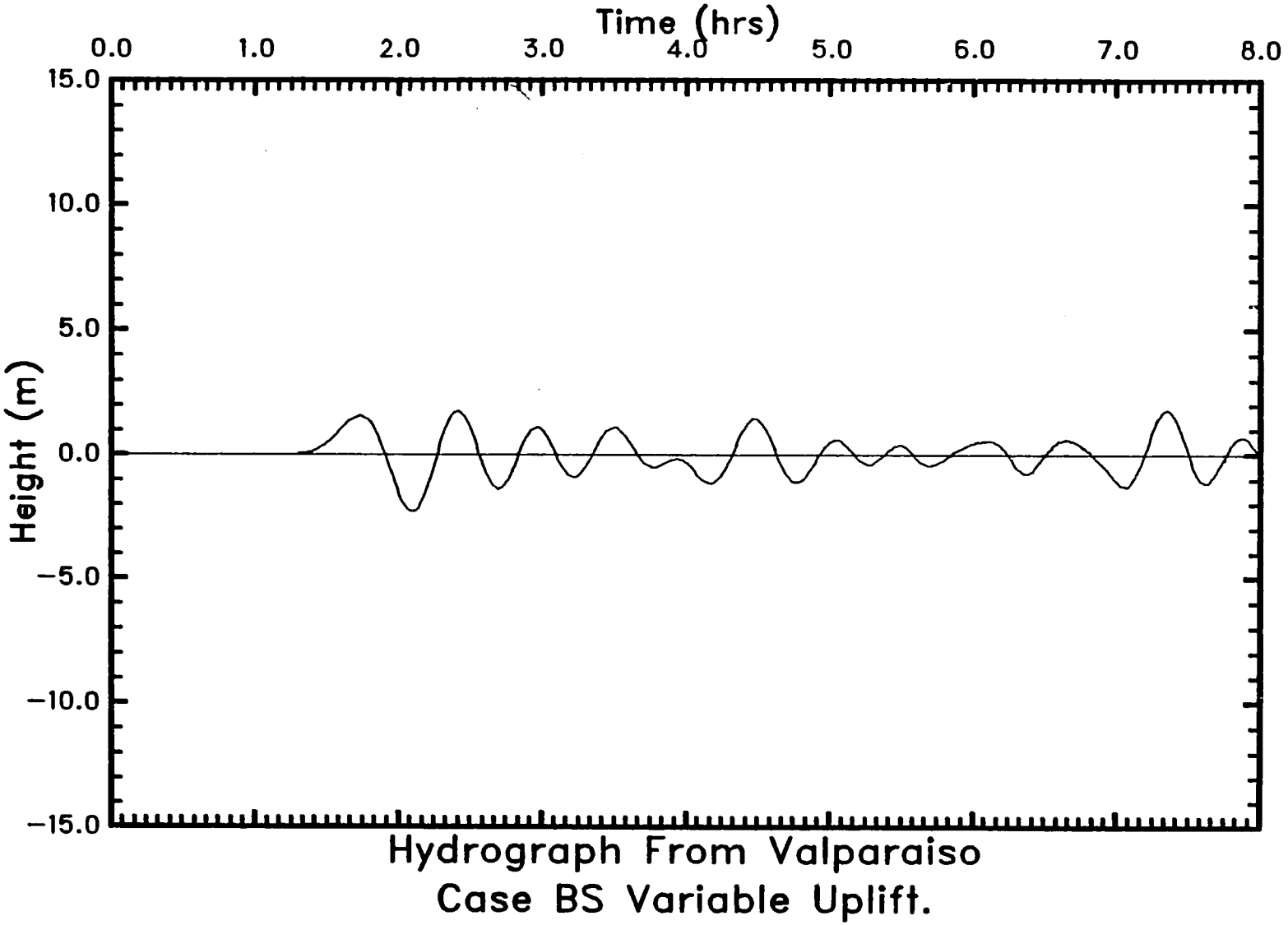

Figure 5.29: Wave elevation as a function of time at the recording point near Valparaiso, Chile. These waves were generated by the variable uplift of the southern portion of Zone B.

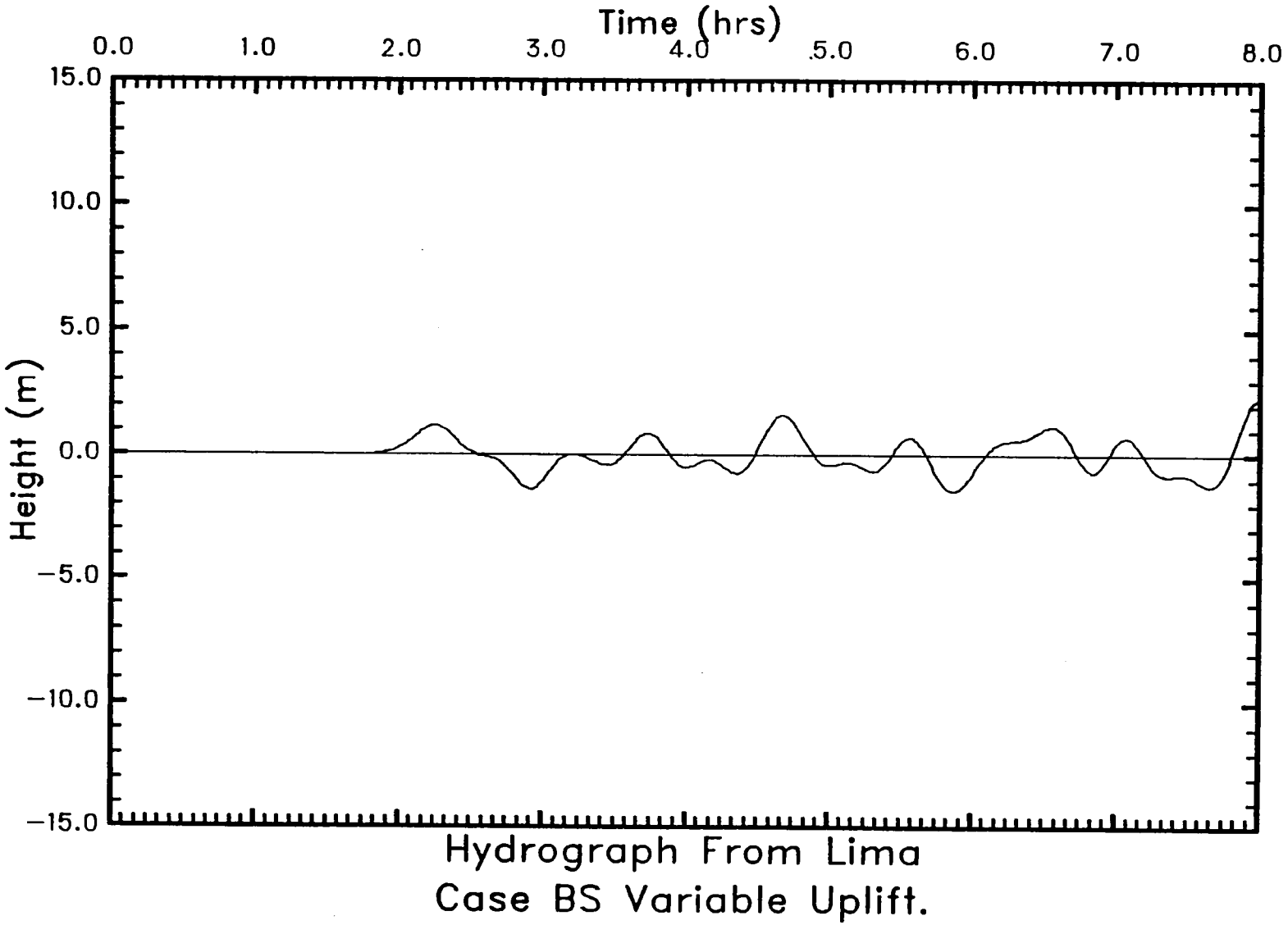

Figure 5.30: Wave elevation as a function of time at the recording point near Lima, Peru. These waves were generated by the variable uplift of the southern portion of Zone B.

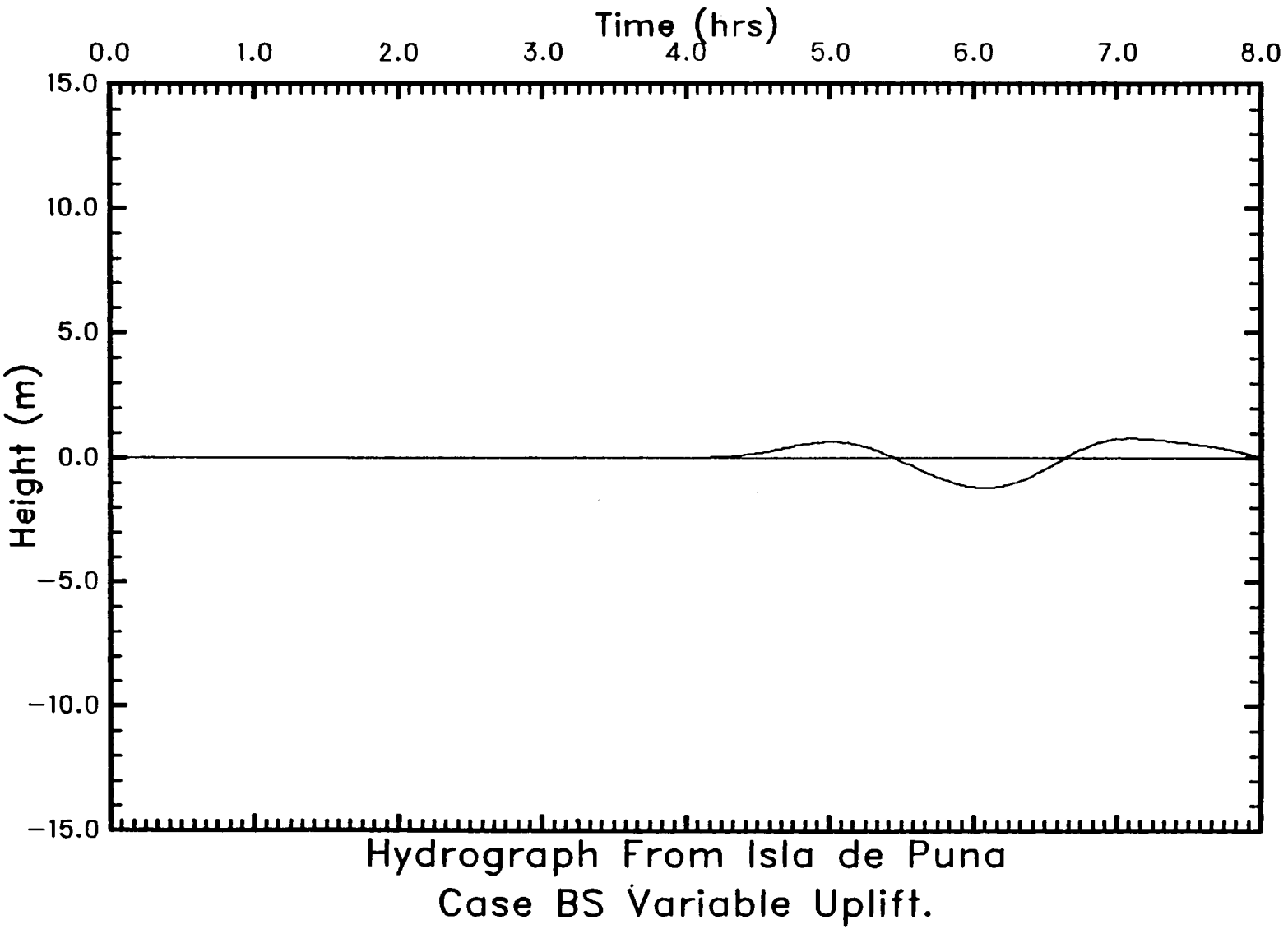

Figure 5.31: Wave elevation as a function of time at the recording point near Isla de Puna, Colombia. These waves were generated by the variable uplift of the southern portion of Zone B.

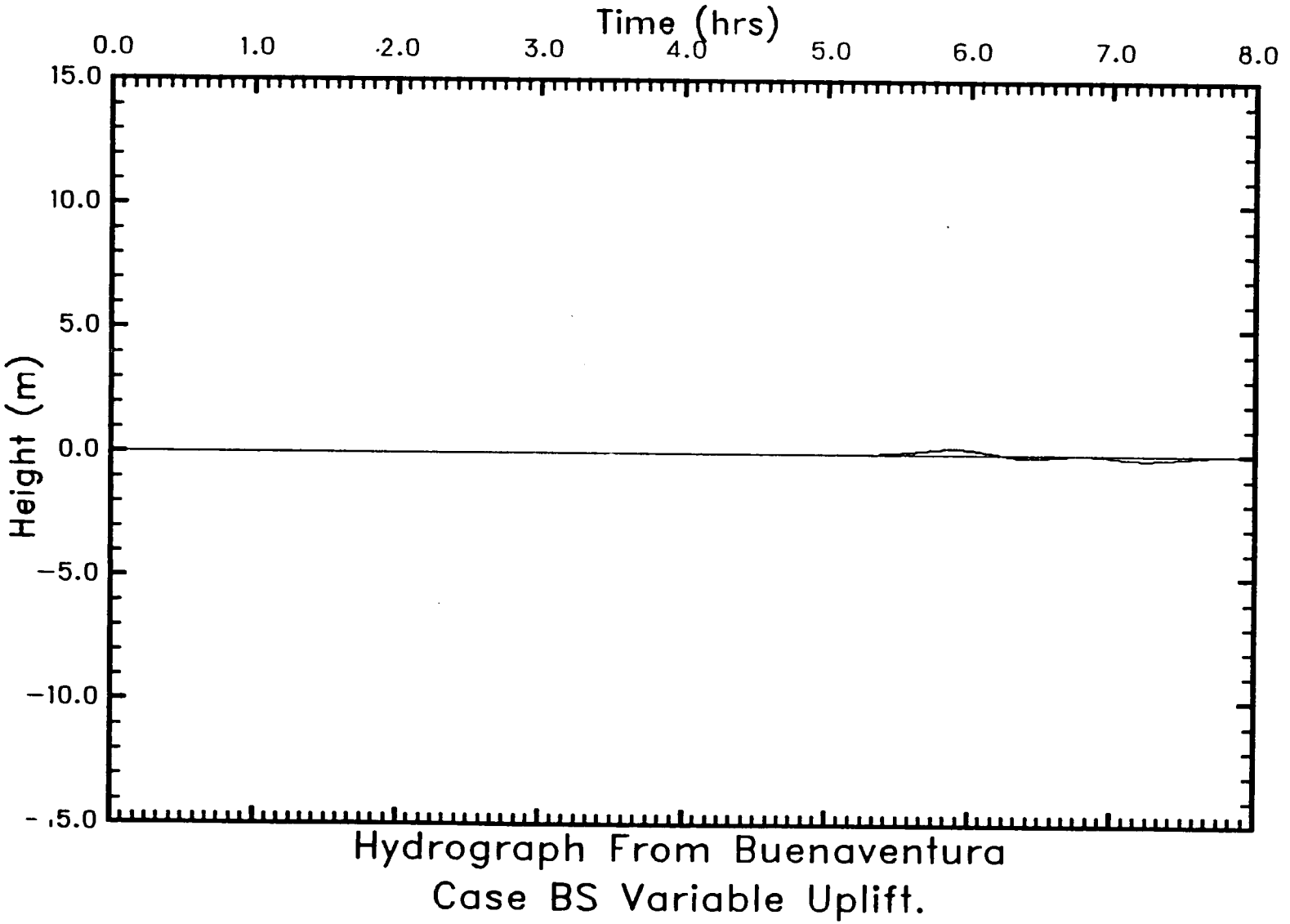

Figure 5.32: Wave elevation as a function of time at the recording point near Buenaventura, Ecuador. These waves were generated by the variable uplift of the southern portion of Zone B.

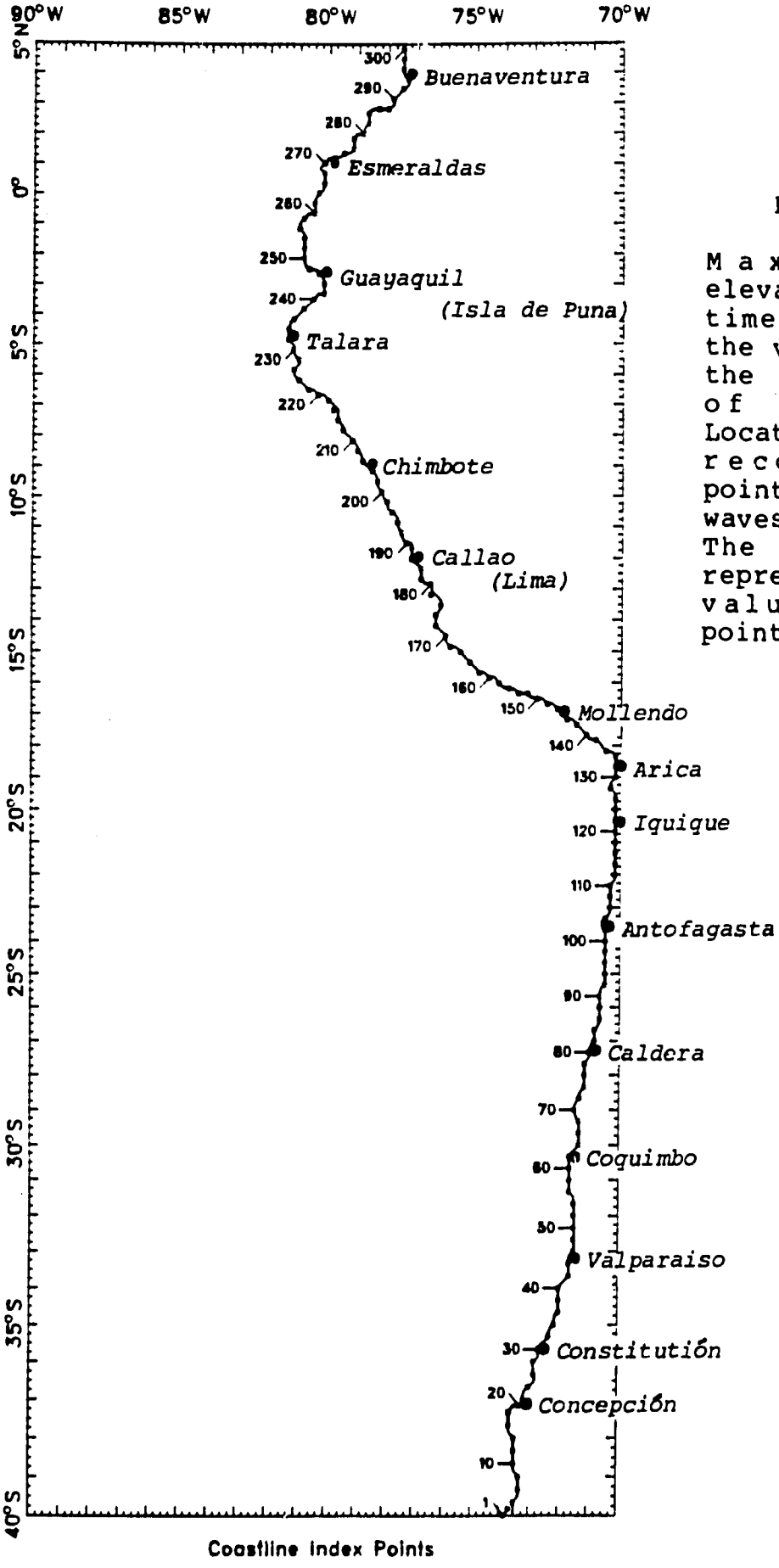

Figure: 5.33

Maximum wave elevations and arrival times of waves from the variable uplift in the southern portion of Zone B. (a) Locations of the 300 recording point points. (b-f) Maximum waves at each point. The horizontal line represents the average value of all 300 points.

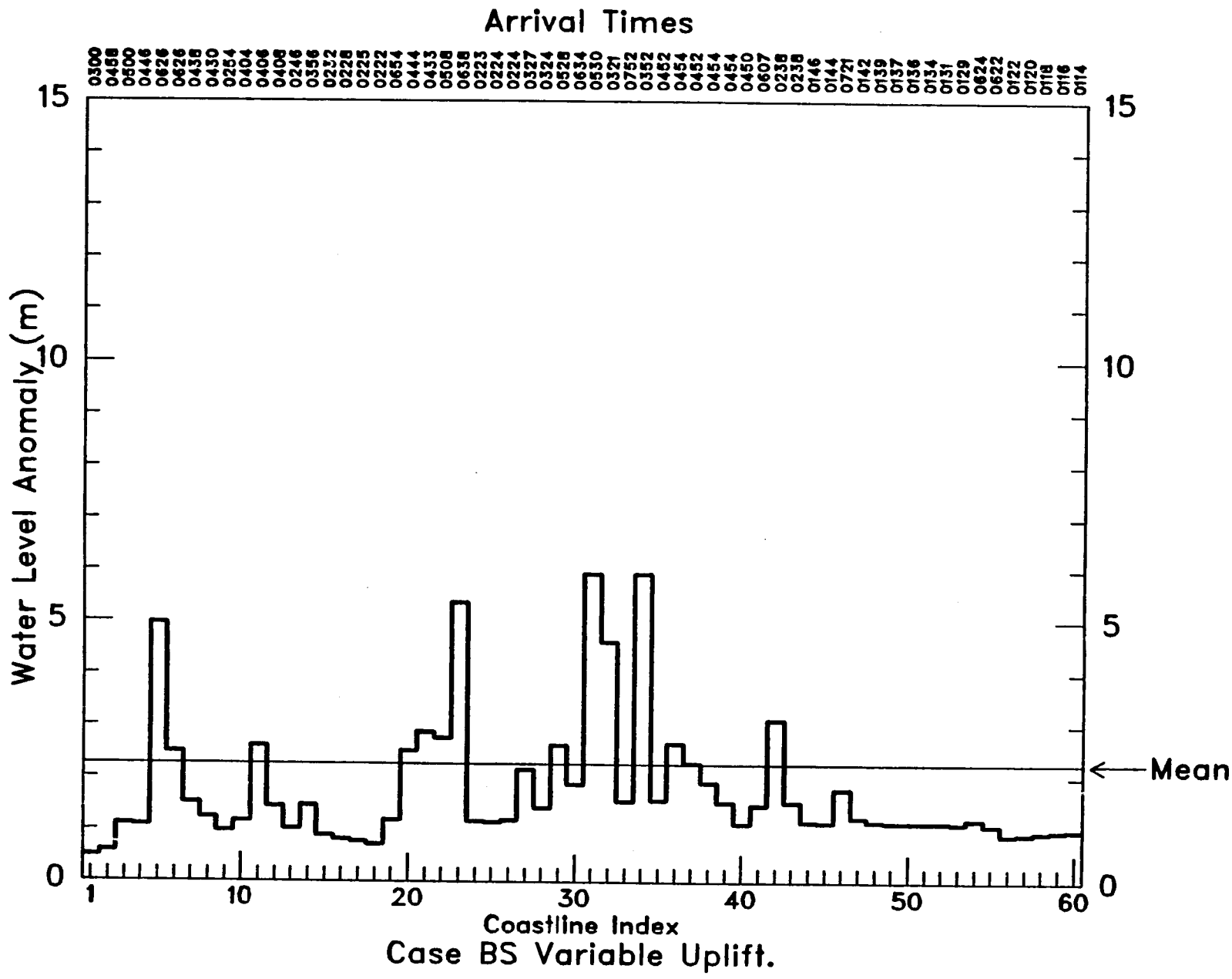
Arrival Times
0300 0458 0500 0446 0626 0626 0438 0430 0254 0404 0406 0408 0246 0356 0232 0228 0225 0222 0654 0444 0433 0508 0638 0223 0224 0224 0327 0324 0528 0634 0530 0321 0752 0352 0452 0454 0452 0454 0454 0450 0607 0238 0238 0146 0144 0721 0142 0139 0137 0136 0134 0131 0129 0624 0622 0122 0120 0118 0116 0114
Water Level Anomaly (m)
0
5
10
15
Mean
1
10
20
30
40
50
60
Coastline Index
Case BS Variable Uplift.

Figure: 5.33 (b)

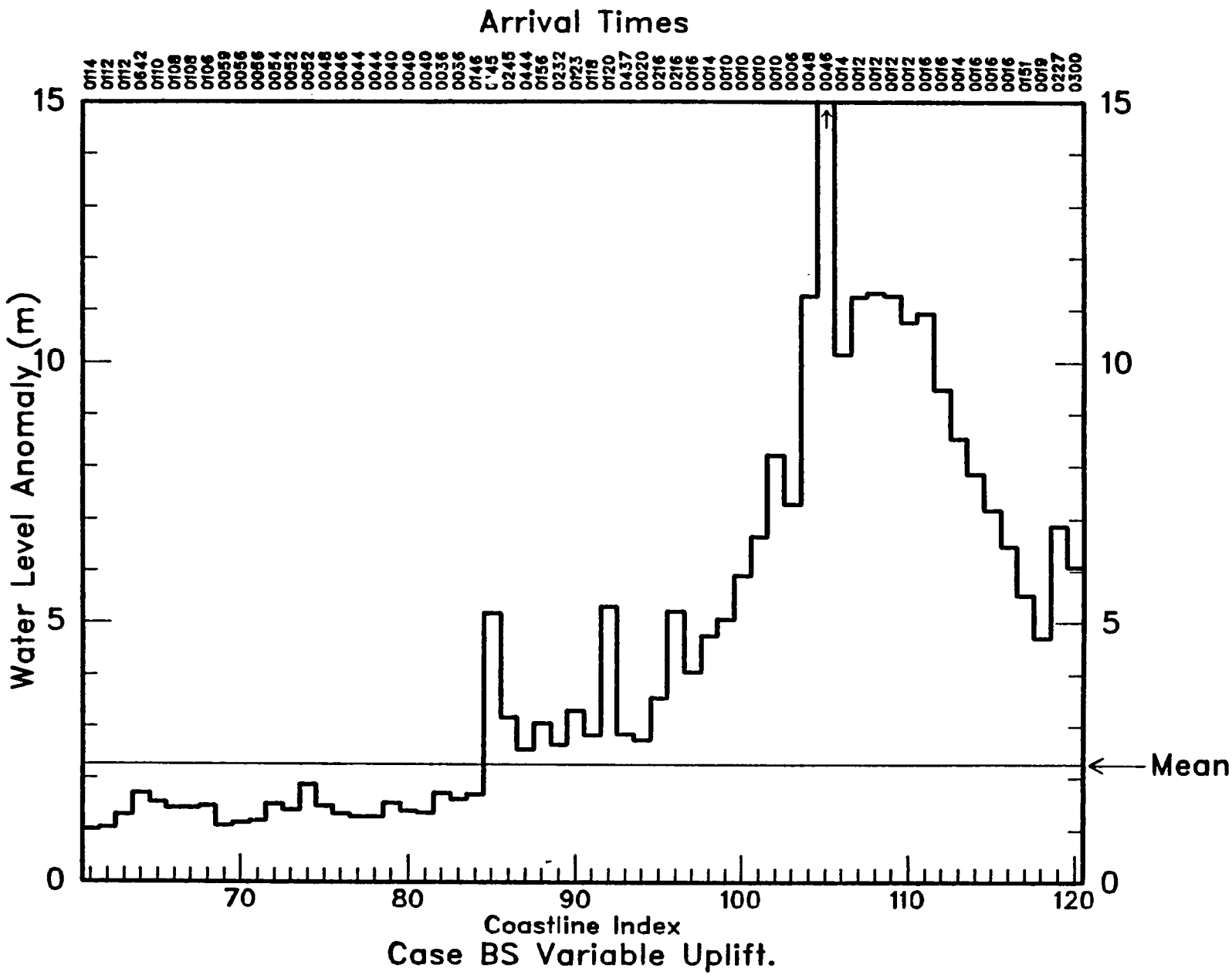
Arrival Times
0114 0112 0112 0642 0110 0108 0108 0106 0059 0056 0056 0054 0052 0052 0048 0046 0044 0044 0040 0040 0040 0036 0036 0146 0145 0245 0444 0156 0232 0123 0118 0120 0437 0020 0216 0216 0016 0014 0010 0010 0010 0010 0006 0048 0046 0014 0012 0012 0012 0012 0016 0016 0014 0016 0016 0016 0151 0019 0227 0300
Water Level Anomaly (m)
15
10
5
0
70
80
90
100
110
120
Coastline Index
Mean
Case BS Variable Uplift.

Figure: 5.33 (c)

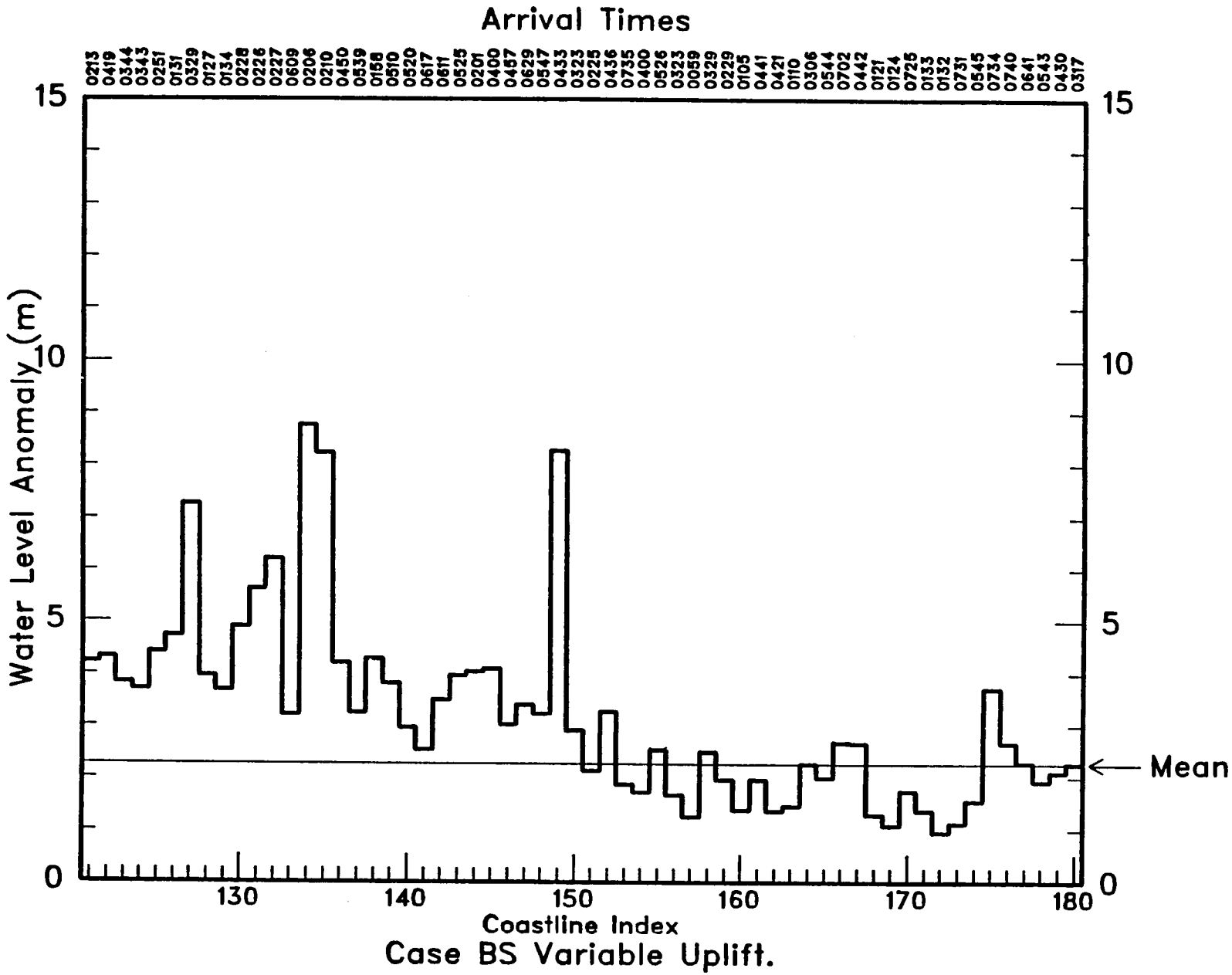
Arrival Times
0213 0419 0344 0343 0251 0131 0329 0127 0134 0228 0226 0227 0609 0206 0210 0450 0539 0158 0510 0520 0617 0611 0525 0201 0400 0457 0629 0547 0433 0323 0225 0436 0735 0400 0526 0323 0059 0329 0229 0105 0441 0421 0110 0306 0544 0702 0442 0121 0124 0726 0133 0132 0731 0545 0734 0740 0641 0543 0430 0317
Water Level Anomaly (m)
0
5
10
15
130
140
150
160
170
180
Mean
Coastline Index
Case BS Variable Uplift.

Figure: 5.33 (d)

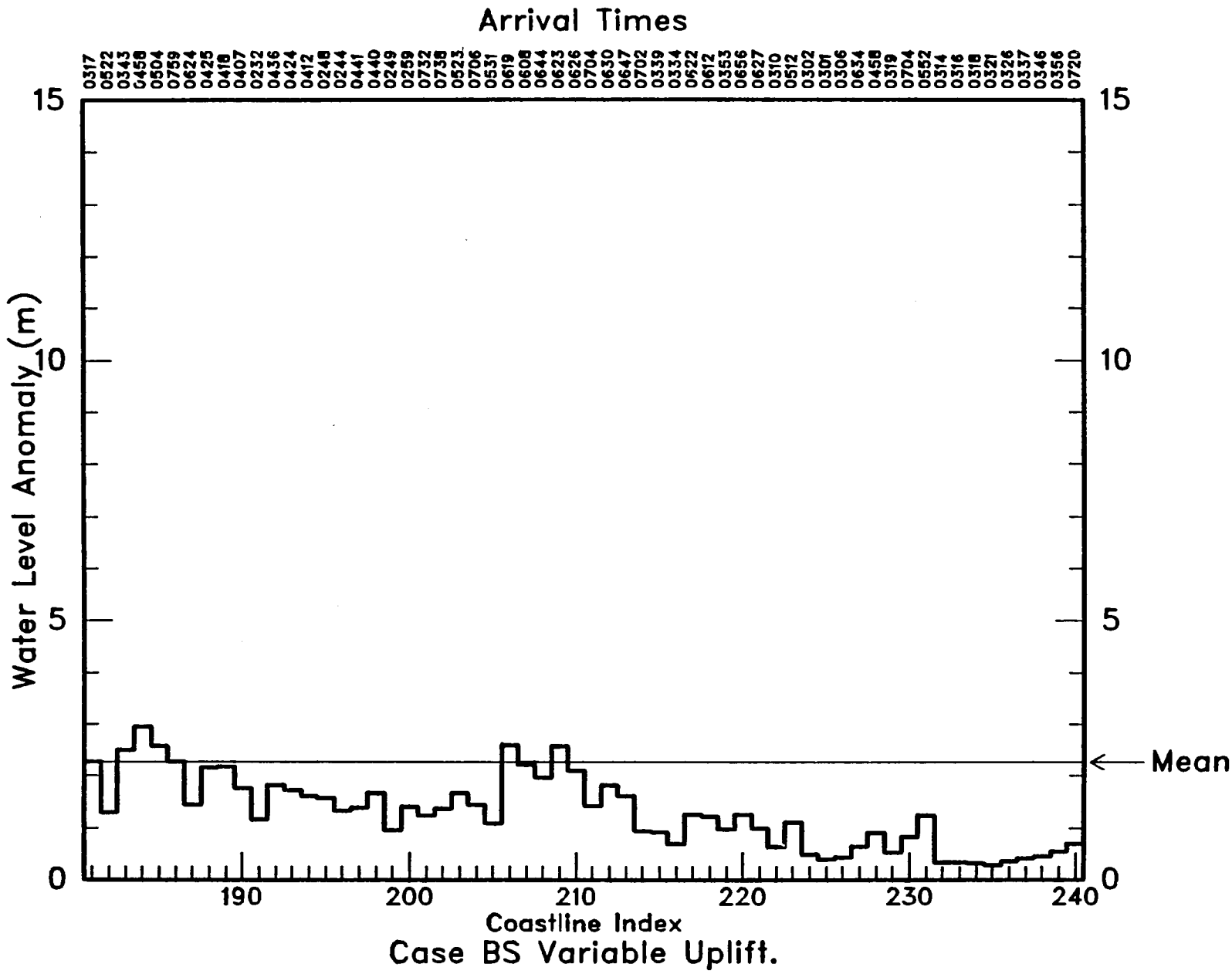
Arrival Times
0317 0522 0343 0458 0504 0759 0624 0425 0418 0407 0232 0436 0424 0412 0248 0244 0441 0440 0249 0259 0732 0738 0523 0706 0531 0619 0608 0644 0623 0626 0704 0630 0647 0702 0339 0334 0622 0612 0353 0656 0627 0310 0512 0302 0301 0306 0634 0458 0319 0704 0552 0314 0316 0318 0321 0326 0337 0346 0356 0720
Water Level Anomaly (m)
15
10
5
0
190
200
210
220
230
240
Coastline Index
Mean
Case BS Variable Uplift.

Figure: 5.33 (e)

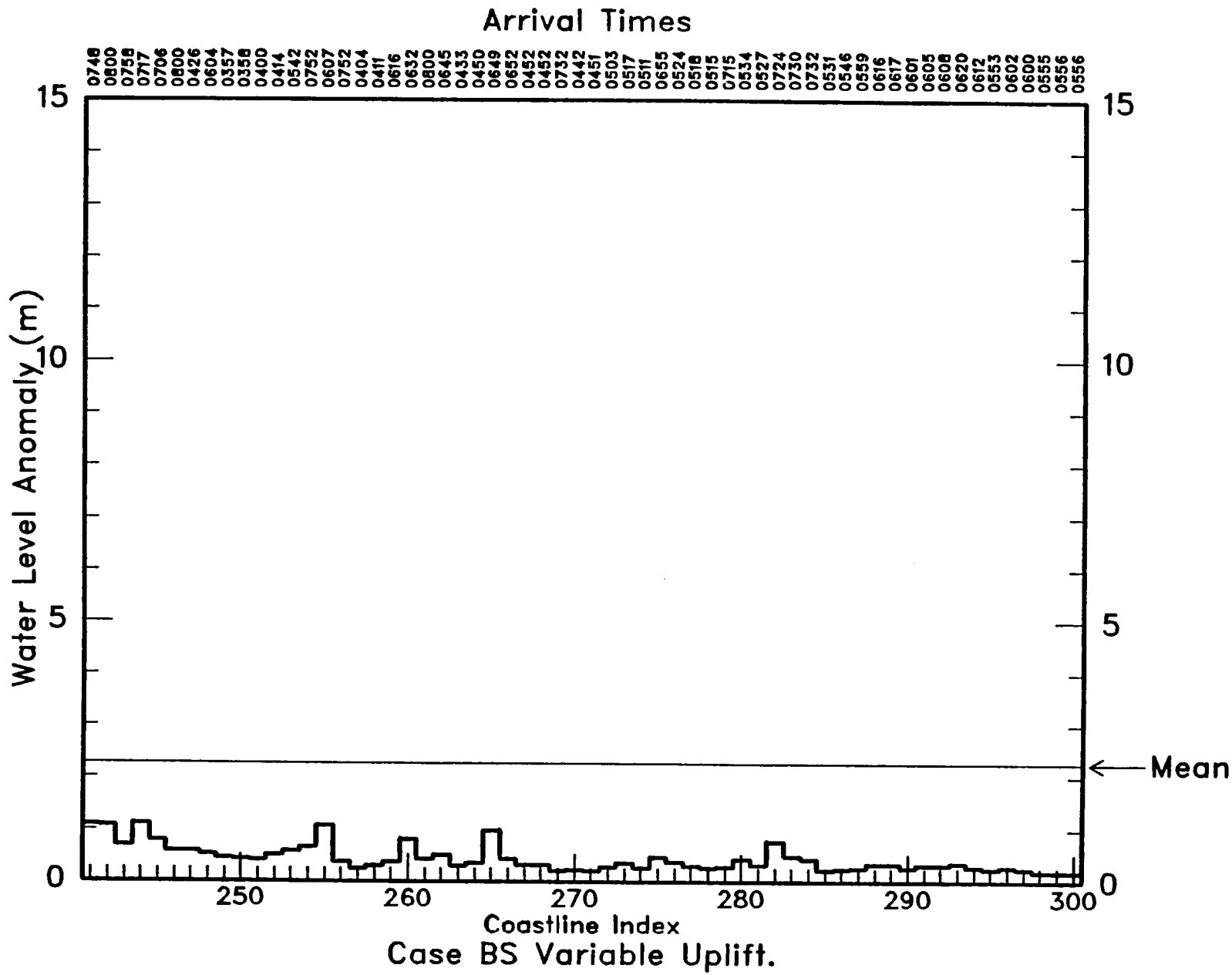

Case BS Variable Uplift.

Figure: 5.33 (f)

5.6 HAZARD ASSESSMENT - ZONE B

The two subzones used to locate hypothetical earthquakes in this zone are oriented quite differently along the South American coast. We discuss the threat from each subzone separately.

5.6.1 Northern Subzone

Both types of uplift produce quite energetic tsunamis. The mean elevation for the uniform case is about 3.1 m, but the mean for the variable case only drops to 2.0 m. Once again, the time series are quite similar in everything but amplitude. Only after 6 or 7 hrs do hydrographs from the different runs show really noticeable differences.

The patterns of wave height distribution are also nearly identical. In both cases the most concentrated threat lies along the coast between Arica and an area southeast of Lima. But high calculated wave elevations are common up and down the coast as far north as Talara and all the way south past Concepcion. Only in the region north of Guayaquil are wave heights consistently low enough to say that little hazard exists.

As we noted earlier, several locations in the far southern end of the coast are subject to surprisingly high waves. This is probably due to local topographic effects.

5.6.2 Southern Subzone

Both of the uplifts in this subzone also produce energetic tsunamis. The mean maximum elevation for the

uniform case is 3.7 m, while that for the variable case is 2.2 m. Again, the distribution patterns are quite similar. In both cases the threat is most severe for the coastal zone which starts just north of Caldera and ends northwest of Mollendo. But waves high enough to pose a potential threat are common as far north as Talara, especially after the uniform uplift. And, as usual, several regions south of the source zone are subject to extreme waves.

One noticeable difference between the two cases is the nature of the threat in the source zone. In the uniform uplift case, most of the section from points 99 to 119 receives waves at least 10 m high as soon as the simulation begins. In the variable uplift case only a relatively few points in that region receive waves that high, and then only after a delay of between 6 and 48 min. This is because the source area ends right at the coastline. In the uniform case the 10 m initial displacement is imposed on these points at the beginning. In the variable uplift case the section with a 10 m displacement is several grid points offshore and it takes time for the first shoreward crest to arrive. Also during that time the crest starts to spread to the north and south, and so the waves reaching the shore are no longer uniform in height along the coast, as they were after the uniform uplift.

5.6.3 Summary

Tsunamis coming out of these two source zones pose a significant threat to the whole South American coast south of Guayaquil. In both cases the immediate vicinity of the uplift receives the highest waves, but coastal areas near the continental bend are also threatened by waves reflecting in that area. This source zone produces the most threatening waves we have yet encountered.

Section 6
SOURCE ZONE C

6.1 INTRODUCTION

Source zone C extends from 25°S to 26°S. The topography of the region is quite similar to that of the southern subzone of zone B. Its location is shown in Figure 6.1. This is a small seismic gap and tsunamis originating here would not be expected to be very energetic.

6.2 UNIFORM UPLIFT CASE

In this situation the entire area depicted in Figure 6.1 moves 3 m upward.

6.2.1 Immediate Effects

The wave contours after one hour (Figure 6.2) confirm our expectation of low waves. The deep water crest height is slightly over 20 cm and the wave is spreading nearly uniformly in all directions. Some intense cells of wave energy do remain in the source zone, however.

6.2.2 Longer Duration Effects

The coastal wave records for this case depict waves of low energy which tend to die out quickly in some cases. At Antofagasta (Figure 6.3), which is closest to the source, the time history contains low amplitude, high frequency waves which persist for 3 to 4 hours and then decrease in amplitude. In contrast, Valparaiso and Arica (Figure 6.4 and 6.5) receive waves of only slightly higher amplitude but much

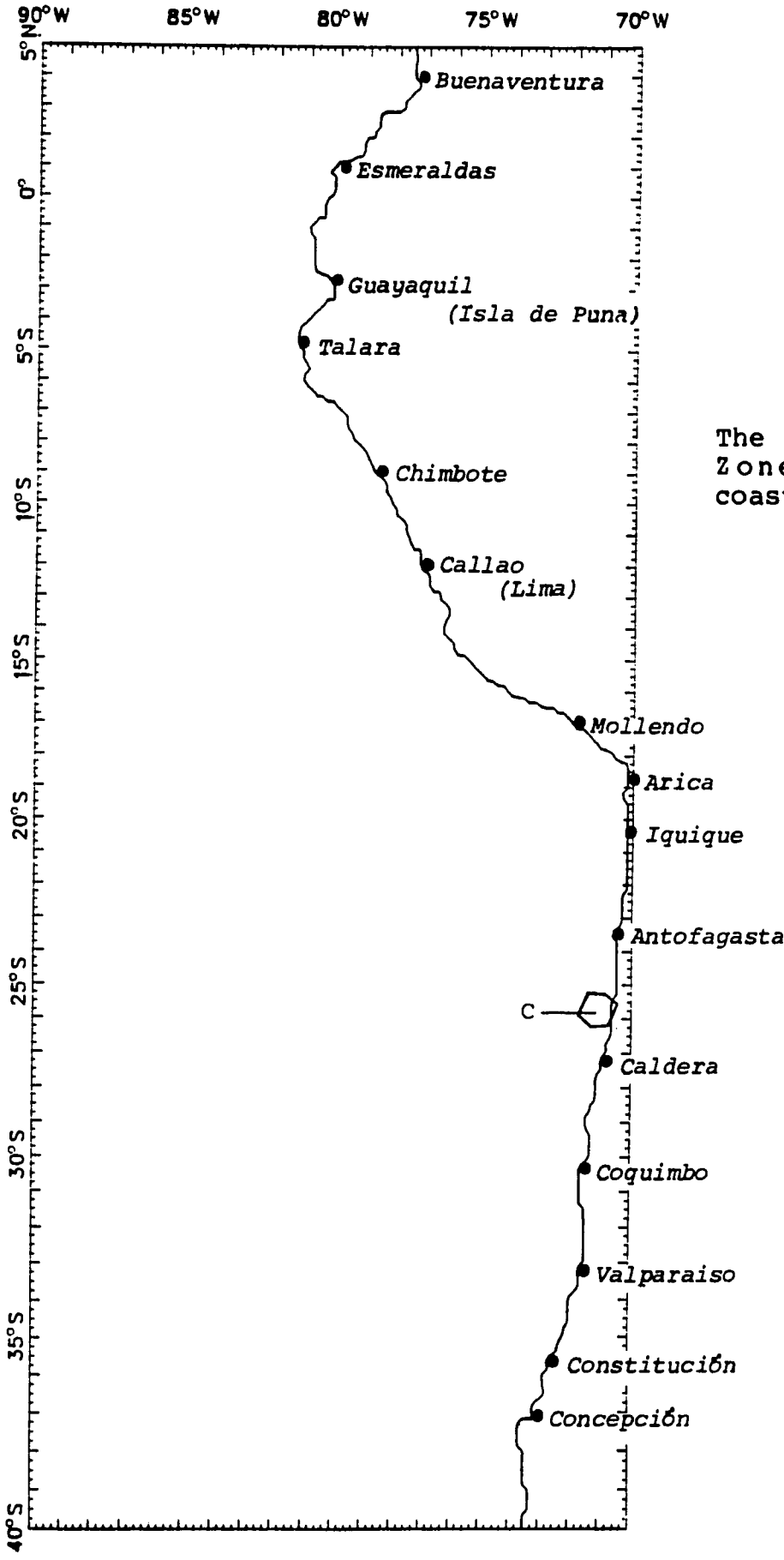

Figure 6.1:

The location of source Zone C along the coastline.

longer period. These persist with only small variations for the full 8 hours.

The locations farther north receive much lower wave energies, although activity near Lima (Figure 6.6) shows signs of increasing after 7 hours. By the time the waves reach Isla de Puna (Figure 6.7) and Buenaventura (Figure 6.8) they are only low, long period disturbances which pose little hazard.

6.2.3 Maximum Wave Heights

The average maximum elevation for this case is quite low--approximately 0.6 m. The highest elevations occur between Caldera and Antofagasta, along the shoreline near the source (see Figures 6.9a-f). Only in this region are the waves really high enough to be considered an unqualified hazard. Some above-average elevations do occur both north and south of the source, especially near Arica and the portion of the continent north of the bend. In general, though, this tsunami seems to pose little threat to coastal areas.

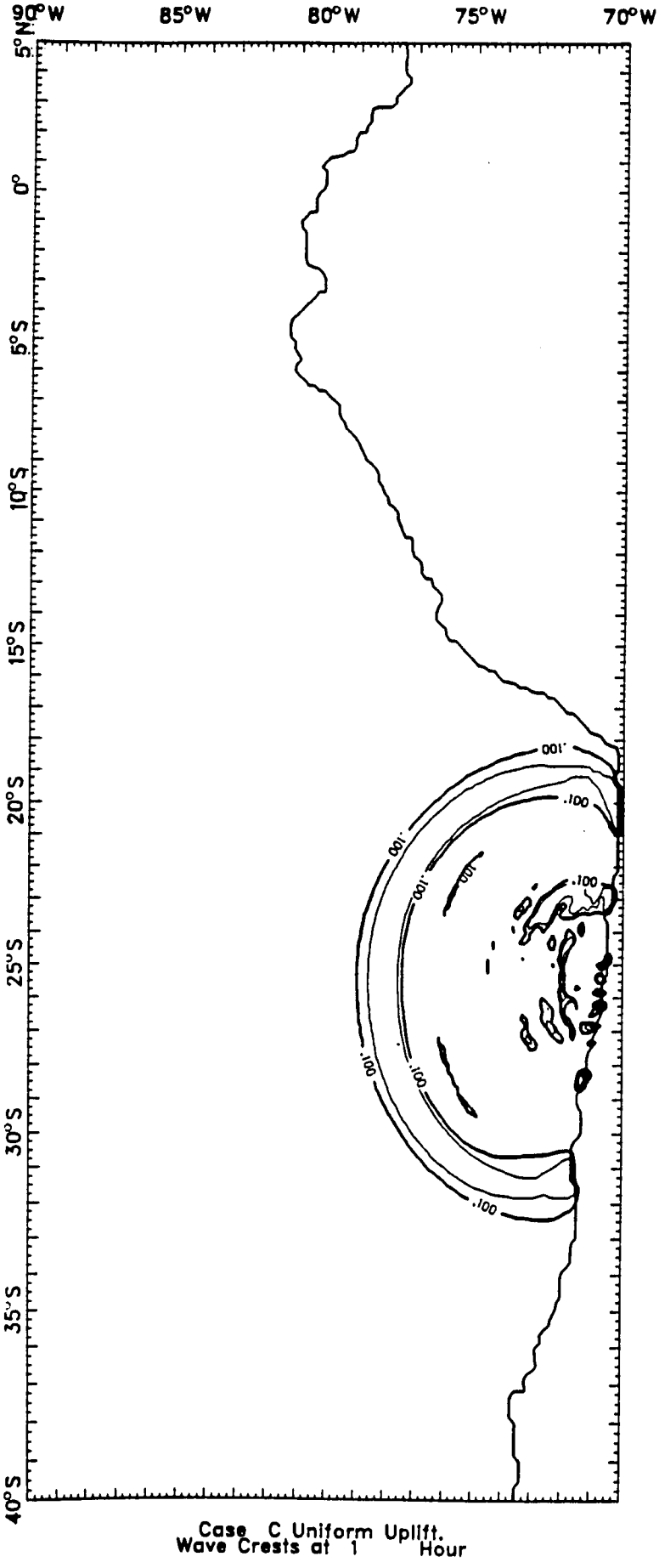

Figure: 6.2

Surface elevation (positive only) one hour after a uniform uplift in source Zone C. Contours correspond to 0.1, 0.2, 0.5, 1.0, and 2.0 m.

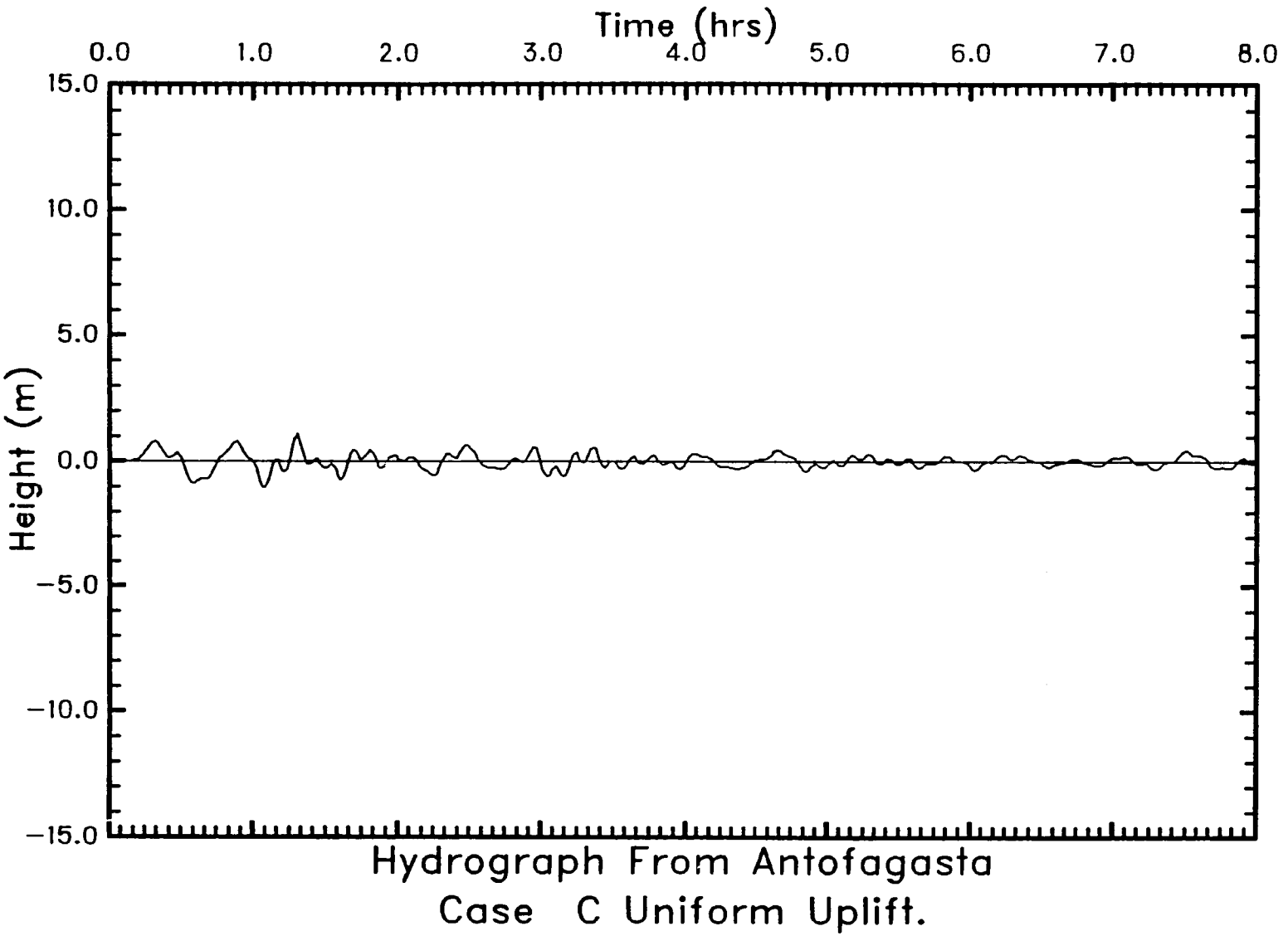

Figure 6.3: Wave elevation as a function of time at the recording point near Antofagasta, Chile. These waves were generated by the uniform uplift of Zone C.

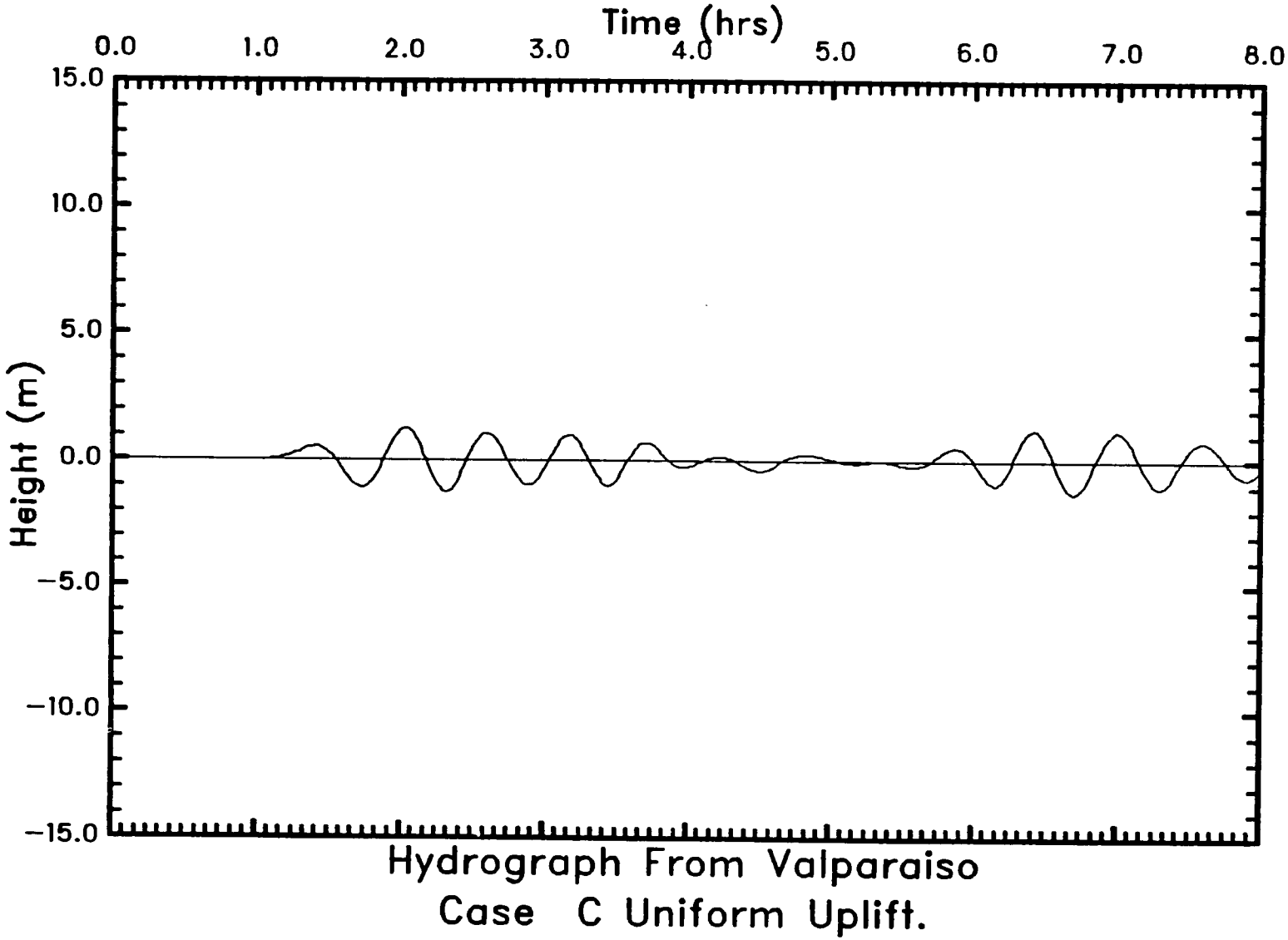

Figure 6.4: Wave elevation as a function of time at the recording point near Valparaiso, Chile. These waves were generated by the uniform uplift of Zone C.

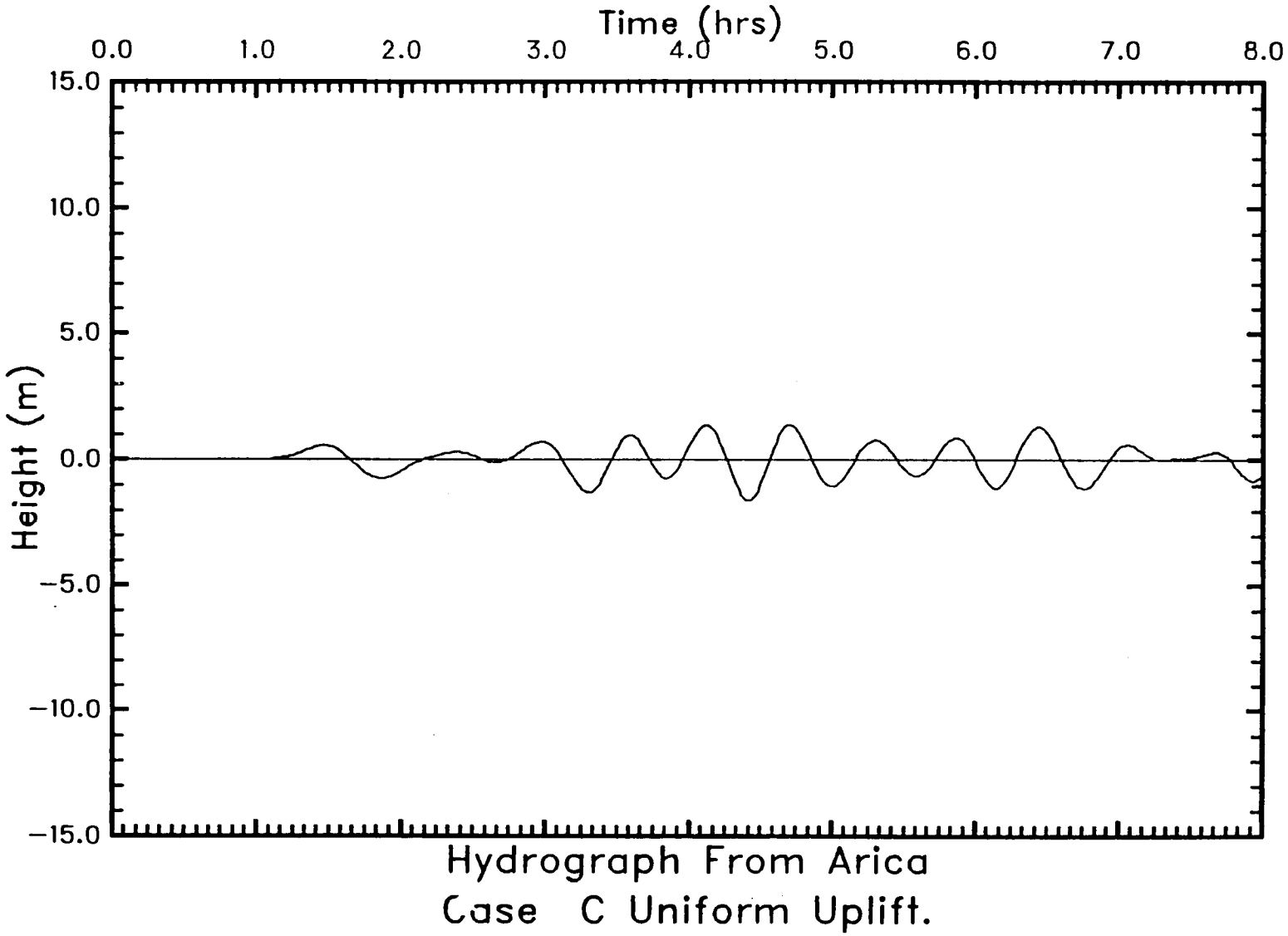

Figure 6.5: Wave elevation as a function of time at the recording point near Arica, Chile. These waves were generated by the uniform uplift of Zone C.

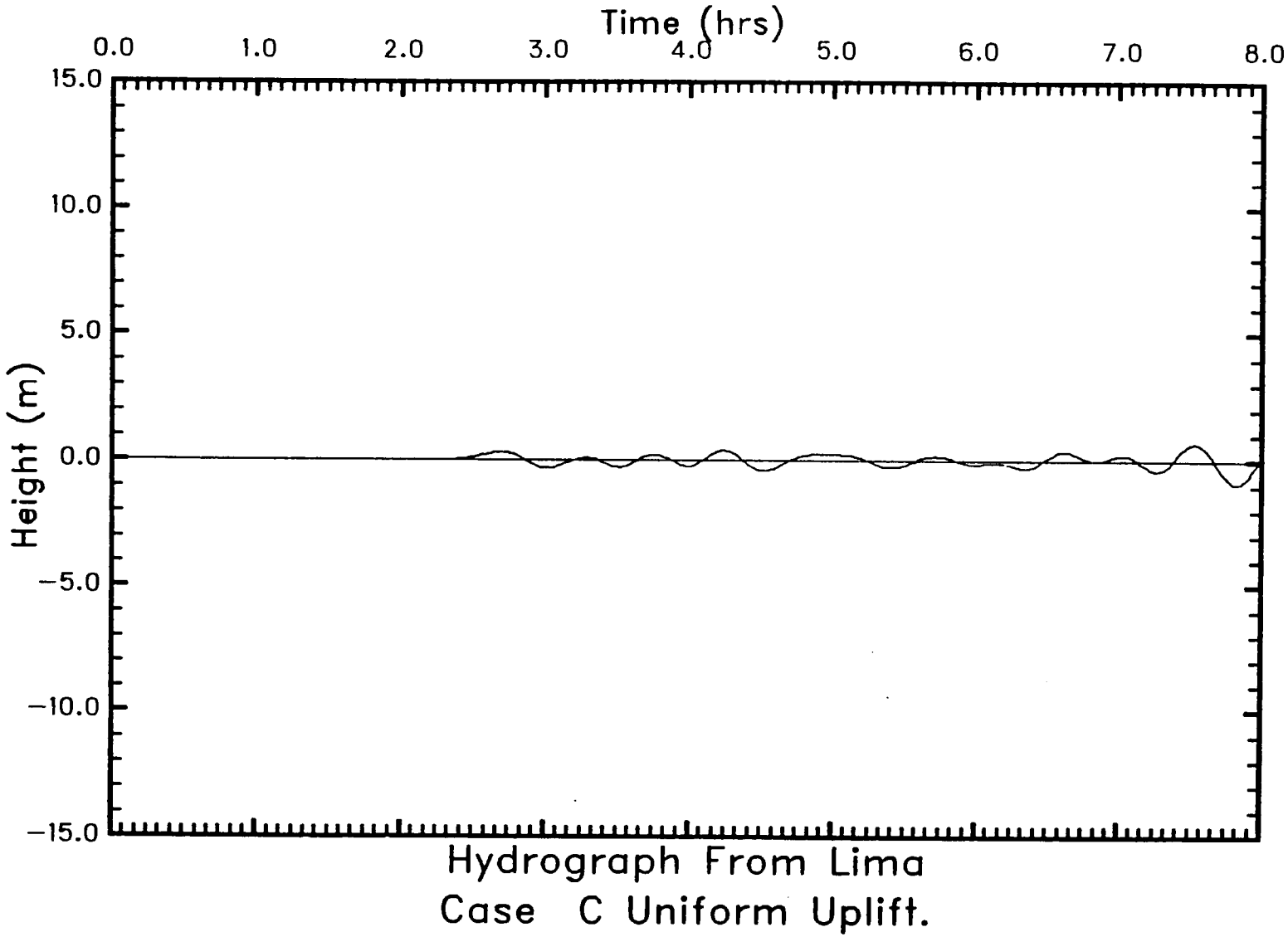

re 6.6: Wave elevation as a function of time at the recording point near Lima, Peru. These waves were generated by the uniform uplift of Zone C.

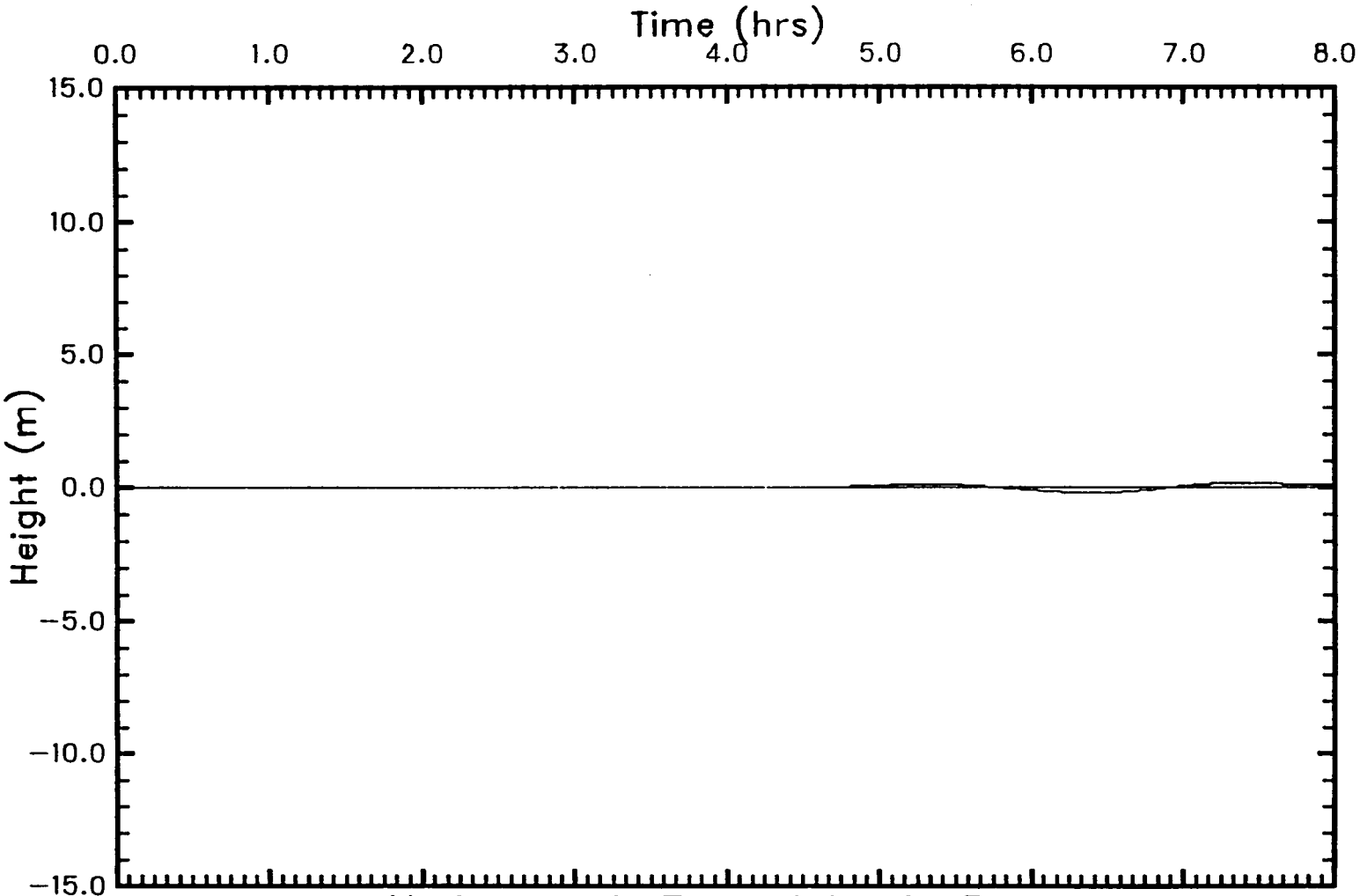

Hydrograph From Isla de Puna
Case C Uniform Uplift.

ıre 6.7: Wave elevation as a function of time at the recording point near Isla de Puna, Colombia. These waves were generated by the uniform uplift of Zone C.

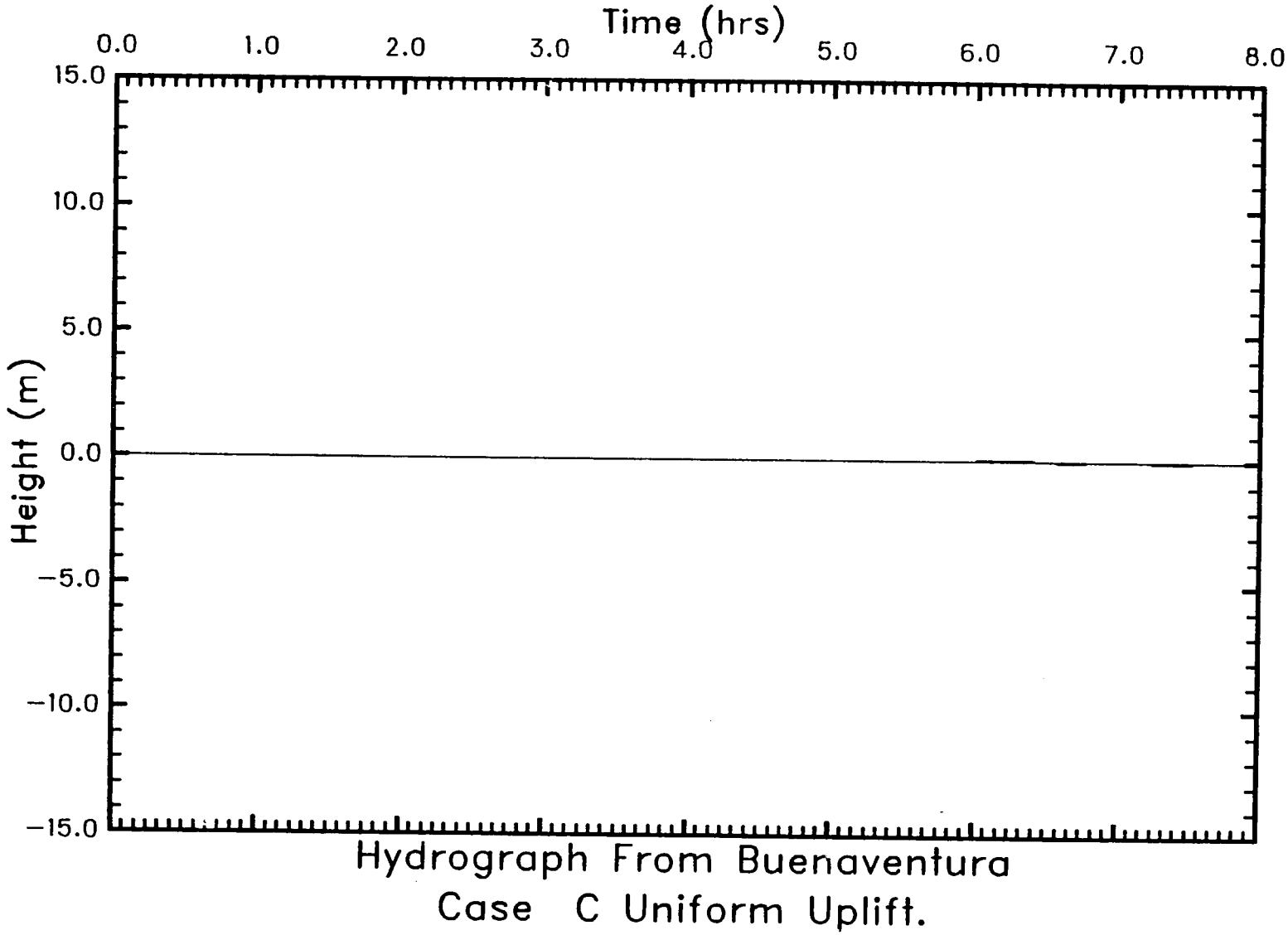

Figure 6.8: Wave elevation as a function of time at the recording point near Buenaventura, Ecuador. These waves were generated by the uniform uplift of Zone C.

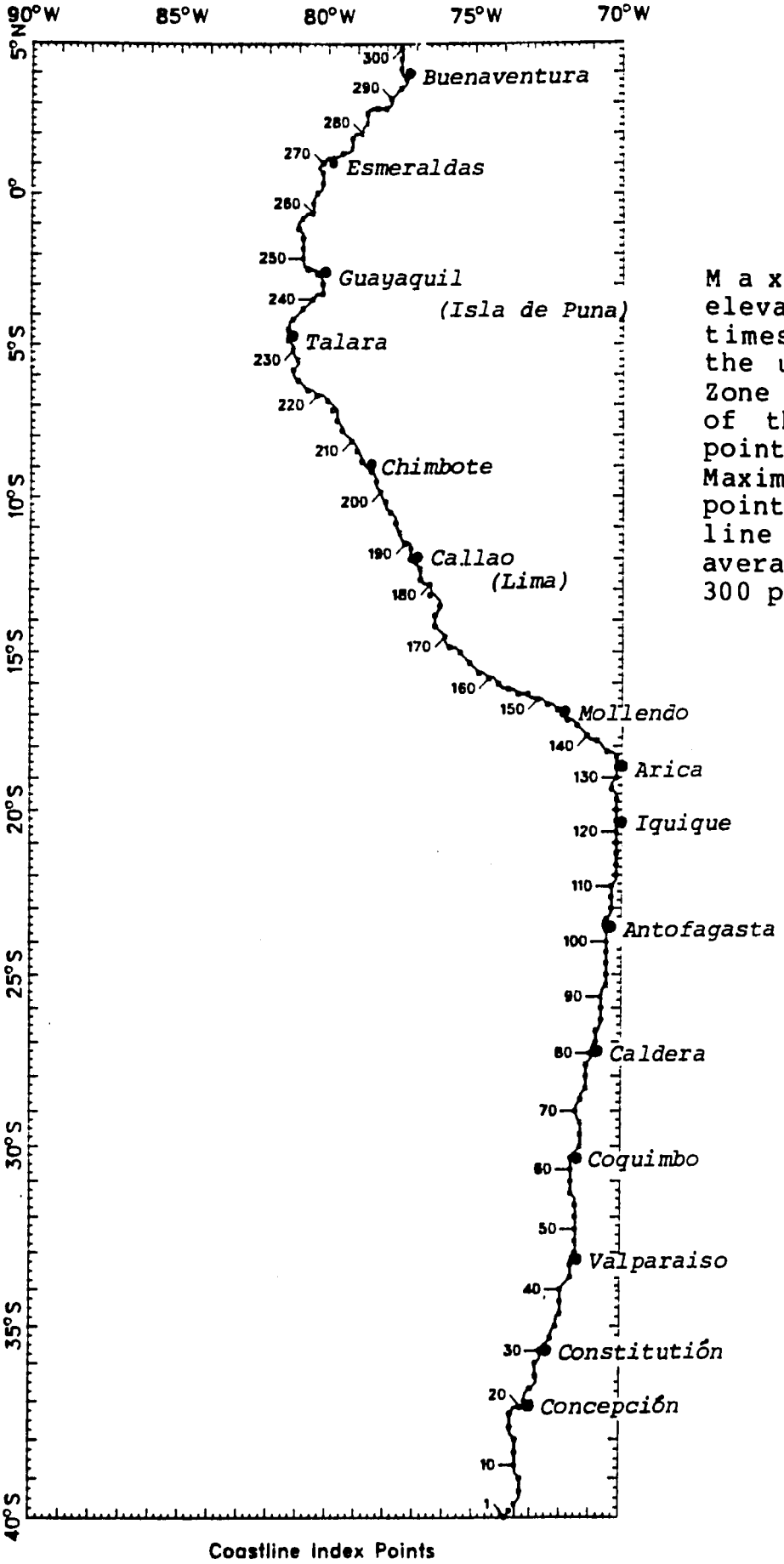

Figure: 6.9

Maximum wave elevations and arrival times of waves from the uniform uplift in Zone C. (a) Locations of the 300 recording point points. (b-f) Maximum waves at each point. The horizontal line represents the average value of all 300 points.

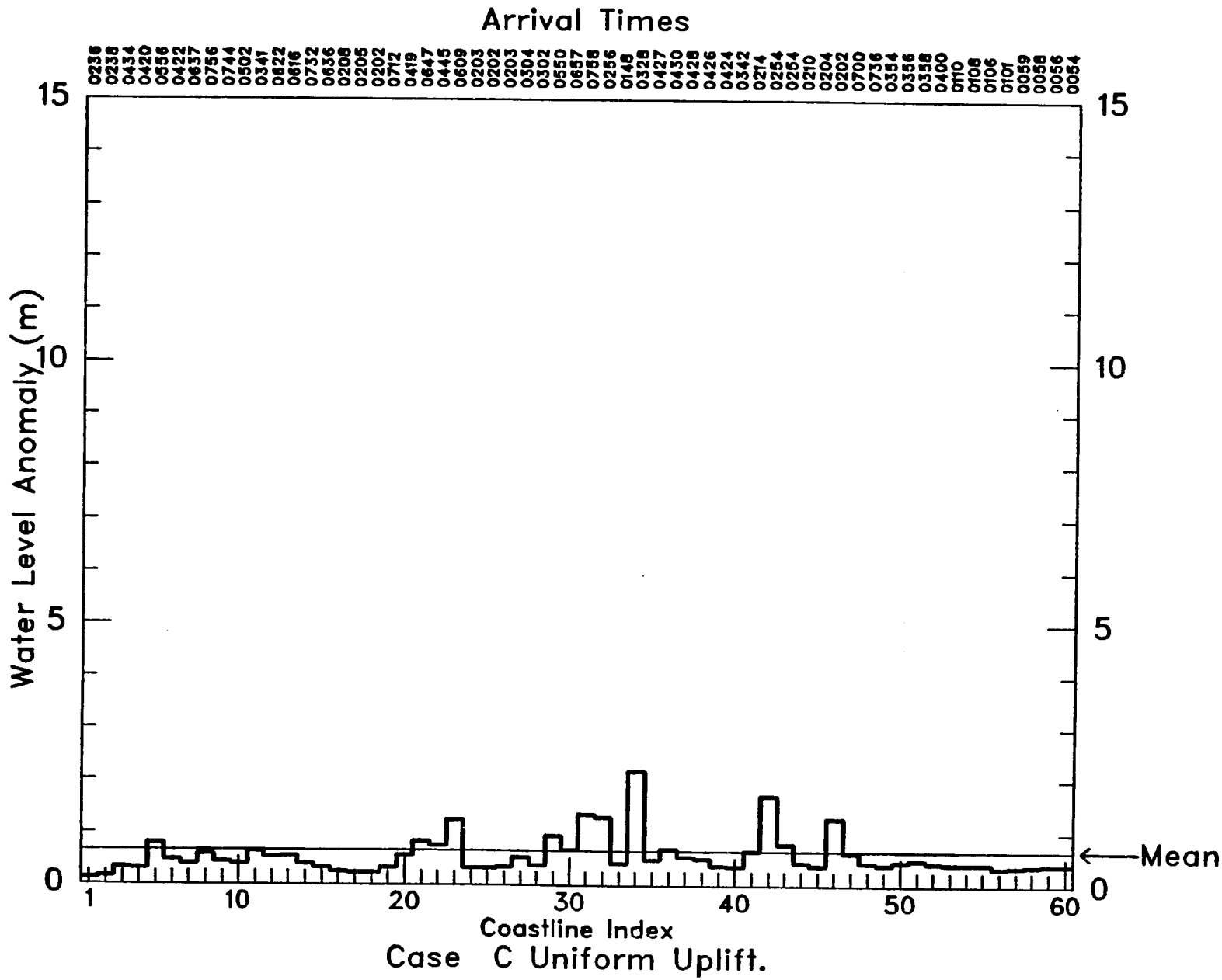
Arrival Times
0236 0238 0434 0420 0556 0422 0637 0756 0744 0502 0341 0622 0616 0732 0636 0208 0205 0202 0712 0419 0647 0445 0609 0203 0202 0203 0304 0302 0550 0657 0758 0256 0148 0328 0427 0430 0428 0426 0424 0342 0214 0254 0254 0210 0204 0202 0700 0736 0354 0356 0358 0400 0110 0108 0106 0101 0059 0058 0056 0054
Water Level Anomaly (m)
15
10
5
0
1
10
20
30
40
50
60
Coastline Index
Mean
Case C Uniform Uplift.

Figure: 6.9 (b)

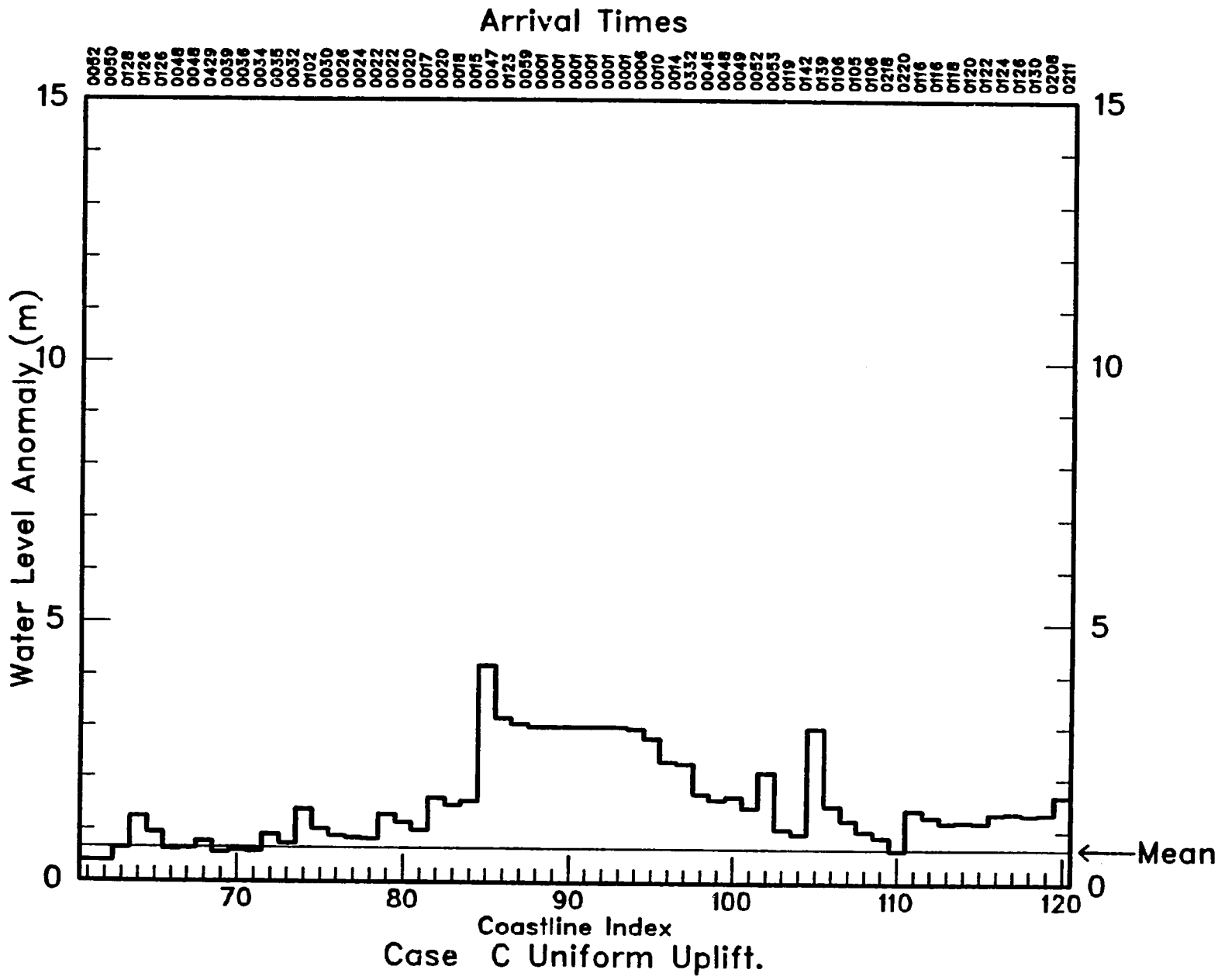
Arrival Times
0052 0050 0128 0126 0126 0048 0048 0429 0039 0036 0034 0035 0032 0102 0030 0026 0024 0022 0022 0020 0017 0020 0018 0015 0047 0123 0059 0001 0001 0001 0001 0001 0001 0001 0006 0010 0014 0332 0045 0048 0049 0052 0053 0119 0142 0139 0106 0105 0106 0218 0220 0116 0116 0118 0120 0122 0124 0126 0130 0208 0211
Water Level Anomaly (m)
15
10
5
0
70
80
90
100
110
120
Coastline Index
Mean
Case C Uniform Uplift.

Figure: 6.9 (c)

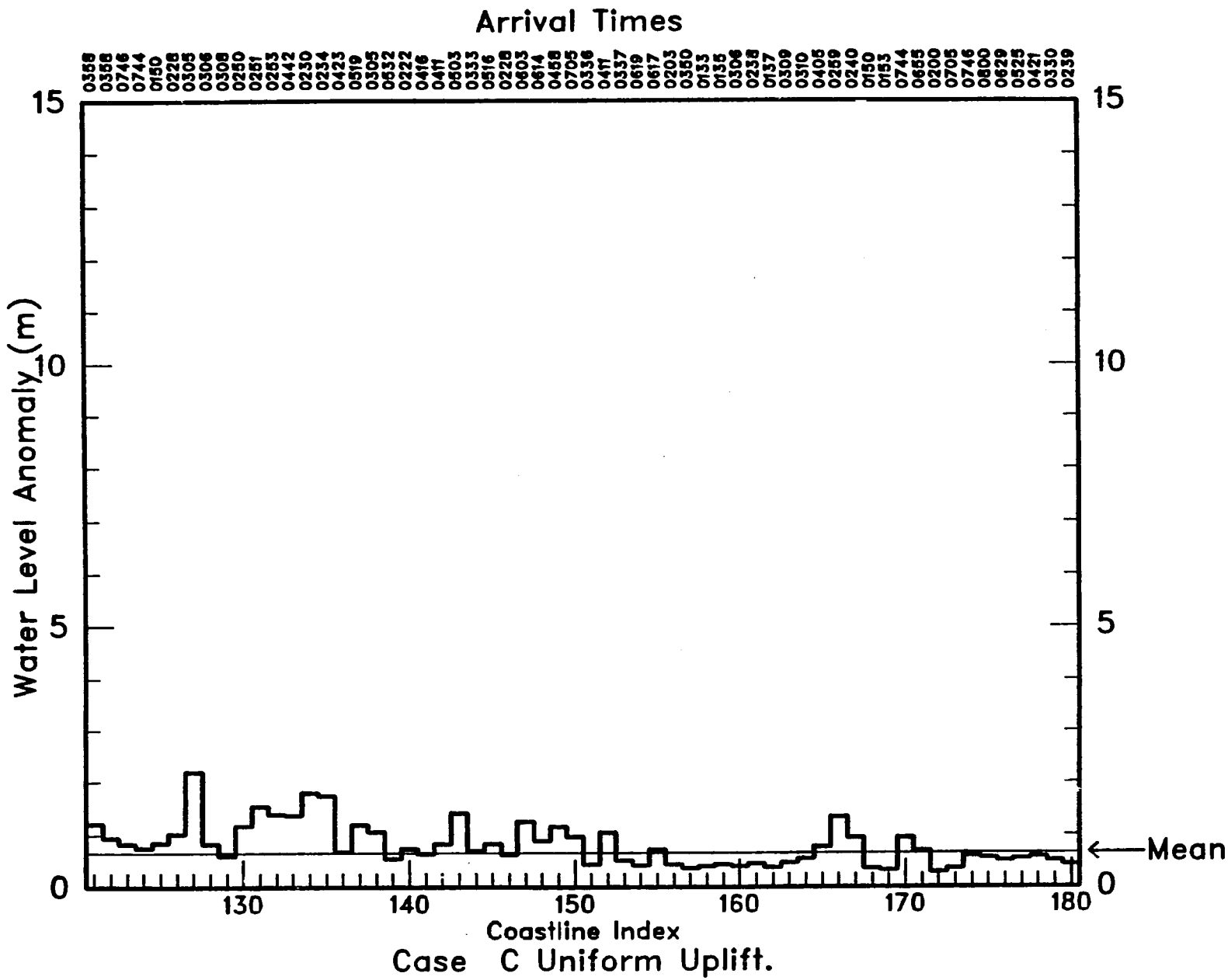
Arrival Times
0358 0358 0746 0744 0150 0228 0305 0306 0308 0250 0251 0253 0442 0230 0234 0423 0519 0305 0632 0222 0416 0411 0503 0333 0516 0228 0603 0614 0458 0705 0336 0411 0337 0619 0617 0203 0350 0153 0135 0306 0238 0137 0309 0310 0405 0259 0240 0150 0153 0744 0655 0200 0705 0746 0800 0629 0525 0421 0330 0239
15
10
5
0
Water Level Anomaly (m)
130
140
150
160
170
180
Coastline Index
Mean
Case C Uniform Uplift.

Figure: 6.9 (d)

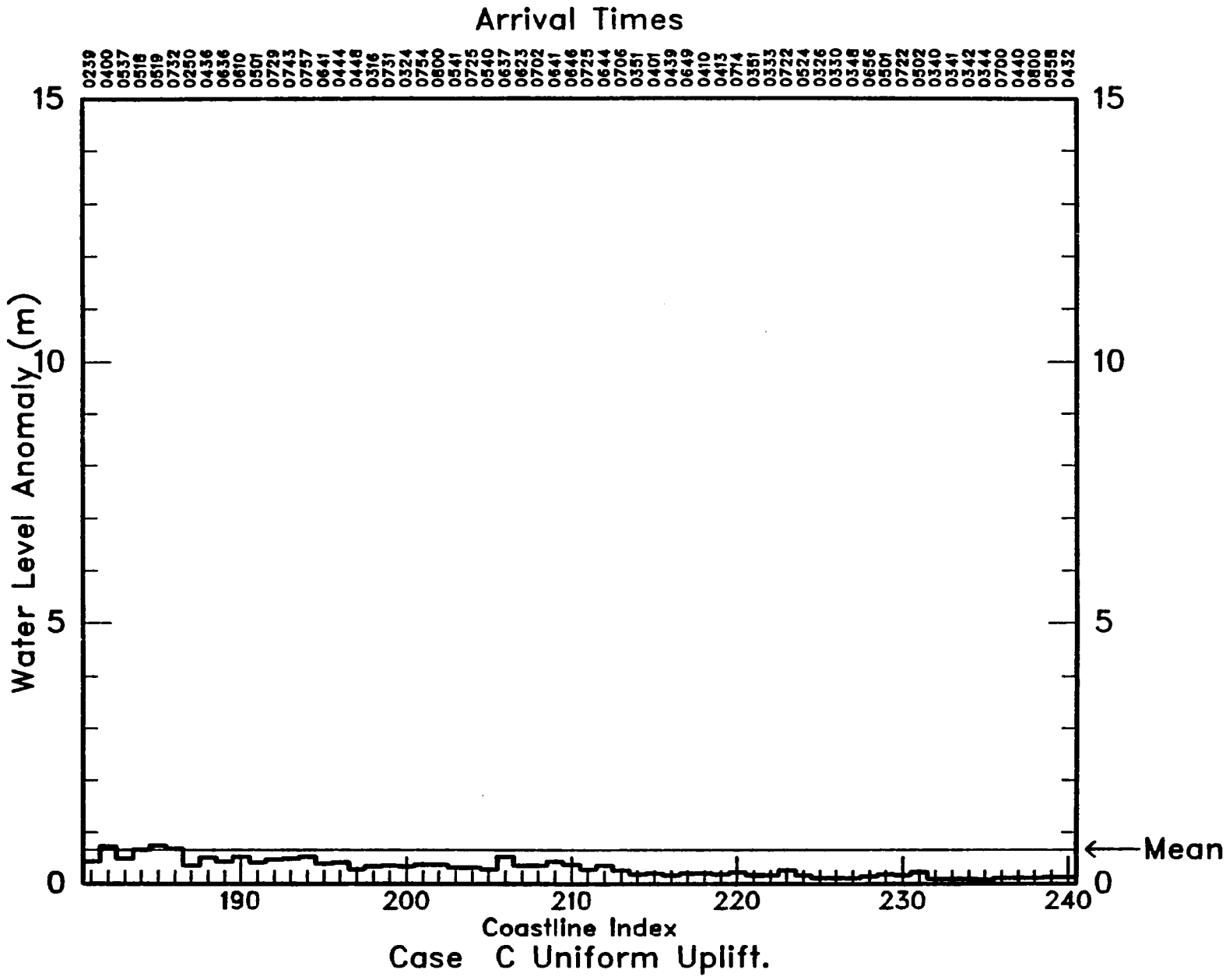
Arrival Times
0239 0400 0537 0518 0519 0732 0250 0436 0636 0610 0501 0729 0743 0757 0641 0444 0448 0316 0731 0324 0754 0800 0541 0725 0540 0637 0623 0702 0641 0646 0725 0644 0706 0351 0401 0439 0649 0410 0413 0714 0351 0333 0722 0524 0326 0330 0348 0656 0501 0722 0502 0340 0341 0342 0344 0700 0440 0800 0558 0432
15
10
5
0
Water Level Anomaly (m)
190
200
210
220
230
240
Coastline Index
Mean
Case C Uniform Uplift.

Figure: 6.9 (e)

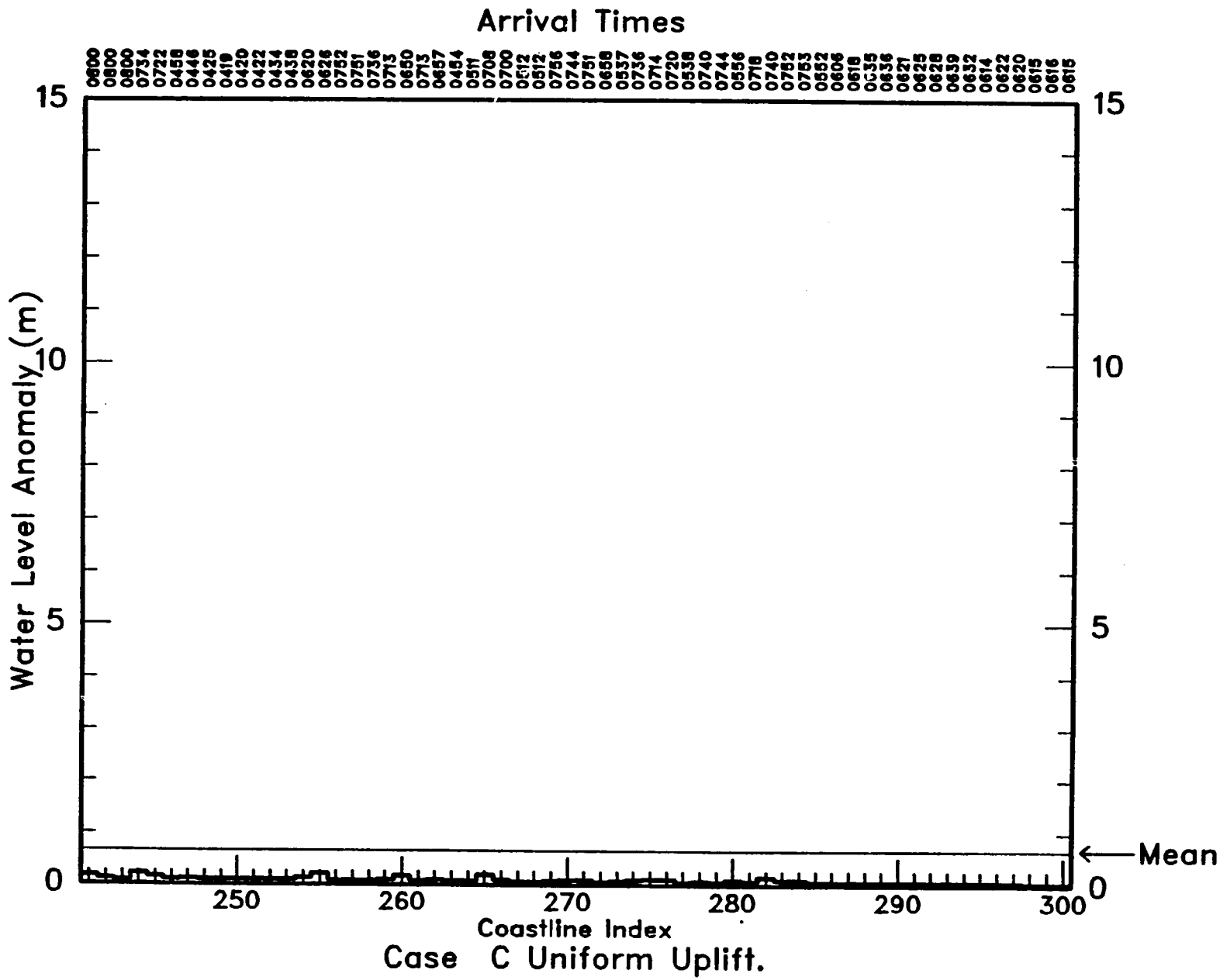
Arrival Times
0800 0800 0800 0734 0722 0458 0446 0425 0419 0420 0422 0434 0438 0620 0626 0752 0751 0736 0713 0650 0713 0657 0454 0511 0708 0700 0512 0512 0756 0744 0751 0658 0537 0736 0714 0720 0538 0740 0744 0556 0716 0740 0752 0753 0552 0606 0618 0635 0636 0621 0625 0628 0639 0632 0614 0622 0620 0615 0616 0615
15
10
5
0
Water Level Anomaly (m)
250
260
270
280
290
300
Coastline Index
Mean
Case C Uniform Uplift.

Figure: 6.9 (f)

6.3 VARIABLE UPLIFT CASE

The maximum uplift for this source is 3 m. As we noted in the previous section, this is not a very energetic source motion.

6.3.1 Immediate Effects

The one hour wave contours (Figure 6.10) show that this wave field spreads out quite evenly. A secondary crest, which is a bit lower than the leading crest and of much shorter wavelength, is apparent. A number of small pockets of wave energy are present along the coast, also.

6.3.2 Longer Duration Effects

The wave hydrographs (Figures 6.11 to 6.16) confirm the low energy levels of this source. Only at Arica do wave elevations approach 1 m. The low level wave activity is present, however, for nearly 8 hours at Antofagasta, Valparaiso, and Arica.

6.3.3 Maximum Elevations

The low energy levels are also apparent in the maximum elevation plots (Figure 6.17a-f). Waves as high as 3 m occur near the source between Caldera and Antofagasta. Clusters of above-average waves do occur near Arica and between Constitucion and Valparaiso, but in general this tsunami does not pose much of a threat.

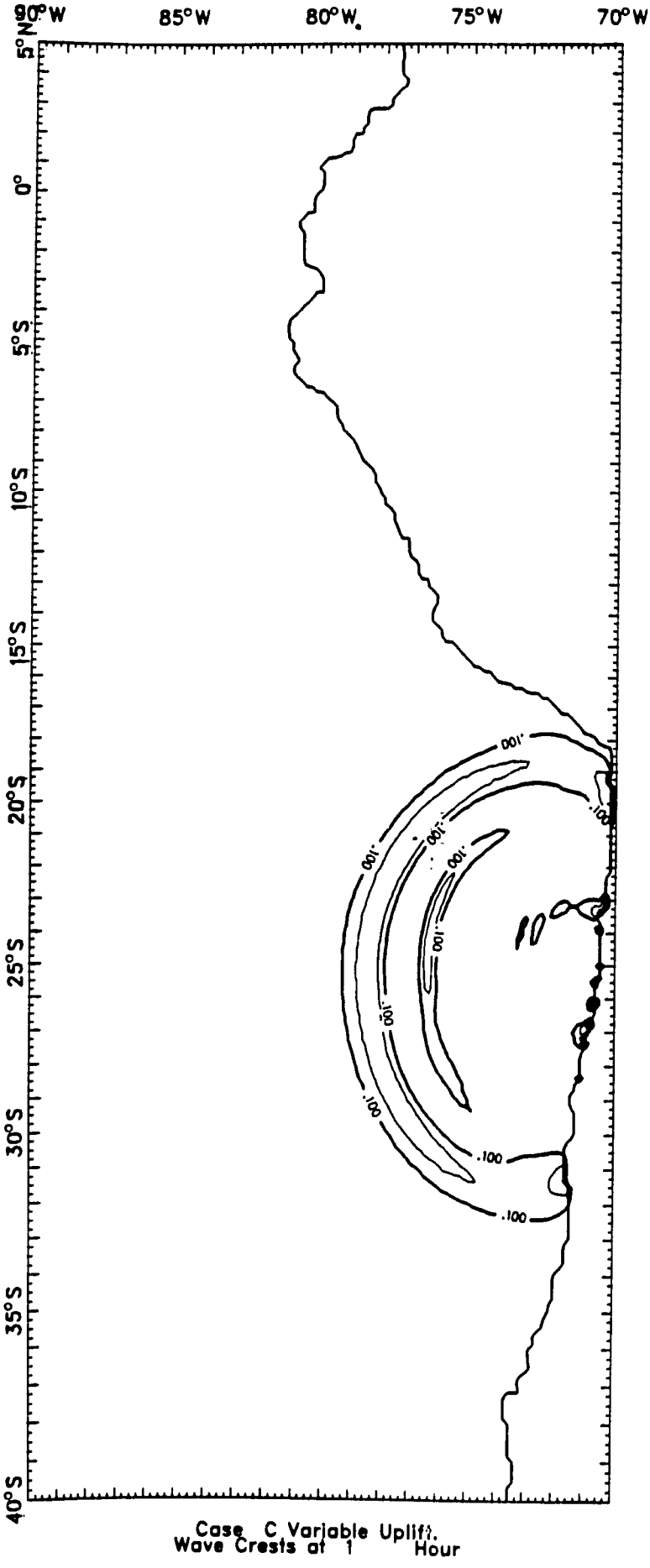

Figure: 6.10

Surface elevation (positive only) one hour after a variable uplift in source Zone C. Contours correspond to 0.1, 0.2, 0.5, 1.0, and 2.0 m.

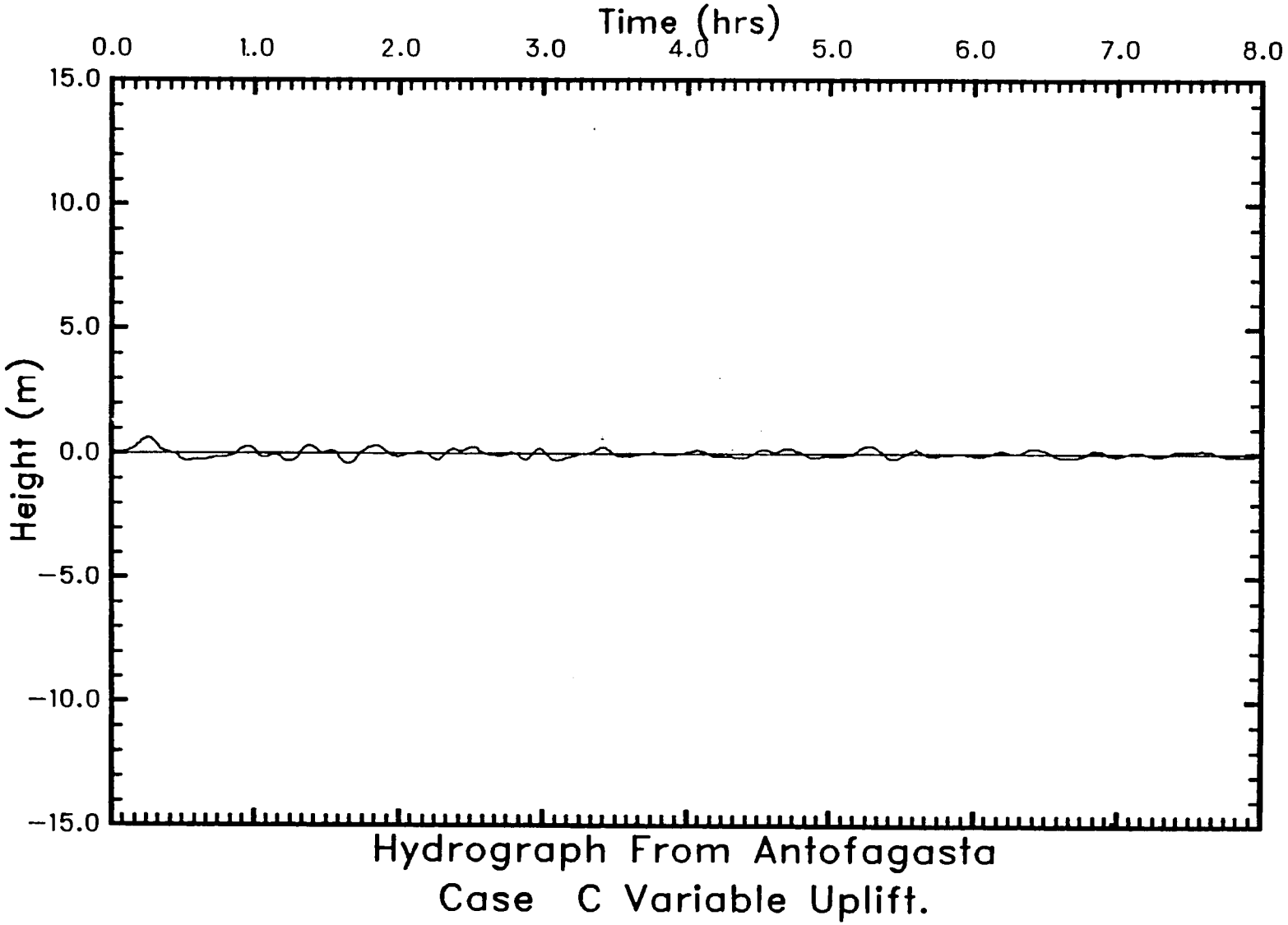

Figure 6.11: Wave elevation as a function of time at the recording point near Antofagasta, Chile. These waves were generated by the variable uplift of Zone C.

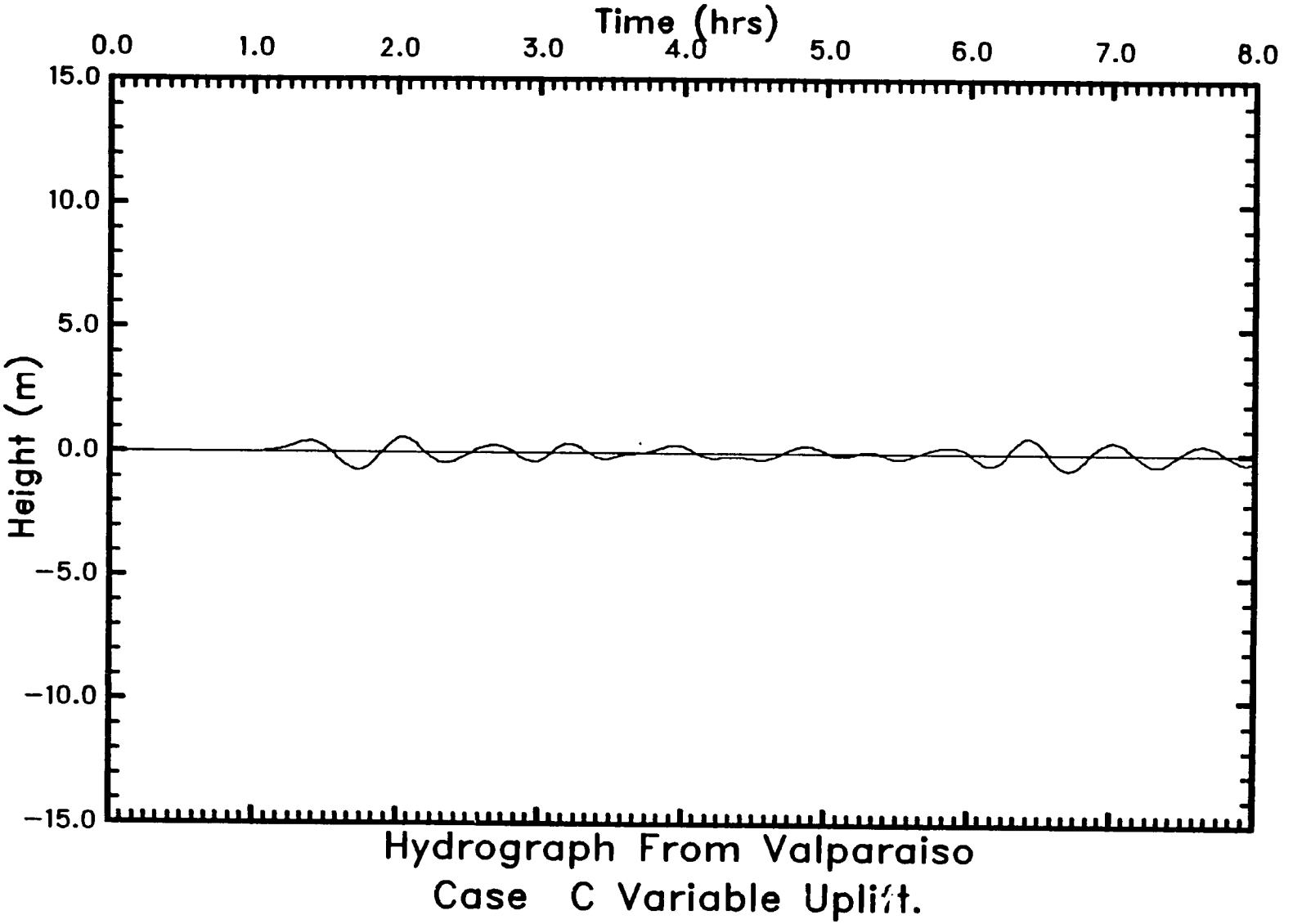

Figure 6.12: Wave elevation as a function of time at the recording point near Valparaiso, Chile. These waves were generated by the variable uplift of Zone C.

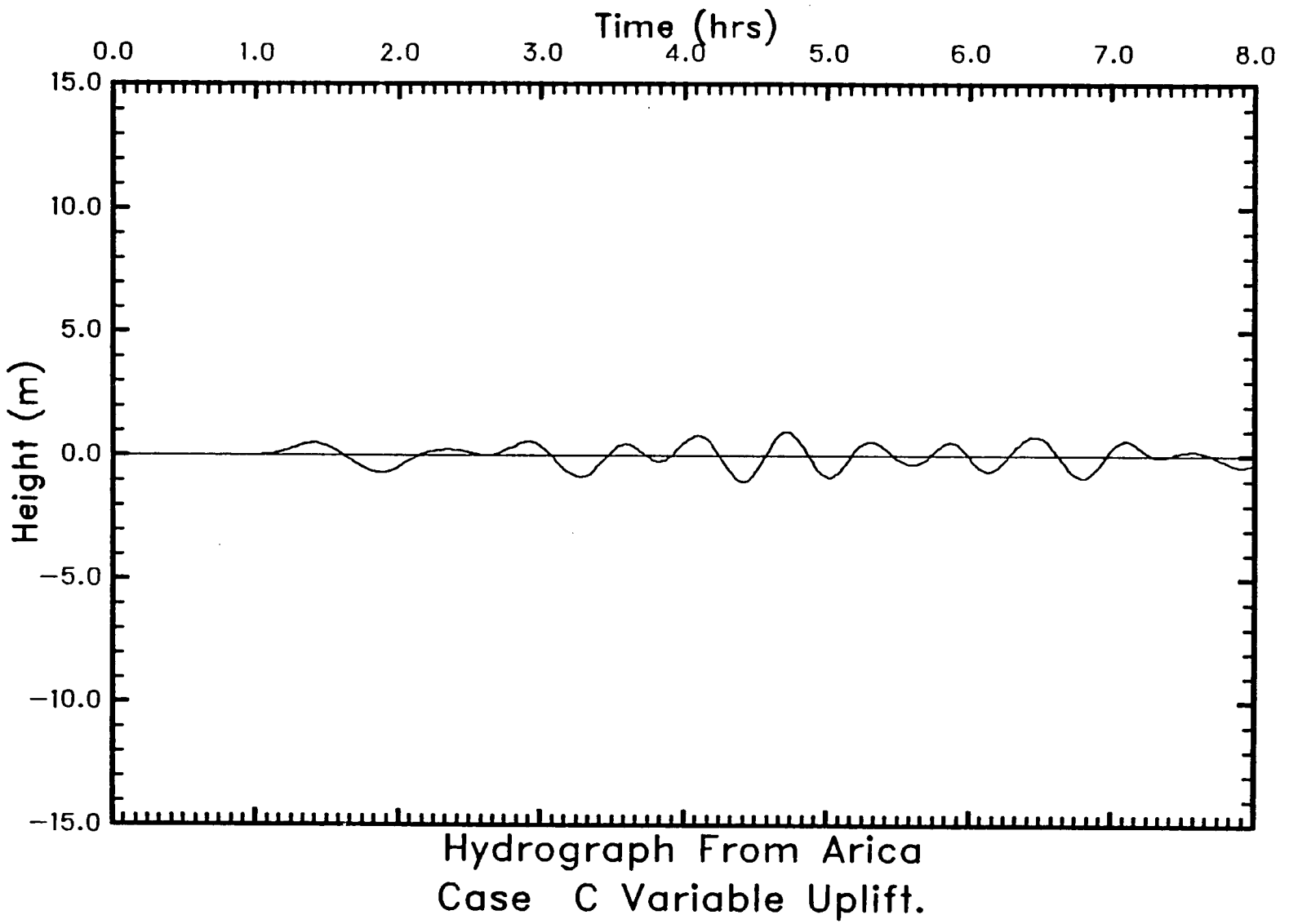

Figure 6.13: Wave elevation as a function of time at the recording point near Arica, Chile.. These waves were generated by the variable uplift of Zone C.

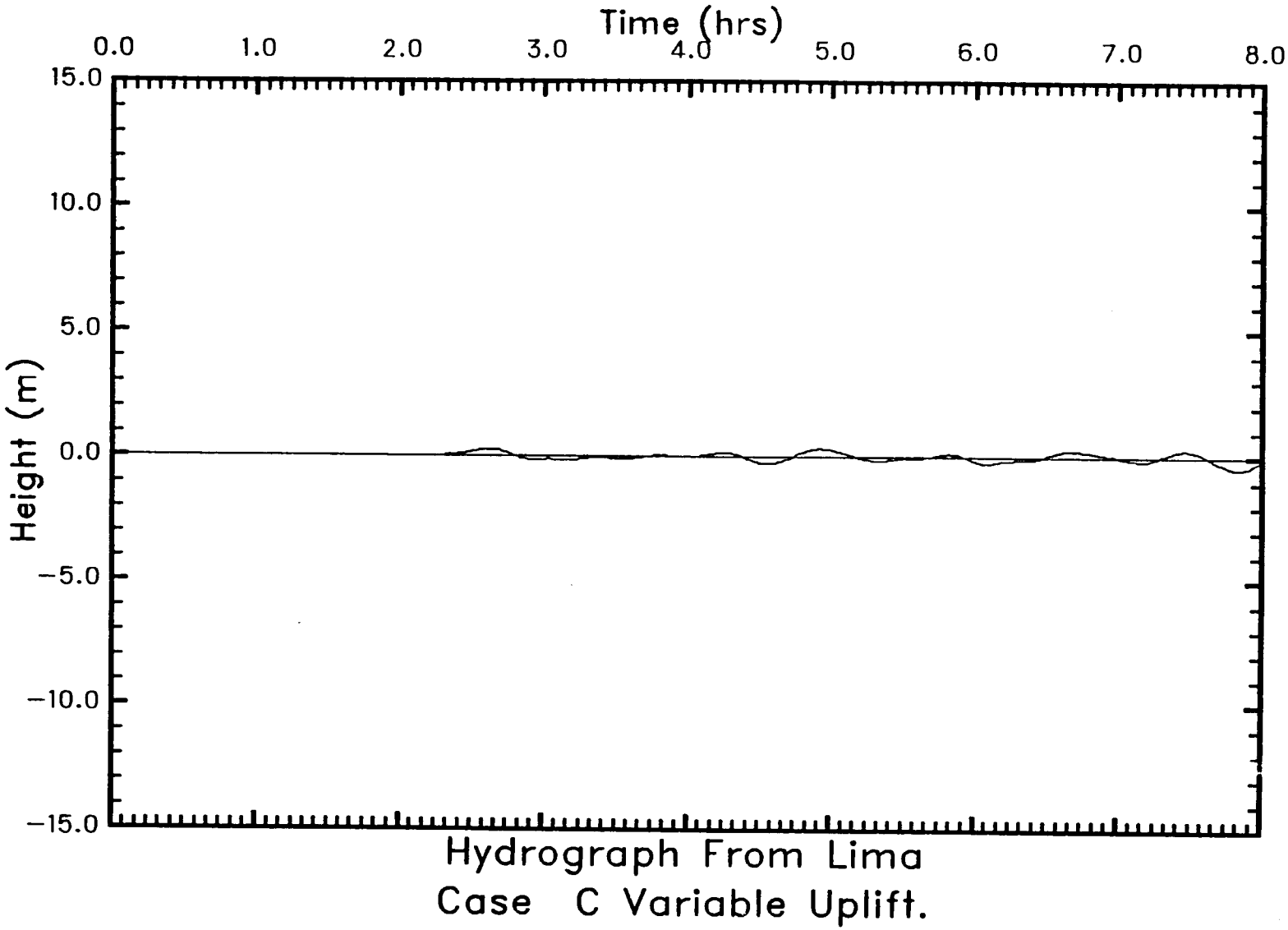

Figure 6.14: Wave elevation as a function of time at the recording point near Lima, Peru. These waves were generated by the variable uplift of Zone C.

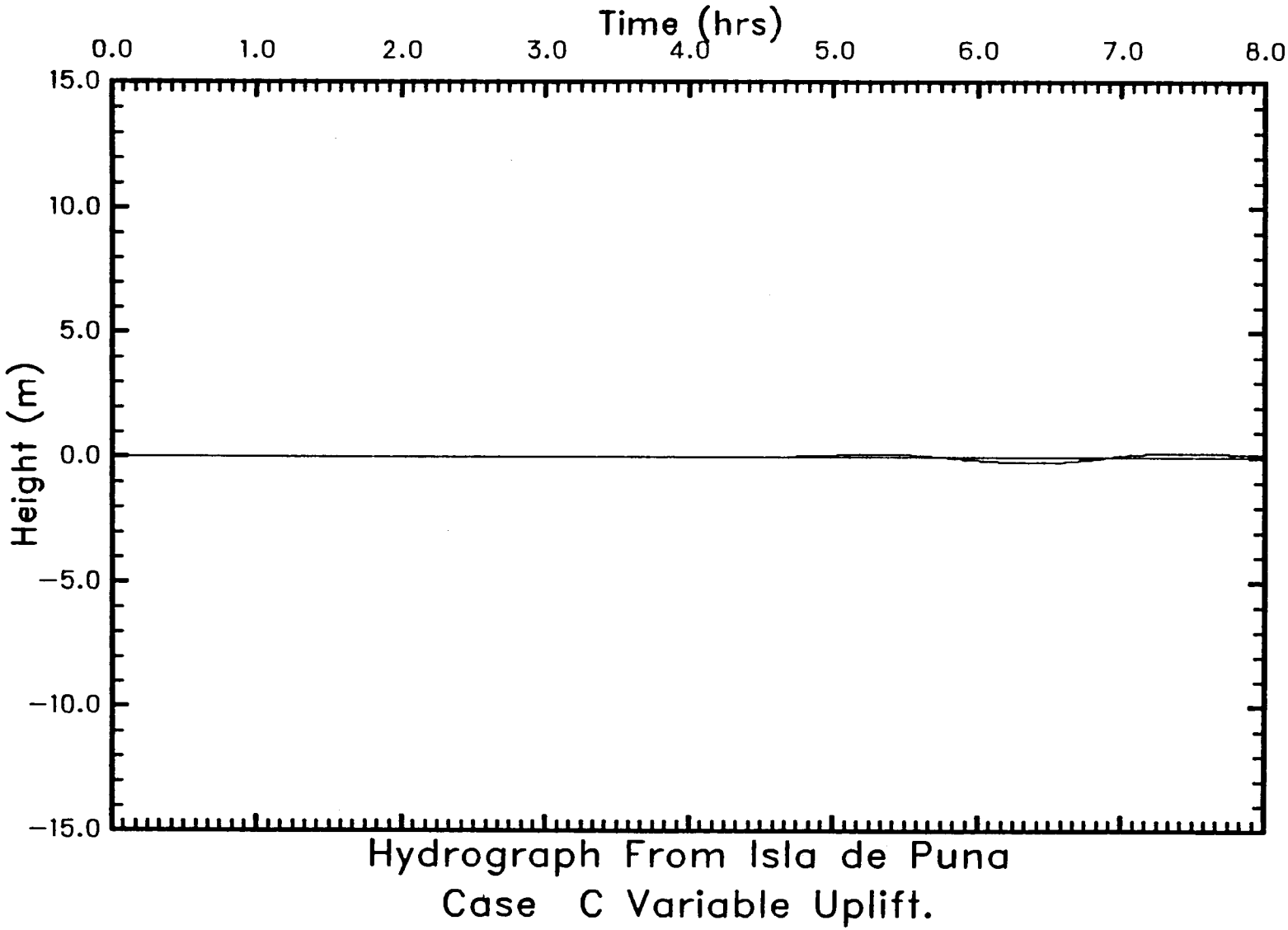

Figure 6.15: Wave elevation as a function of time at the recording point near Isla de Puna, Colombia. These waves were generated by the variable uplift of Zone C.

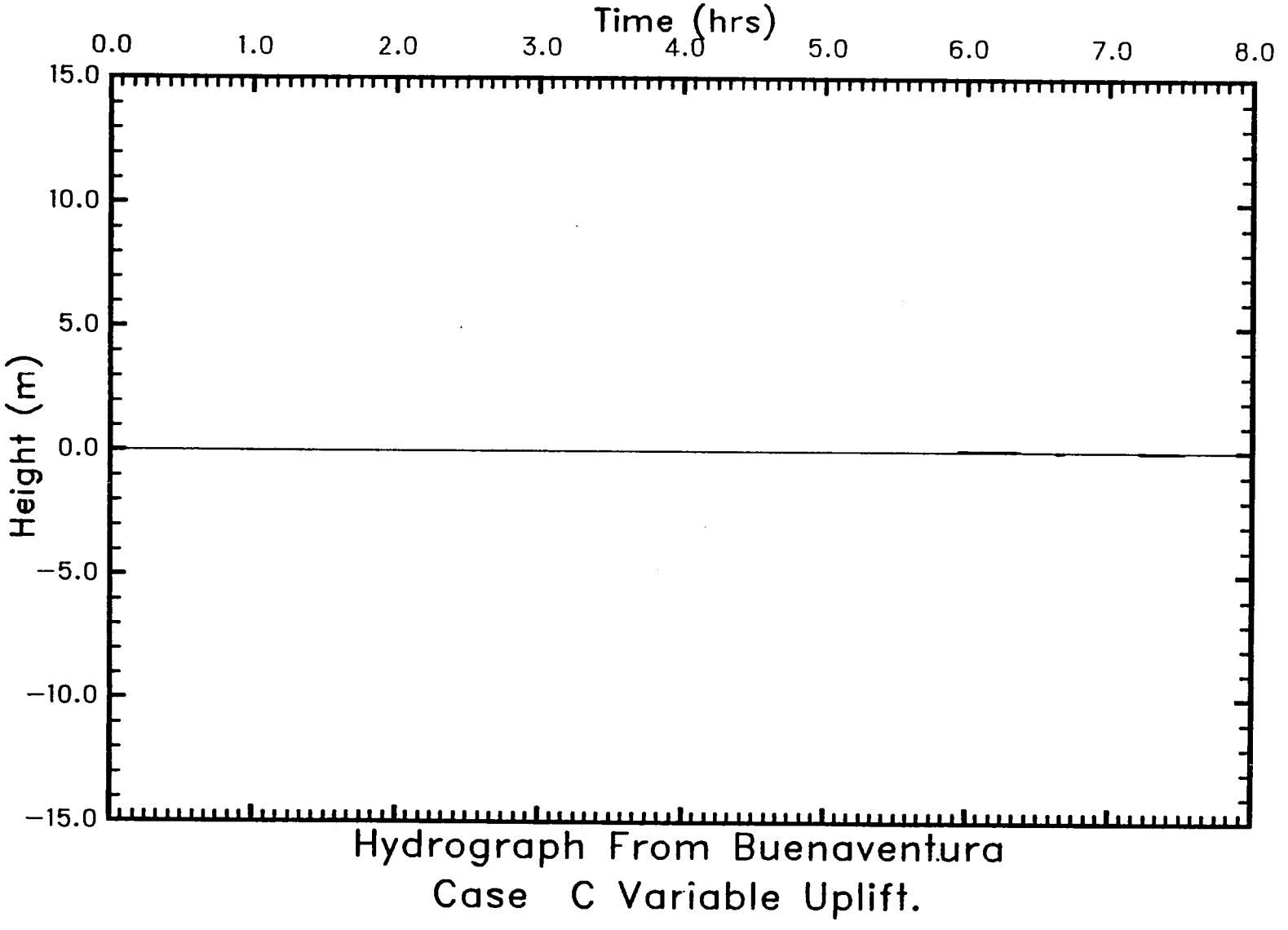

Figure 6.16: Wave elevation as a function of time at the recording point near Buenaventura, Ecuador. These waves were generated by the variable uplift of Zone C.

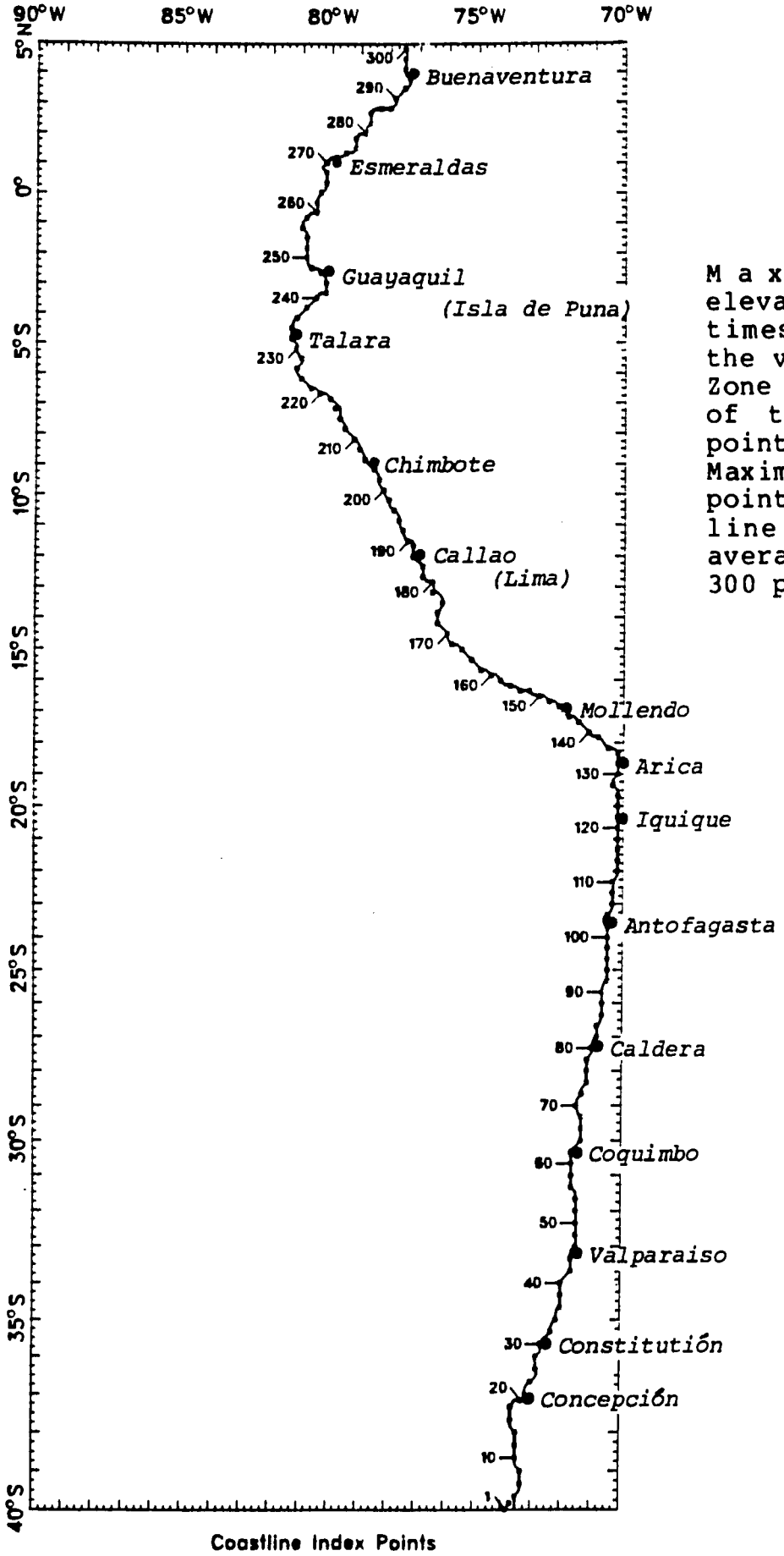

Figure: 6.17

Maximum wave elevations and arrival times of waves from the variable uplift in Zone C. (a) Locations of the 300 recording point points. (b-f) Maximum waves at each point. The horizontal line represents the average value of all 300 points.

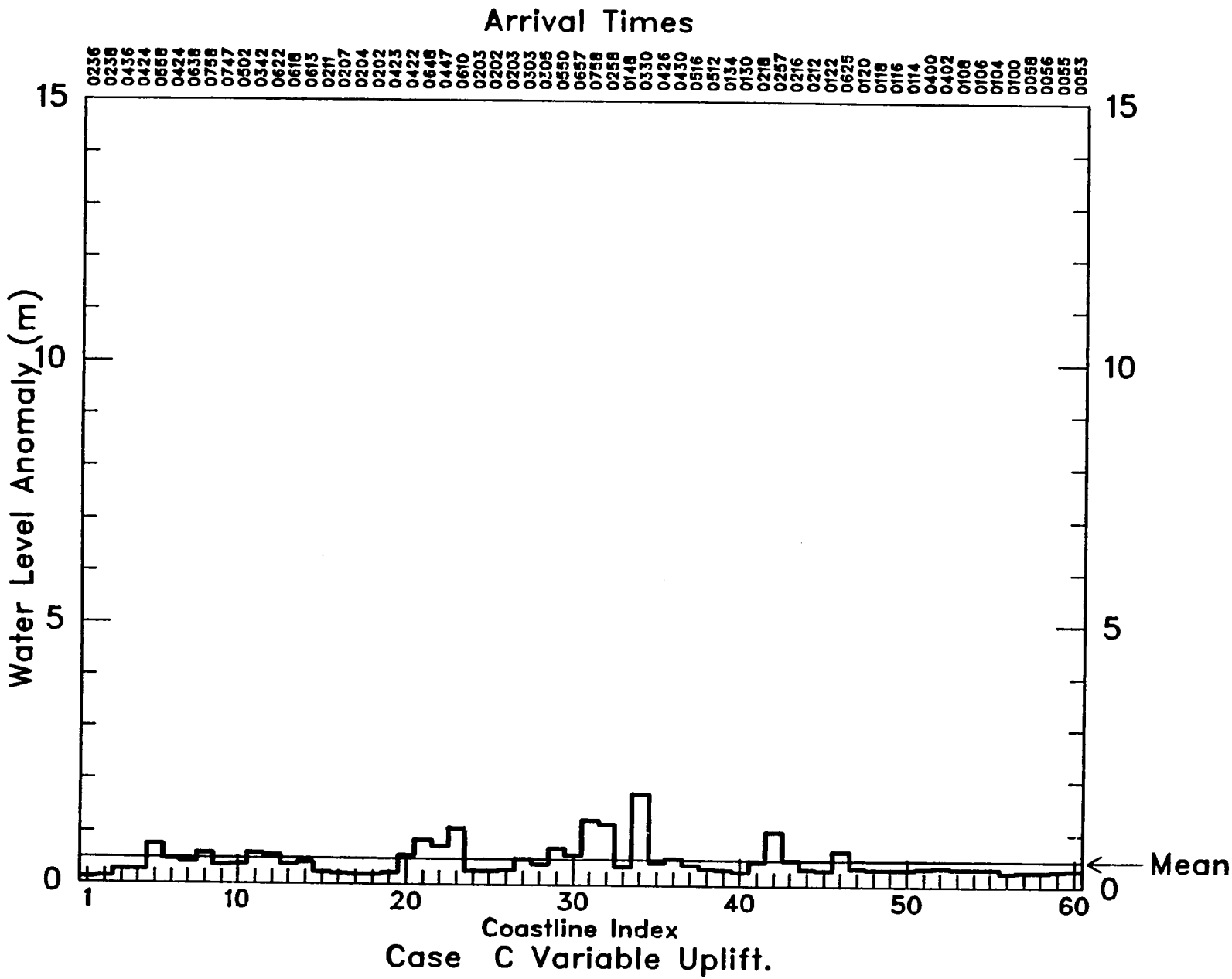
Arrival Times
0236 0238 0436 0424 0558 0424 0638 0758 0747 0502 0342 0622 0618 0613 0211 0207 0204 0202 0423 0422 0648 0447 0610 0203 0202 0203 0303 0305 0550 0657 0758 0258 0148 0330 0426 0430 0516 0512 0134 0130 0218 0257 0216 0212 0122 0625 0120 0118 0116 0114 0400 0402 0108 0106 0104 0100 0058 0056 0055 0053
Water Level Anomaly (m)
15
10
5
0
1
10
20
30
40
50
60
Coastline Index
Mean
Case C Variable Uplift.

Figure: 6.17 (b)

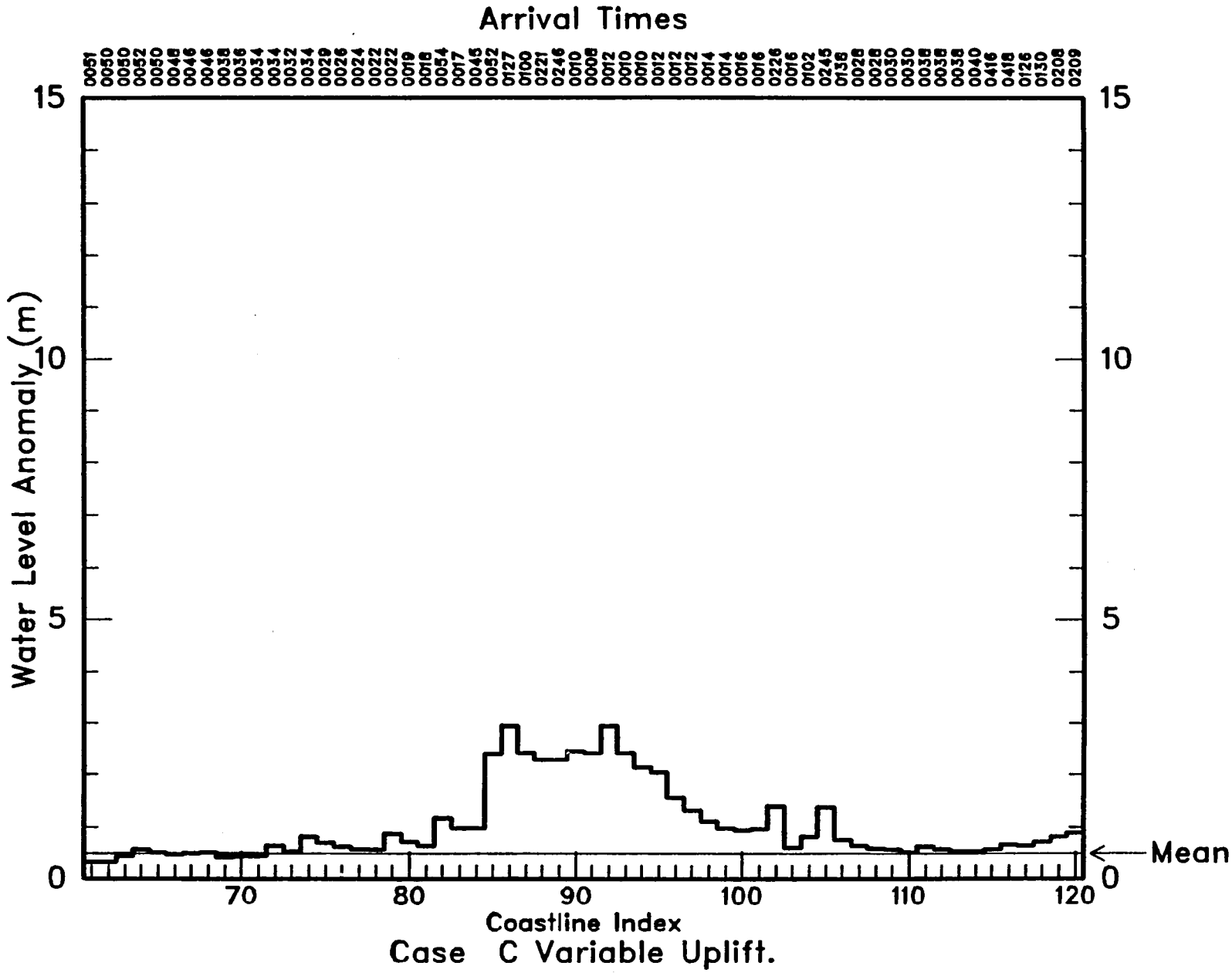
Arrival Times
0051 0050 0050 0052 0050 0048 0046 0046 0038 0036 0034 0034 0032 0034 0029 0026 0024 0022 0022 0019 0018 0054 0017 0045 0052 0127 0100 0221 0246 0010 0008 0012 0010 0010 0012 0012 0012 0014 0014 0016 0016 0226 0016 0102 0245 0138 0028 0028 0030 0030 0038 0038 0038 0040 0416 0418 0126 0130 0208 0209
15
10
5
0
Water Level Anomaly (m)
70
80
90
100
110
120
Coastline Index
Mean
Case C Variable Uplift.

Figure: 6.17 (c)

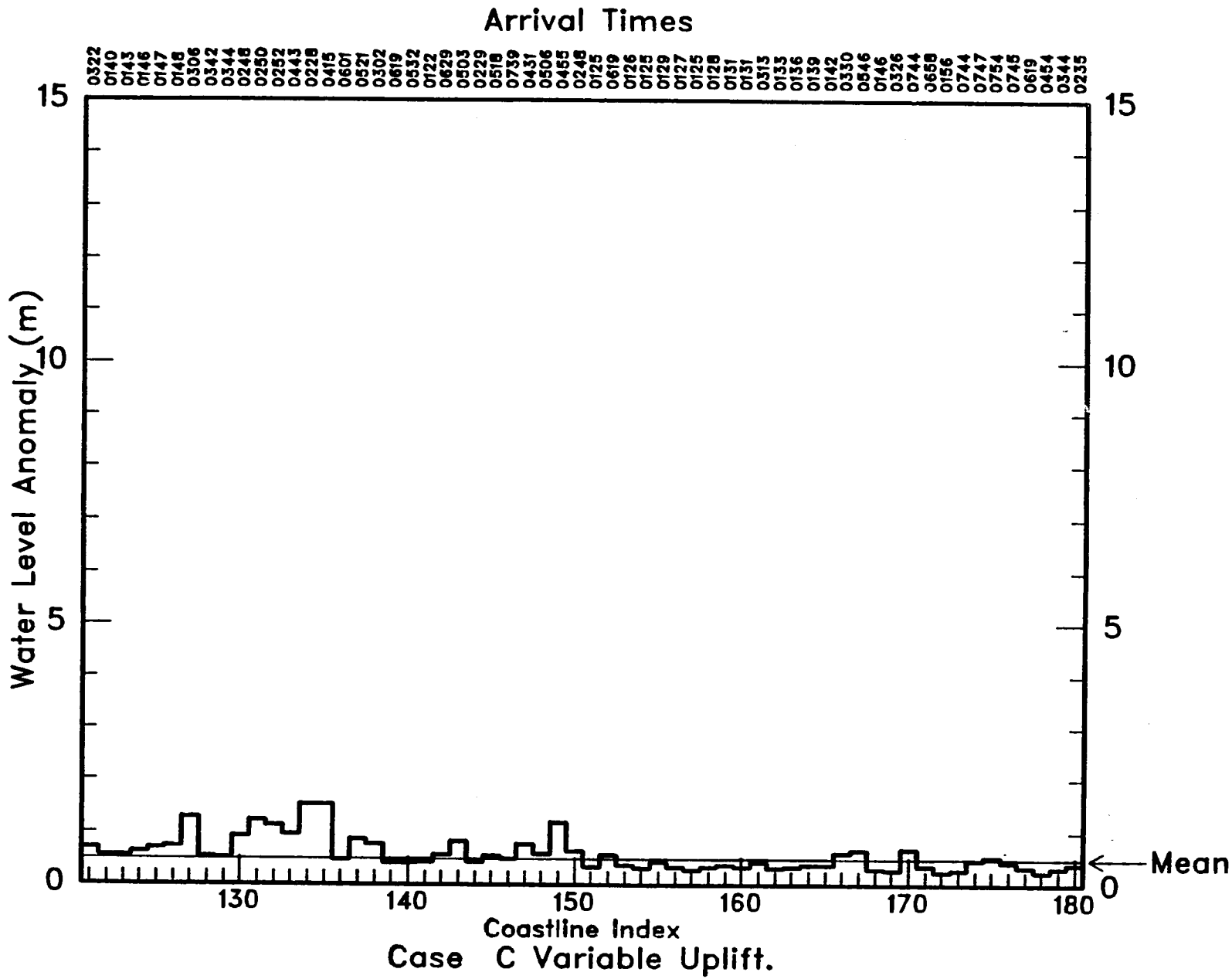
Arrival Times
0322 0140 0143 0146 0147 0148 0306 0342 0344 0248 0250 0252 0443 0228 0415 0601 0521 0302 0619 0532 0122 0629 0503 0229 0518 0739 0431 0506 0455 0248 0125 0619 0126 0125 0129 0127 0125 0128 0131 0131 0313 0136 0139 0142 0330 0546 0146 0326 0744 0658 0156 0744 0747 0754 0745 0619 0454 0344 0235
Water Level Anomaly (m)
15
10
5
0
130
140
150
160
170
180
Coastline Index
Mean
Case C Variable Uplift.

Figure: 6.17 (d)

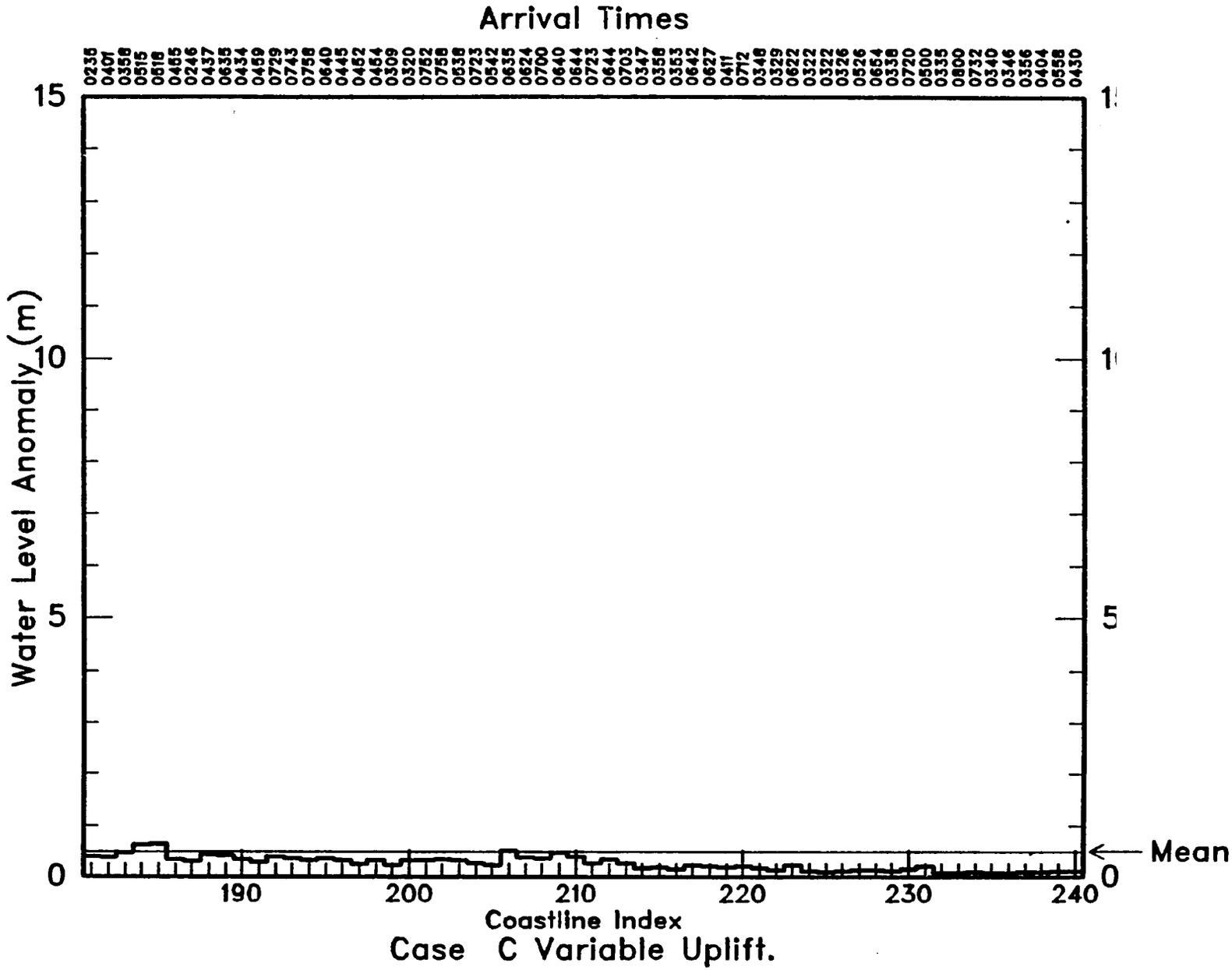
Arrival Times
0235 0401 0358 0515 0518 0455 0246 0437 0635 0434 0459 0729 0743 0758 0640 0445 0452 0454 0309 0320 0752 0758 0538 0723 0542 0635 0624 0700 0640 0644 0723 0644 0703 0347 0358 0353 0642 0627 0411 0712 0348 0329 0622 0322 0322 0326 0526 0654 0338 0720 0500 0335 0800 0732 0340 0346 0356 0404 0558 0430
Water Level Anomaly (m)
15
10
5
0
190
200
210
220
230
240
Coastline Index
Mean
Case C Variable Uplift.

Figure: 6.17 (e)

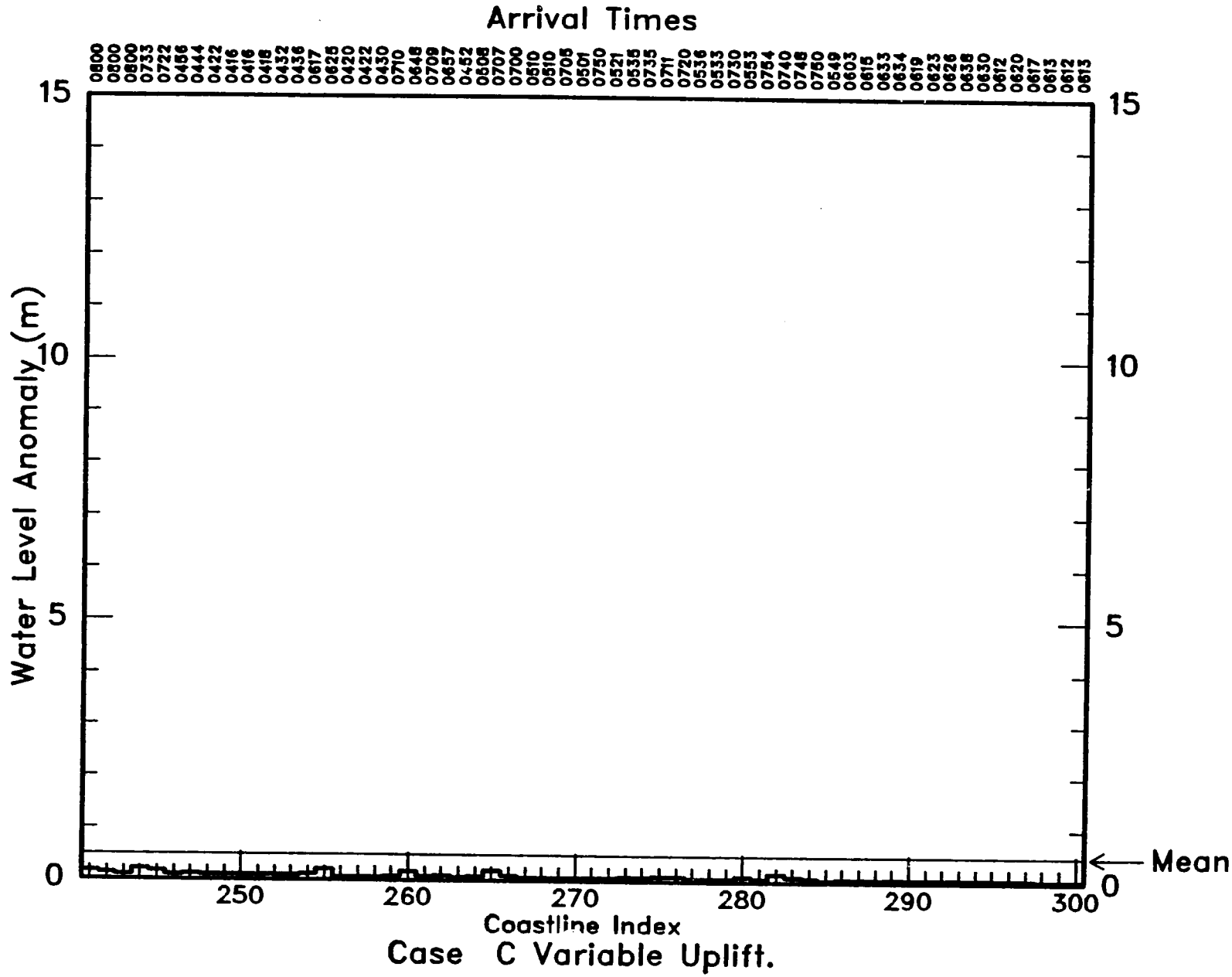
Arrival Times
0800 0800 0800 0733 0722 0456 0444 0422 0416 0416 0418 0432 0436 0617 0625 0420 0422 0430 0710 0648 0709 0657 0452 0508 0707 0700 0510 0510 0705 0501 0750 0521 0535 0735 0711 0720 0536 0533 0730 0553 0754 0740 0748 0750 0549 0603 0615 0633 0634 0619 0623 0626 0638 0630 0612 0620 0617 0613 0612 0613
Water Level Anomaly (m)
15
10
5
0
250
260
270
280
290
300
Coastline Index
Mean
Case C Variable Uplift.

Figure: 6.17 (f)

6.4 HAZARD ASSESSMENT - SOURCE C

As we have already seen, the tsunamis generated in this zone are not very energetic. The mean elevations for the uniform and the variable uplift simulations are roughly 0.7 m and 0.5 m. Only in the vicinity of the source, between Caldera and Antofagasta, do waves approach 3.0 m high in either case. Farther north and south of the source we see wave elevations between 1 and 2 m, but whether or not these pose a threat we cannot say without further study.

We do notice that elevations are consistently above average in the vicinity of the continental bend, indicating that wave energy does get trapped there. We also note that the entire coast north of Chimbote is practically unaffected by this tsunami.

Section 7
SOURCE ZONE D

7.1 INTRODUCTION

Source zone D extends from 33°S to 35°S. The source is oriented along the trench axis rather than the coastline. The general trend of the trench is toward the southwest and thus the source zones tend to send their wave energy toward the northwest initially. The source area is depicted in Figure 7.1

7.2 UNIFORM UPLIFT CASE

The generating motion for this case is a uniform 8 m displacement over the entire area indicated in Figure 7.1.

7.2.1 Immediate Effects

The contours of wave height one hour after generation (Figure 7.2) show that the waves are spreading fairly uniformly outward from the source. The highest portion of the leading crest is propagating toward the northwest. A large concentration of wave energy remains in the source zone, however.

7.2.2 Longer Duration Effects

The waves emanating from this source again exhibit a decrease in intensity as they get farther away. At Valparaiso (Figure 7.3) the waves are initially quite high and persist for the entire simulation. The waves at Antofagasta

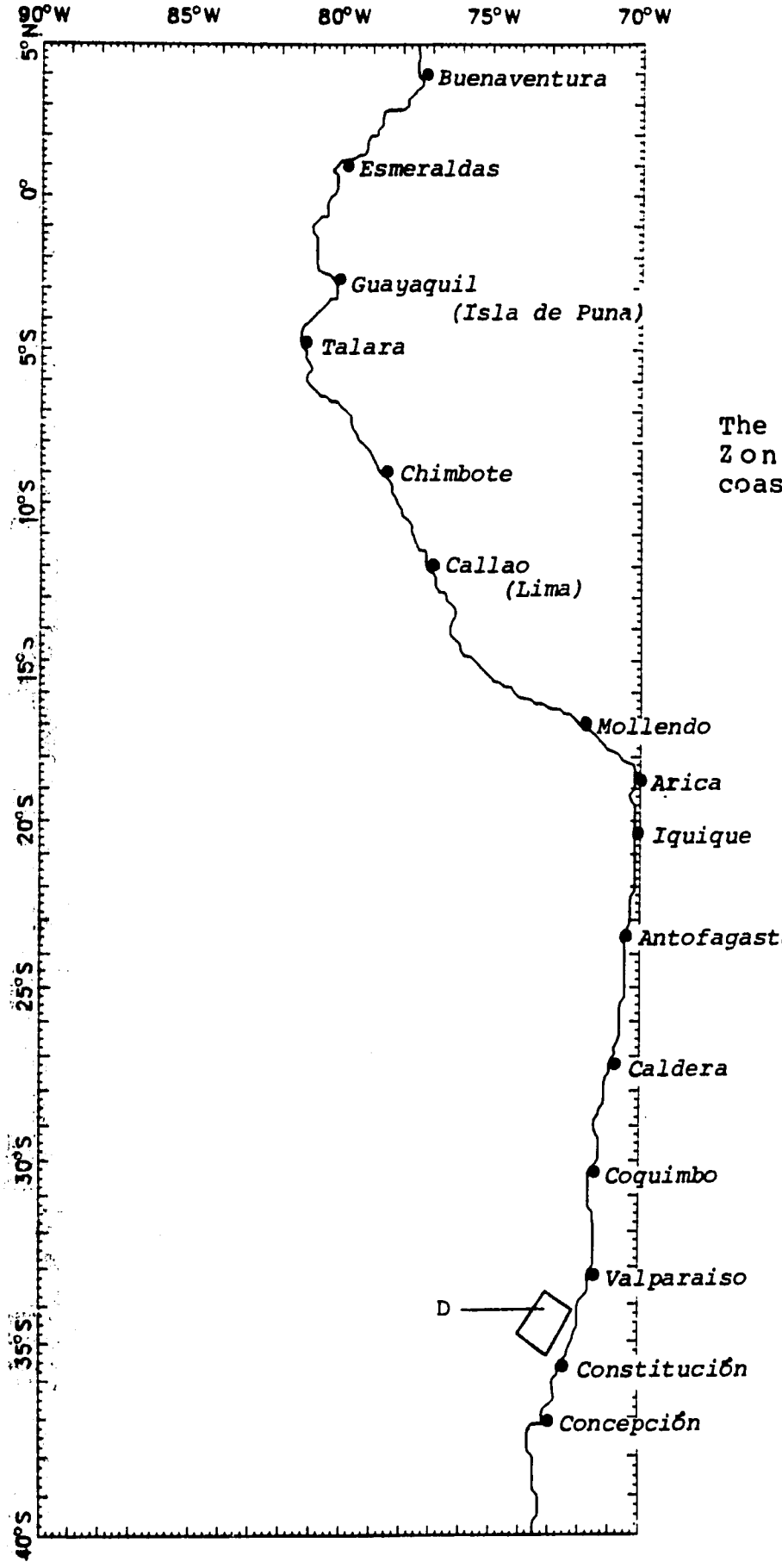

Figure 7.1:

The location of source Zone D along the coastline.

(Figure 7.4) also persist, but at much reduced amplitude. The waves reaching Arica (Figure 7.5) are higher than those at Antofagasta, but have much longer periods. They do seem to die off slowly. Waves near Lima (Figure 7.6) are fairly low and long and do not pose much threat. Waves at Isla de Puna and Buenaventura (Figures 7.7 and 7.8) do not appear to contain significant energy.

7.2.3 Maximum Elevations

The patterns of maximum elevations for this case are shown in Figure 7.9a-f. The mean level for these waves is roughly 1.8 m, which is high enough so that waves at or above-average are at least a potential hazard. Not surprisingly, the highest waves by far occur between the southern end of the model zone (at 40°S) and Coquimbo, along the shore close to the source. The region from Arica north around the continental bend to Chimbote receives waves which are somewhat higher than those in regions to the north or south of there. This is probably a reversal of the open ocean propagation effect indicated in case A and the northern subzone of case B. Here the waves originate in the south and cross the deep, relatively flat Chile Basin before being refracted up onto the shelf, where the transition from deep to shallow water amplifies the wave crests. Once again, the coastlines of Ecuador and Colombia receive only quite small waves.

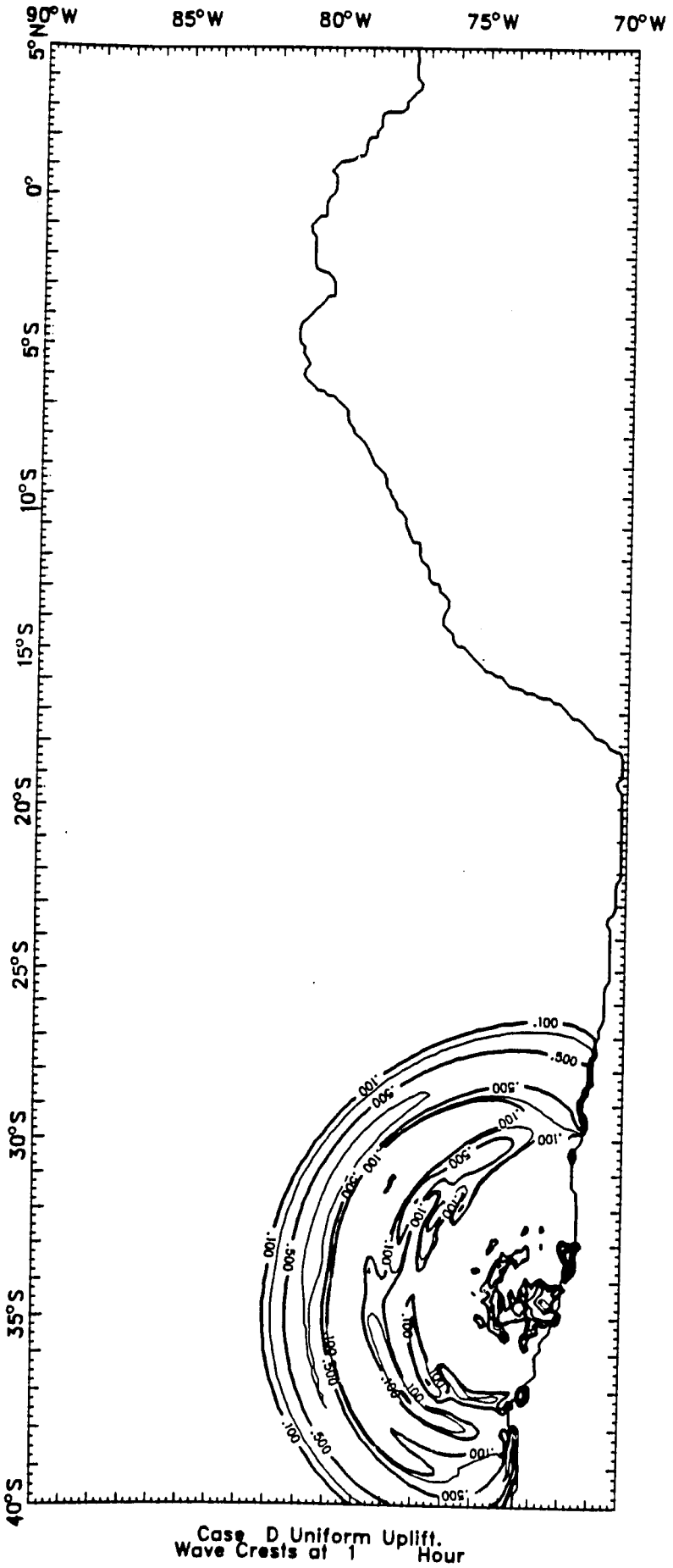

Figure: 7.2

Surface elevation (positive only) one hour after a uniform uplift in source Zone D. Contours correspond to 0.1, 0.2, 0.5, 1.0, and 2.0 m.

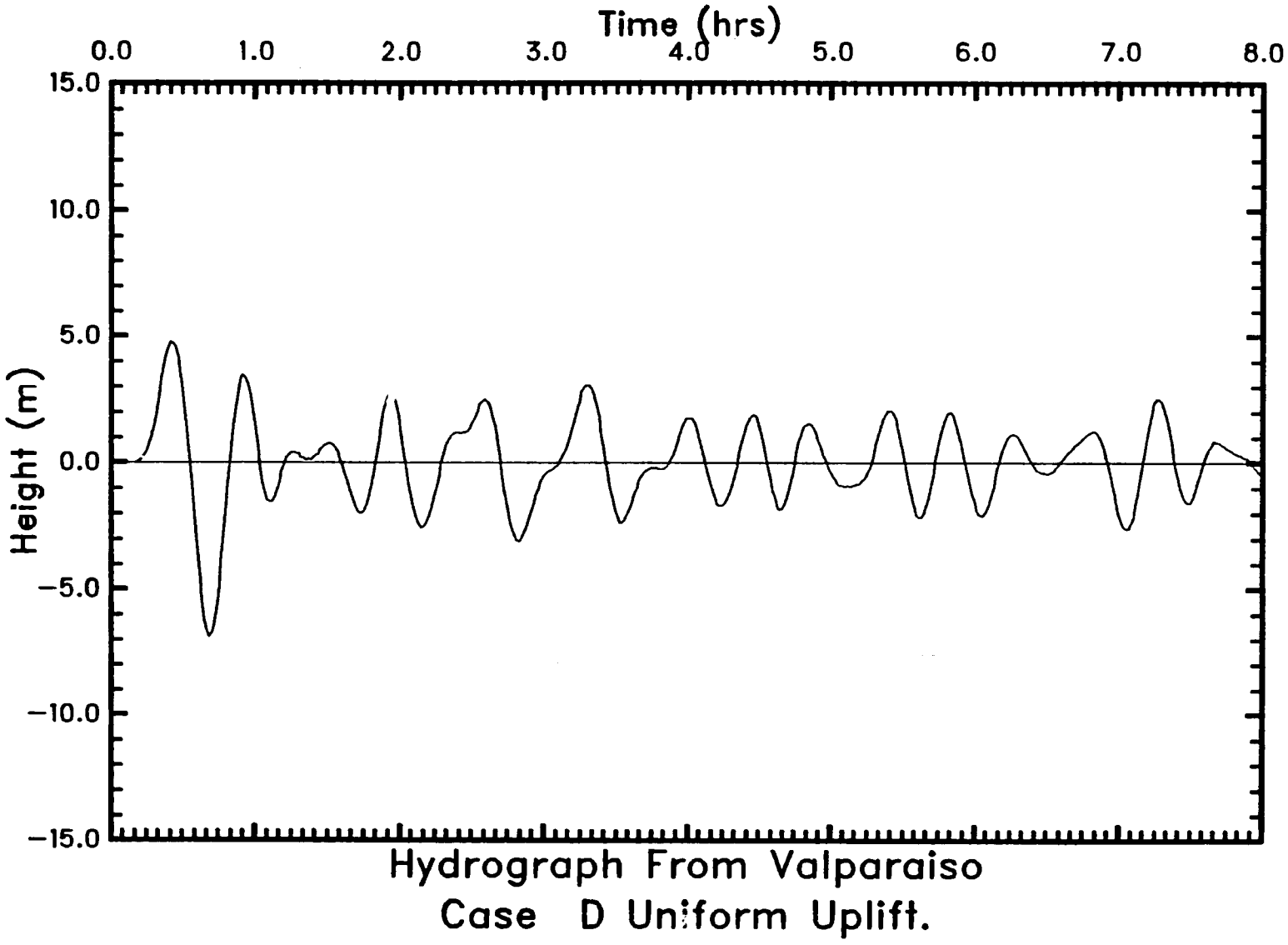

Figure 7.3: Wave elevation as a function of time at the recording point near Valparaiso, Chile. These waves were generated by the uniform uplift of Zone D.

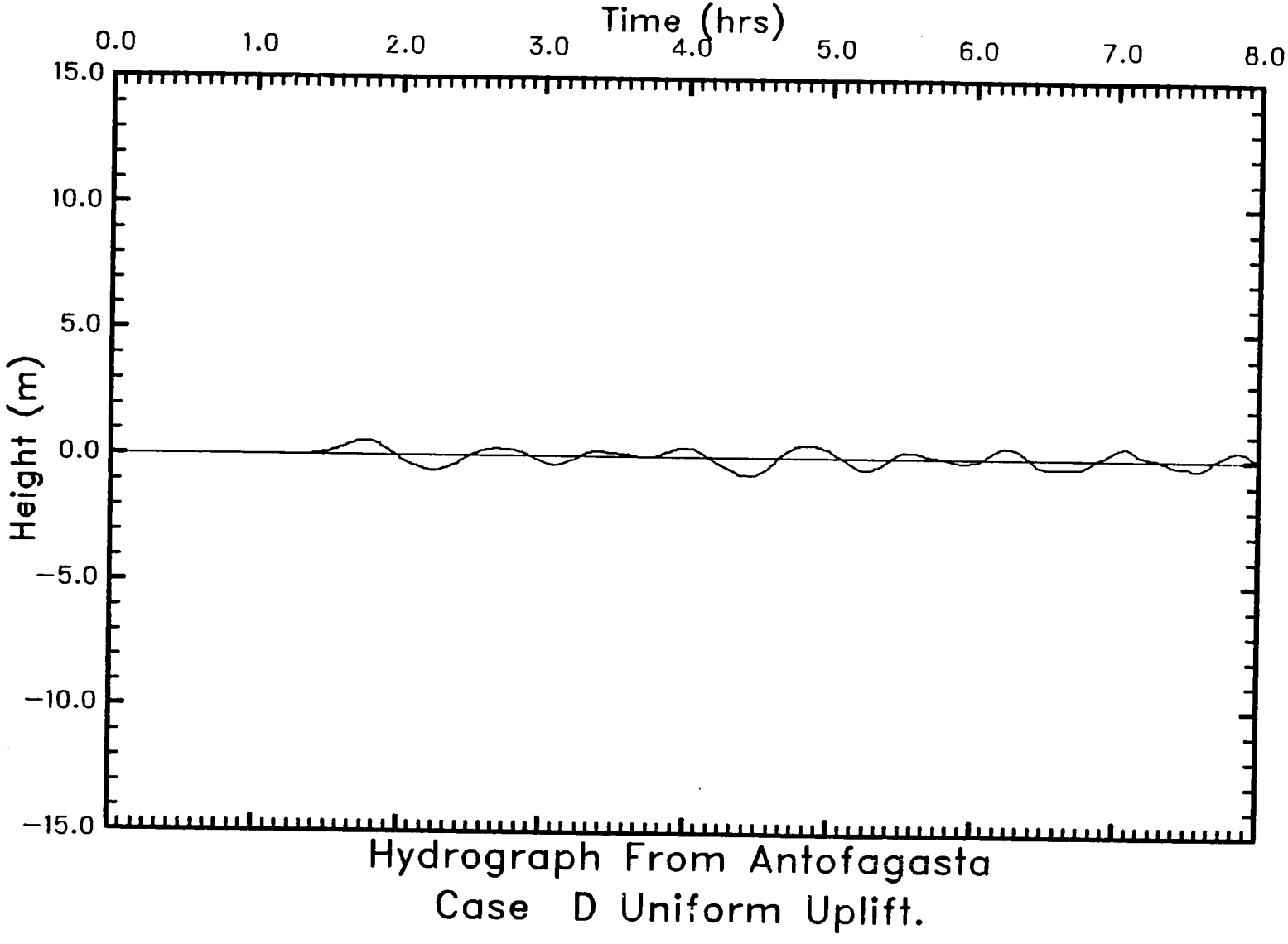

Figure 7.4: Wave elevation as a function of time at the recording point near Antofagasta, Chile. These waves were generated by the uniform uplift of Zone D.

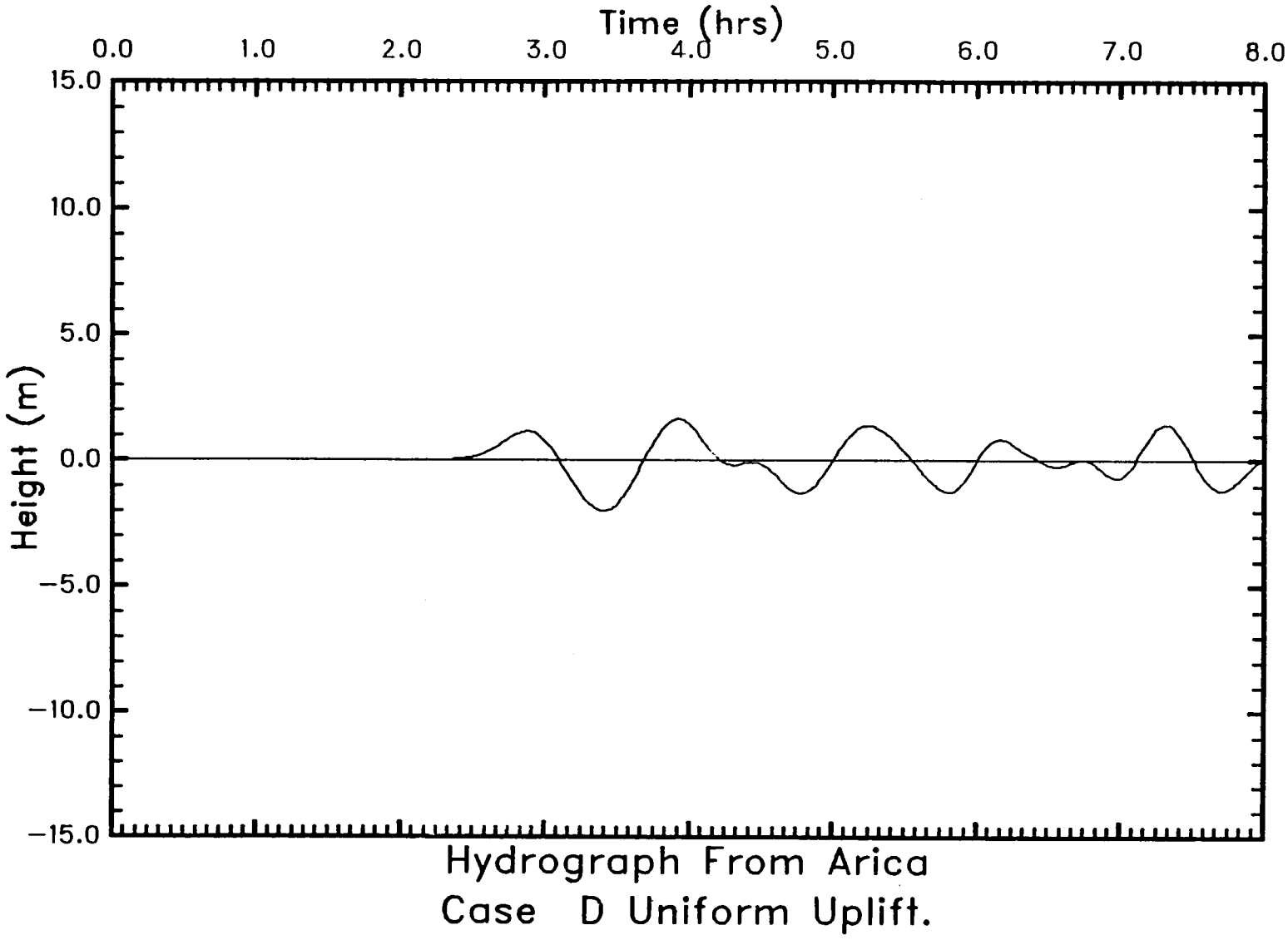

Figure 7.5: Wave elevation as a function of time at the recording point near Arica, Chile. These waves were generated by the uniform uplift of Zone D.

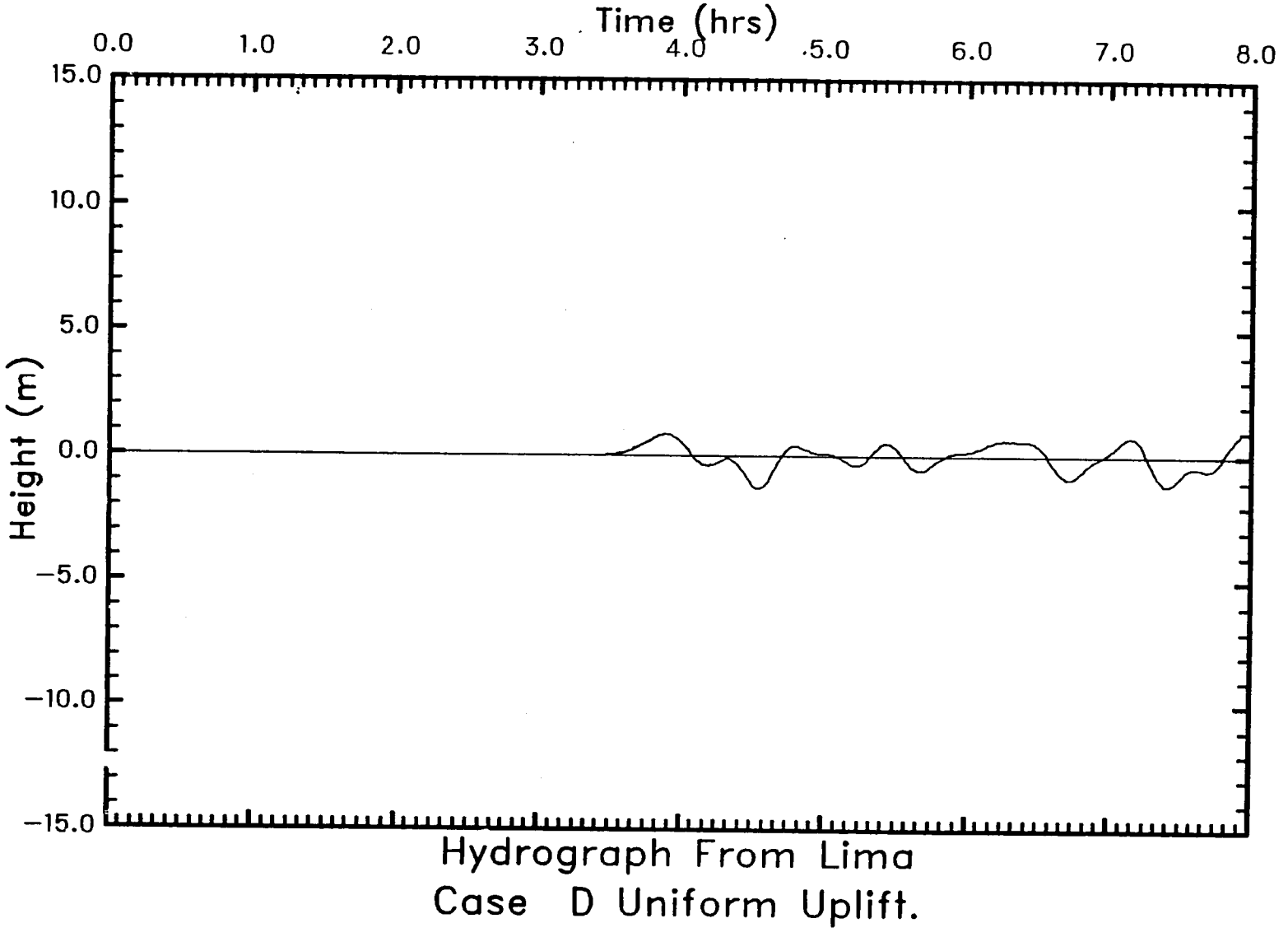

Figure 7.6: Wave elevation as a function of time at the recording point near Lima, Peru. These waves were generated by the uniform uplift of Zone D.

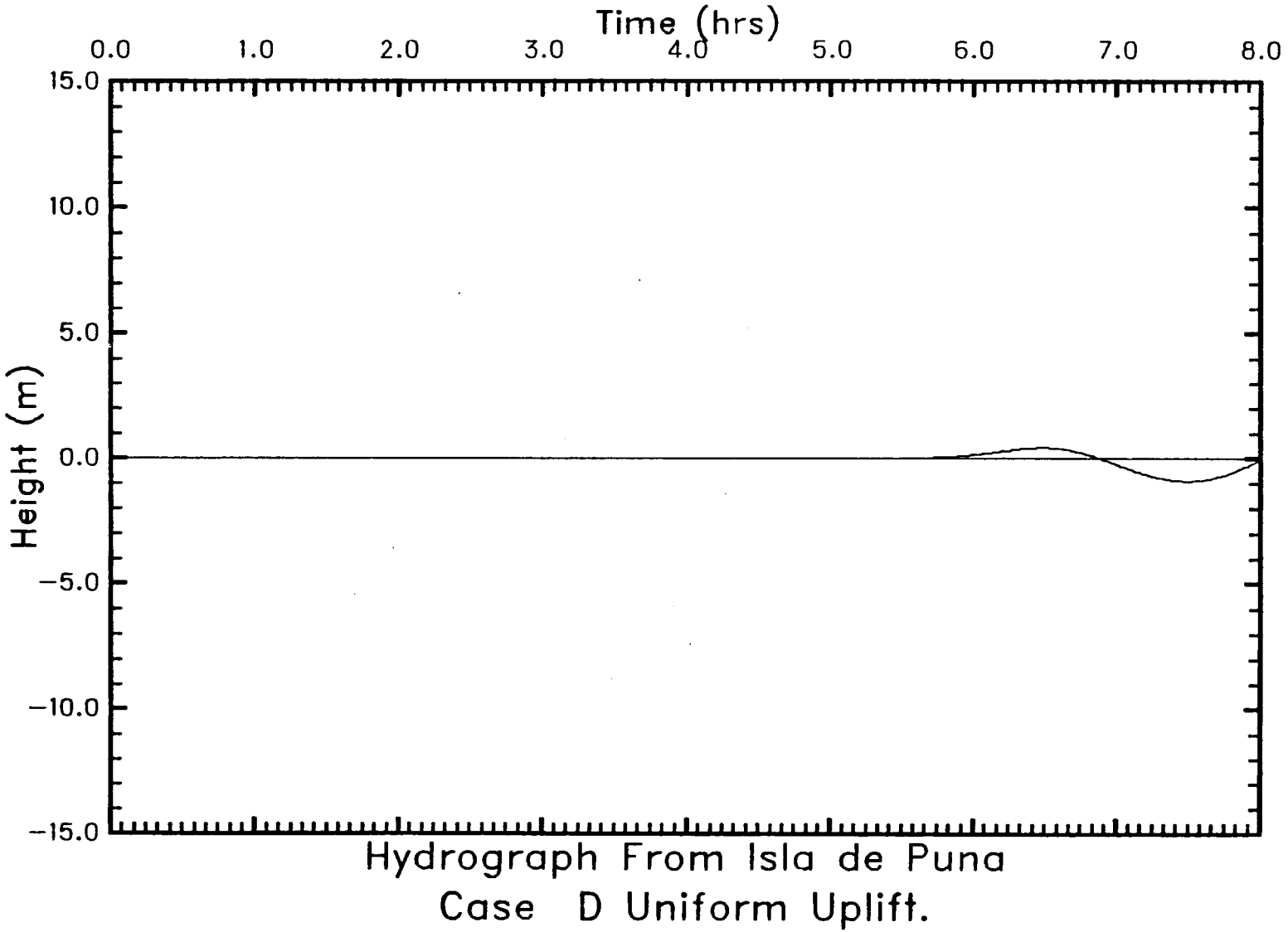

Figure 7.7: Wave elevation as a function of time at the recording point near Isla de Puna, Colombia. These waves were generated by the uniform uplift of Zone D.

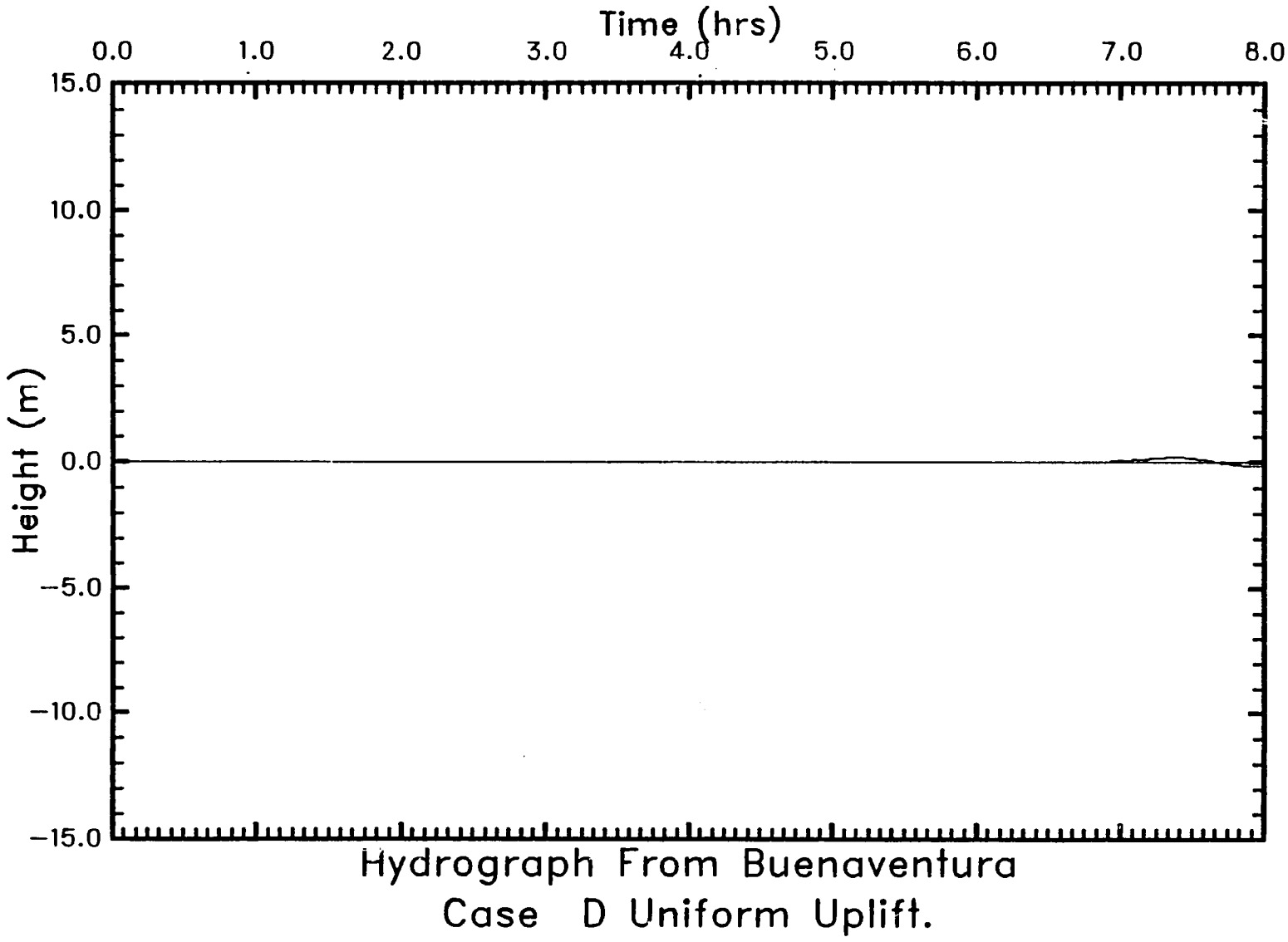

Figure 7.8: Wave elevation as a function of time at the recording point near Buenaventura, Ecuador. These waves were generated by the uniform uplift of Zone D.

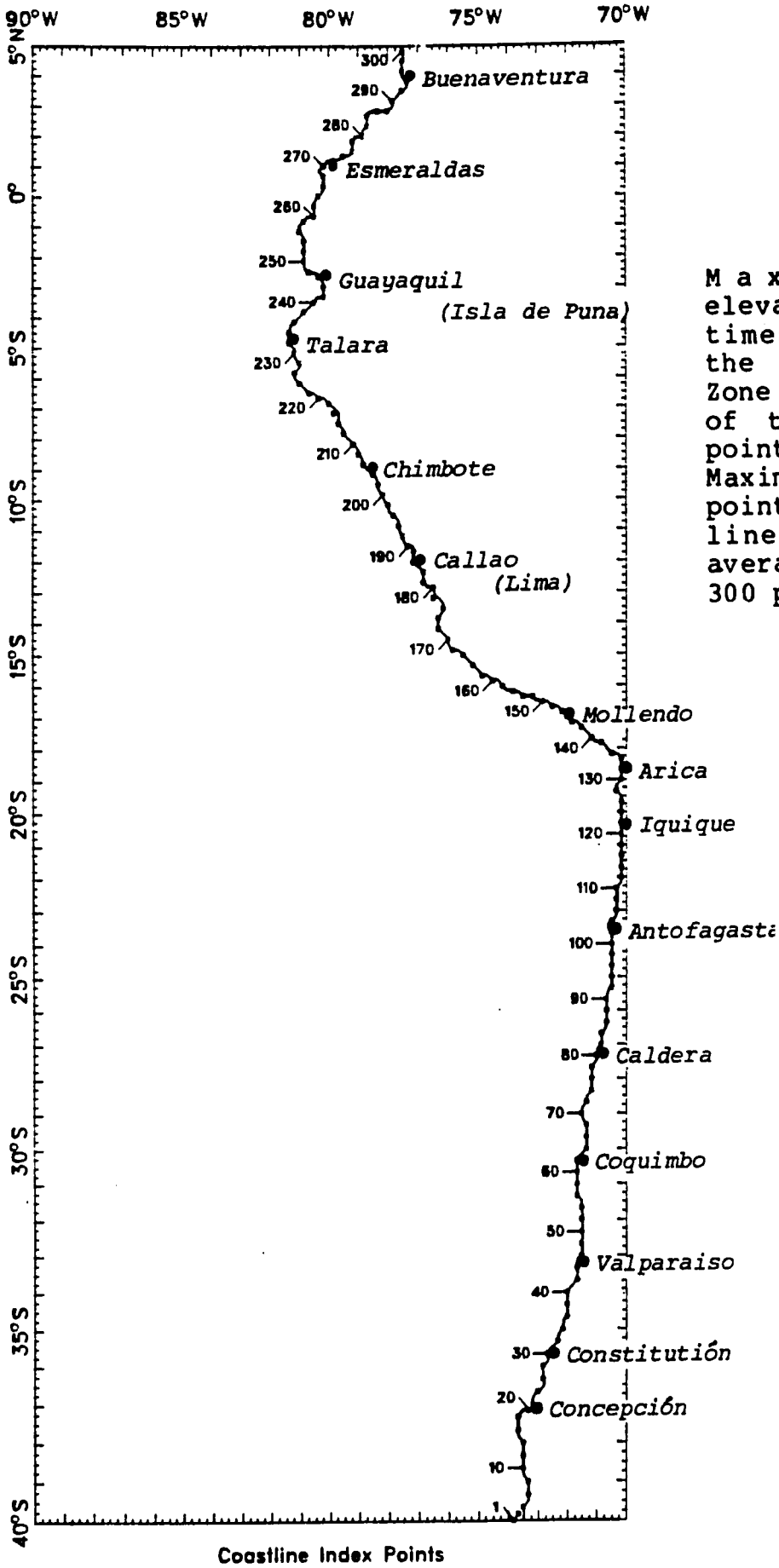

Figure: 7.9

Maximum wave elevations and arrival times of waves from the uniform uplift in Zone D. (a) Locations of the 300 recording point points. (b-f) Maximum waves at each point. The horizontal line represents the average value of all 300 points.

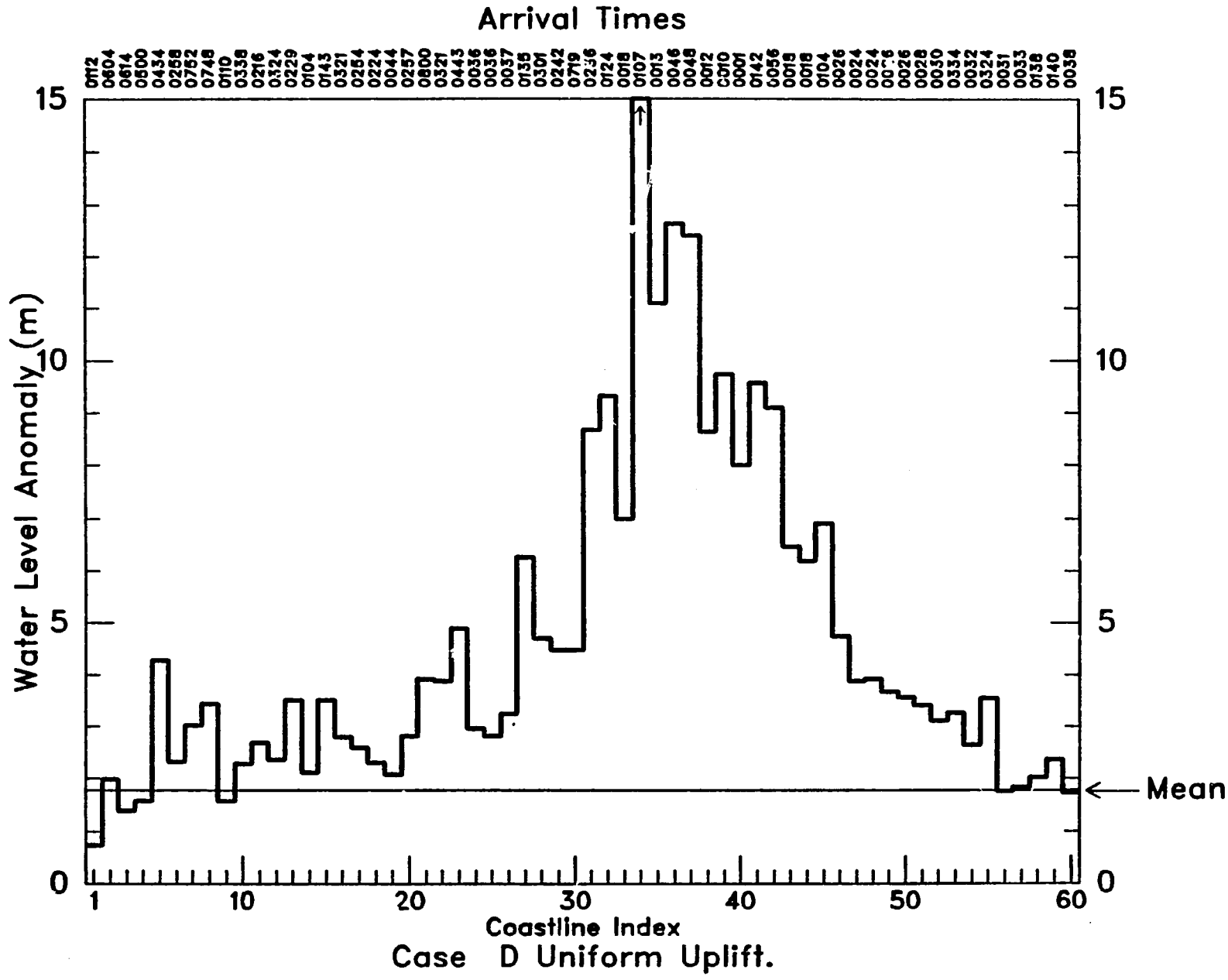
Arrival Times
Water Level Anomaly (m)
15
10
5
0
1
10
20
30
40
50
60
Coastline Index
Mean
Case D Uniform Uplift.

Figure: 7.9 (b)

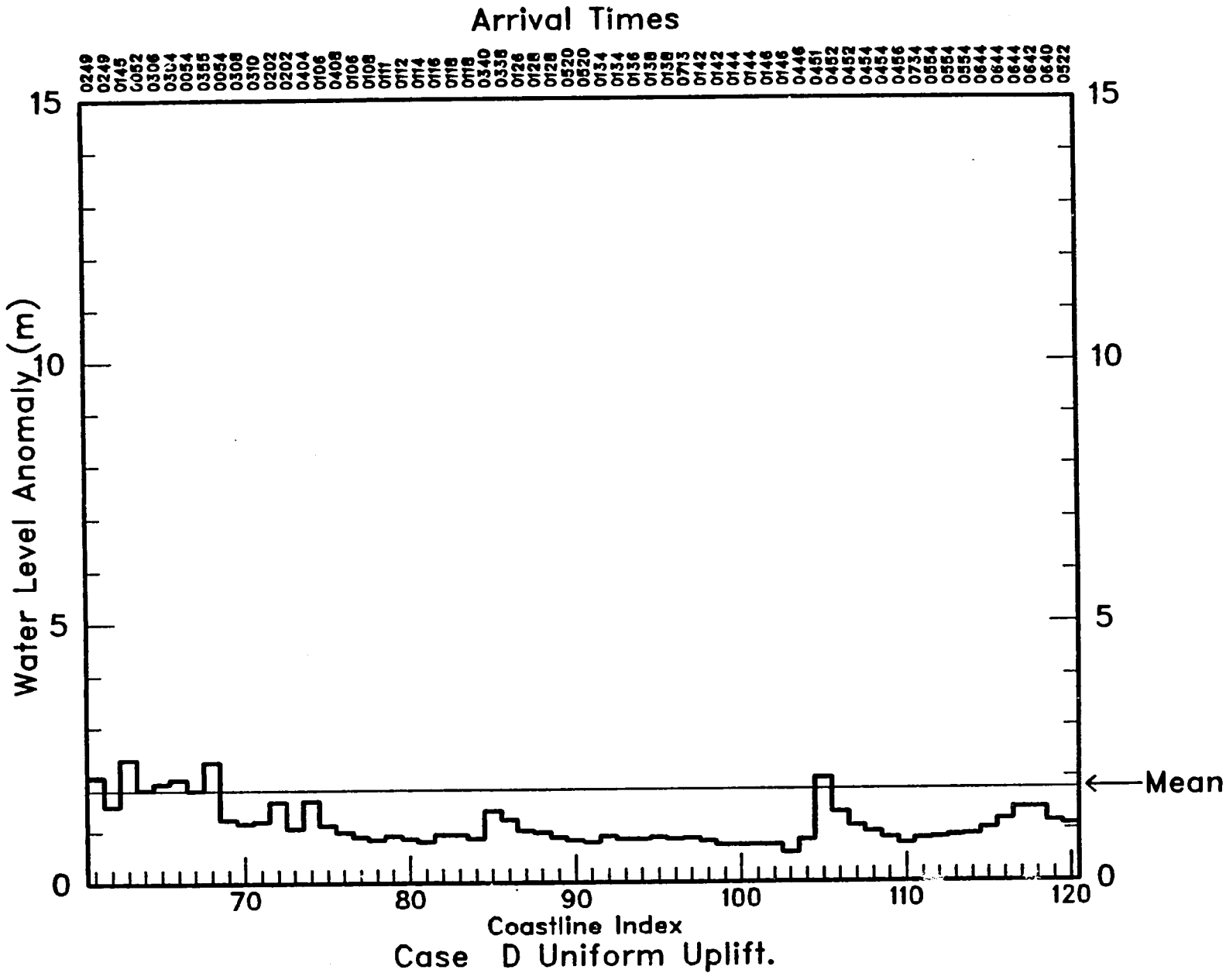
Arrival Times
0249 0249 0145 0052 0306 0304 0054 0355 0054 0308 0310 0202 0202 0404 0106 0408 0106 0108 0111 0112 0114 0116 0118 0118 0340 0338 0126 0128 0128 0520 0520 0134 0134 0136 0138 0138 0713 0142 0142 0144 0144 0146 0146 0446 0451 0452 0452 0454 0454 0456 0734 0554 0554 0554 0644 0644 0644 0642 0640 0522
Water Level Anomaly (m)
15
10
5
0
70
80
90
100
110
120
Mean
Coastline Index
Case D Uniform Uplift.

Figure: 7.9 (c)

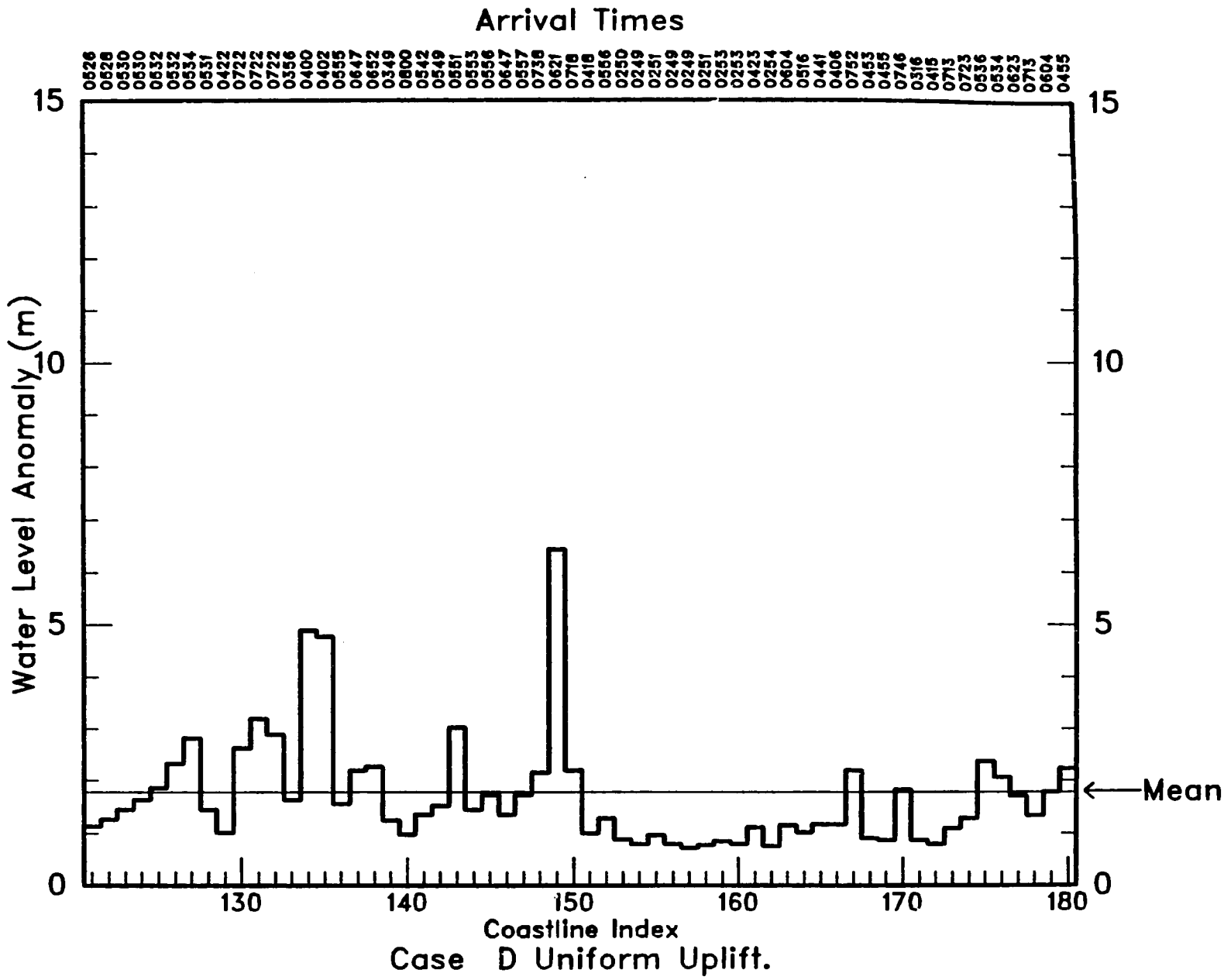
Arrival Times
0526 0528 0530 0530 0532 0532 0534 0531 0422 0722 0722 0722 0356 0400 0402 0555 0647 0652 0349 0800 0542 0549 0551 0553 0556 0647 0557 0738 0621 0718 0418 0556 0250 0249 0251 0249 0249 0251 0253 0253 0423 0254 0604 0516 0441 0406 0752 0453 0455 0746 0316 0415 0713 0723 0536 0534 0623 0713 0604 0455
15
10
5
0
Water Level Anomaly (m)
130
140
150
160
170
180
Coastline Index
Mean
Case D Uniform Uplift.

Figure: 7.9 (d)

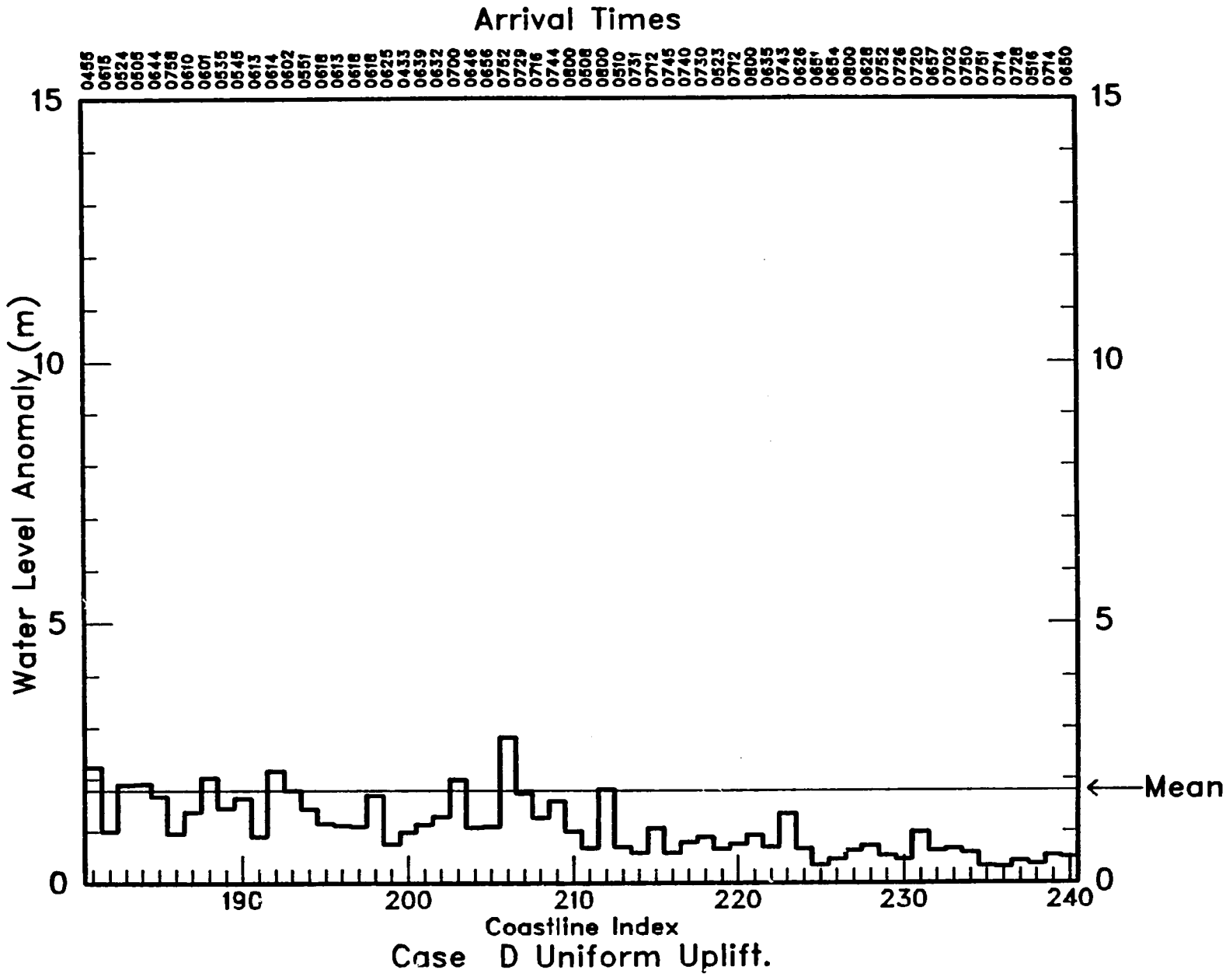
Arrival Times
0455 0615 0524 0505 0644 0758 0610 0601 0535 0545 0613 0614 0602 0551 0618 0613 0618 0618 0625 0433 0639 0632 0700 0646 0656 0752 0729 0716 0744 0800 0508 0800 0510 0731 0712 0745 0740 0730 0523 0712 0800 0635 0743 0626 0651 0654 0800 0628 0752 0726 0720 0657 0702 0750 0751 0714 0728 0516 0714 0650
Water Level Anomaly (m)
0
5
10
15
190
200
210
220
230
240
Coastline Index
Mean
Case D Uniform Uplift.

Figure: 7.9 (e)

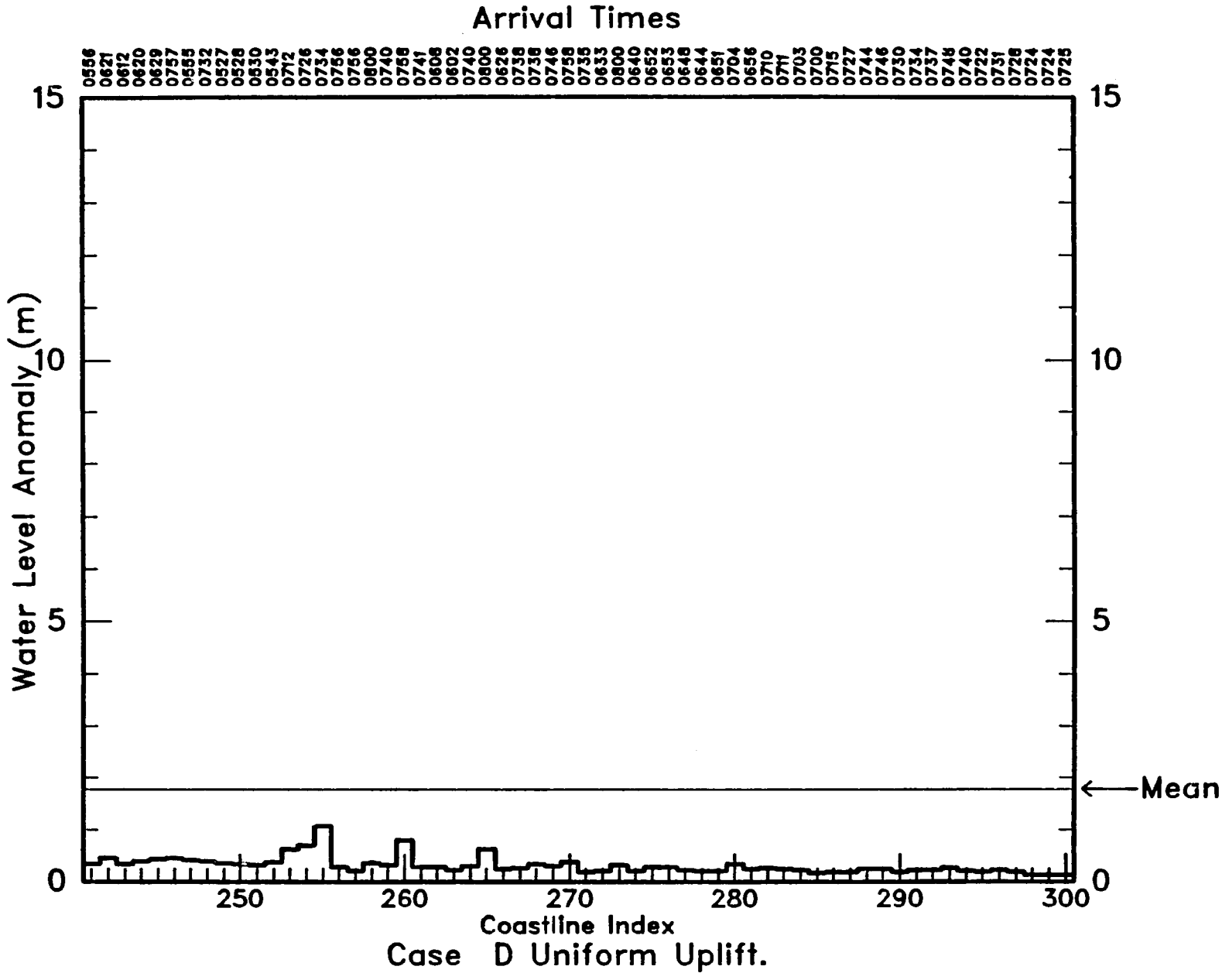
Arrival Times
0556 0621 0612 0620 0629 0757 0555 0732 0527 0528 0530 0543 0712 0726 0734 0756 0756 0800 0740 0758 0741 0608 0602 0740 0800 0626 0738 0738 0746 0758 0735 0633 0800 0640 0652 0653 0648 0644 0651 0704 0656 0710 0711 0703 0700 0715 0727 0744 0746 0730 0734 0737 0748 0740 0722 0731 0728 0724 0724 0725
15
10
5
0
Water Level Anomaly (m)
250
260
270
280
290
300
Coastline Index
Mean
Case D Uniform Uplift.

Figure: 7.9 (f)

7.3 VARIABLE UPLIFT CASE

The displacement pattern for this case covers the entire area indicated in Figure 7.1. The maximum uplift is 8 m.

7.3.1 Immediate Effects

The wave elevation contours after one hour appear in Figure 7.10. The leading crest spreads uniformly out from the source, with a slight orientation toward the west by northwest. A very well-defined secondary crest follows closely behind. This is probably the continental reflection. Several coastal areas are subject to concentrations of wave elevation at this time.

7.3.2 Longer Duration Effects

The wave elevation time series for this case indicate that wave energy drops off quickly with distance from the source. At Valparaiso (Figure 7.11) the waves start out quite high and slowly diminish, although after 8 hours the crest height is still about 1 m. In contrast, the waves are almost totally damped out at Antofagasta (Figure 7.12).

The waves reaching Arica (Figure 7.13) are long and low and gradually diminish. At the three northern locations (Figures 7.14 to 7.16) the waves are very long and smooth and create only a minimal disturbance.

7.3.3 Maximum Elevations

The maximum elevation plots (Figure 7.17a-f) also reflect the gradually diminishing nature of this wave field.

The average maximum is about 1.1 m. The region of highest waves extends from the southern end of the model area to just north of Coquimbo. All through this region waves are of average to well-above-average height. The most consistently threatened area extends from near Concepcion to just north of Valparaiso. The only other areas of nearly comparable height are close to Arica and in the area just northwest of Mollendo. The waves around Chimbote also hover near the mean, but in general most areas away from the source do not seem threatened.

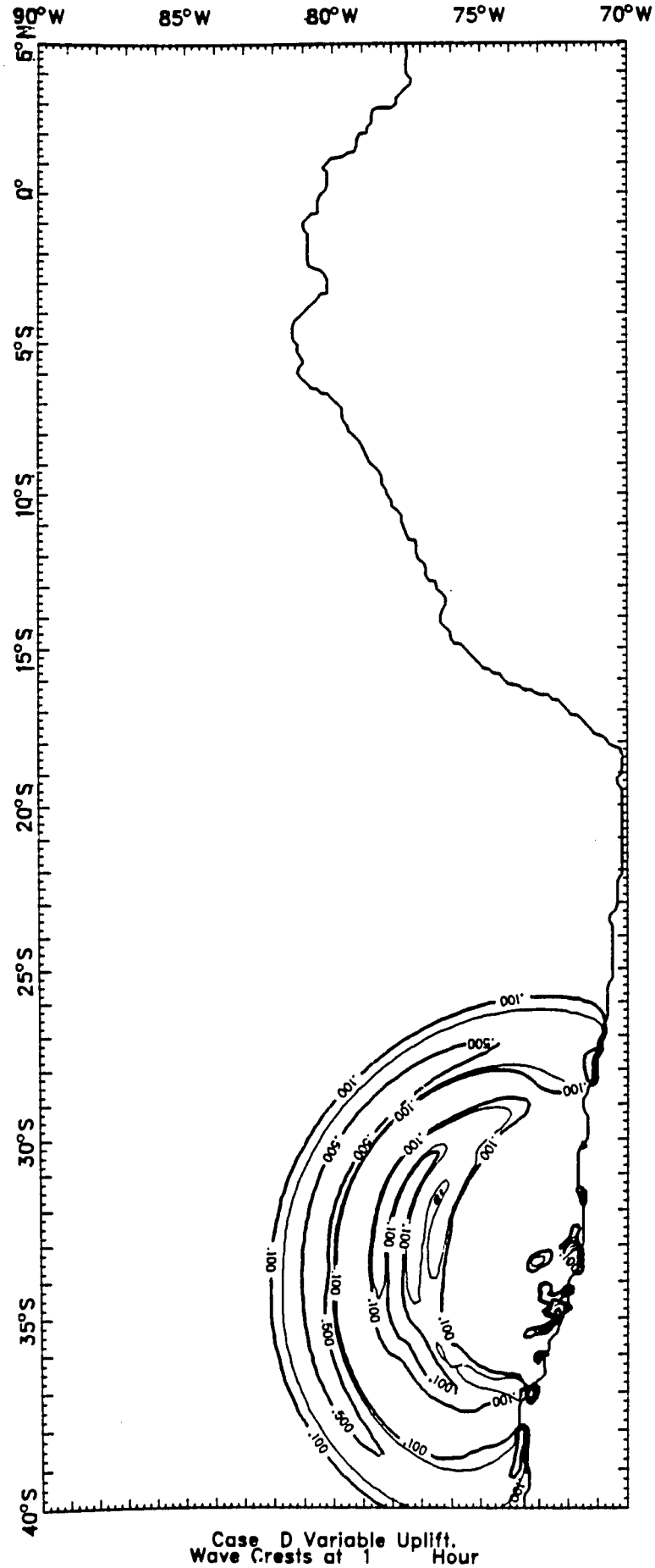

Figure: 7.10

Surface elevation (positive only) one hour after a variable uplift in source Zone D. Contours correspond to 0.1, 0.2, 0.5, 1.0, and 2.0 m.

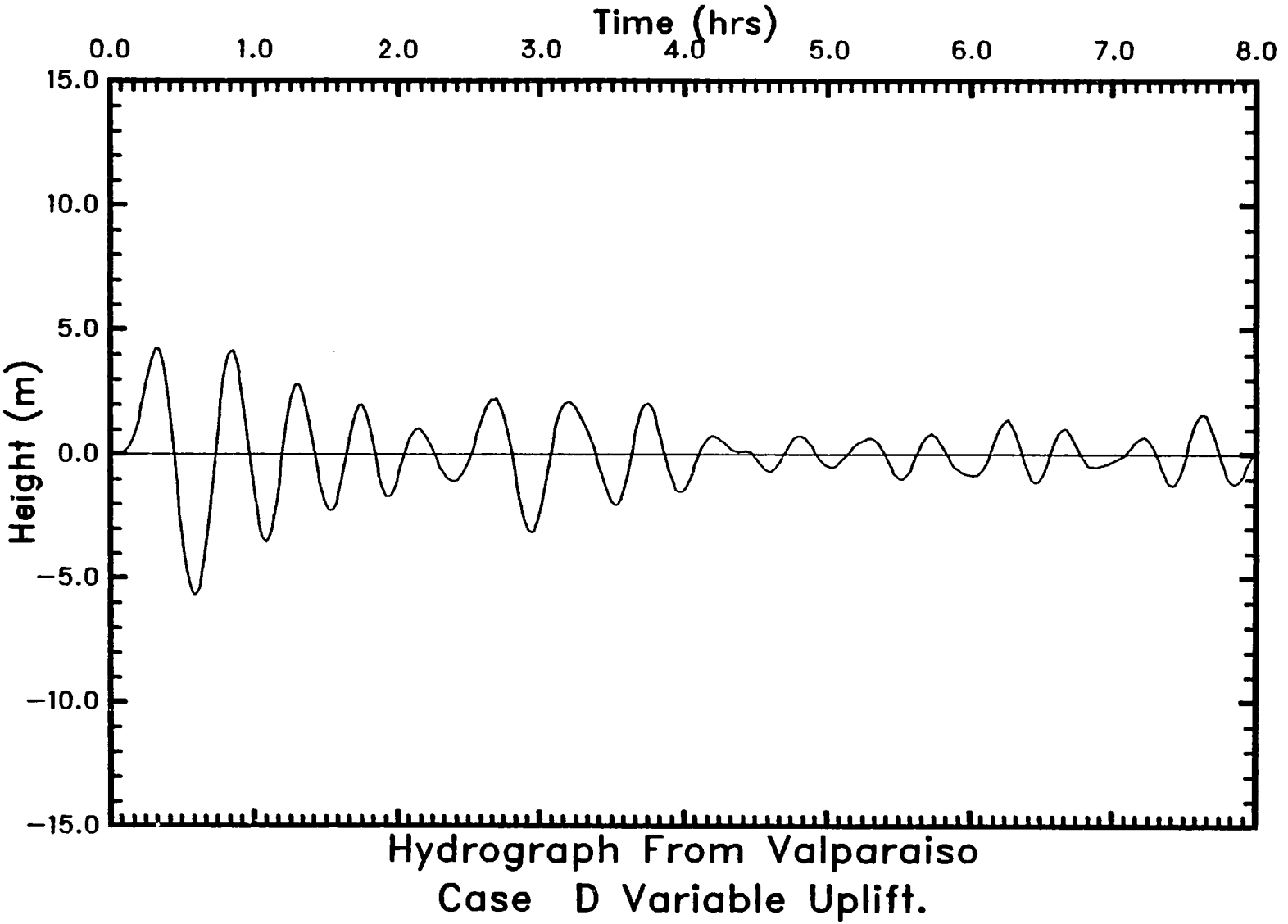

Figure 7.11: Wave elevation as a function of time at the recording point near Valparaiso, Chile. These waves were generated by the variable uplift of Zone D.

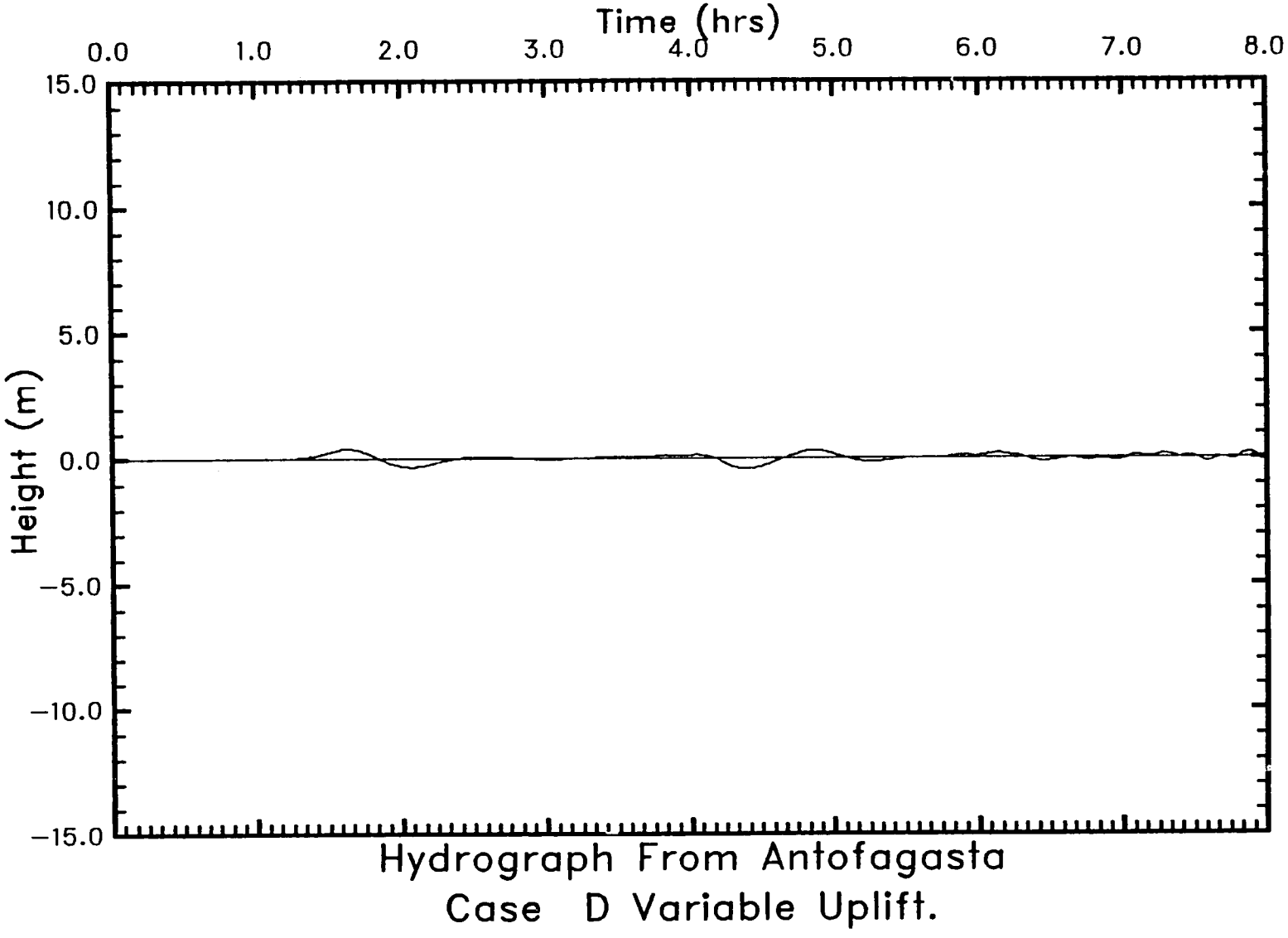

Figure 7.12: Wave elevation as a function of time at the recording point near Antofagasta, Chile. These waves were generated by the variable uplift of Zone D.

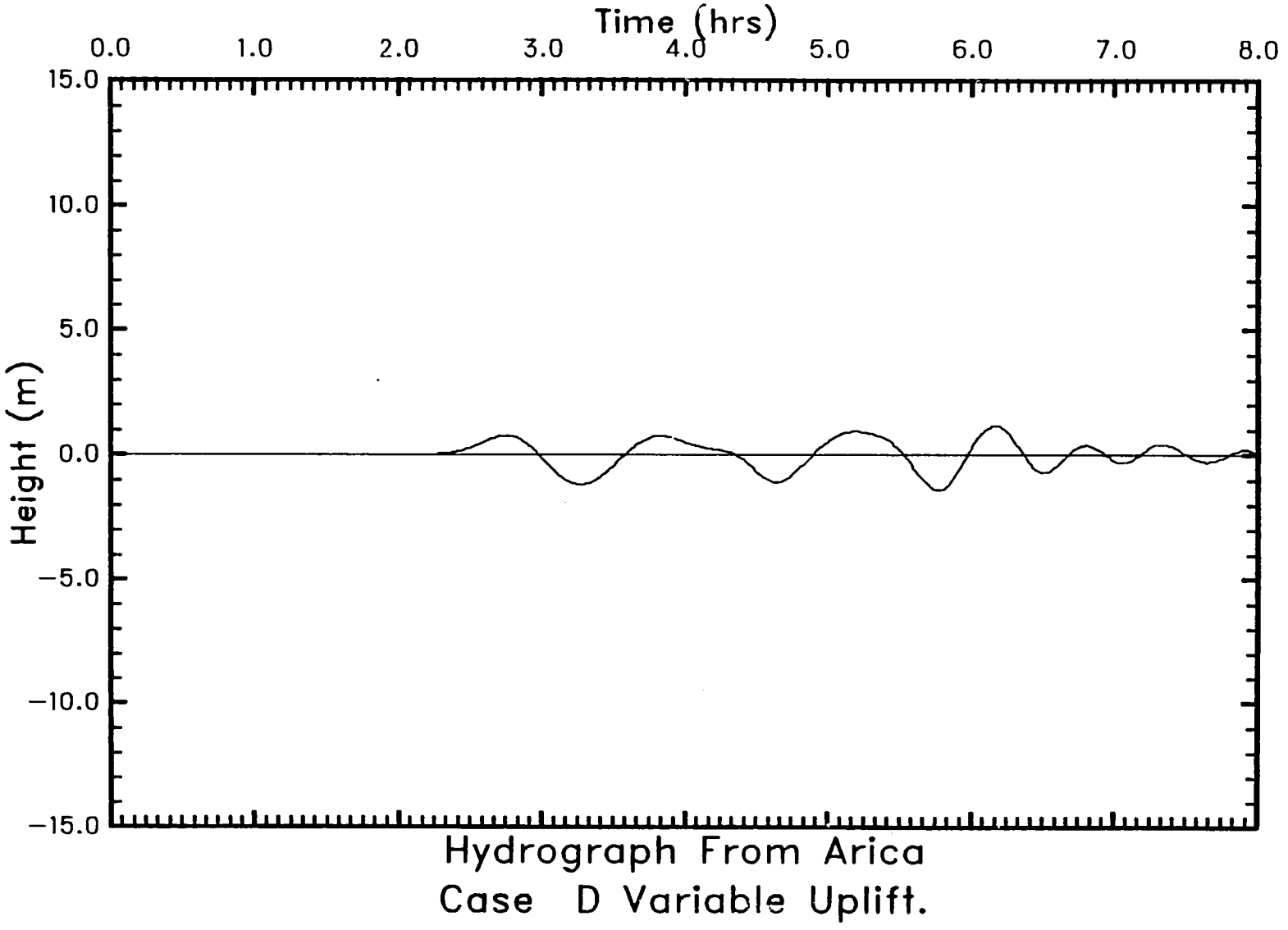

Figure 7.13: Wave elevation as a function of time at the recording point near Arica, Chile. These waves were generated by the variable uplift of Zone D.

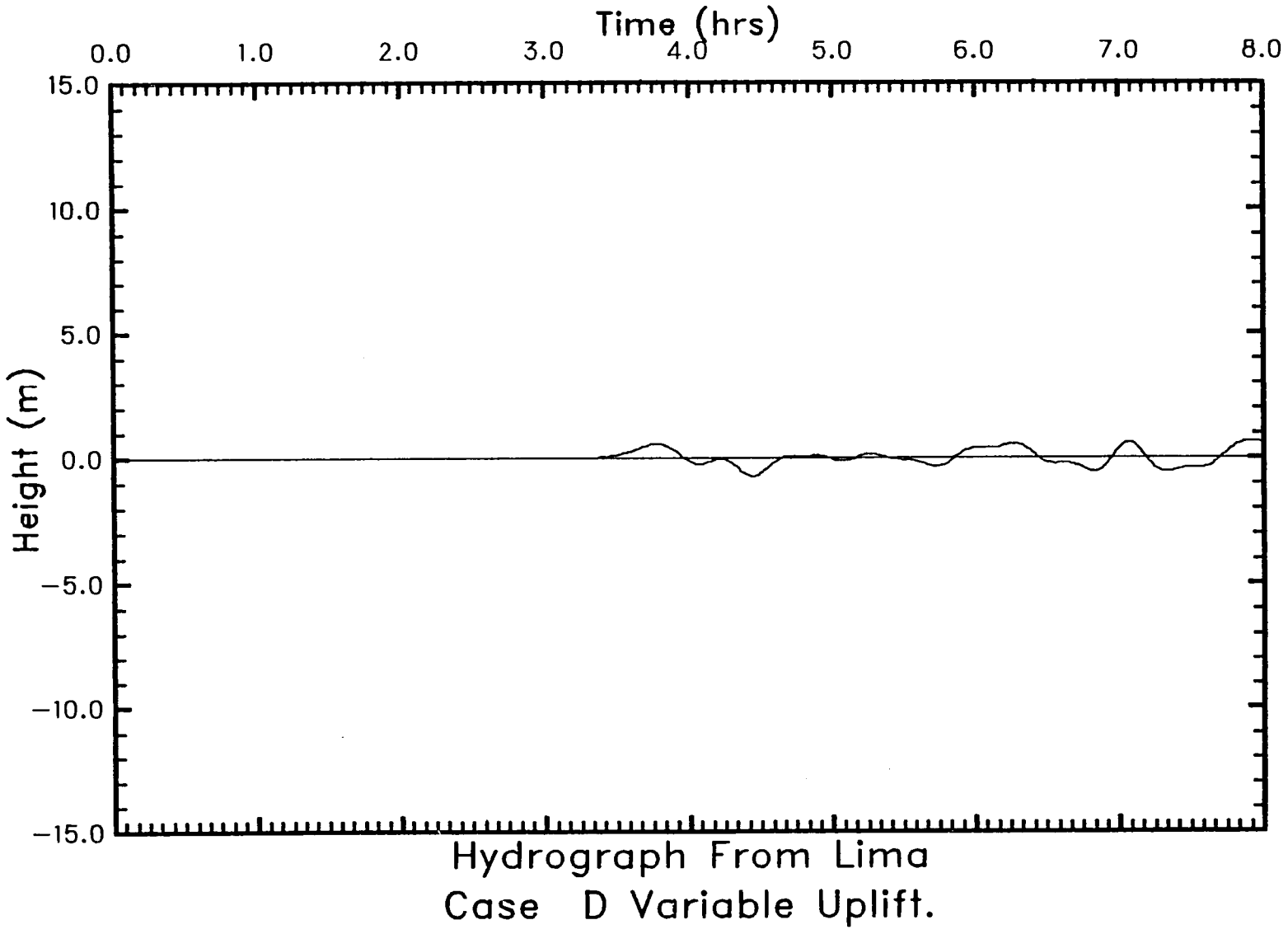

Figure 7.14: Wave elevation as a function of time at the recording point near Lima, Peru. These waves were generated by the variable uplift of Zone D.

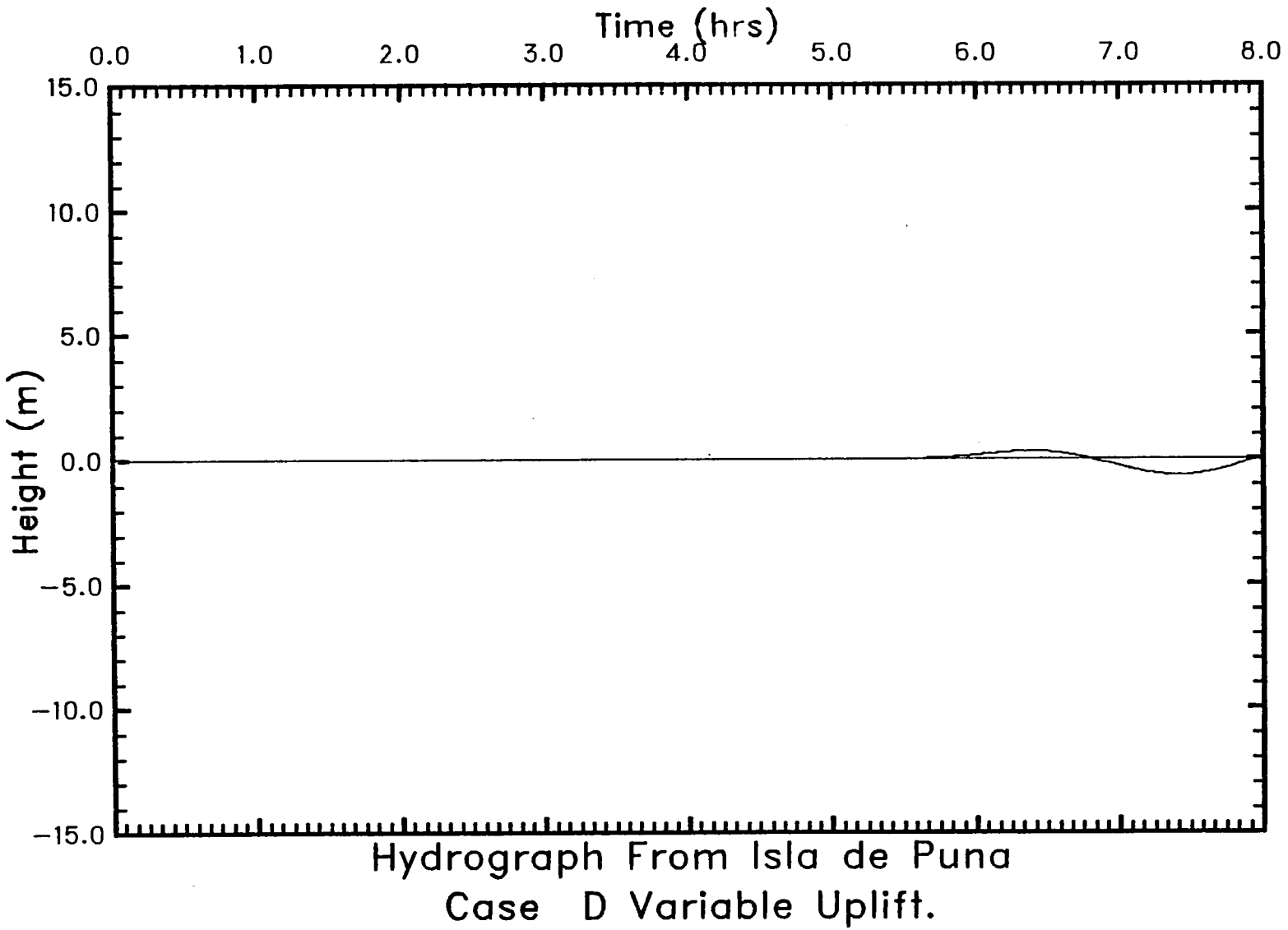

Figure 7.15: Wave elevation as a function of time at the recording point near Isla de Puna, Colombia. These waves were generated by the variable uplift of Zone D.

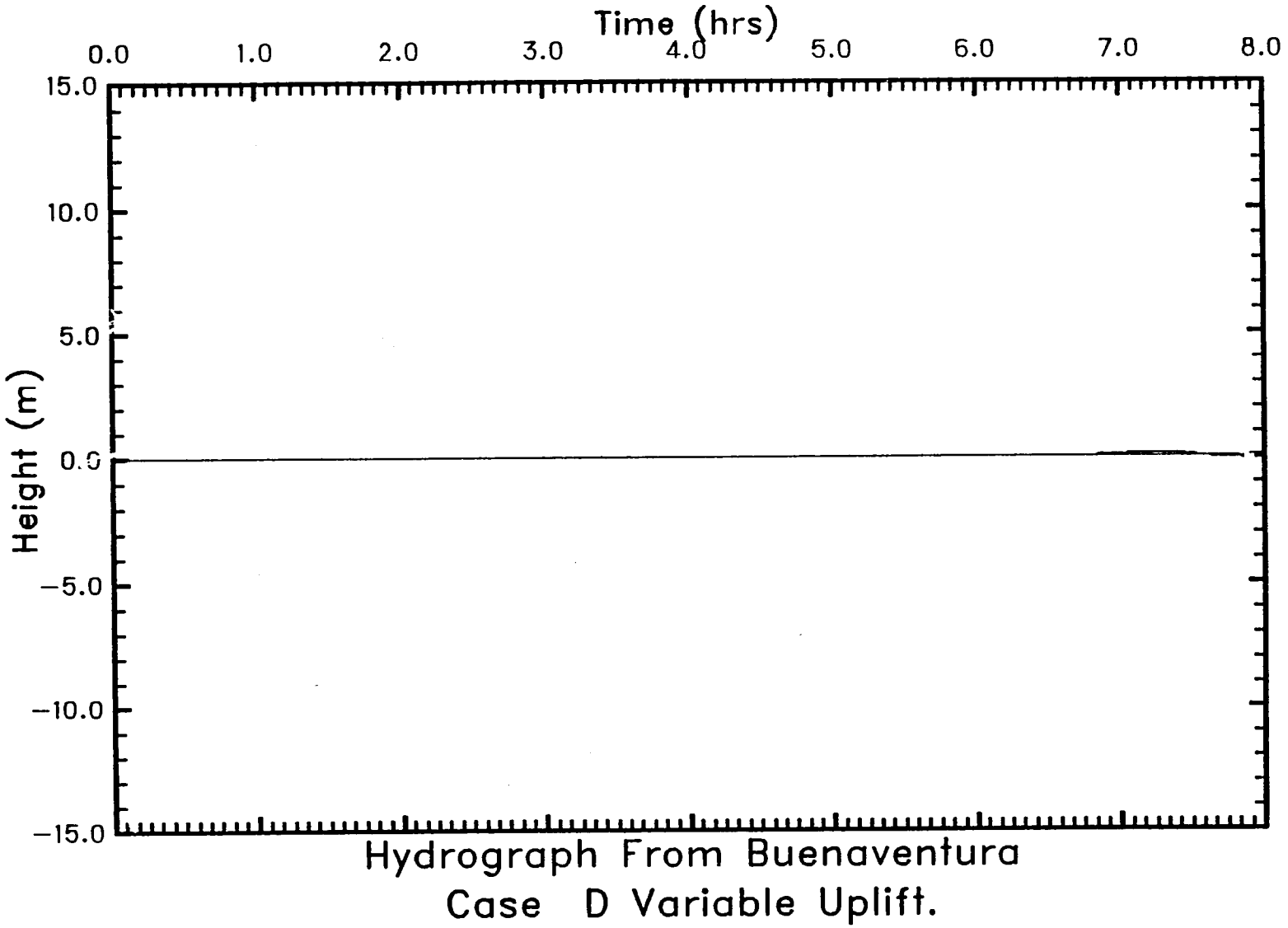

Figure 7.16: Wave elevation as a function of time at the recording point near Buenaventura, Ecuador. These waves were generated by the variable uplift of Zone D.

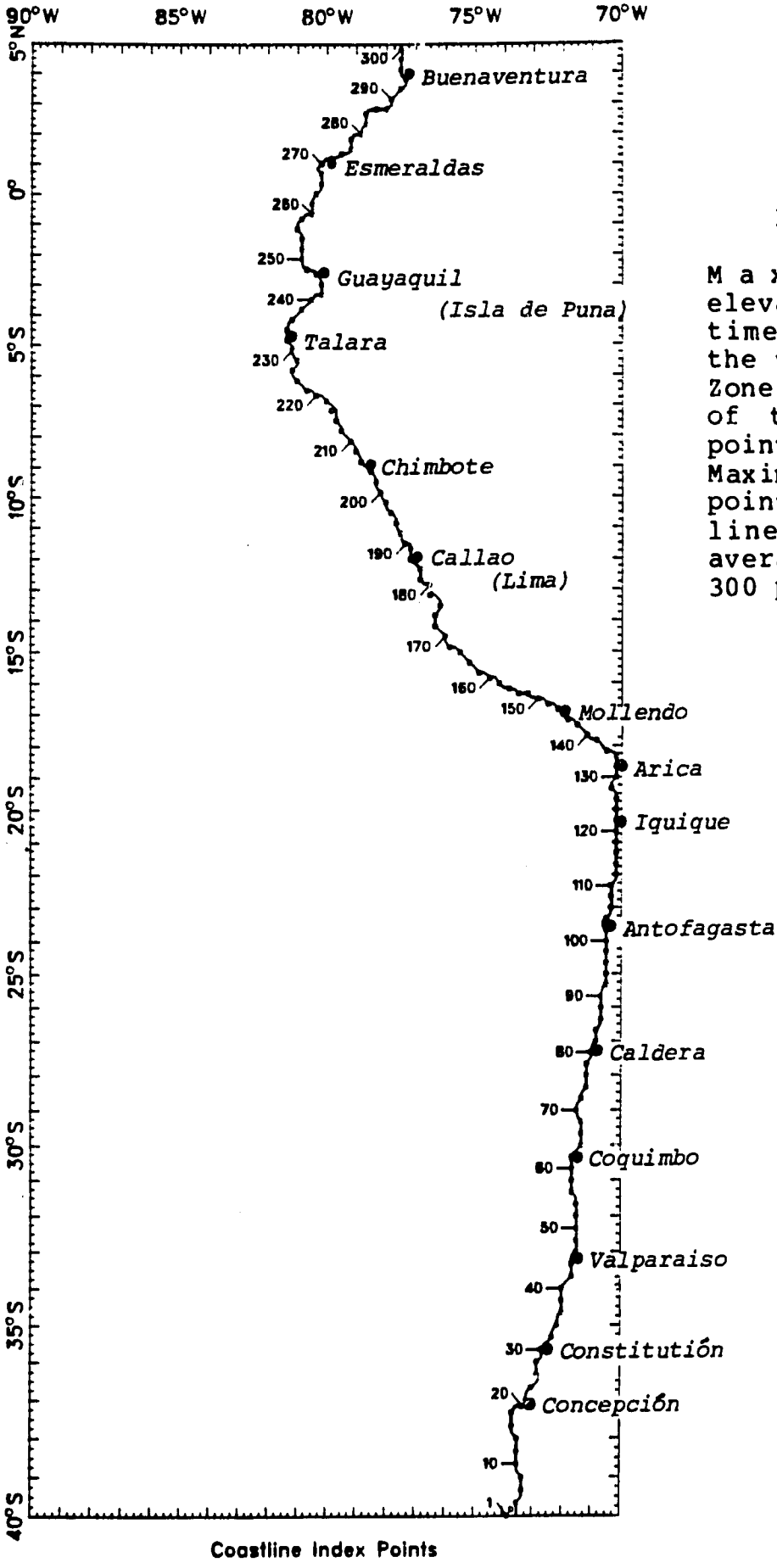

Figure: 7.17

Maximum wave elevations and arrival times of waves from the variable uplift in Zone D. (a) Locations of the 300 recording point points. (b-f) Maximum waves at each point. The horizontal line represents the average value of all 300 points.

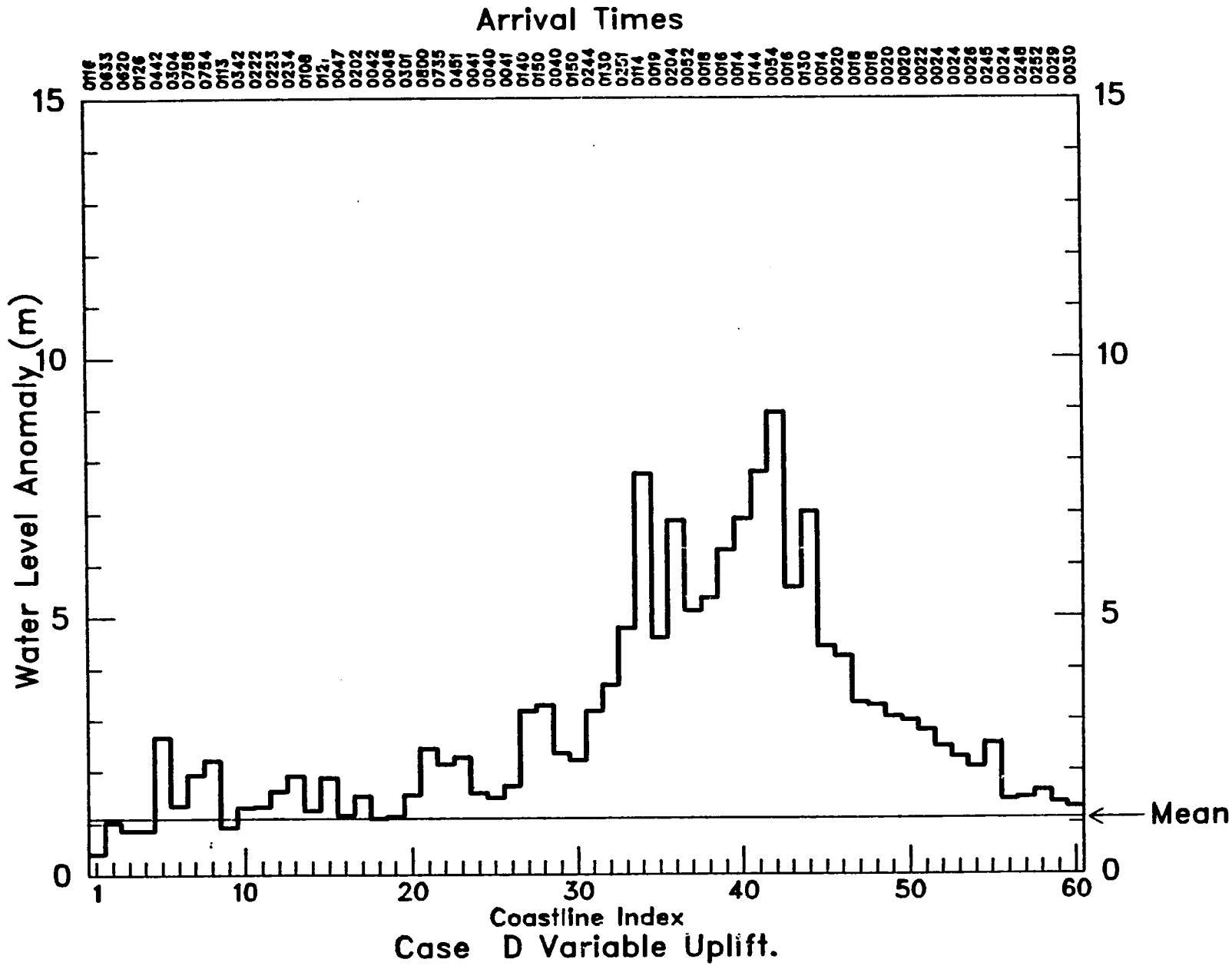
Arrival Times
Water Level Anomaly (m)
15
10
5
0
1
10
20
30
40
50
60
Coastline Index
Mean
Case D Variable Uplift.

Figure: 7.17 (b)

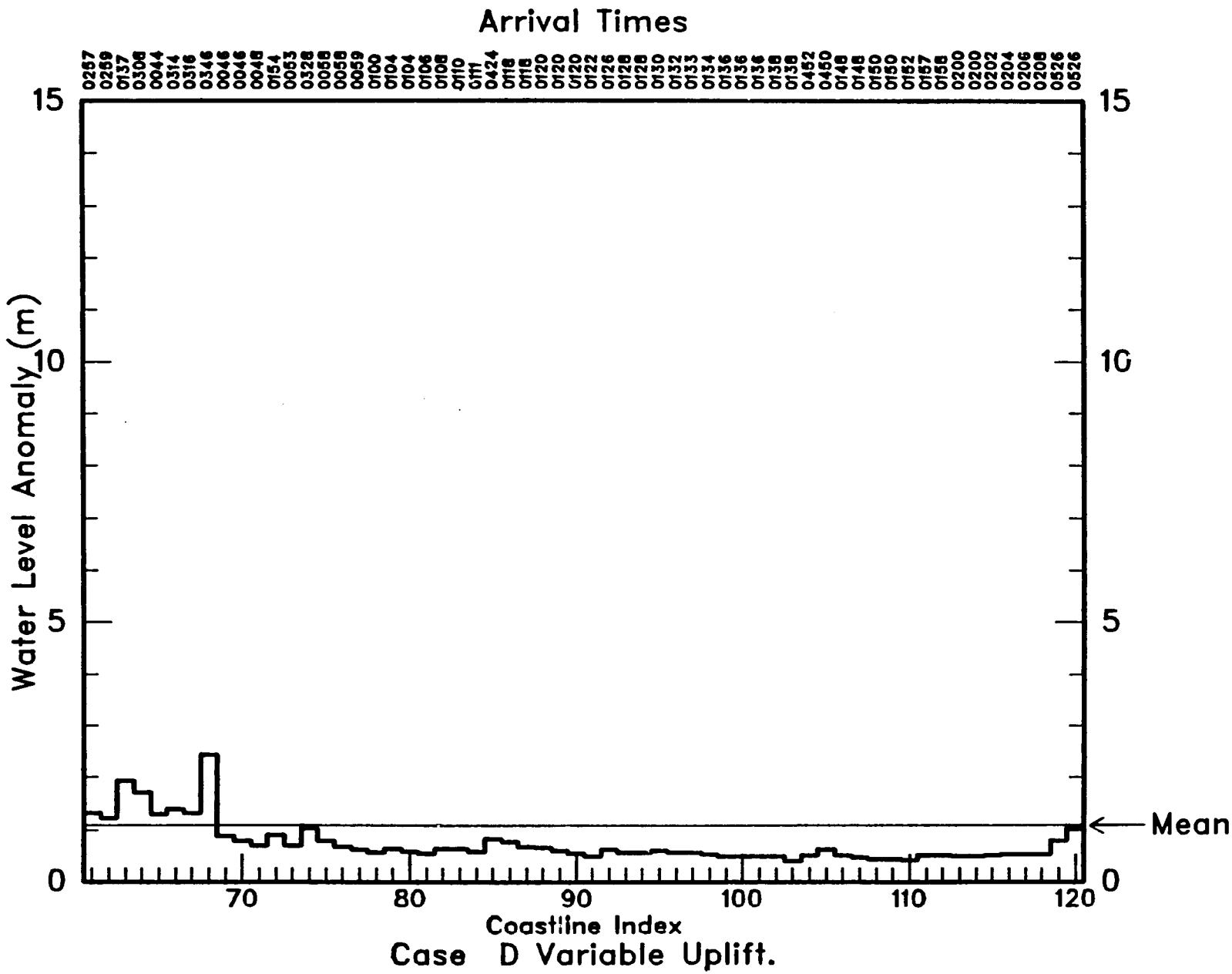
Arrival Times
0257 0259 0137 0308 0044 0314 0316 0346 0046 0046 0048 0154 0053 0328 0058 0058 0059 0100 0104 0104 0106 0108 0110 0111 0424 0118 0118 0120 0120 0120 0122 0126 0128 0128 0130 0132 0133 0134 0136 0136 0138 0138 0452 0450 0148 0148 0150 0150 0152 0157 0158 0200 0200 0202 0204 0206 0208 0526 0526
15
10
5
0
Water Level Anomaly (m)
70
80
90
100
110
120
Coastline Index
Mean
Case D Variable Uplift.

Figure: 7.17 (c)

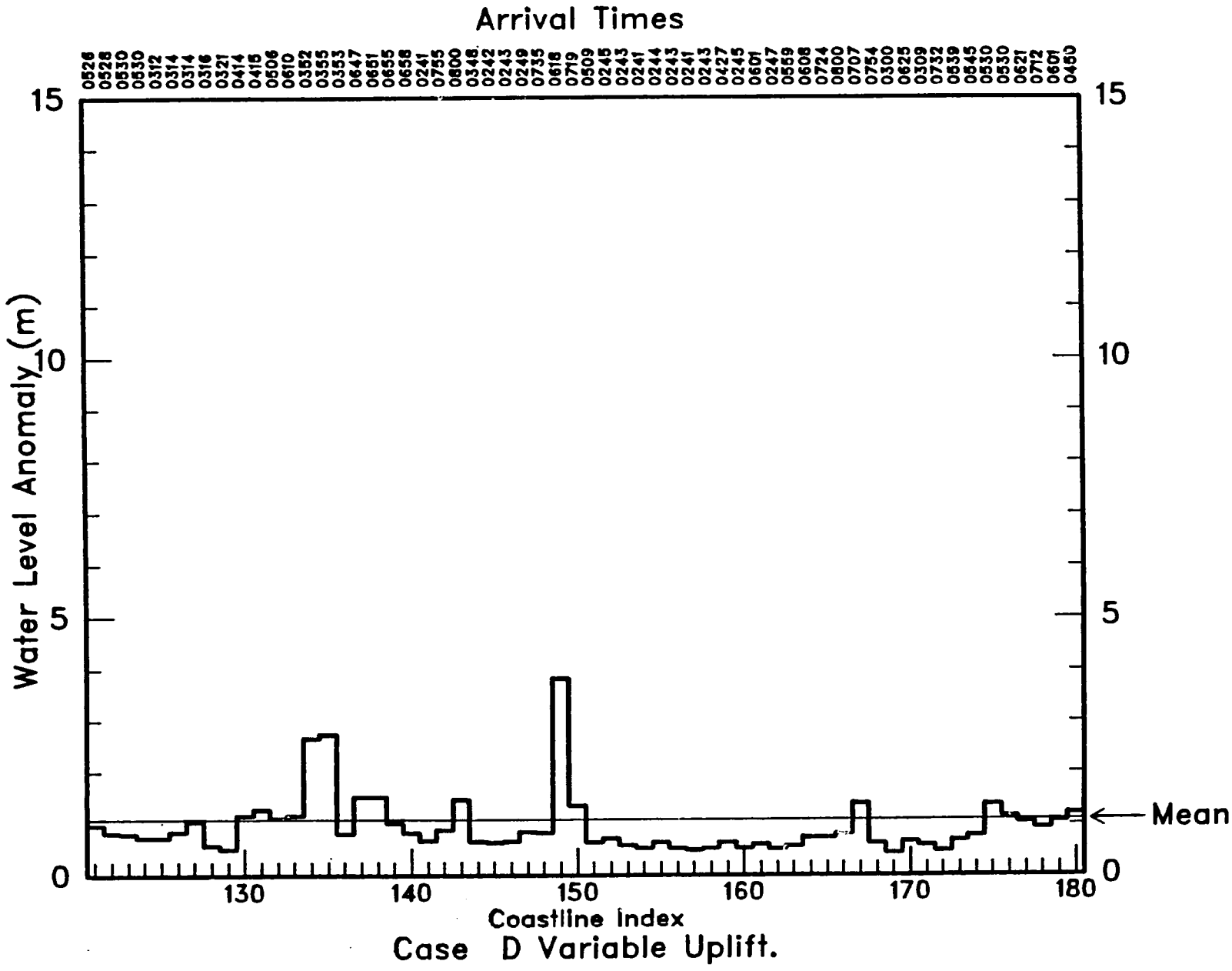
Arrival Times
0526 0528 0530 0530 0312 0314 0314 0316 0321 0414 0415 0506 0610 0352 0355 0353 0647 0661 0655 0658 0241 0755 0800 0348 0242 0243 0249 0735 0618 0719 0509 0245 0243 0241 0244 0243 0241 0243 0427 0245 0601 0247 0559 0608 0724 0800 0707 0754 0300 0625 0309 0732 0539 0545 0530 0530 0621 0712 0601 0450
15
10
5
0
Water Level Anomaly (m)
130
140
150
160
170
180
Coastline Index
Mean
Case D Variable Uplift.

Figure: 7.17 (d)

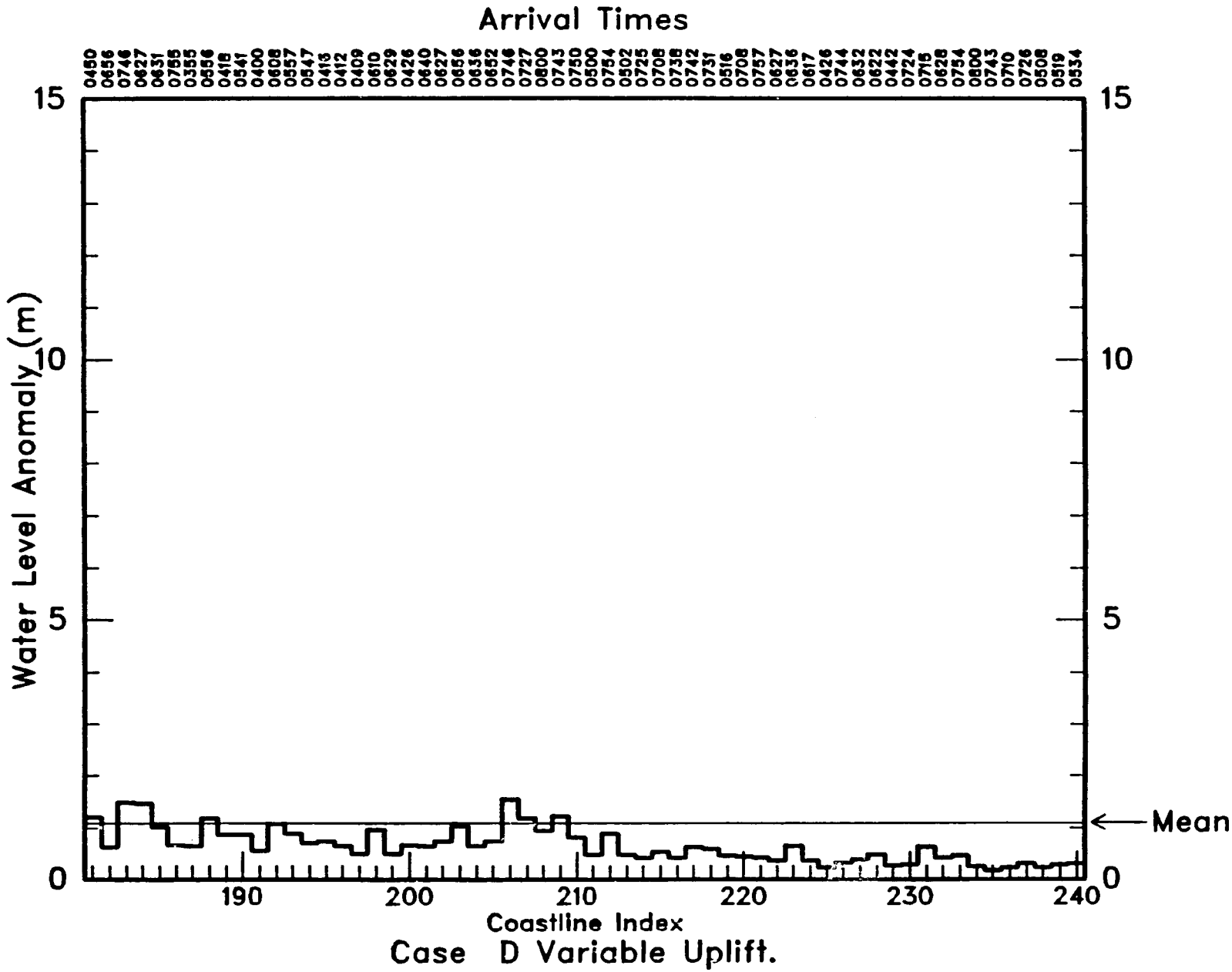
Arrival Times
0450 0656 0746 0627 0631 0755 0355 0556 0418 0541 0400 0608 0557 0547 0413 0412 0409 0610 0629 0426 0640 0627 0656 0636 0652 0746 0727 0800 0743 0750 0500 0754 0502 0725 0708 0758 0742 0731 0516 0708 0757 0627 0636 0617 0426 0744 0632 0622 0442 0724 0716 0628 0754 0800 0743 0710 0726 0508 0519 0534
15
10
5
0
Water Level Anomaly (m)
190
200
210
220
230
240
Coastline Index
Mean
Case D Variable Uplift.

Figure: 7.17 (e)

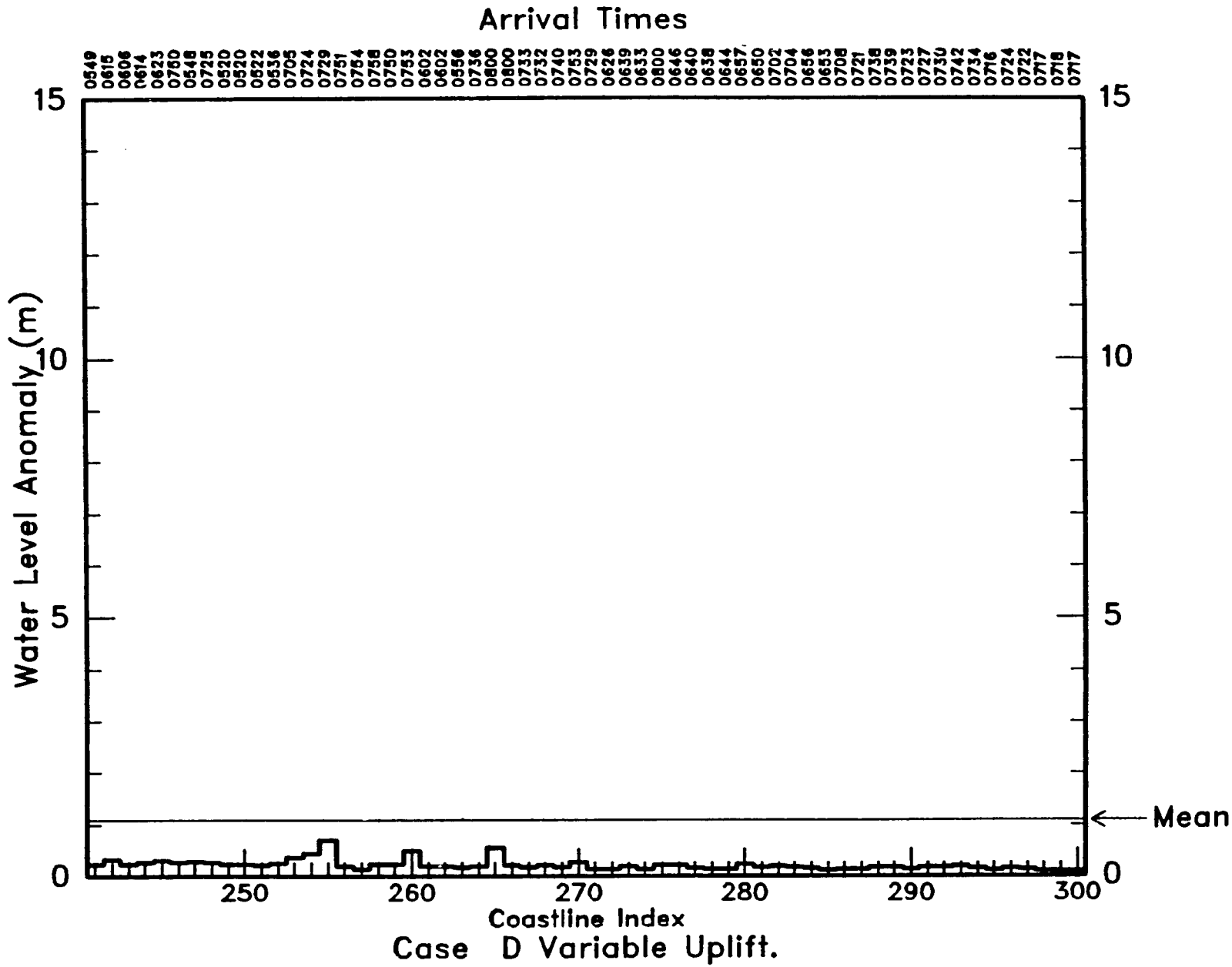
Arrival Times
0549 0615 0606 0614 0623 0760 0548 0725 0520 0520 0522 0536 0705 0724 0729 0751 0754 0758 0750 0753 0602 0602 0556 0736 0800 0800 0733 0732 0740 0753 0729 0626 0639 0633 0800 0646 0640 0638 0644 0657 0650 0702 0704 0656 0653 0708 0721 0738 0739 0723 0727 0730 0742 0734 0716 0724 0722 0717 0718 0717
15
10
5
0
Water Level Anomaly (m)
250
260
270
280
290
300
Coastline Index
Mean
Case D Variable Uplift.

Figure: 7.17 (f)

7.4 HAZARD ASSESSMENT - SOURCE ZONE D

This source zone produces small, but moderately energetic tsunamis. The mean elevation values are 1.1 m for the variable uplift and 1.8 for the uniform uplift. The hydrographs are quite similar in both cases, except at Valparaiso. The wave record for the variable uplift case is much more regular than that for the uniform case. The amplitudes of the two records are quite comparable though.

In both cases the highest waves occur in the vicinity of the source. The entire coast from the southern end of the model zone to near Coquimbo is under severe or potentially severe threat. The coast north of Coquimbo is relatively quiet up to the area around Arica. Here reflections and trapping work to produce scattered threatening waves. These recur intermittently to around Chimbote. North of there the threat is greatly reduced.

Section 8
SOURCE ZONE E

8.1 INTRODUCTION

This zone is not only the largest used in this study, but also the largest ever postulated. It is nearly twice as long as the 1000 km uplift zone of the 22 May 1960 earthquake which occurred off the southern coast of Chile. Such a widespread event would generate a truly catastrophic tsunami. The extent of the zone is depicted in Figure 8.1.

Because of the unusual length of the zone we could not assume an instantaneous uplift. Instead, we specified approximately how long a section a rupture propagating at 3.5 km/sec could uplift in 60 sec (one model time step). Then 10 areas, each roughly the same length, were marked off. The model specifies that these blocks, one after the other in sequence from north to south, are displaced instantaneously at a rate of one block per time step. This process serves as a discrete approximation to the continuous uplift process which the sea floor would actually undergo.

8.2 UNIFORM UPLIFT CASE

The source motion for this case consists of a 10 m vertical uplift for each block in sequence.

8.2.1 Immediate Effects

As the wave contours one hour after generation show (Fig. 8.2), the results of this uplift are catastrophic.

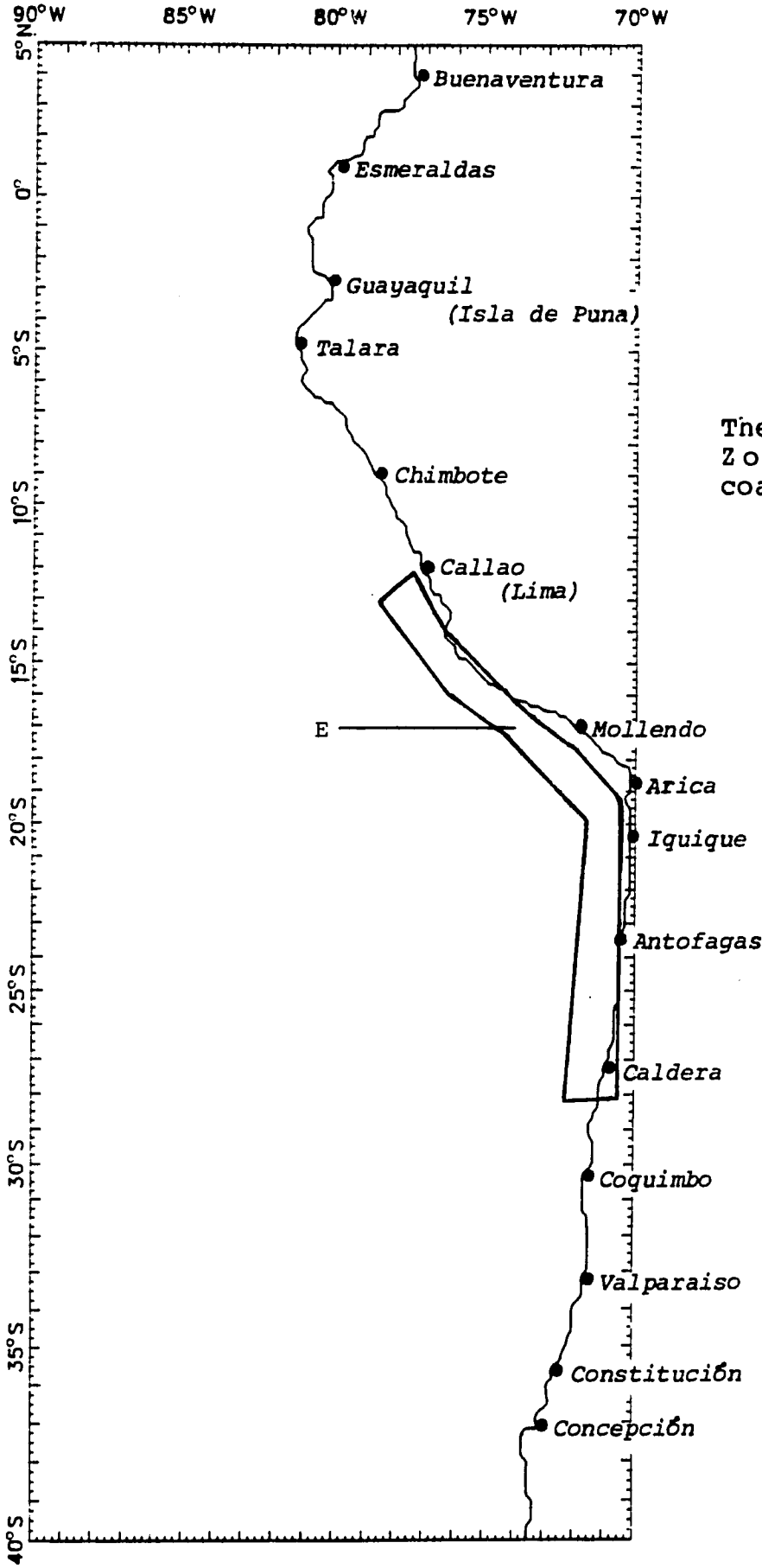

Figure 8.1:

The location of source Zone E along the coastline.

The leading wave extends approximately 29° of latitude. The highest point on the wave, denoted by the small, unlabelled, heavy ellipse between 22°S and 24°S, is over 10 m. The sea behind the leading wave is chaotic, the result of two dominant wave regimes--one moving southwestward and one moving westward--interacting as they cross. Many areas of high waves are apparent on the coast.

8.2.2 Longer Duration Effects

The time series at the various recording points show that this tsunami produces not only very intense waves but also waves of long duration. Note in examining these pictures that the vertical scale is now 20 m, rather than the 15 m used in cases A to D.

The waves at Valparaiso (Fig. 8.3) are initially only 3 m high, but gradually increase in height to between 4 and 6 m. By the end of the simulation they seem to be growing. At Antofagasta (Fig. 8.4) the opposite happens. The waves start high and then rapidly die off to a less spectacular (but still dangerous) 2-3 m height.

Arica (Fig. 8.5) is continually struck by long, high waves, although none are as awesome as the initial 17 m crest. The wave energy level in this record remains high throughout the simulation.

The waves at Lima (Fig. 8.6), like those at Valparaiso, start off slowly, if a 5 m crest can be called a slow start, and gradually increase, until a crest 11 m high arrives nearly 5 hrs. after the uplift. Again, the waves are highly active throughout the simulation.

Isla de Puna (Fig. 8.7) receives the usual very long waves which slowly increase. The final wave calculated is 4·m high. Only at Buenaventura (Fig. 8.8) do we record low waves throughout the simulation.

8.2.3 Maximum Elevations

The maximum elevation plots (Fig. 8.9a-f) depict graphically the threat posed by this event. The mean level calculated is about 6.8 m. The source region, of course, is struck by extreme waves almost immediately, but no section of the coast is free of at least a potential threat. The normally protected region north from Talara is once again much quieter than any other portion of the coast, but even here waves 2 to 3 m high occur in some areas.

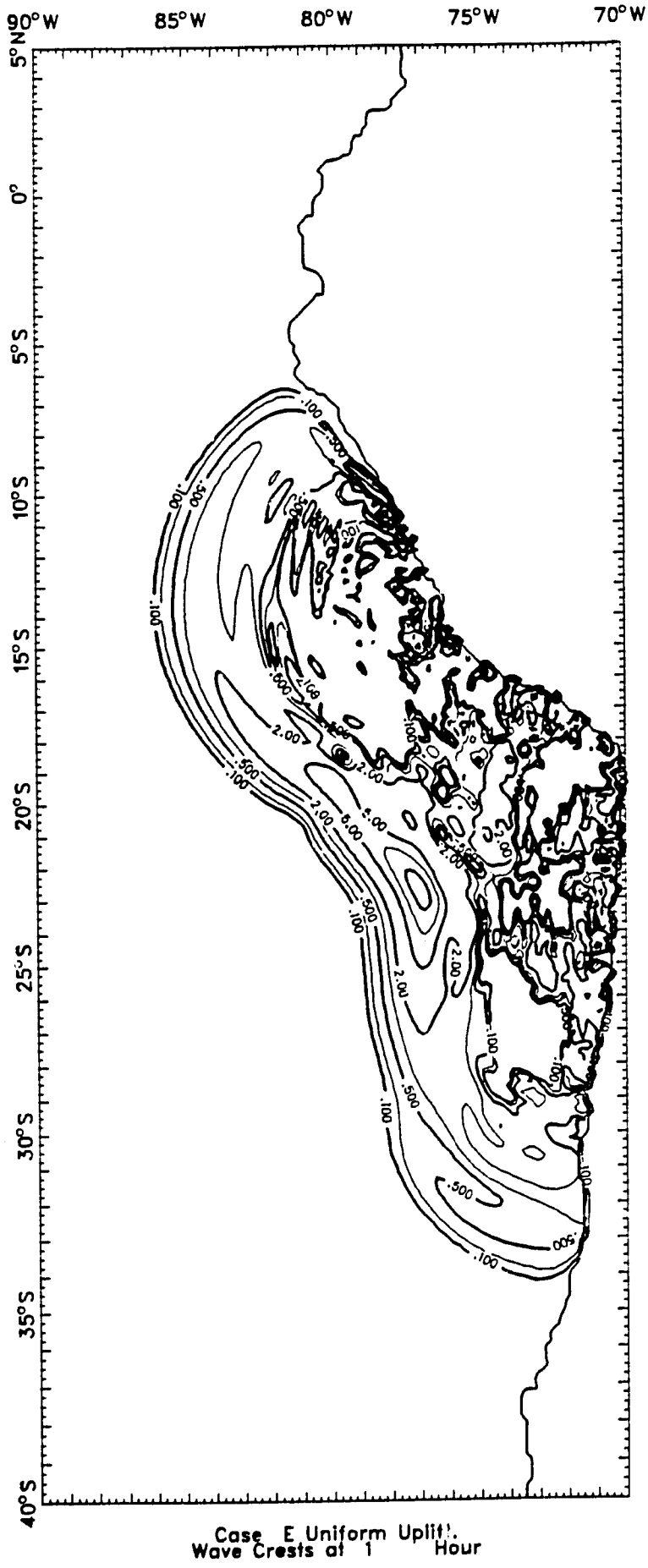

Figure: 8.2

Surface elevation (positive only) one hour after a uniform uplift in sour e Zone E. Contours correspond to 0.1, 0.2, 0.5, 1.0, 2.0, 7.5, and 10 m.

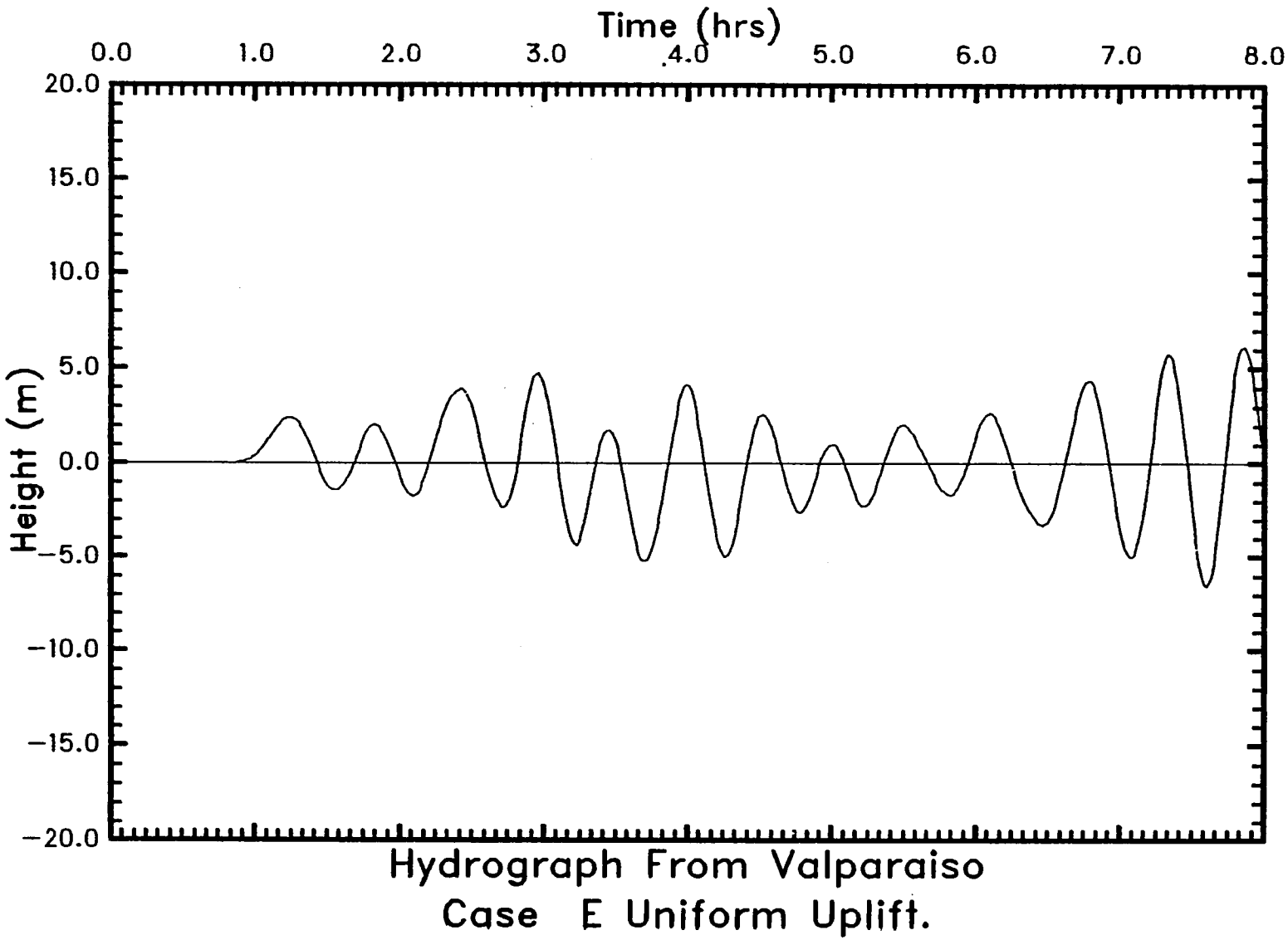

Figure 8.3: Wave elevation as a function of time at the recording point near Valparaiso, Chile. These waves were generated by the uniform uplift of Zone E.

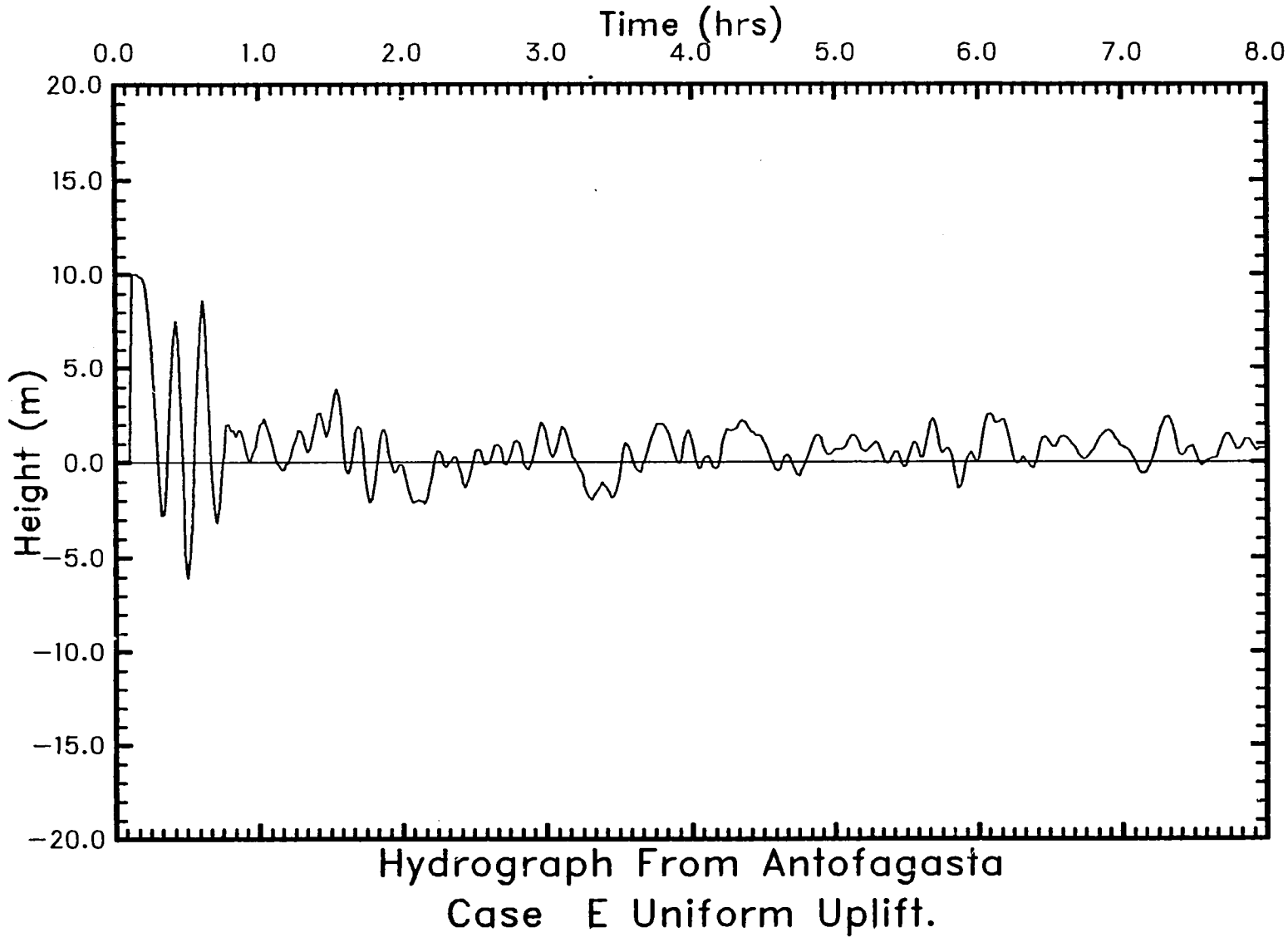

Figure 8.4: Wave elevation as a function of time at the recording point near Antofagasta, Chile. These waves were generated by the uniform uplift of Zone E.

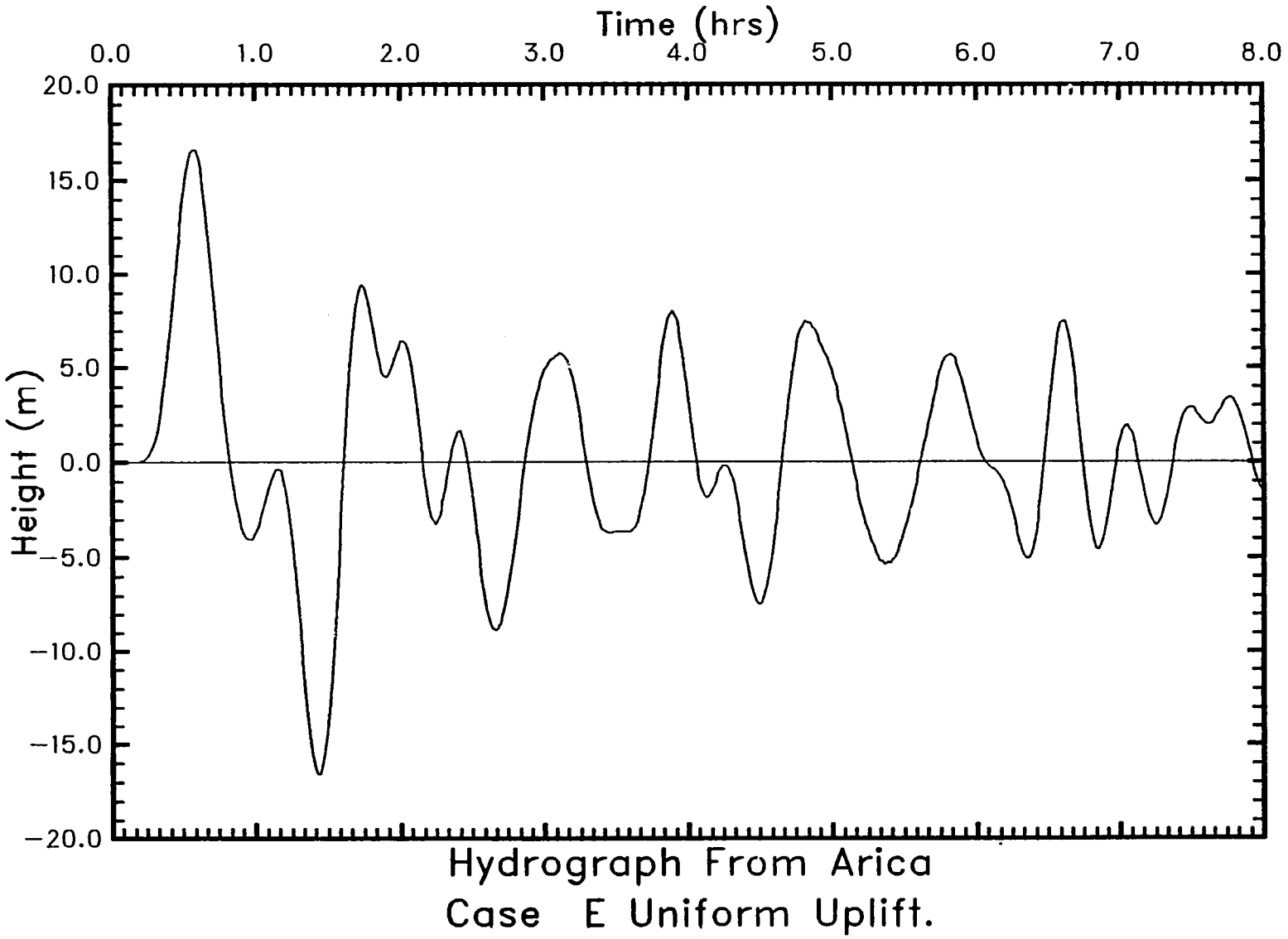

Figure 8.5: Wave elevation as a function of time at the recording point near Arica, Chile. These waves were generated by the uniform uplift of Zone E.

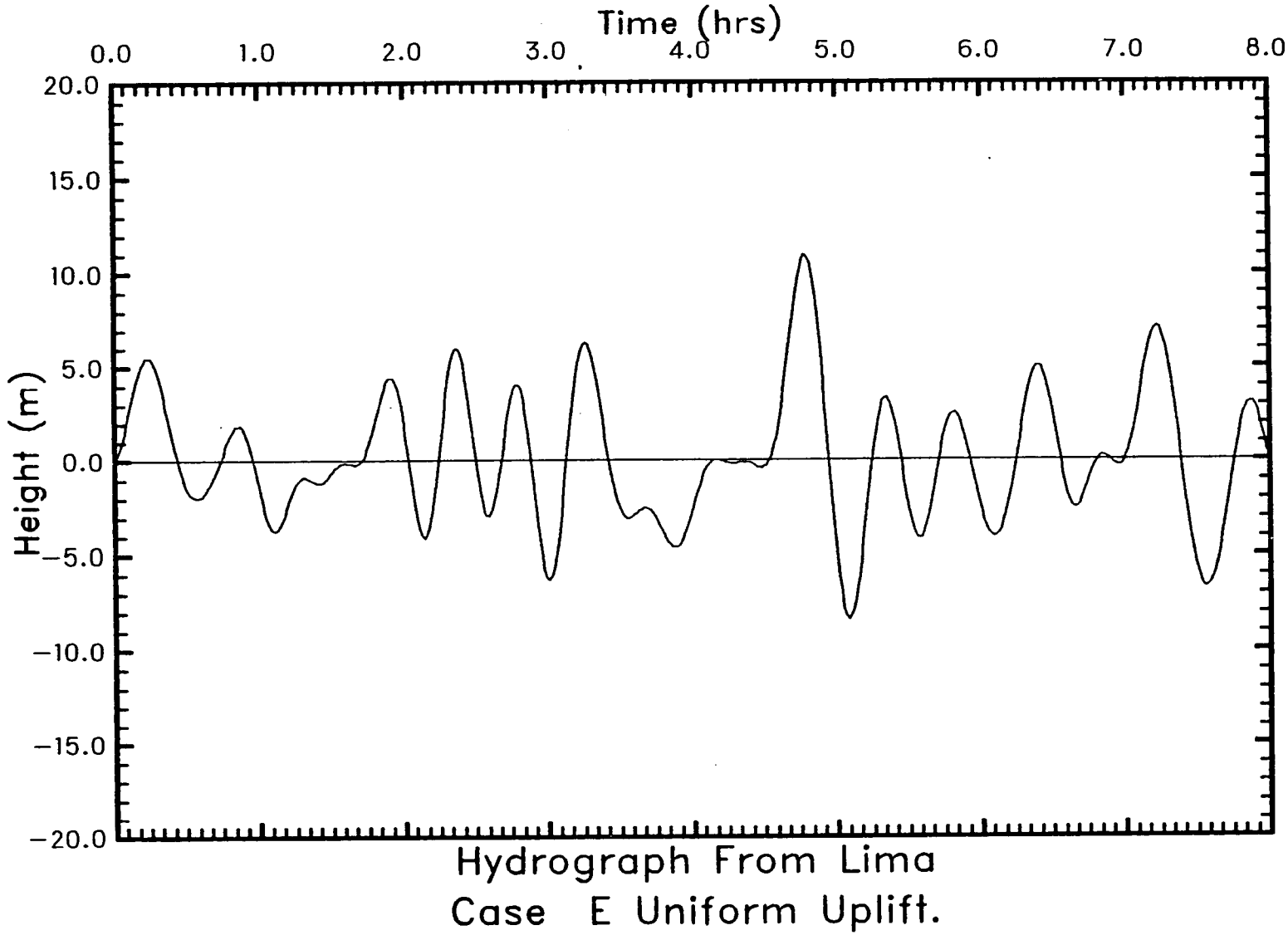

Figure 8.6: Wave elevation as a function of time at the recording point near Lima, Peru. These waves were generated by the uniform uplift of Zone E.

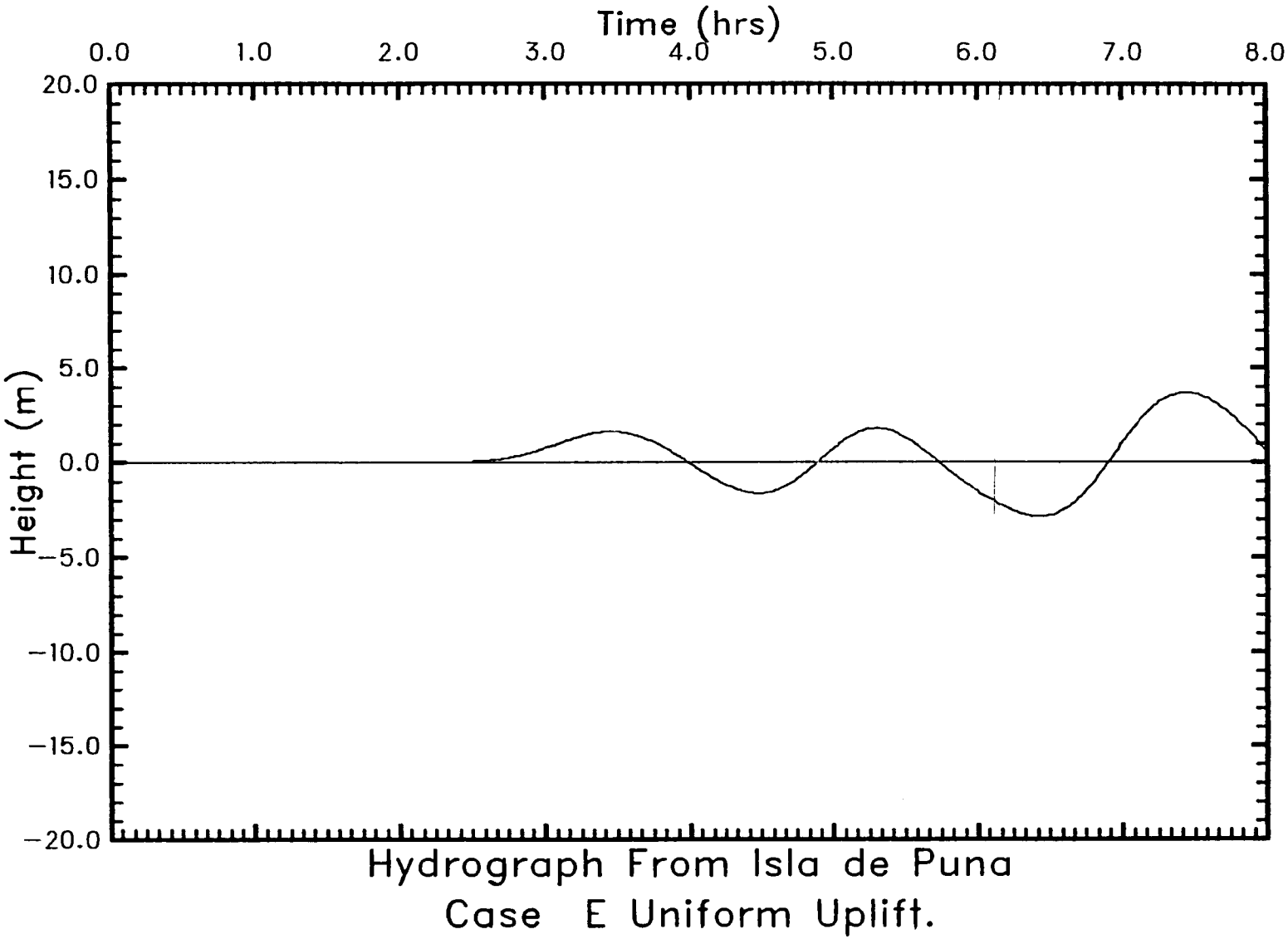

Figure 8.7: Wave elevation as a function of time at the recording point near Isla de Puna, Colombia. These waves were generated by the uniform uplift of Zone E.

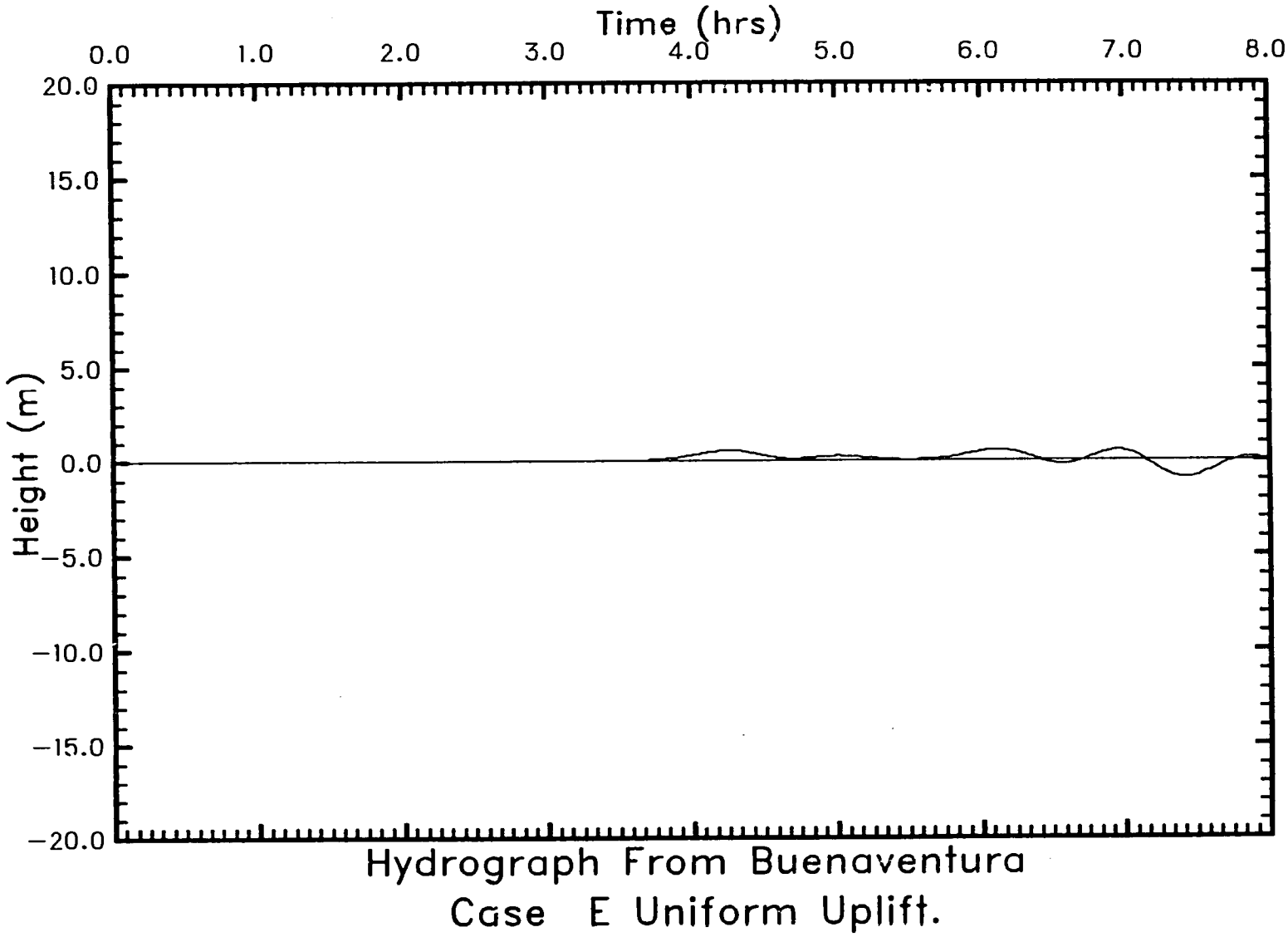

Figure 8.8: Wave elevation as a function of time at the recording point near Buenaventura, Ecuador. These waves were generated by the uniform uplift of Zone E.

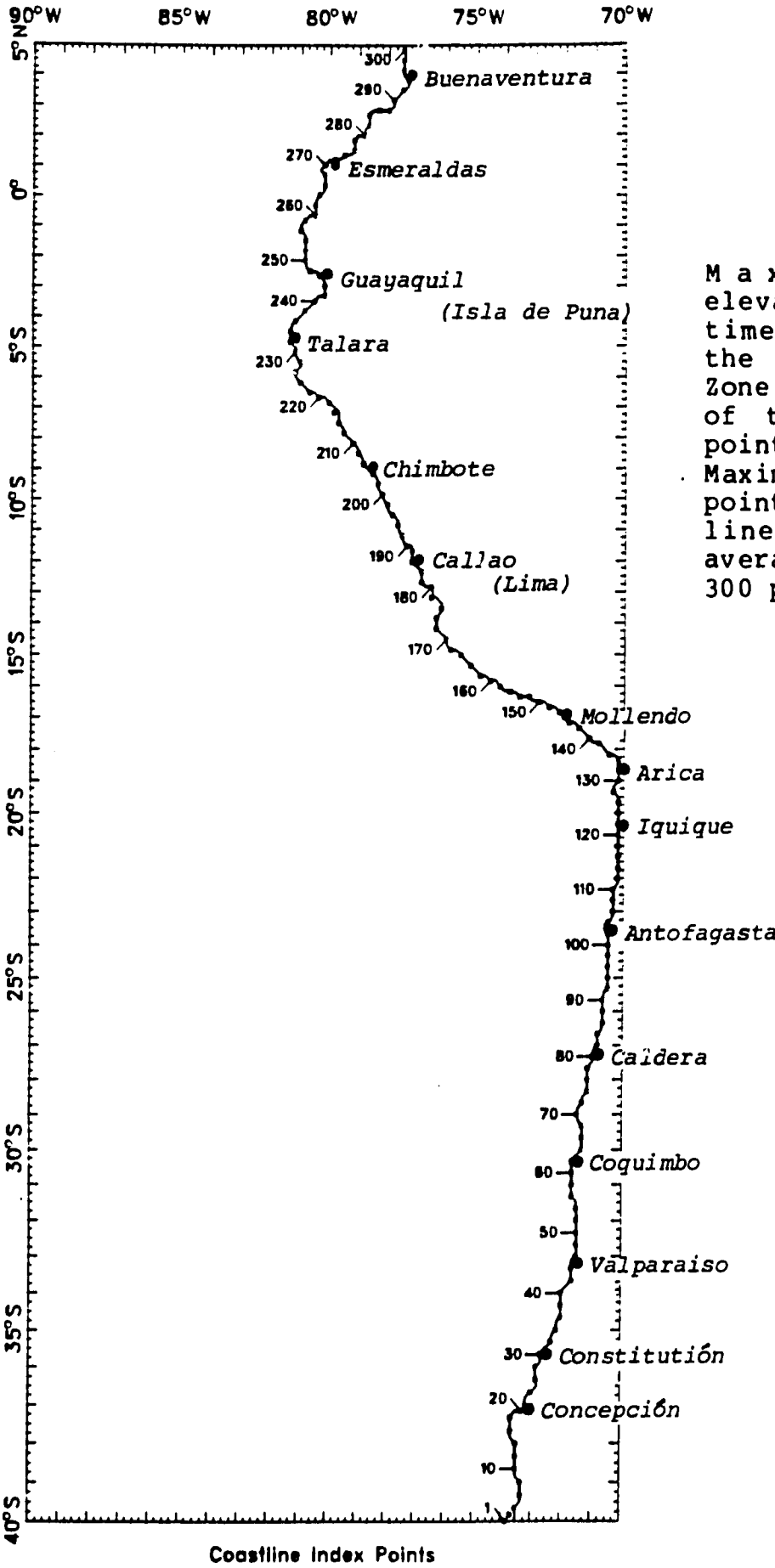

Figure: 8.9

Maximum wave elevations and arrival times of waves from the uniform uplift in Zone E. (a) Locations of the 300 recording point points. (b-f) Maximum waves at each point. The horizontal line represents the average value of all 300 points.

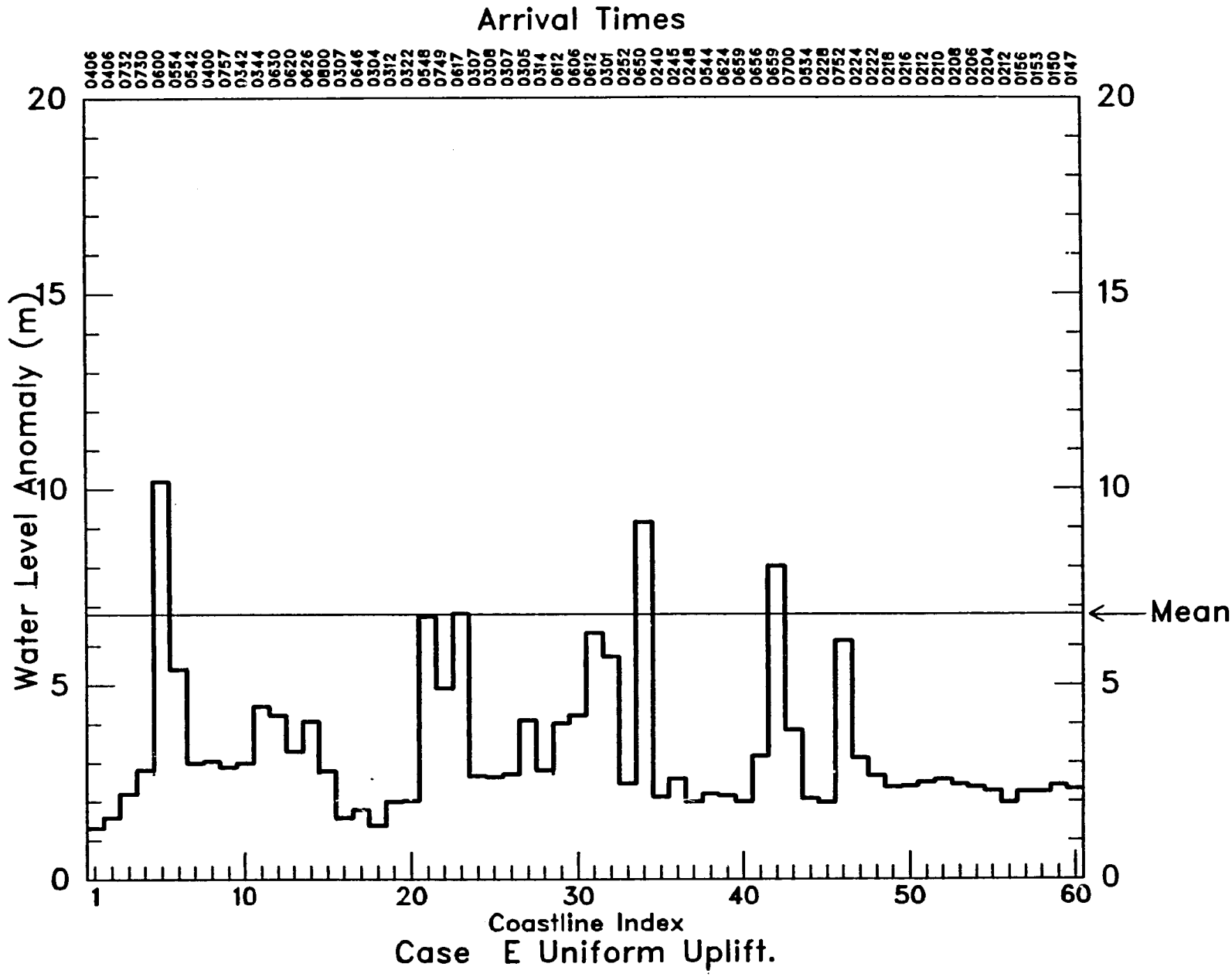
Arrival Times
0406 0406 0732 0730 0600 0554 0542 0400 0757 0342 0344 0630 0620 0626 0800 0307 0646 0304 0312 0322 0548 0749 0617 0307 0308 0307 0305 0314 0612 0606 0612 0301 0252 0650 0240 0245 0248 0544 0624 0659 0656 0659 0700 0534 0228 0752 0224 0222 0218 0216 0212 0210 0208 0206 0204 0212 0156 0153 0150 0147
Water Level Anomaly (m)
0
5
10
15
20
Mean
1
10
20
30
40
50
60
Coastline Index
Case E Uniform Uplift.

Figure: 8.9 (b)

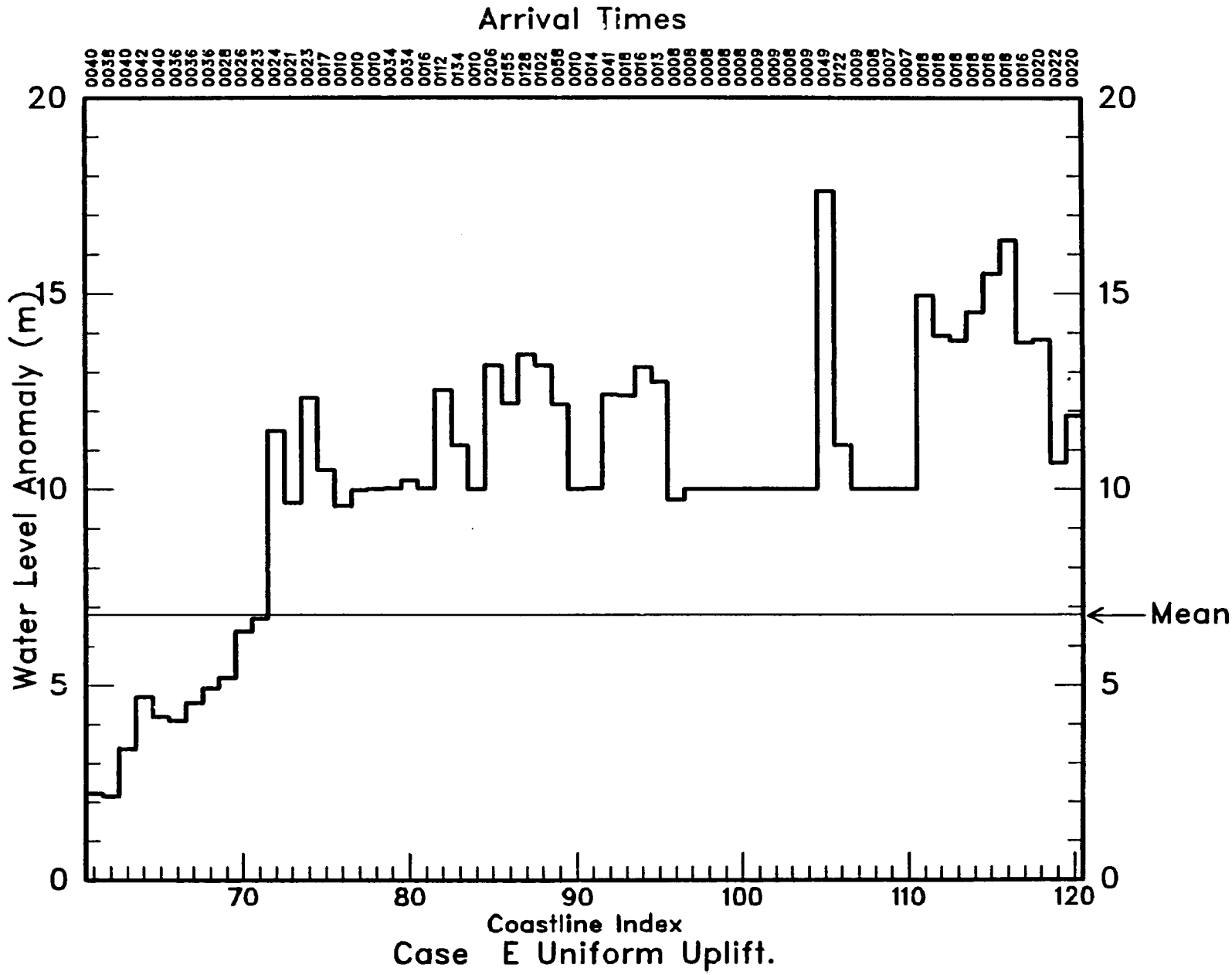
Arrival Times
0040 0038 0040 0042 0040 0036 0036 0036 0028 0026 0023 0024 0021 0023 0017 0010 0010 0010 0034 0034 0016 0112 0134 0010 0206 0155 0128 0102 0058 0010 0014 0041 0018 0016 0013 0008 0008 0008 0008 0009 0009 0008 0009 0049 0122 0009 0008 0007 0007 0018 0018 0018 0018 0018 0018 0016 0020 0022 0020
Water Level Anomaly (m)
0
5
10
15
20
70
80
90
100
110
120
Coastline Index
Mean
Case E Uniform Uplift.

Figure: 8.9 (c)

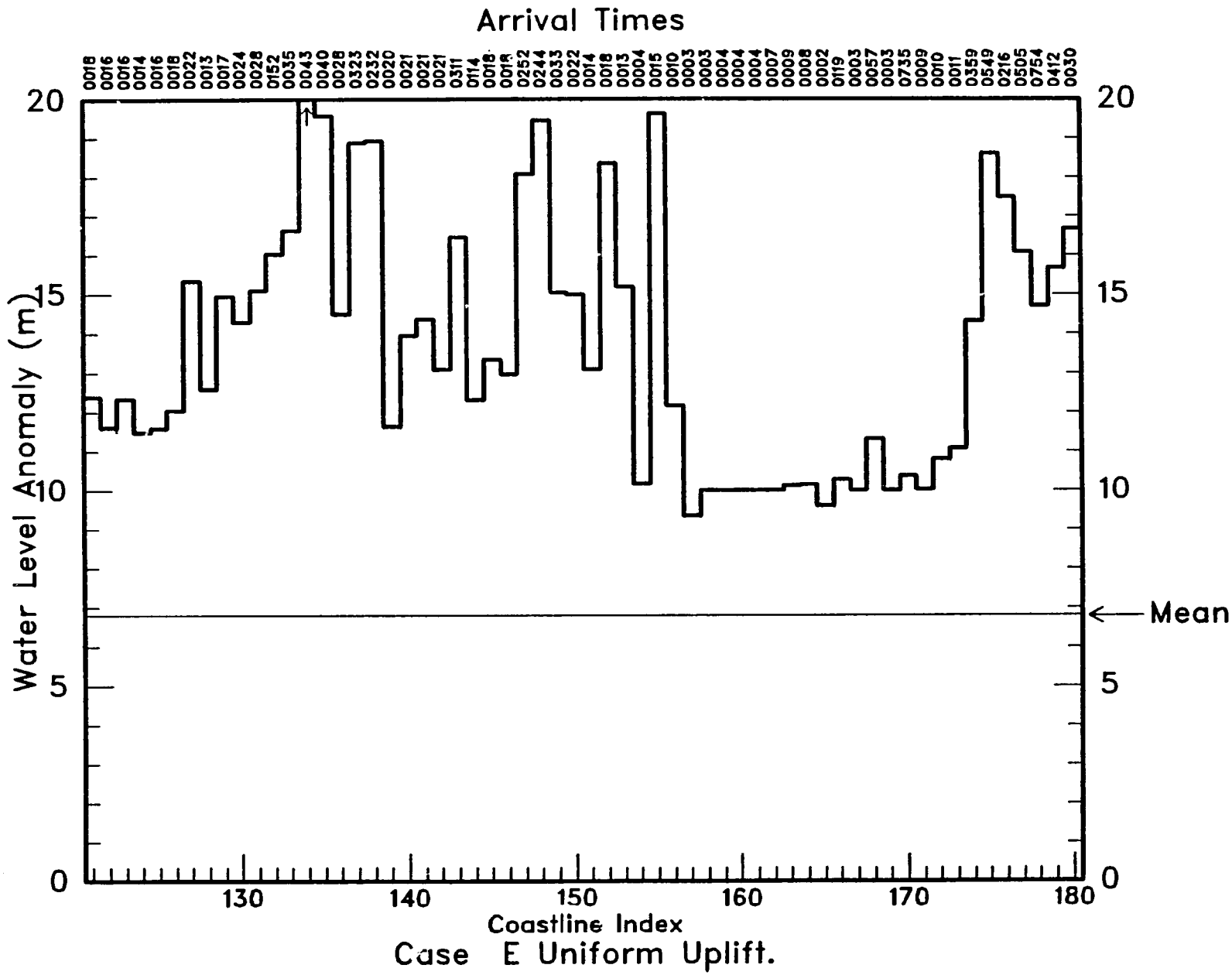
Arrival Times
0018 0016 0016 0014 0016 0018 0022 0013 0017 0024 0028 0152 0035 0043 0040 0028 0323 0232 0020 0021 0021 0021 0311 0114 0018 0018 0252 0244 0033 0022 0014 0018 0013 0004 0015 0010 0003 0003 0004 0004 0004 0007 0009 0008 0002 0119 0003 0057 0003 0735 0009 0010 0011 0359 0549 0216 0505 0754 0412 0030
Water Level Anomaly (m)
0
5
10
15
20
Mean
130
140
150
160
170
180
Coastline Index
Case E Uniform Uplift.

Figure: 8.9 (d)

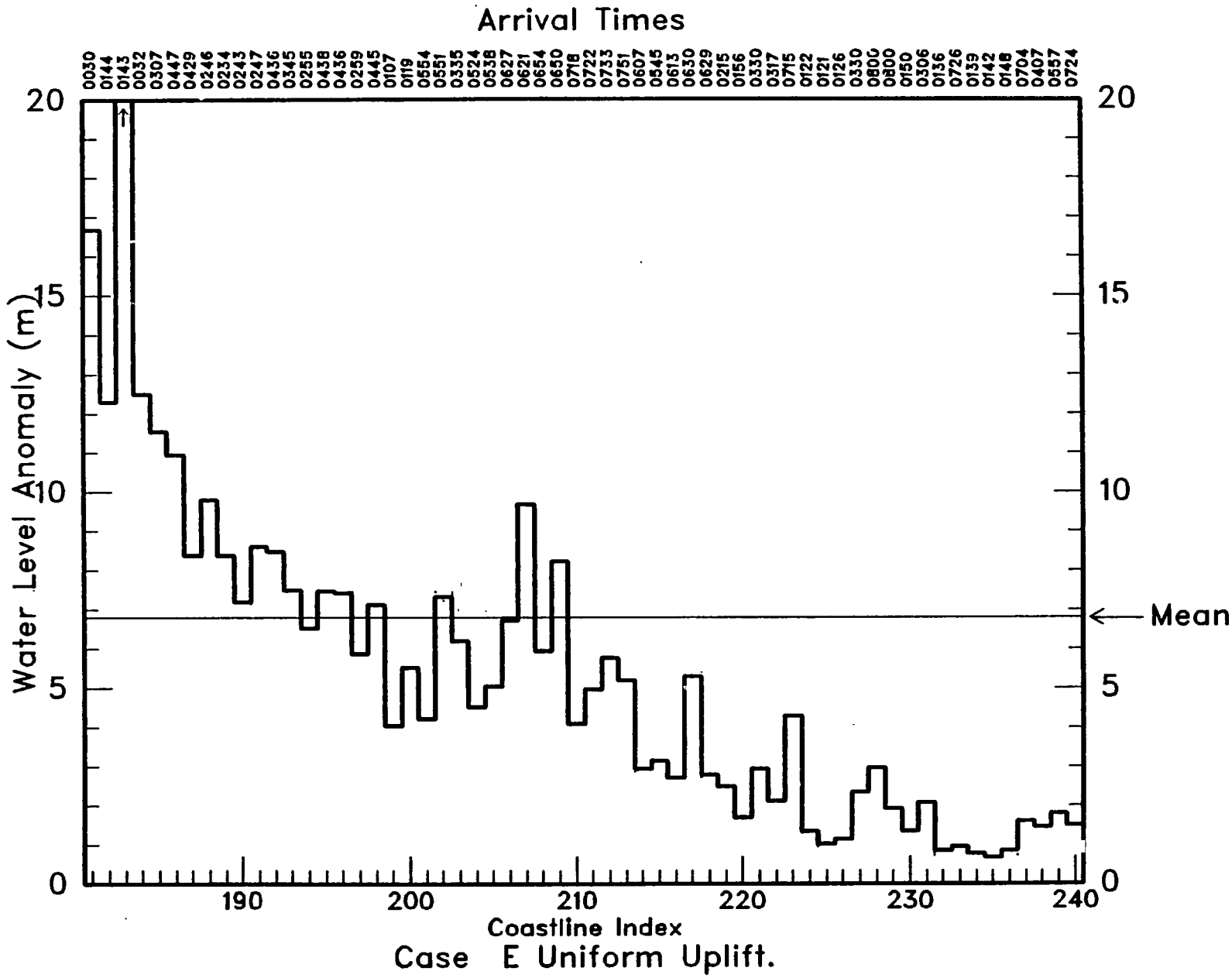

Case E Uniform Uplift.

Figure: 8.9 (e)

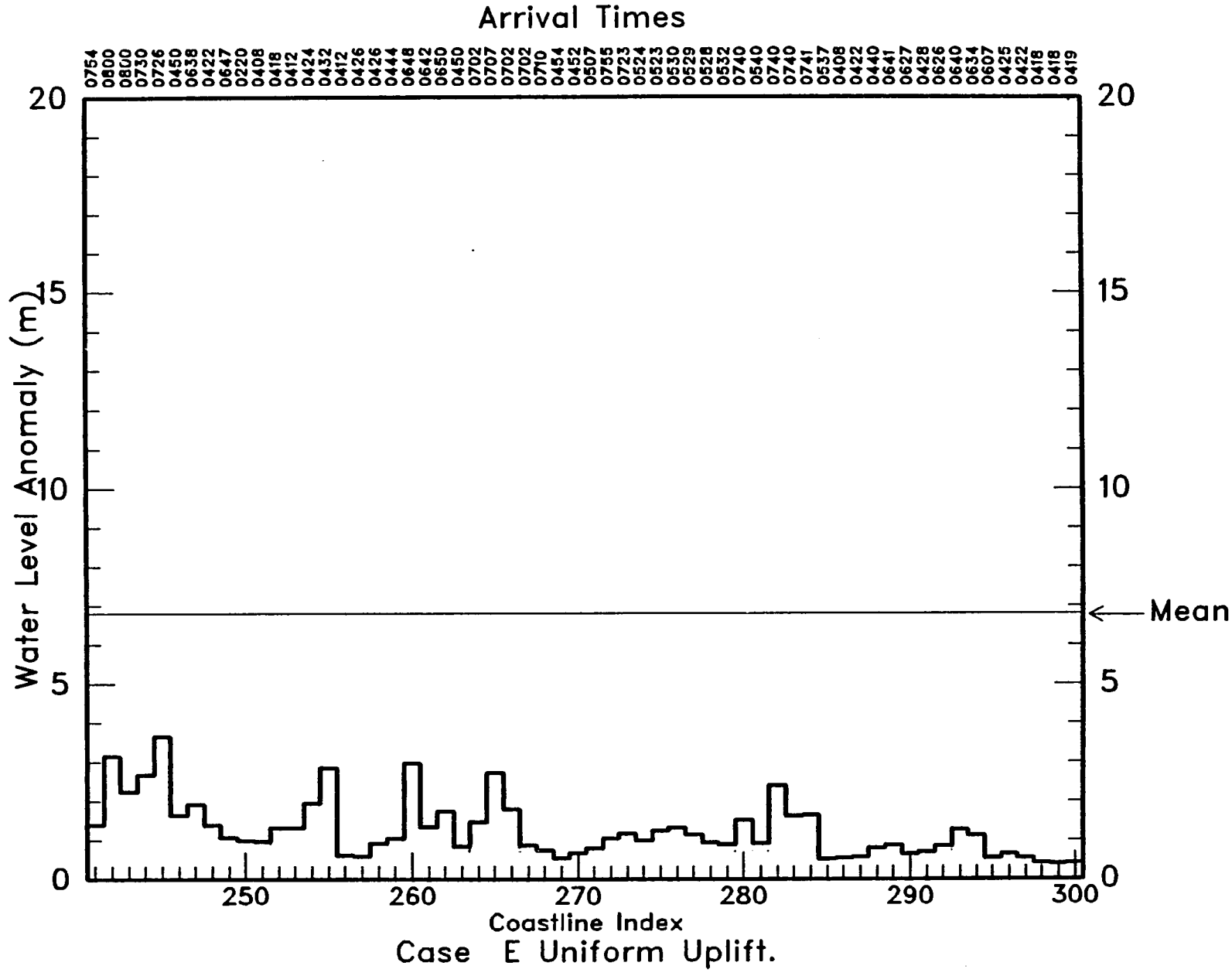
Arrival Times
0754 0800 0800 0730 0726 0450 0638 0422 0647 0220 0408 0418 0412 0424 0432 0412 0426 0426 0444 0648 0642 0650 0450 0702 0707 0702 0702 0710 0454 0452 0507 0755 0723 0524 0523 0530 0529 0528 0532 0740 0540 0740 0740 0741 0537 0408 0422 0440 0641 0627 0428 0626 0640 0634 0607 0425 0422 0418 0418 0419
Water Level Anomaly (m)
0
5
10
15
20
Mean
250
260
270
280
290
300
Coastline Index
Case E Uniform Uplift.

Figure: 8.9 (f)

8.3 VARIABLE UPLIFT CASE

The ultimate uplift pattern used in this simulation is the consolidation of two separate uplift patterns. The first extends parallel to the trench from the northern end of zone E to the bend in the continent near 20°S. The second extends parallel to the trench from the bend to the southern end of zone E. The two patterns, both with a maximum uplift of 10 m, overlap in the bend region. In the overlap region the higher of the two patterns at each point is used in the simulation.

8.3.1 Immediate Effects

The surface elevation contours after one hour are shown in Figure 8.10. The leading wave is quite well established and extends over nearly 25° of latitude. It is clearly the result of the interference of two separate wave regimes--one propagating to the southwest from the coast north of the bend and one propagating west from the coast south of the bend. The maximum wave height is nearly 6 m in deep water.

The sea behind the leading wave is quite complicated, since it is made up of a number of smaller waves arising out of the interference pattern. Wave energies are concentrated all along the coast, especially near the bend.

8.3.2 Longer Duration Effects

High waves are apparent at all of the recording stations from Valparaiso to Lima (Figures 8.11 to 8.14). In all four stations the waves persist for many hours, although amplitudes at Antofagasta are heavily damped.

At Isla de Puna the waves are very long and appear to be growing as the simulation ends (Figure 8.15). But little wave activity appears at Buenaventura (Figure 8.16).

8.3.3 Maximum Elevations

It is not surprising, in light of the hydrographs, that the maximum elevation plots (Figure 8.17a-f) show that high waves occur all along the coast from the southern end to Talara. And even north of there waves 2 m high occur occasionally. The overall wave level of this tsunami is quite high, with a mean of roughly 4.3 m. This event is definitely the most threatening that we have discussed.

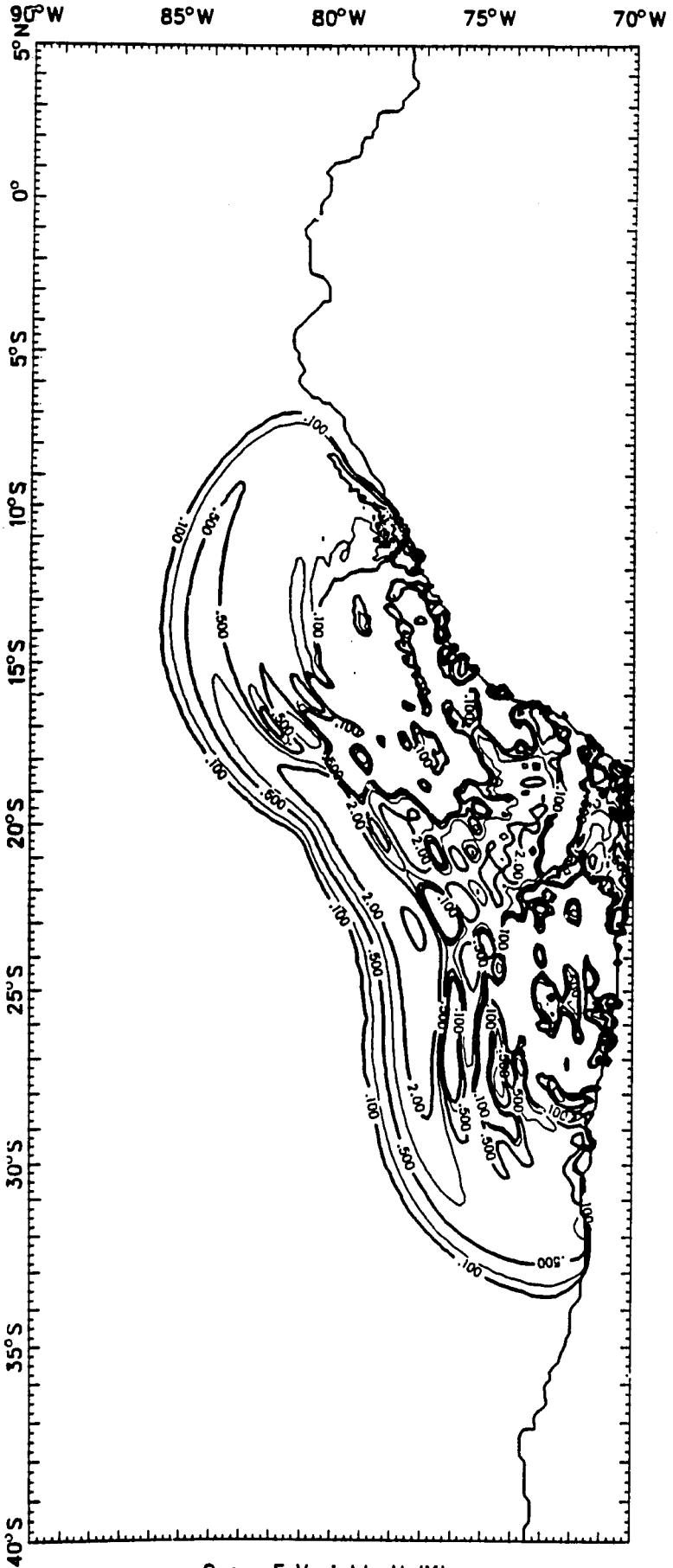

Case E Variable Uplift.
Wave Crests at 1 Hour

Figure: 8.10

Surface elevation (positive only) one hour after a variable uplift in source Zone E. Contours correspond to 0.1, 0.2, 0.5, 1.0, 2.0, 7.5, and 10 m.

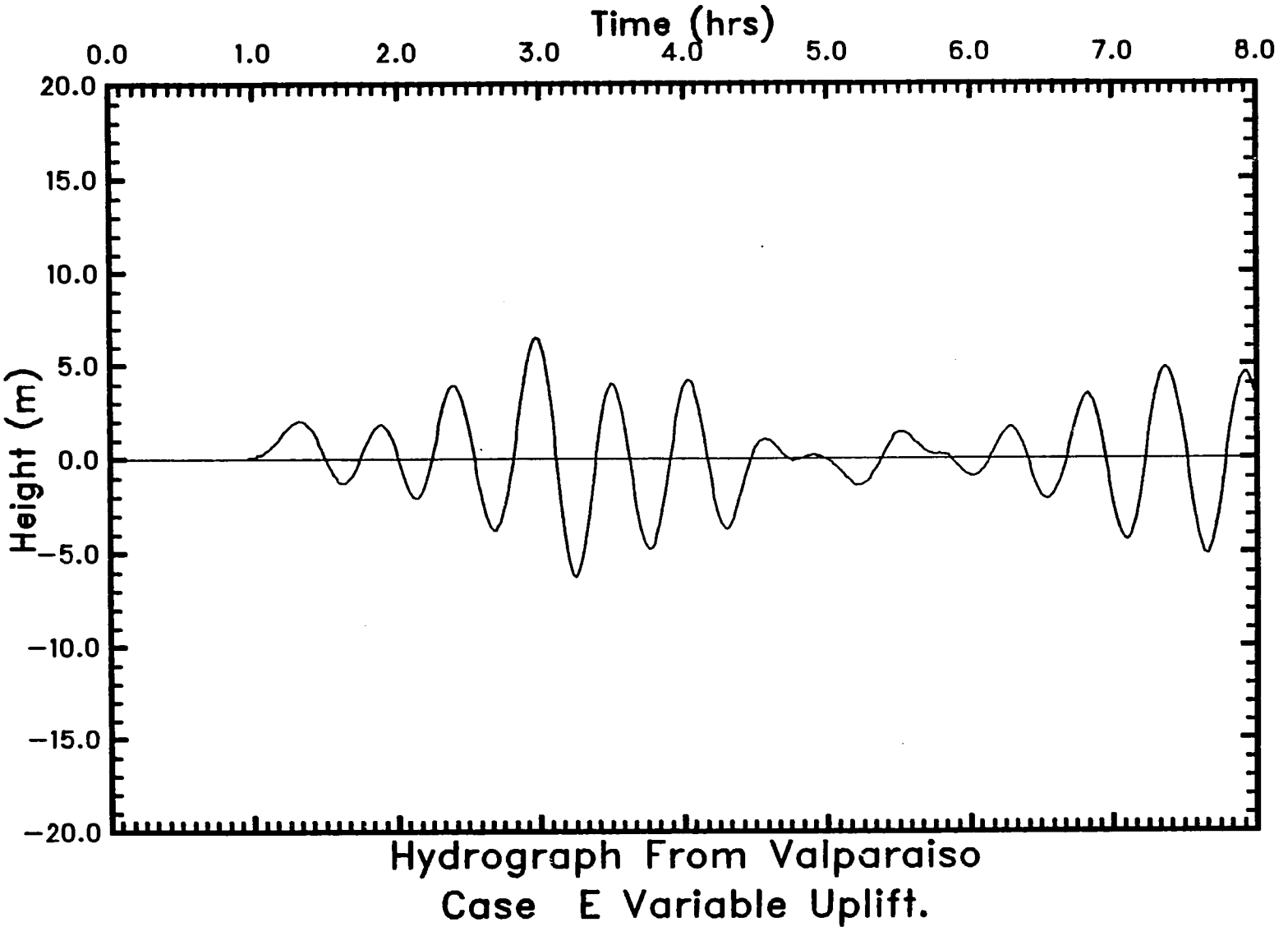

Figure 8.11: Wave elevation as a function of time at the recording point near Valparaiso, Chile. These waves were generated by the variable uplift of Zone E.

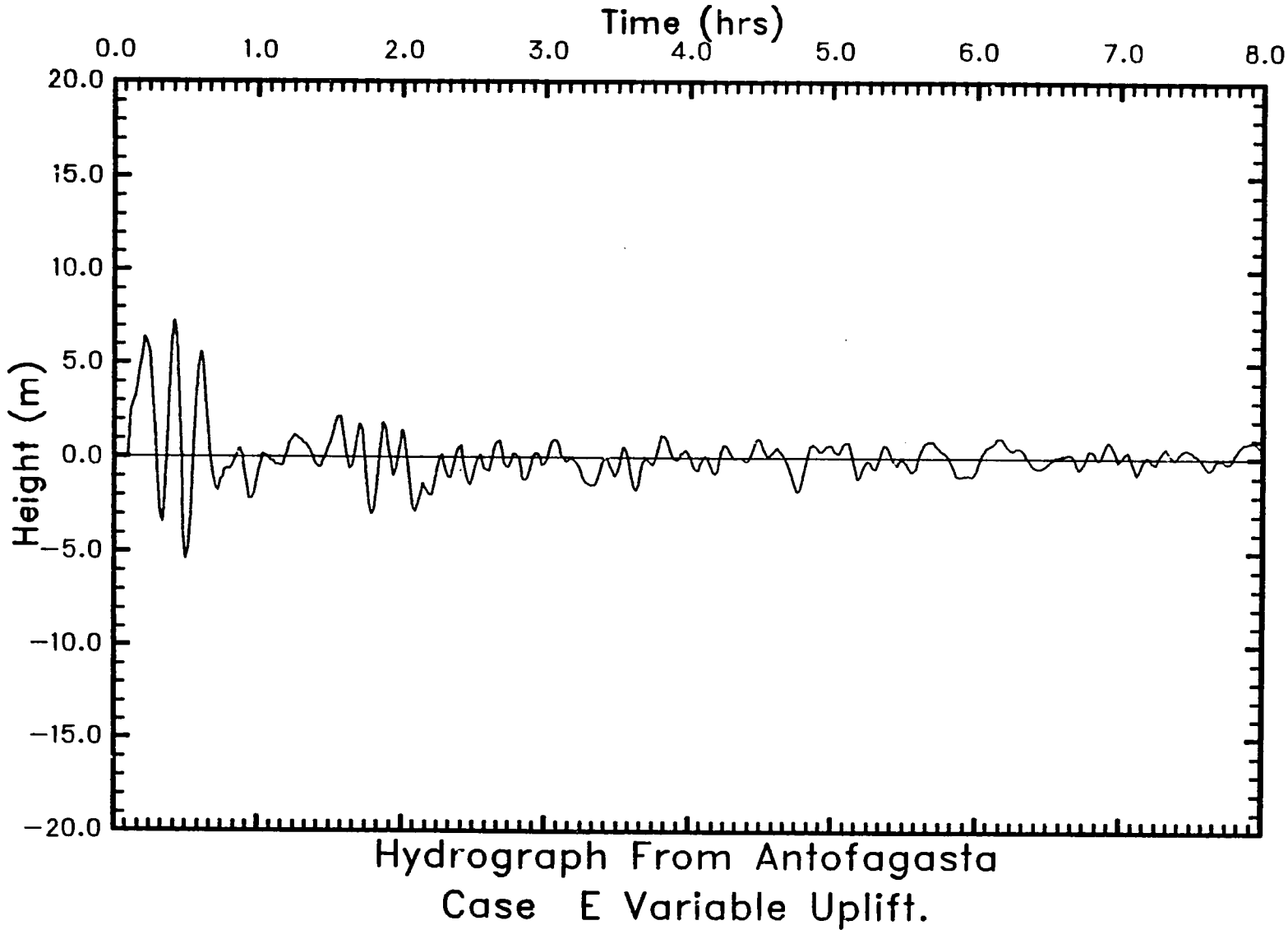

Figure 8.12: Wave elevation as a function of time at the recording point near Antofagasta, Chile. These waves were generated by the variable uplift of Zone E.

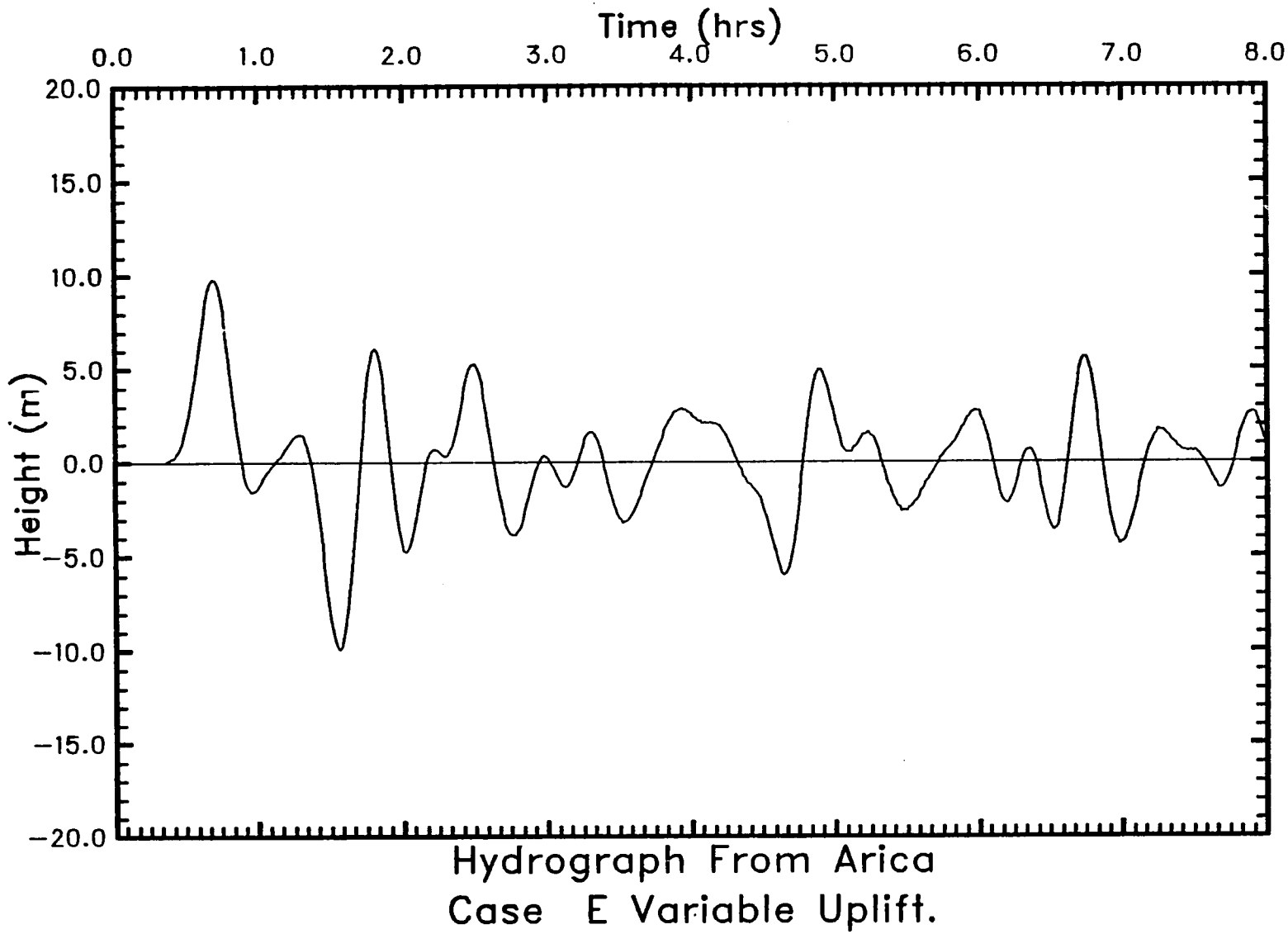

Figure 8.13: Wave elevation as a function of time at the recording point near Arica, Chile. These waves were generated by the variable uplift of Zone E.

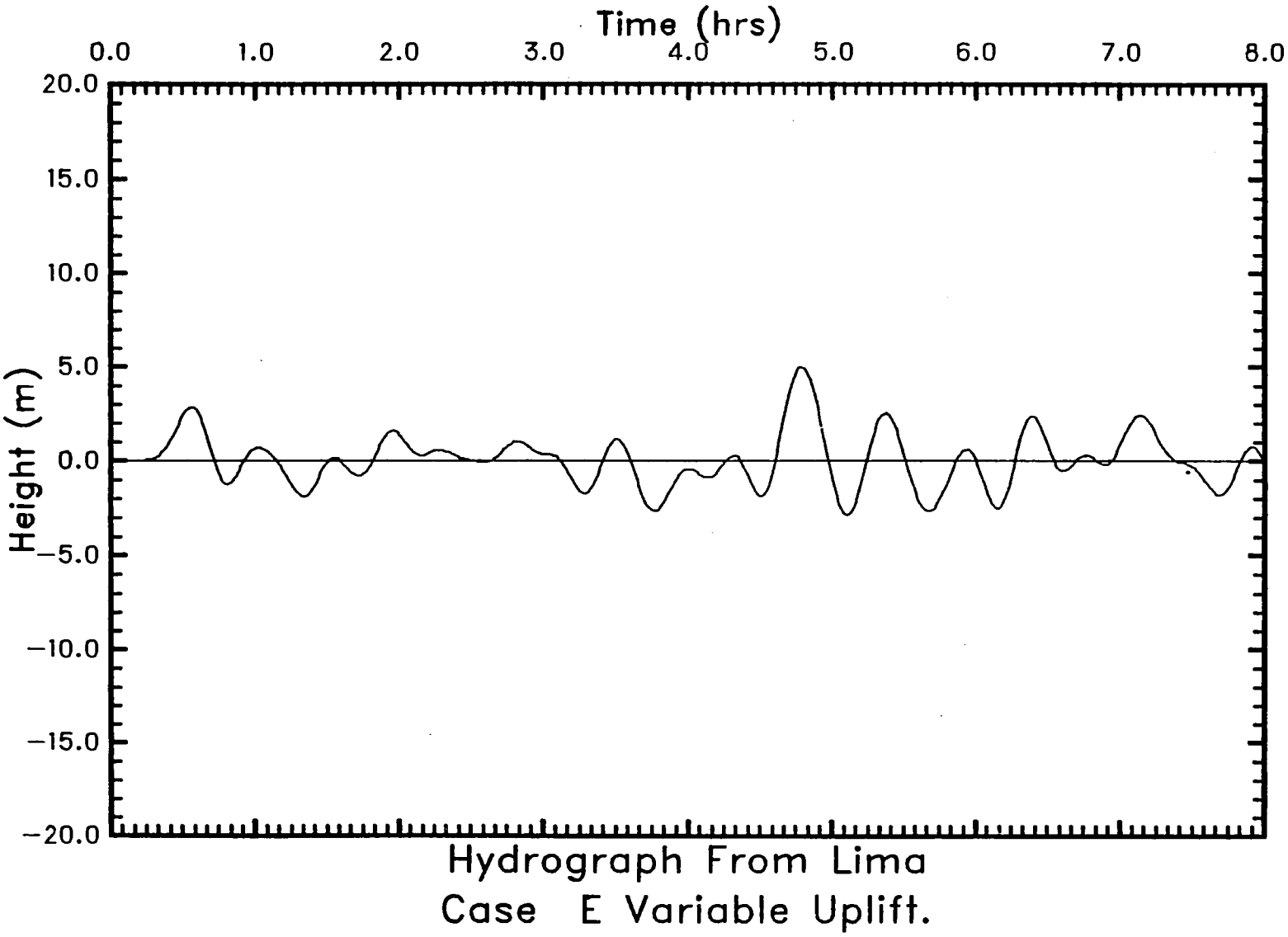

Figure 8.14: Wave elevation as a function of time at the recording point near Lima, Peru. These waves were generated by the variable uplift of Zone E.

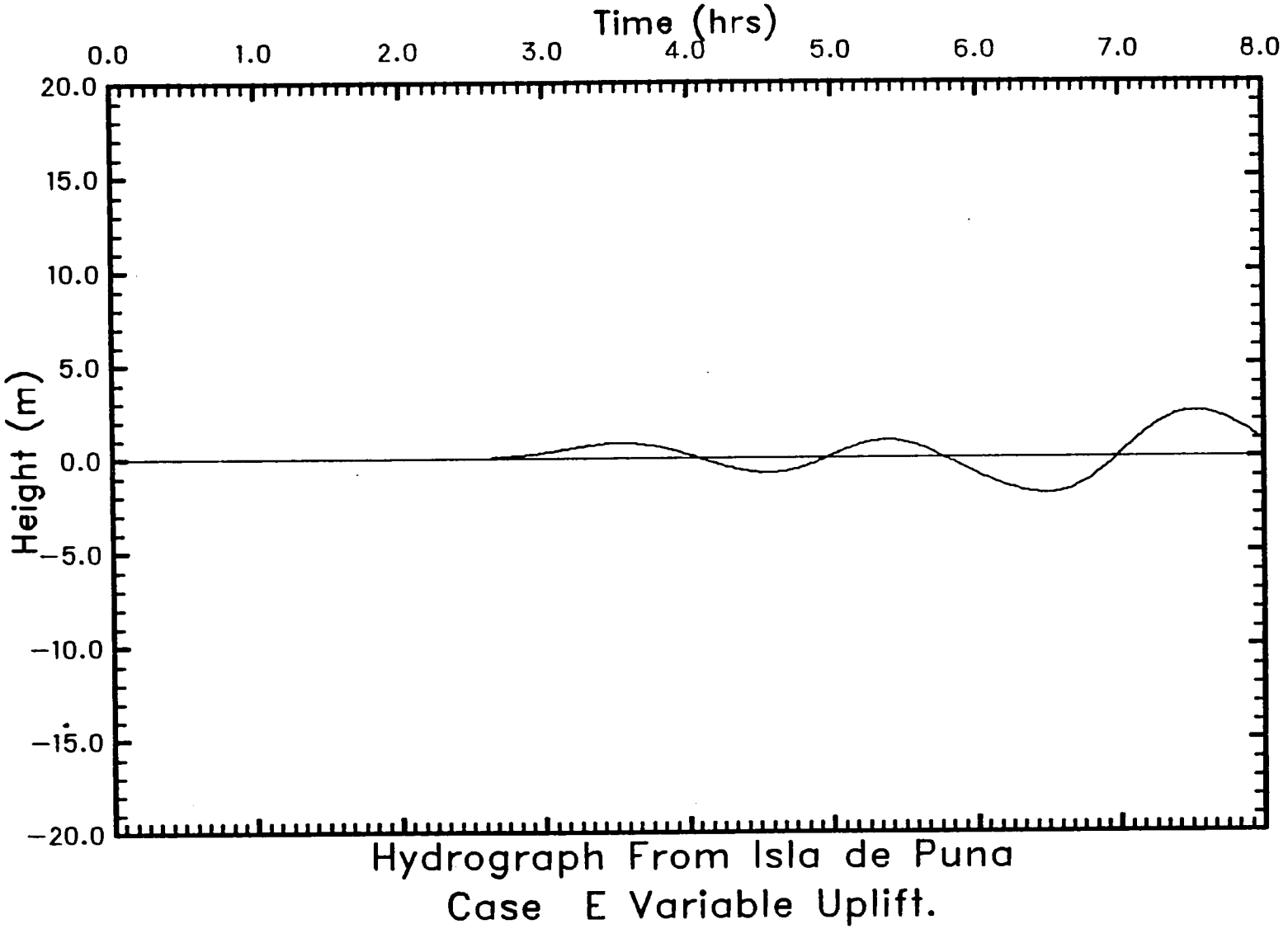

Figure 8.15: Wave elevation as a function of time at the recording point near Isla de Puna, Colombia. These waves were generated by the variable uplift of Zone E.

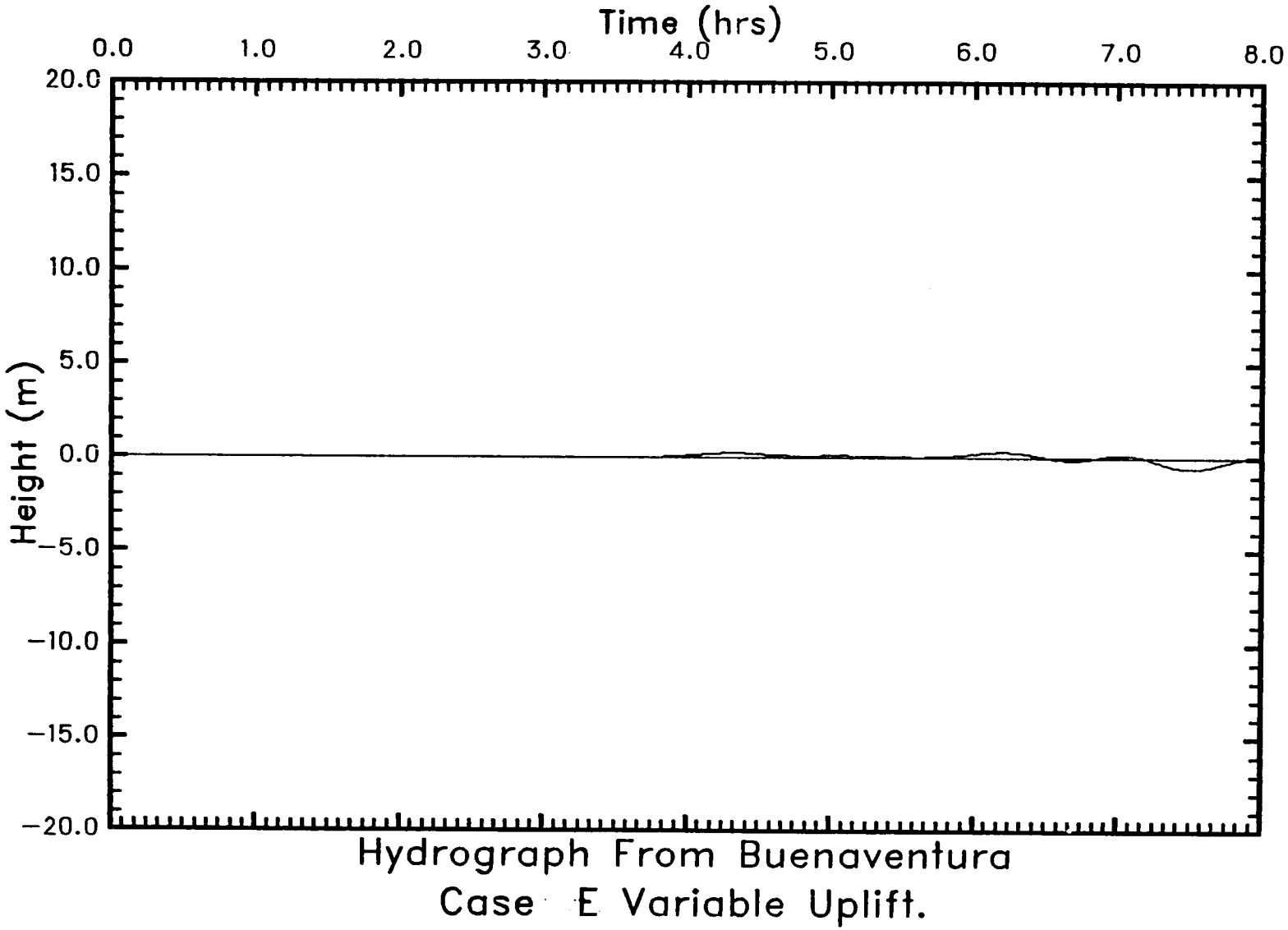

Figure 8.16: Wave elevation as a function of time at the recording point near Buenaventura, Ecuador. These waves were generated by the variable uplift of Zone E.

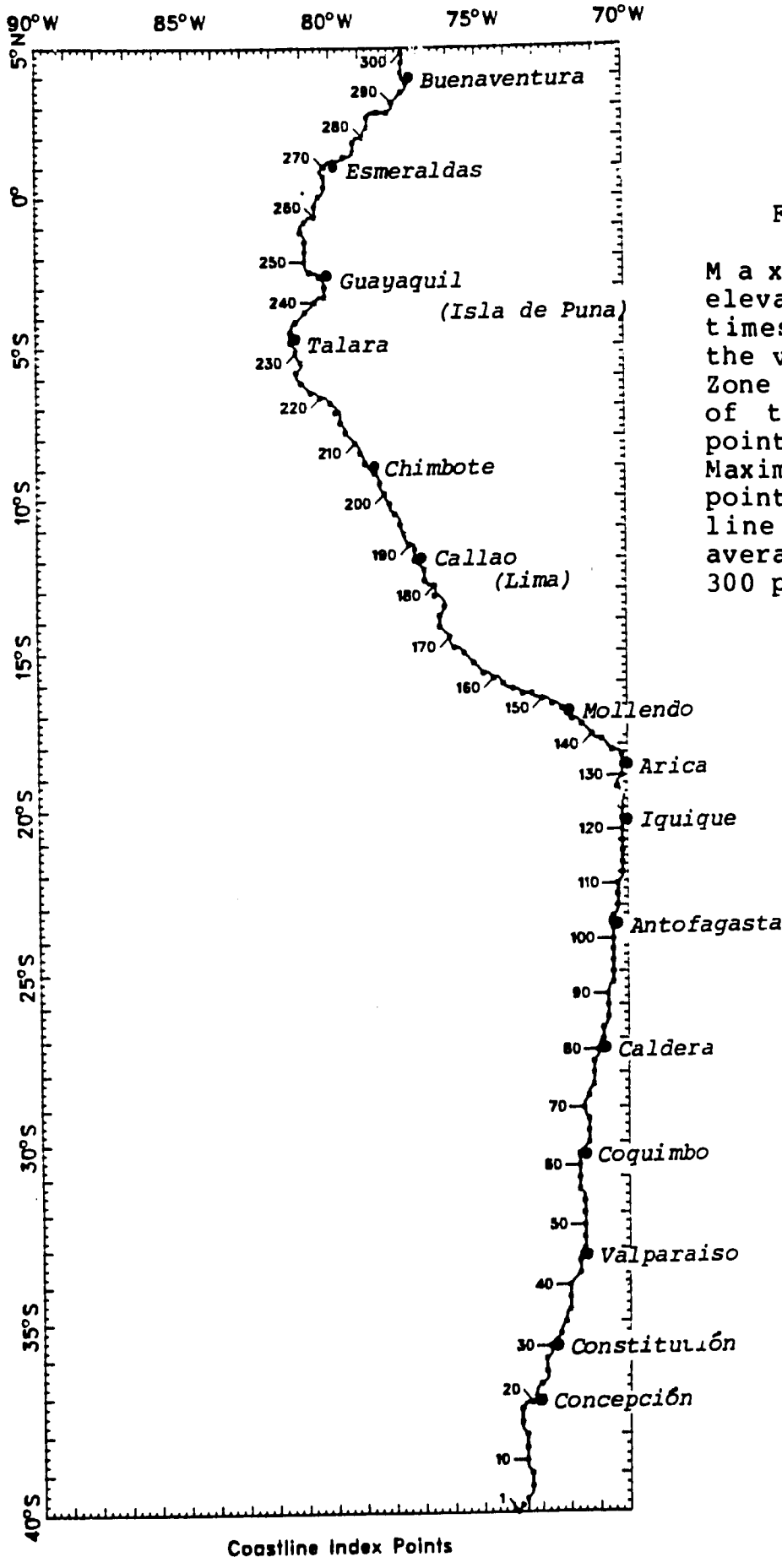

Figure: 8.17

Maximum wave elevations and arrival times of waves from the variable uplift in Zone E. (a) Locations of the 300 recording point points. (b-f) Maximum waves at each point. The horizontal line represents the average value of all 300 points.

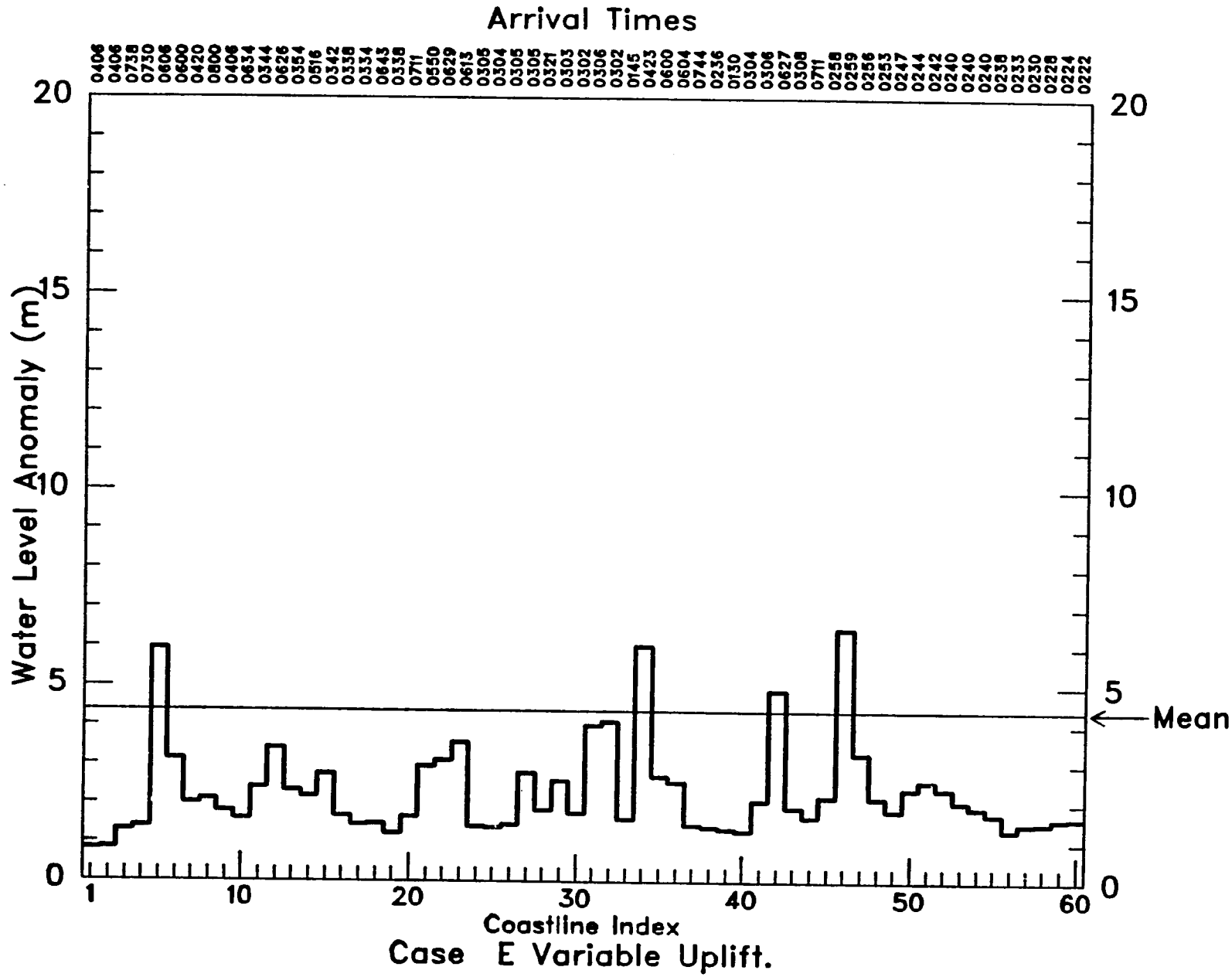
Arrival Times
0406 0406 0738 0730 0606 0600 0420 0800 0406 0634 0344 0626 0354 0516 0342 0338 0334 0643 0338 0711 0550 0629 0613 0305 0304 0305 0305 0321 0303 0302 0306 0302 0145 0423 0600 0604 0744 0236 0130 0304 0306 0627 0308 0711 0258 0259 0256 0253 0247 0244 0242 0240 0240 0240 0238 0233 0230 0228 0224 0222
Water Level Anomaly (m)
0
5
10
15
20
Mean
1
10
20
30
40
50
60
Coastline Index
Case E Variable Uplift.

Figure: 8.17 (b)

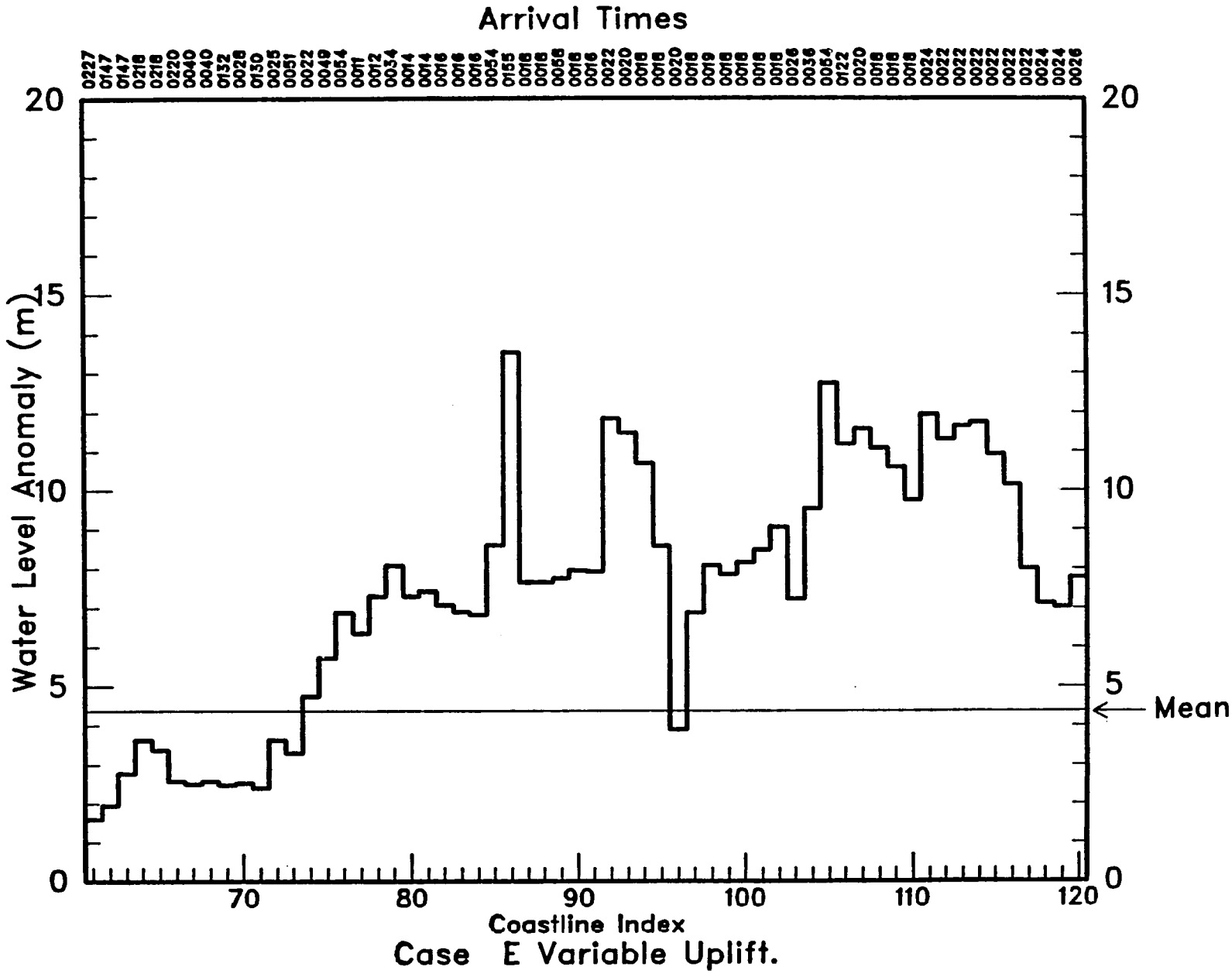
Arrival Times
0227 0147 0147 0218 0218 0220 0040 0040 0132 0028 0130 0025 0051 0022 0049 0054 0011 0012 0034 0014 0016 0016 0016 0054 0155 0016 0016 0056 0016 0016 0022 0020 0016 0016 0020 0016 0019 0016 0016 0016 0016 0026 0036 0054 0122 0020 0016 0016 0016 0024 0022 0022 0022 0022 0022 0024 0024 0026
Water Level Anomaly (m)
0
5
10
15
20
70
80
90
100
110
120
Coastline Index
Mean
Case E Variable Uplift.

Figure: 8.17 (c)

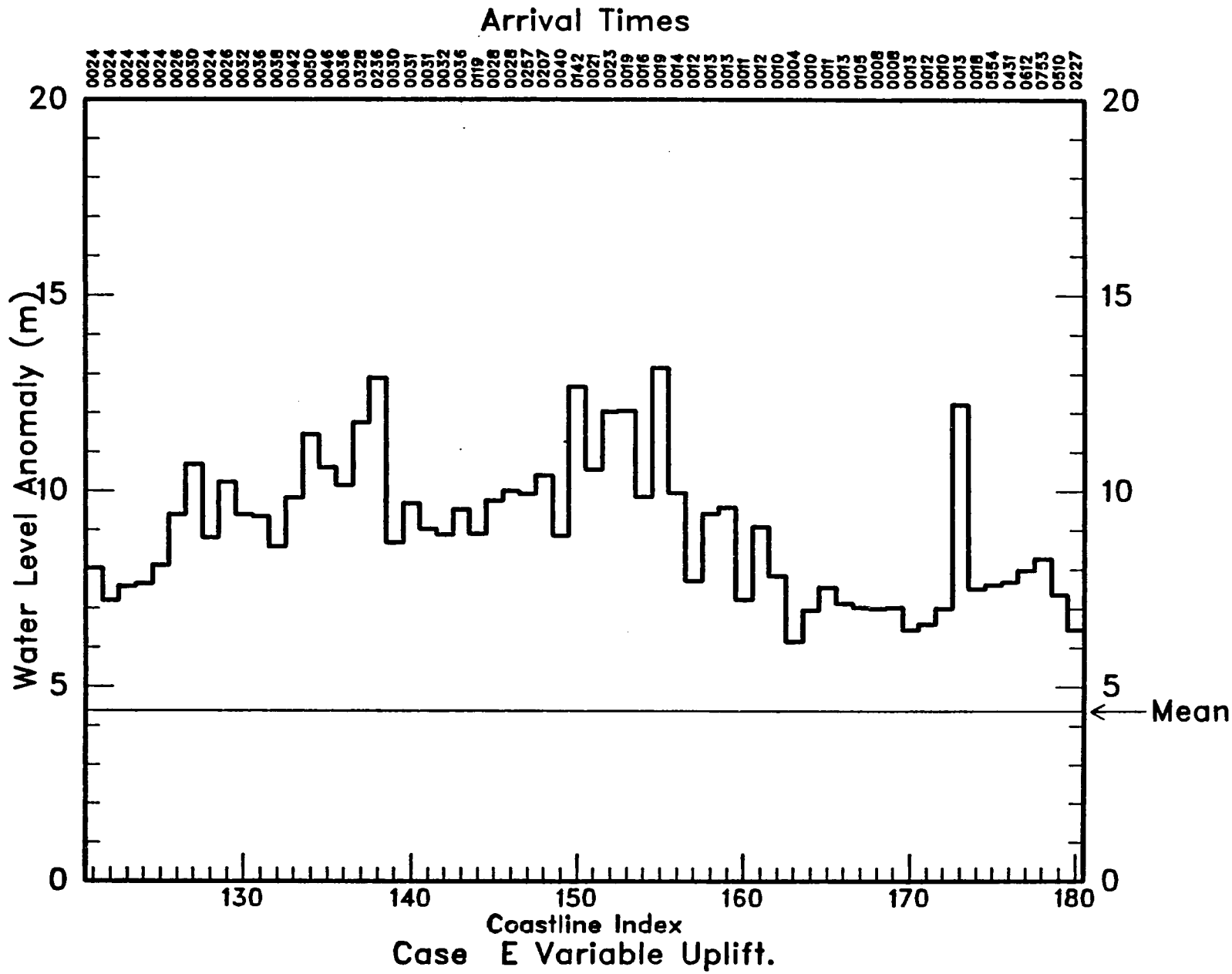
Arrival Times
0024 0024 0024 0024 0026 0030 0024 0026 0032 0036 0038 0042 0050 0046 0036 0328 0236 0030 0031 0031 0032 0036 0119 0028 0257 0207 0040 0142 0021 0023 0019 0016 0019 0014 0012 0013 0013 0011 0012 0010 0004 0010 0011 0013 0105 0008 0008 0013 0012 0010 0013 0018 0554 0431 0612 0753 0510 0227
Water Level Anomaly (m)
0
5
10
15
20
130
140
150
160
170
180
Coastline Index
Mean
Case E Variable Uplift.

Figure: 8.17 (d)

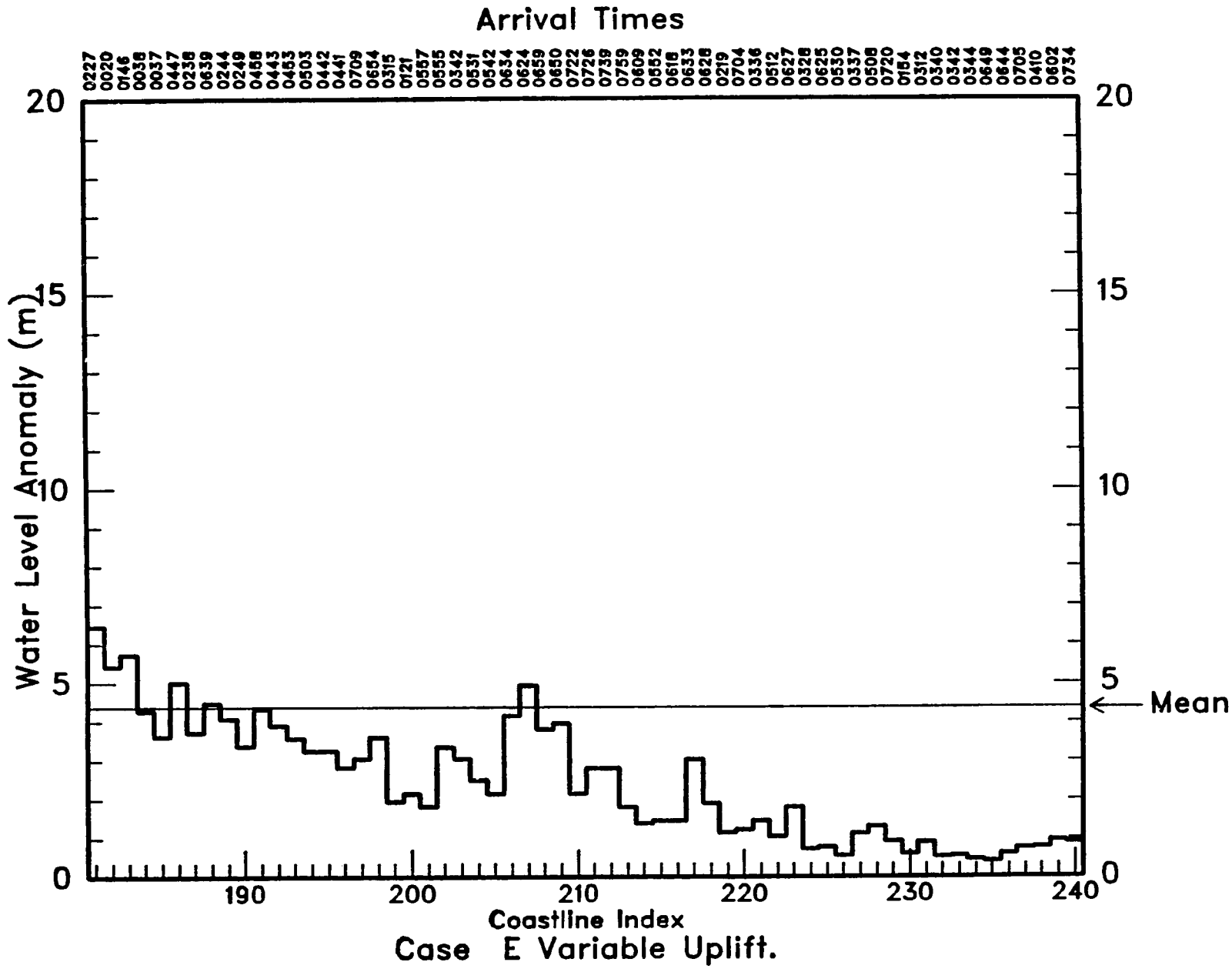
Arrival Times
0227 0020 0146 0038 0037 0447 0238 0639 0244 0249 0458 0443 0453 0503 0442 0441 0709 0654 0315 0121 0557 0555 0342 0531 0542 0634 0624 0659 0650 0722 0726 0739 0759 0609 0552 0618 0633 0628 0219 0704 0336 0512 0627 0328 0625 0530 0337 0508 0720 0154 0312 0340 0342 0344 0649 0644 0705 0410 0602 0734
Water Level Anomaly (m)
0
5
10
15
20
Mean
190
200
210
220
230
240
Coastline Index
Case E Variable Uplift.

Figure: 8.17 (e)

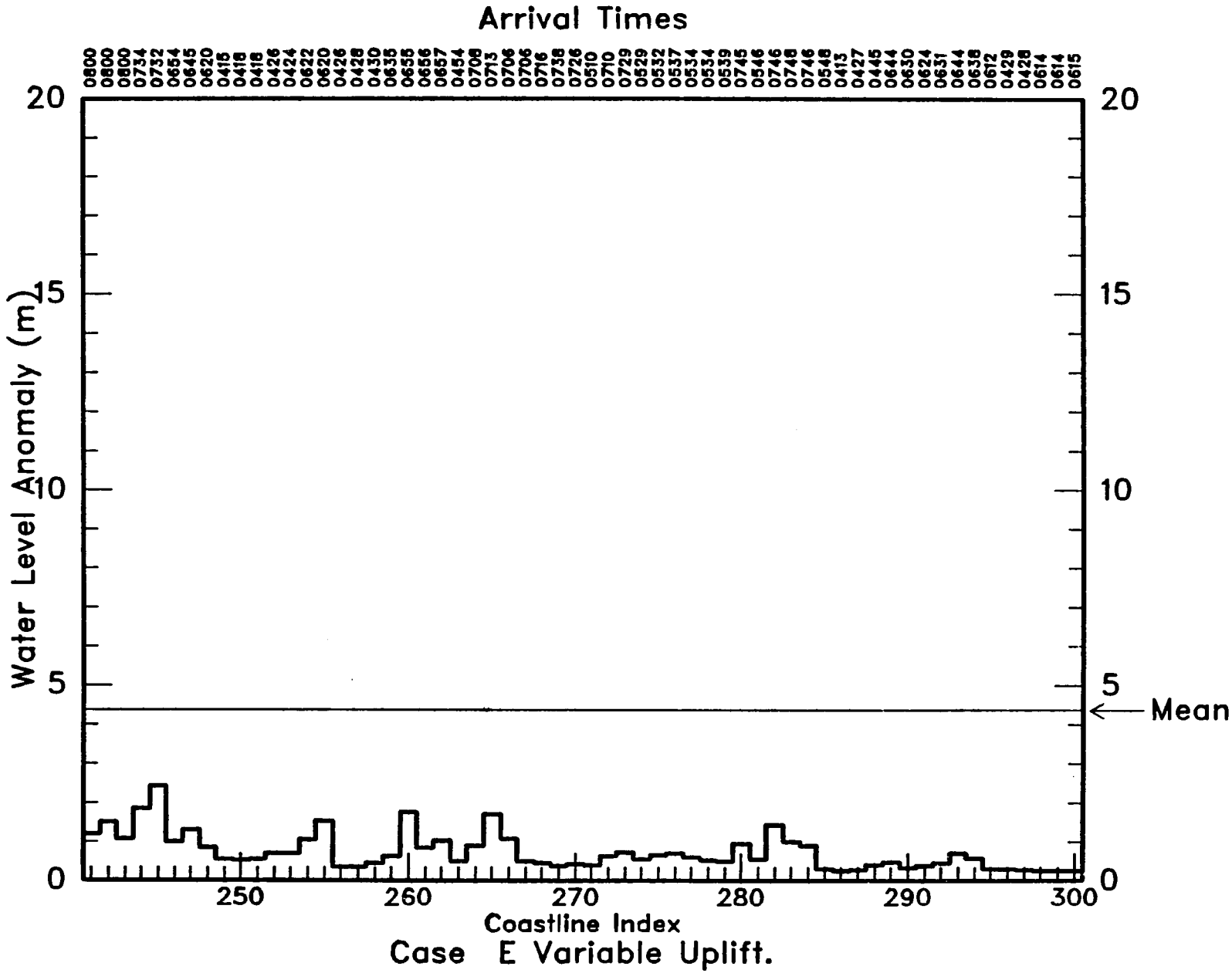
Arrival Times
0800 0800 0800 0734 0732 0654 0645 0620 0415 0418 0426 0424 0622 0620 0426 0428 0430 0635 0655 0656 0657 0454 0708 0713 0706 0706 0716 0738 0726 0510 0710 0729 0529 0532 0537 0534 0534 0539 0745 0546 0746 0748 0746 0548 0413 0427 0445 0644 0630 0624 0631 0644 0638 0612 0429 0428 0614 0614 0615
Water Level Anomaly (m)
0
5
10
15
20
250
260
270
280
290
300
Coastline Index
Mean
Case E Variable Uplift.

Figure: 8.17 (f)

8.4 HAZARD ASSESSMENT - SOURCE ZONE E

Uplift in this source zone produces the most uniformly threatening tsunami. Maximum wave heights have been higher in other simulations, but the breadth of the source area ensures that this event directly threatens more of the coastline than any other. The area of concentrated hazard begins south of Caldera and, if we use a 3 m elevation as the lower limit for a serious threat, continues almost unrelieved to the area between Callao and Chimbote. Although the threat is not uniform along here, making a distinction between facing a 7 m wave and a 12 m wave seems pointless. Both are going to be highly destructive in most cases.

As is usual, locally high waves occur at various locations outside the immediate source area. Only north of Talara do wave elevations fall regularly below 1 m. And even there an occasional potentially threatening 2 to 3 m wave occurs.

In summary, our expectations are confirmed. Tsunamis generated by this source would indeed threaten severe destruction for almost all of the South American west coast.

Section 9
CONCLUSIONS AND RECOMMENDATIONS

9.1 INTRODUCTION

In the preceding eight sections we have discussed the nature of the tsunami problem, the means we have chosen to examine it, and the results of our investigations. The next logical step is to draw conclusions based on our results and make recommendations concerning how these results can be applied. However, before we present our conclusions, we would like first to remind the reader of what we have and have not done.

What we have not done is to predict tsunami wave heights on the beaches of South America as the result of offshore earthquakes. Nor have we predicted specific earthquakes and their resulting tsunamis. In fact, we have not done any predicting at all.

What we have done is to examine an area of known high earthquake potential, the Pacific coast of South America, and to use existing seismic theory to identify places in the area which could possibly (or even probably) be the sites of future large earthquakes. We postulated that earthquakes in these areas would produce tsunamis, and then used existing modeling techniques to simulate what would happen to the ocean surface if the hypothetical earthquakes were indeed tsunamigenic.

Because of the modeling approach that we have taken, we have not attempted to predict onshore wave heights. Rather, we are concerned with the pattern of wave elevation

at points just offshore (a distance of roughly $1/12^{o}$ in latitude or longitude, depending on the location) in water no shallower than 20 m.

We cannot emphasize strongly enough that the patterns of wave height up and down the coast are much more informative than the actual heights. The absolute heights are very much dependent on the way in which we modeled the specific source motion. Because we are dealing with a linear model we could raise or lower the bottom displacement and produce a corresponding proportional change in the offshore waves. But the fact that wave height distribution patterns look similar whether we use the broadband uniform uplift or the more restricted variable uplift leads us to conclude that the model results are, within limits, relatively insensitive to the choice of uplift. Thus we feel confident that, although these results cannot be used in a predictive sense, they can provide valuable information about the general nature and severity of the tsunami threat to coastal South America.

9.2 CONCLUSIONS

We can draw two types of conclusions from this study. The first is an assessment of the threat to the whole coast from tsunamis originating in various source areas. The second is an assessment of the threat to specific locations from tsunamis generated anywhere along the coast.

9.2.1 Threat from Specific Earthquakes

It is obvious from our results that some of the hypothetical tsunami sources are more threatening than others. We can preface our examination of this by asking the question: If an earthquake were to occur in the locations

postulated, with the mechanism postulated, how bad would the tsunami be?

A tsunami generated in source zone E would be the most widely destructive event studied. It produces high waves (not necessarily the highest ones calculated in this study) over roughly 25° of coastline. Even in areas where the wave heights are below the average for this case, they could still be a threat.

The tsunamis coming out of the two subzones of zone B are the next most threatening. Their extreme waves are pretty well localized, but they still produce high water levels at locations well-removed from the source. The tsunamis coming from the southern subzone are the slightly more energetic of the two.

The tsunamis from zone A are only slightly less of a threat than those from zone B. The seismic moments of the earthquakes in the two zones are nearly equal, but the uplift used in zone A is a little more than half that of zone B. The result is a lower overall threat level, although, once again, effects from zone A are felt far from the source.

Tsunamis from zones D and C are not much of a threat outside the immediate source area. Source zone C is by far the least threatening of the generating areas.

9.2.2 Threats to Specific Areas

A second fact that we can note from this study is that some coastal areas respond strongly to all of the tsunamis. Are there areas which are consistently threatened?

The most immediate threat to coastal areas from each of these tsuanamis is on the shore directly opposite the source area. This is true both for the wide-spread sources, such as E, and the small sources, such as C. Since the sources occur in various parts of the coast, no one area is consistently threatened in this way. All coastal locations are equally at peril if a tsunamigenic earthquake occurs closeby.

However, we have noted some similarities in response pattern which seem to occur almost without regard to the source location. For example, several locations south of Valparaiso respond strongly to any tsunami propagating along the coast. We cannot, as yet, say whether or not this response is due to the topography of the locations themselves or some quirk in the model. But this consistent response, if real, would bear further study.

Another apparent trend is the strong response in locations close to the bend in the shoreline near 18°S. In almost every case where the source area was not in the bend region we see stronger-than-average responses at Iquique, Arica, and positions northward along the coast. The geometry of this region seems to be such that wave energy is easily focussed and trapped there. Thus the whole region is consistently threatened by tsunamis from a variety of locations.

Two other effects we see consistently are that waves near Antofagasta damp out very rapidly and that little strong wave energy reaches the coasts of Ecuador and Colombia. The first effect is presumably due to Antofagasta's location on a promontory with little offshore continental shelf (see Figure 2.3). This configuration may not be conducive to the buildup of wave energy.

The second effect is presumably due to a sheltering effect brought on by the gentle bend of the coastline to the northeast beginning at 5°S or so. Waves following the coast northward apparently disperse much of their energy into the shallow water over the Carnegie Ridge, and only a small portion follows the curve of the coast. It would seem that the tsunami threat to this portion of the coast comes from local earthquakes rather than earthquakes occuring off Peru or Chile.

9.2.3 Summary

These conclusions can be summarized in four simple statements.

- The greatest threat to life and property is to coastal areas within or close to the edge of the tsunami source. All of the hypothetical earthquakes pose this type of a threat.
- Most of these source motions produce tsunamis which can result in threatening waves at a considerable distance from the source.
- The coastal communities in the vicinity of the continental bend are continually threatened by tsunamis from almost any source.
- Several localities between 30°S and 40°S are similarly threatened.

9.3 HISTORICAL PERSPECTIVE

It is not possible to test our results against historical records to determine any exact correspondence between the model and actual situations. Very little is known about exact focal mechanisms for tsunamigenic

earthquakes in the region. The one exception is the 1960 Chilean earthquake. But the only tsunami data available are runup heights and wave gauge records. Both of these are recorded either on shore or much closer to shore than our calculations allow.

We can, however, use the historical record to confirm some of the trends we see in our results. An examination of the information in Appendix A is sufficient to point out several facts. The first is that, indeed, most South American tsunamigenic earthquakes produce the greatest wave damage in the source area and reports of water levels as high as 10, 15, or 20 m above MSL are not unheard of.

The second fact is that a number of historical events have caused destruction at sites well-removed from the source. For example, the 1730 tsunami orginating near Valparaiso caused destruction at Concepcion, over 400 km to the south, and the 1877 tsunami originating near Iquique caused damage at Callao, nearly 700 km to the northwest.

This general agreement between our model results and historical precedent does not, of course, guarantee that our conclusions are completely accurate. It does, however, lead us to believe that much of what we have determined can prove quite useful in tsunami hazard planning and research.

9.4 RECOMMENDATIONS

We feel that the results obtained in this study can be used in a number of areas. Among these are disaster education, disaster planning, and future research.

- Education - These results show quite graphically how tsuanamis generated off the South American

coast can threaten population and economic centers. This type of information can be used to educate the affected populace and their leaders as to the magnitude of the threat and the need for a high level of tsunami preparedness.

- Planning - These results, by themselves or in conjunction with historical data, can be used by disaster preparedness authorities in making plans for coping with tsunami hazards when they do occur. Emphasis can be placed on relief for areas likely to be hardest hit, for example.
- Research - These results have shown that certain areas seem to be more threatened than others by specific events. The next logical step would be to establish which of these areas is heavily populated enough or economically important enough that a large tsunami would cause severe damage. These areas could then be studied in detail, using even finer-resolution modeling techniques to assess the local hazard due to onshore runup and flooding. This type of study could then be used by local authorities to plan detailed disaster assistance and hazard mitigation procedures.

This study provides a good deal of information about the near-source threat from possible tsunamigenic earthquakes in the Peru-Chile Trench. It has a number of uses, both as it stands and as fuel for more intense study. We feel that this document, and the companion far-field study funded by AID, make a significant contribution to our knowledge of the tsunami hazard to the Pacific community.

Apendix A
SOUTH AMERICAN TSUNAMIS

The section of the western coast of South America from southern Ecuador to southern Chile has had a long history of tsunami-producing earthquakes. Both Berninghausen (1962) and Soloviev and Go (1969) list a tsunami in 1562 as the earliest verifiable event. Soloviev and Go point out that Peruvian Indian legends talk of earthquakes and floods from the ocean dating back before the reign of the Incas.

We have compiled a list of destructive tsunamis for the period from 1562 to 1966. An examination of several of the tsunami catalogs shows some wide discrepancies in reports on various events, especially prior to about 1860. Great confusion can exist about exact dates, severity of waves, casualties, and damage. We have applied two criteria to determine whether or not to include an event in this appendix. The first is that the event must appear in all three of the sources we used (Berninghausen, 1962; Iida et al., 1967; and Soloviev and Go, 1969). This lends a measure of accuracy to the list, since in many instances each of these documents used different sources to verify records. The second is that the tsunamis must have caused some degree of damage.

We have listed the date of the earthquake, the approximate location of the epicenter (using geographical names rather than latitudes and longitudes), a short summary of the tsunami activity on the South American coast, and an indication of far-field damage caused by the tsunami. If a dollar value for damage is listed, no attempt has been made to convert it to 1981 dollars (unless noted on the table.)

TSUNAMIS ORIGINATING IN SOUTH AMERICA (1562-1966)

DATE	EARTHQUAKE LOCATION	NEAR-SOURCE EFFECTS	FAR-FIELD EFFECTS
1562	Concepcion, Chile	Waves felt for a distance of 1200 km along the coast. Numerous deaths.	
8 Feb 1572	Concepcion, Chile	The portions of Concepcion not destroyed by the earthquake were swept away by the waves. 2000 deaths.	
16 Dec 1575	Epicenter between 39°S and 41°S	Severe wave damage to Valdivia. 100 deaths. Wave damage was localized in source area.	
Nov 1604	Arequipa, Peru	Waves felt 1200 km along the coast. Severe damage to Arica, causing the town to be relocated. 74 deaths.	
15 Mar 1657	Interior of Chile, 36°S to 39°S	Wave damage to Concepcion was heavy. Approximately 40 deaths.	
20 Oct 1687	Lima, Peru	Wave destroyed Pisco and caused many deaths. Approximately 500 deaths at Callao.	Waves 0.5 m high recorded on the northeast shore of Honshu, Japan. Waves observed on Okinawa.
8 Jul 1730	Valparaiso, Chile	Waves felt 1000 km along the coast. Valparaiso was flooded. Concepcion was largely destroyed. 2 or 3 deaths.	Some flooding on northeastern Honshu.
28 Oct 1746	Callao, Peru	Most of Callao destroyed by waves. 4800 deaths. Several smaller towns were destroyed.	

DATE	EARTHQUAKE LOCATION	NEAR-SOURCE EFFECTS	FAR-FIELD EFFECTS
May 1751	Concepcion, Chile	Concepcion destroyed by the combined effects of the earthquake and the tsunami. A settlement on the island of Juan Fernandez was washed away.	
11 Apr 1819	Copiapo, Chile	The tsunami was felt 800 km away. Caldera suffered considerable damage.	Waves as high as 2 m in Hawaii.
19 Nov 1822	Valparaiso, Chile	Some tsunami damage. Waves over 3 m high at Valparaiso.	
20 Feb 1835	Concepcion, Chile	Severe damage to Concepcion and Talcahuano. Waves as high as 7-9 m. Several deaths.	
13 Aug 1868	Arica, Chile	Severe damage to Arica. Many smaller villages were destroyed. Waves as high as 15 m reported. As many as 25,000 deaths from the earthquake and tsunami.	Waves were observed all over the Pacific. Some damage in New Zealand. Waves as high as 5 m. Much lower waves along Australia. Waves several meters high observed in Hawaii, and as high as 3 m in Japan.

DATE	EARTHQUAKE LOCATION	NEAR-SOURCE EFFECTS	FAR-FIELD EFFECTS
9 May 1877	Iquique, Chile	Near the epicenter the mean water rise was 10 m. Rise from 2-6 m at Iquique. Much damage to coastal villages with waves as high as 10 m. Some damage at Antofagasta. Little damage at Caldera, but waves up to 2 m were recorded. Waves with 2 m amplitudes at Valparaiso. Some damage and loss of life at Callao, with waves persisting for several days. At least 100-200 deaths due to the tsunami.	Waves of 1 m observed along the Mexican coast. Damage and loss of life on the island of Hawaii. 5 deaths. Waves as high as 5 m were observed. Waves up to 2 m were reported in Samoa, Fiji, and New Zealand. Much flooding in Japan and several drownings were reported. Waves as high as 3 m were observed.
23 Jan 1878	Arequipa-Iquique	Damage and flooding in coastal areas near the source.	
4 Dec 1918	Caldera, Chile	Waves as high as 5 m were noted at Caldera.	
10 Nov 1922	Coquimbo, Chile	Waves up to 7 m high at Caldera caused some damage. Waters at Coquimbo rose as high as 7 m. Much of the city was destroyed and several hundred drownings were reported.	Some damage was done at Hilo by waves up to 2 m. Waves were observed in Samoa, New Zealand, Australia, and the Philippines. Some damage was done in Japan.
19 Apr 1955	Central Chile	Flooding at Coquimbo. The villages of Tongo and La Serena were damaged. One death.	

DATE	EARTHQUAKE LOCATION	NEAR-SOURCE EFFECTS	FAR-FIELD EFFECTS
22 May 1960	Southern Chile	Severe damage throughout the South American coast. Waves as high as 25 m near the source. Over 300 lives lost. Many coastal towns and villages were destroyed.	$30,000 damage in Crescent City, California. $50,000 damage to Pago Pago, Samoa. $22 million damage in Hawaii. 61 deaths, several hundred injuries. 199 deaths in Japan. Thousands of boats and structures lost. Waves observed all over the Pacific.
20 Nov 1960	Northwest Peru	Extensive damage along the Peruvian coast by waves up to 9 m high. 15-50 deaths.	
17 Oct 1966	Lima, Peru	A 3.5 m wave was observed at Callao. Several small towns were destroyed.	Waves were observed all around the Pacific.

Appendix B
NUMERICAL TECHNIQUE

In order to solve the long wave equations used in this study, we applied the multioperational, alternating direction implicit (ADI) algorithm described by Leendertsee (1967). At each computational cell the wave height anomaly, η, at time $n\Delta t$ is averaged over the cell area centered at $i\Delta\phi$ and $j\Delta\theta$. The flux $U_{i,j}$ is taken at the center of the left-hand face of the cell and the flux $V_{i,j}$ is taken at the center of the lower side.

The following notation is used to express the finite-difference analogs of the continuum equations. For any variable (use α as a representative name) at time $n\Delta t$ and location $i\Delta\phi$ and $j\Delta\theta$

$$\alpha^{n}_{i,j} = \alpha(i\Delta\phi,\ j\Delta\phi,\ n\Delta t) \tag{B.1}$$

$$\frac{\partial\alpha}{\partial t} \approx \frac{1}{2\Delta t}\left(\alpha^{n+1}_{i,j} - \alpha^{n-1}_{i,j}\right) \tag{B.2}$$

$$\frac{\partial\alpha}{\partial x} \approx \frac{1}{2\Delta x}\left(\alpha^{n}_{i+1,j} - \alpha^{n}_{i-1,j}\right). \tag{B.3}$$

and

$$\overline{\alpha^{n}_{i,j}}^{xy} = 1/4\left(\alpha^{n}_{i-1,j}+\alpha^{n}_{i-1,j+1}+\alpha^{n}_{i,j-1}+\alpha^{n}_{i,j}\right) \tag{B.4}$$

The cycle of computations is separated into two operations. During the first half cycle (from time $n\Delta t$ to $(n+1)\ \Delta t$), η and U are calculated implicitly along a line of constant latitude. The finite-difference analogs used for (2.1) and (2.3) are

$$U_{i,j}^{n+1} - U_{i,j}^{n-1} + \frac{2\Delta t g\ h_{i,j}}{R\Delta\phi\ \sin\ \theta}\left(\eta_{i+1,j}^{n+1} - \eta_{i-1,j}^{n+1}\right) - 2f\Delta t\ \overline{V}_{i,j}^{n\,xy} = 0 \quad \text{(B.5)}$$

$$\eta_{i,j}^{n+1} - \eta_{i,j}^{n-1} + \frac{2\Delta t}{R\Delta\phi\ \sin\ \theta}\left(U_{i+1,j}^{n+1} - U_{i-1,j}^{n+1}\right) + \frac{2\Delta t}{R\Delta\theta\ \sin\ \theta}$$

$$\left[(V\ \sin\ \theta)_{i,j+1}^{n} - (V\ \sin\ \theta)_{i,j-1}^{n}\right] = 0 \quad \text{(B.6)}$$

These equations yield a system of linear algebraic equations whose coefficient matrix can be solved quite efficiently.

The computational cycle is completed by implicit computation of V and η with the finite-difference analogs of (2.2) and (2.3)

$$V_{i,j}^{n+1} - V_{i,j}^{n-1} + \frac{2\Delta t g h_{i,j}}{R\Delta\theta}\left(\eta_{i,j+1}^{n+1} - \eta_{i,j-1}^{n+1}\right) + 2f\Delta t\overline{V}_{i,j}^{n\,xy} = 0 \quad , \quad \text{(B.7)}$$

$$\eta_{i,j}^{n+1} - \eta_{i,j}^{n-1} + \frac{2\Delta t}{R\Delta\theta\ \sin\ \theta}\left[(V_{\sin}\theta)_{i,j+1}^{n+1} - (V\ \sin\ \theta)_{i,j-1}^{n+1}\right]$$

$$+ \frac{2\Delta t}{R\Delta\phi\ \sin\ \theta}\left(U_{i+1,j}^{n} - U_{i-1,j}^{n}\right) = 0 \quad \text{(B.8)}$$

These equations are solved in the same manner as (B.5) and (B.6).

The numerical characteristics of the ADI algorithm used here were studied in detail during the course of a previous U.S. Army Corps of Engineers-sponsored research program. A succinct method of examining the numerical phase speed is to determine the dispersion relation of the numerical scheme. If we assume that a single Fourier component of frequency ω is the solution for a rotating, constant depth basin we find that the dispersion relation for linear free gravity waves is

$$(\sin \theta)^2 = \frac{\sigma^2 + \gamma^2(a^2+b^2) + \gamma^4 a^2 b^2}{1 + \gamma^2(a^2+b^2) + \gamma^4 a^2 b^2}, \qquad (B.9)$$

where

$\theta = \omega \Delta t$ non-dimensional frequency

$\sigma = f \Delta t$ non-dimensional Coriolis parameter

$a = 2 \sin (k_x \Delta x)/2$

$b = 2 \sin (k_y \Delta y)/2$

k_x, k_y = x,y-components of wave number

$\gamma = \sqrt{gh} \cdot \Delta t/\Delta s$ (Courant number).

The above is valid for a square grid ($\Delta y = \Delta x = \Delta s$). Equation (B.9) states that the linear algorithm is stable for all γ provided only that $\sigma^2 < 1$. However, the accuracy of θ, and hence of the phase speed for given wave length, is

dependent upon both γ and σ. The condition for accurate rendition of θ (phase speed) for given wave length is that

$$\sigma^2 \ll 1 \tag{B.10a}$$

and

$$\gamma^2(a^2+b^2) \ll 1 , \tag{B.10b}$$

in which case (B.9) reduces nearly to the exact relation

$$\theta^2 = \sigma^2 + \gamma^2(k\Delta x)^2 , \tag{B.11}$$

where k is the wave number magnitude. For $\gamma = 1$, which is the usual upper bound for explicit schemes, (B.10b) simply states that the wave should be well resolved by the grid, i.e., $k\Delta x \ll 1$. One can use a larger γ and remain stable, but only for those waves for which $k\Delta x \ll 1/\gamma$ will one have an accurate rendition of propagation speeds.

If the depth varies in a step-wise manner, as it does in this application to tsunami generation and propagation, then (B.9) and (B.11) are valid locally. It is fortuitous that a grid scale (10') and a time step (60 sec) give a Courant number (γ) near unity for the deepest portions of the modeled area. Hence the shorter waves in the <u>shallower</u> margins, even though they are not well resolved, will maintain accurate propagation speeds according to (B.10b). The propagation of tsunami along the coast will at least be numerically accurate.

REFERENCES

Abe, K., 1975: Reliable estimation of the seismic moment of large earthquakes. J. Phys. Earth, 23, 381-390.

Aida, I., 1978: Reliability of a tsunami source model derived from fault parameters. J. Phys. Earth, 26, 57-73.

Bennett, A. F., 1976: Open boundary conditions for dispersive waves. J. Atmos. Sci., 33, 176-182.

Berninghauses, W. H., 1962: Tsunamis reported from the west coast of South America. Bulletin of Seismolog. Soc. of America, 52, 915-921.

Billings, M., 1954: Structural Geology, 2nd ed. Prentice-Hall, Englewood Cliffs, NJ., 514pp.

Brandsma, M., D. Divoky and L.-S. Hwang, 1975: Seawave-A revised model for tsunami applications. Tetra Tech Inc., Pasadena, CA., NTIS: PB-252-705.

Chen, M., D. Divoky and L.-S. Hwang, 1975: Nearfield tsunami behavior. Tetra Tech Inc., Pasadena, CA., Tech. Rept. NSF-RA-F-75-121, NTIS: PB-252-427.

Chinnery, M. A. and R. G. North, 1975: The frequency of very large earthquakes. Science, 190, 1197-1198.

Garcia, A. W., 1976: Effect of source orientation and location in the Peru-Chile Trench on tsunami amplitude along the Pacific Coast of the continental United States. U. S. Army Engineer Waterways Experiment Station, Rept H-76-2, NTIS: AD-AO32991.

Hammack, J. L., 1973: A note on tsunamis: their generation and propagation in an ocean of uniform depth. J. Fluid Mech., 60, 769-799.

Hebenstreit, G. T., 1981: Assessment of tsunami hazard presented by possible seismic events: Far-field effects. Tech. Rept. SAI-82-599-WA, Science Applications, Inc., McLean, VA.

Hebenstreit, G. T., E. N. Bernard, and A. C. Vastano, 1980: Applications of improved numerical techniques to the tsunami response of island systems. J. Phys. Oceanogr., 10, 1134-1140.

Iida, K., D. C. Cox and G. Pararas-Carayannis, 1967: Preliminary catalog of tsunamis occurring in the Pacific Ocean. Hawaii Inst. of Geophys. Report HIG-67-10, Univ. of Hawaii, Honolulu.

Kajiura, K., 1963: The leading wave of tsunami. Bull., Tokyo Earthquake Res. Inst., 41, 535-571.

Kanamori, H., 1977: The energy release in great earthquakes. J. Geophys. Res., 82, 2981-2987.

Kelleher, J. A., 1972: Rupture zones of large South American earthquakes and some predictions. J. Geophys. Res., 77, 2087-2103.

Kelleher, J., J. Savino, H. Rowlett and W. McCann, 1974: Why and when great thrust earthquakes occur along island arcs. J. Geophys. Res., 79, 4889-4899.

Le Pichon, X., 1968: Sea-floor spreading and continental drift. J. Geophys. Res., 73, 3661-3697.

Lee, J. J., 1980: Distant and local tsunamis in coastal regions. Tech. Rept. NSF/RA-80-0511, Dept. of Civil Eng., Univ. of Southern California, Los Angeles, CA., NTIS: PB81-211-047.

Leendertse, J. J., 1967: Aspects of a computational model for long-period water-wave propagation. Tech. Memo RM-5294-PR, The Rand Corp.

McCann, W. R., S. P. Nischenko, L. R. Sykes, and J. Krause, 1978: Seismic gaps and plate tectonics-seismic potential for major plate boundaries. Proceedings of Conference VI: Methodology for identifying seismic gaps and soon-to-break gaps. U. S. Geol. Surv. Open-File Report 78-943, 441-584.

Mansinha, L. and D. E. Smylie, 1971: The displacement fields of inclined faults. Bull., Seismol. Soc. of America, 61, 1433-1440.

Momoi, T., 1964: Tsunami in the vicinity of a wave origin [1]. Bull, Tokyo Earthquake Res. Inst., 42, 133-146.

Mungall, J. C. H. and R. O. Reid, 1978: A radiation boundary condition for radially-spreading non-dispersive gravity waves. Texas A&M Univ., Dept. Of Oceanography, Ref 78-2-T, 63pp.

NOAA, 1971: Tsunami travel-time charts for use in the Tsunami Warning System (Revised 1971 Edition). National Ocean Survey, NOAA, Rockville, MD., NTIS: COM-71-00918.

Pararas-Carayannis, G. and J. Calebaugh, 1977: Catalog of tsunamis in Hawaii. Report SE-4, World Data Center A for Solid Earth Geophysics, NOAA/EDIS, Boulder, Colo.

Purcaru, G. and H. Berckhemer, 1978: A magnitude scale for very large earthquakes. Tectonophysics, 49, 189-198.

Silgado, E. 1978: Recurrence of tsunamis in the western coast of South America. Marine Geodesy, 1, 347-354.

Sklarz, M. A., L. Q. Spielvogel, and H. G. Loomis, 1979: Numerical simulation of the 29 November 1975 island of Hawaii tsunami by the finite-element method. J. Phys. Oceanogr., 9, 1022-1039.

Soloviev, S. L. and Ch. N. Go, 1969: Catalog of tsunamis in the Pacific (main data), Academy of Sciences, USSR, Moscow.

Stauder, W., 1973: Mechanism and spatial distribution of Chilean earthquakes with relation to the subduction of the oceanic plate. J. Geophys. Res., 78, 5033-5061.

Stauder, W., 1975: Subduction of the Nazca Plate under Peru as evidenced by focal mechanisms and by seismicity, J. Geophys. Res., 80, 1053-1064.

Tuck, E. O. and L. -S. Hwang, 1972: Long wave generation on a sloping beach. J. Fluid Mech., 51, 449-461.

Yamashita, T. and R. Sato, 1974: Generation of tsunami by a fault model, J. Phys. Earth, 22, 415-440.